Controlling Deformation Errors in the Contour Method for Residual Stress Measurement

Thesis

Faculty of Science, Technology, Engineering and Mathematics

School of Engineering and Innovation

Materials Engineering Group

Controlling Deformation Errors in the Contour Method for Residual Stress Measurement

Beverly Stewart

February 2019

A thesis submitted to the School of Engineering and Innovation of the Open University for the Degree of Doctor of Philosophy

Abstract

The contour method is being increasingly utilised for characterising residual stresses in engineering components because it has the ability to measure a two-dimensional map of residual stresses on a plane of interest [1], it is not limited by the size or geometry of the component and is insensitive to microstructural variations. It involves carefully cutting a component into two halves and measuring the resulting deformation on the cut surfaces due to the relaxation of residual stresses. The measured deformation data is used to back calculate a map of the original residual stresses acting normal to the plane of the cut [2].

Similar to other mechanical strain relief techniques the contour method is based on elastic relaxation of residual stresses and the cutting technique for material removal should not induce residual stress and plastic deformation. However, there is an assumption unique to the contour method and that is the width of the cut must be constant. Usually wire EDM is employed for cutting as it imposes minimal stress on the material. In practice, the stresses near the cut tip can cause a deviation from the cutting requirement, referred to as the bulge error or elastic bulging. These deformation errors can cause significant bias errors in the contour method stress results. The aim of this research is to understand how to control and correct deformation errors that occur during the cutting step of the technique to help to obtain accurate and reliable residual stress measurements made with the contour method.

In the first part of this thesis the iterative FE based (2D) bulge correction procedure first published by Prime and Kastengren [3] is investigated and applied for a compact tension, C(T), cross-weld specimen that appeared to show bulge error in the residual stresses measured by the contour method [4]. The procedure is also extended to perform a more complex 3D bulge correction. A simpler procedure, which calculates directly the stress error due to bulge, has been developed and applied for the case study.

Following this, numerical mode I stress intensity factor (SIF) correlations were developed for a finite plate with a uniform far field tension loading in the plane stress and plane strain condition to improve the understanding of the factors that influence the bulge error. Then a new analytical solution based on the linear elastic fracture mechanics mode I SIF is developed and validated to replace the cumbersome iterative FE procedure to estimate the bulge error. This solution is used to develop a set of stress error correlations for periodic cosine stress functions to predict the magnitude of stress errors due to bulging in contour method measurements. Finally, a set of guidelines are developed to assist practitioners of the contour method to decide on a suitable approach to correct for the bulge error.

Acknowledgement

Firstly, I am very thankful to my supervisors Dr. Foroogh Hosseinzadeh and Prof. John Bouchard for their continuous guidance, advice and support throughout my project. I would also like to say a special thank you to Dr. Michael Prime for his invaluable discussions and advice during my work. I have learned a great deal from you all.

I would like to thank The Open University for funding my PhD project and all my colleagues for their friendship and support. Many thanks to Peter Ledgard and Stan Hiller for their kind help when needed and useful discussions during my work.

Finally, I would like to say a special thank you to my family who have always encouraged and supported me greatly throughout all my endeavours in life. Most of all, I am thankful to my husband Stephen for his continuous love, support and encouragement and who I could not have completed this project without.

Preface

This thesis is submitted for the degree of Doctor of Philosophy of The Open University, United Kingdom. The work described in this thesis was performed in the School of Engineering and Innovation, Faculty of Science, Technology, Engineering and Mathematics, between March 2015 and February 2019, under the supervision of Dr. Foroogh Hosseinzadeh and Prof. Peter John Bouchard.

Except for where clearly referenced, the work is entirely the author's own work. None of the work referred to in this thesis has been submitted for another degree or qualification in this or any other university. Some of the results of this work has been published in conference proceedings as listed below:

Conference paper

Stewart, B., et al. Investigating bulge correction in the contour method for residual stress measurement of a compact tension weld specimen. in 7th International Conference on Mechanics and Materials in Design. 11-15 June 2017. Albufeira/Portugal

Table of contents

Chapter 1: Introduction

Residual stress is that which remains in a body that is stationary and at equilibrium with its surroundings (in the absence of external forces) [5]. These stresses are generated during most manufacturing processes involving material deformation, heat treatment, machining or processing operations that transform the shape or change the properties of a material [6]. The contribution of the residual stresses can be beneficial or harmful, dependent on the sign (i.e. tensile or compressive) and location of the residual stresses [1]. Accordingly, residual stress analysis is a compulsory stage in the design of parts and structural elements and in the estimation of their reliability under real service conditions [6]. However, the processes that bring about residual stresses are often complex and analytical predictions only provide approximate solutions of the residual stress magnitude and distribution. Numerical analyses have been increasingly employed to predict residual stress in engineering structures but the reliability of the results is highly dependent on the assumptions which have to be made. Therefore, experimental methods have become important to measure these stresses and validate analytical and numerical predictions.

There are many different methods available for measuring residual stresses in different types of components have been developed [6]. Mechanical stress relaxation methods rely on the measurement of deformations due to the release of residual stresses upon removal of material from the specimen [6]. The contour method is one such technique, first published in detail in 2000 [2], which is appealing because provides high resolution maps of the residual stress distribution normal to a plane of interest [1] and can be applied with equipment that is generally available in workshops and inspection laboratories. The method is also not limited by the specimen size and geometry. And unlike diffraction techniques, the contour method is not sensitive to microstructural variations. Although the contour method has many advantages, it is the youngest technique to measure residual stresses and needs further development to deal with potential sources of error and uncertainties in the assumptions to implement the technique [1].

The experimental procedure involves cutting through the specimen cross-section using wire Electric Discharge Machining (EDM) and measuring the surface height profiles of the cut surfaces using a coordinate measuring machine or a laser profilometer [1]. Finite element modelling is then used to determine the normal stresses required to restore the deformed cut surface shape back to its original flat shape [2]. This requires the assumption that a precisely flat cut is created when sectioning the component. However, assuming a flat cut

is overly restrictive and the fundamental assumption for the contour method is that the cut removes a constant width of material thereby creating a fixed slot width when measured relative to the original state of the body [3]. A deviation from this occurs during cutting, the stresses within the remaining material will redistribute to maintain interior equilibrium [1] and results in a stress concentration at the cut tip that elastically deforms, i.e. stretches or contracts, the material at the cut tip. Since the physical cut width is fixed by the EDM wire size, this causes the width of material removed to vary along the cut length which creates slot width errors. This error, also referred to as the 'bulge error' [3], can cause significant bias in the contour method results if not dealt with [3].

This PhD project was undertaken to understand the origins and influence of the slot width error in residual stress measurements made with the contour method. The novel numerical and analytical approaches proposed in this thesis have the potential to simplify correcting contour measurements for the slot width error, thereby helping to improve the accuracy and reliability of residual stress measurements.

1.1 Outline of the thesis

The layout of the thesis is as follows:

Chapter two provides an overview of the characteristics of residual stresses and the available techniques for measuring residual stresses. The contour method measurement technique is described and the sources of cutting errors are outlined. The published literature on the deformation errors in the contour method is reviewed as this is the main focus of this research. As the cutting process in the contour method can be seen as a slow-moving blunt crack, the stress intensity factor is introduced based on linear elastic fracture mechanics to characterise the stresses and displacements at the crack tip. Finally, the main aims and methodologies in this research are set out.

In Chapter 3 the proposed bulge correction procedure is carefully studied to correct contour method residual stress measurements. The capability of the procedure to correct complex (varying) stress distributions is evaluated by using two-dimensional and three-dimensional FE modelling. The case study was a stainless steel (Esshete 1250) compact tension, C(T), welded specimen where residual stresses had been previously measured using neutron diffraction, incremental slitting and the contour method [4]. From this work an alternative method is proposed and applied to calculate the corrected stresses which simplifies the time-consuming procedure to correct for the bulge error in contour measurements.

One of the main aims of this research is to understand the fundamental theory of the bulge error to determine when it arises. Chapter 4 starts with a proof of the hypothesis that the bulge error is dependent on the stress concentration at the cut tip using the stress intensity factor. Then a new analytical solution to calculate the bulge displacement is presented based on fracture mechanics crack tip displacement field equations. The new approach is then validated with numerical predictions of the bulge error using 2D and 3D models subjected to idealised stress distributions and real residual stress measurements made with the contour method.

The contour method technique is appealing because it is simple to implement but the need to correct residual stress measurements for the bulge error may be a drawback. For that reason, Chapter 5 investigates possible correlations between the stress error due to bulging and the stress intensity factor parameter to predict the level of stress error associated with the bulge in contour measurements. The aim of this work is to determine the magnitude of the bulge error in contour method stress results to enable the practitioner to decide whether to correct for it.

In Chapter 6 the current and new proposed approaches to estimate and correct contour measurements for the bulge error are discussed and guidelines are provided. Finally, the main conclusions and suggestions for future work throughout this research is presented in Chapter 7.

Chapter 2: Literature review

Residual stresses can be beneficial or detrimental to the performance of a material or the life of a component. Consequently, it is important to have reliable methods for the measurement of these stresses and to understand the level of information they can provide [5]. There are several residual stress measurement techniques that have different spatial resolution and penetration capabilities [1]. The main focus of this research is the contour method technique.

This chapter provides an overview of the origin and types of residual stresses and the three categories of residual stress measurement techniques (non-destructive, destructive and semi-destructive). Then a detailed description of the contour method theory, assumptions and experimental procedures is presented and the advantages of the contour method are discussed. Followed by a summary of the cutting errors in the contour method and a review of the two deformation errors which is the main focus of this research, that is plasticity and bulging or “varying cut width”. The current published literature on correcting for deformation errors in the contour method is reviewed and the steps of the iterative finite element procedure proposed by Prime and Kastengren [3] to correct contour measurements for the bulge error is established. Then the basic linear elastic fracture mechanics concepts are introduced and the available methods to estimate the stress intensity factor are considered. Finally, the needs and gaps in the contour method are identified and the individual aims and methodology for this research are outlined.

2.1 Residual stresses

Residual stresses are “locked-in” [7] stresses that exist in materials and structures, independent of the presence of any external loads. Residual stresses in a body originate from geometrical misfits [5] between different regions or phases in a material. These give rise to macro or micro stresses or both can be present in a component. Figure 2 - 1 shows different external load mechanisms and the expected profile of the induced residual stresses. The interaction between misfits and the restraint of the surrounding material determines the magnitude of residual stresses induced and their length scales [5].

The mechanical properties of materials and structural components, such as fatigue life and corrosion resistance, can be considerably influenced by the presence of residual stresses [7]. These stresses can enhance the strength of a material or cause premature failure, depending on the sign and location of the residual stresses [1]. The presence of tensile

residual stresses is generally harmful since they can cause fatigue failure and stress corrosion cracking [8]. Welding is an example of a manufacturing process that produces harmful tensile stresses and these stresses usually show very steep residual stress to distance gradients [9]. They are commonly relaxed by stress relief annealing and post-weld heat treatments (PWHT) are routinely applied to welds in safety critical plant [10]. One of the most effective means of prolonging the fatigue life of a component is by placing the surface in residual in-plane compression. Most commonly this is achieved by the introduction of plasticity local to the surface region [10] by techniques such as shot peening, laser peening, water-jet peening, ultrasonic peening and roller burnishing. In shot peening, the surface is repeatedly impacted by hard millimetre sized 'shot' [10]. Whereas the laser peening process offers a much deeper peened surface, whereby the workpiece surface is subjected to planar laser shocks (pulses) from high-powered lasers [11]. In water-jet peening a water jet at high pressures impinges on the surface of the workpiece, inducing compressive residual stresses and surface hardening at the same level as in shot peening [12]. Ultrasonic peening process uses a hand tool based on a piezoelectric transducer [13]. In the roller burnishing process, also called surface rolling, the surface is cold worked by a hard and highly polished roller or set of rollers [14]. The ability to measure residual stresses is important in understanding material failure and to predict the life of engineering structures.

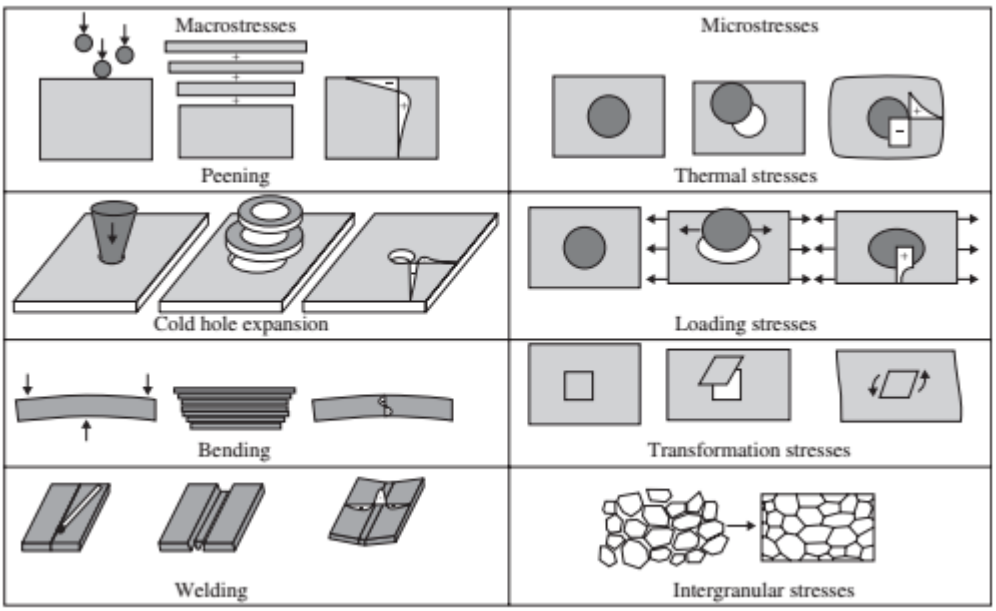

Figure 2 - 1: Ways in which macro and micro residual stresses are created in materials from engineering processes [5].

2.2 Types of residual stresses

Residual stresses are characterised by the length scale over which they self-equilibrate [5]. Figure 2 - 2 illustrates the types of residual stresses and how they equilibrate over different length scales. Type I or macro stresses are in equilibrium over the entire cross section of a component, type II or intergranular stresses are in equilibrium over a single grain or several grains and type III stresses are in equilibrium at a scale smaller than a grain size at the subatomic scale. Macro stresses can typically arise through the interaction between mis fitting parts within an assembly, and through generation of chemical, thermal, and plastically induced misfits between different regions within one part [15]. This is in contrast to intergranular stresses which typically arise in multi-phase materials due to the incompatibility between different grains, for example from differences in slip behaviour [10], and the subatomic stresses which usually arise from crystal defects such as dislocations.

Type II and III stresses have zero resultant force over the measurement volumes that macro residual stresses can be measured and therefore have negligible influence on longer length scale stresses. However, the occurrence of many misfits of a shorter scale may have a cumulative effect such that they give rise to stresses at a longer scale. For example, the cumulative presence of many geometrically necessary dislocations can give rise to plastic strain gradients and thereby macroscale misfits and stresses of type I [10]. In the structural integrity assessment of engineering components attention is focused on type I macro stresses [5], therefore it is this type of residual stress which is of interest in this research and is referred to throughout this thesis.

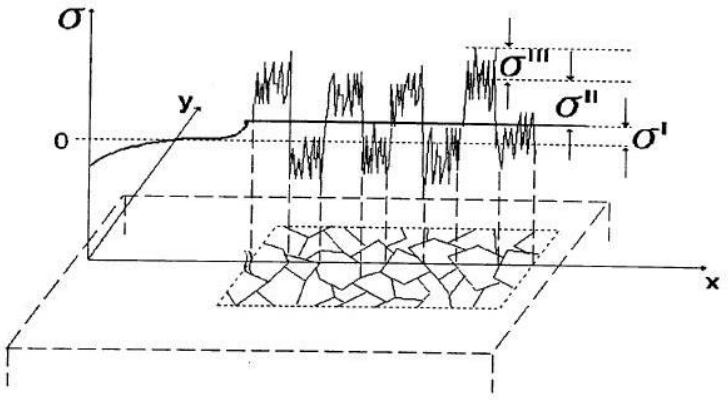

Figure 2 - 2: Categorisation of residual stresses according to length scales [16].

2.3 Residual stress measurement techniques

Experimental techniques to measure residual stresses that develop within engineering components are essential to validate analytical or numerical predictions. In practice, residual stresses cannot be measured directly [17], instead techniques such as mechanical stress-relaxation methods or diffraction methods, measure fundamental quantities, such as elastic strain or displacement, that can be related to stress. Residual stress measurement techniques are generally classified as destructive, semi-destructive or non-destructive. When developing a stress measurement strategy, it is imperative that techniques are chosen which are sensitive to the relevant length scale (macroscopic or microscopic) and that sensitivities to shorter length scales do not affect the reliability of the measurements [18]. In effect, residual stresses are three dimensional and may have large stress gradients to maintain equilibrium conditions, therefore it is important to consider the required spatial resolution and the depth over which they can penetrate. Figure 2 - 3 shows the penetration capabilities versus spatial resolution of different measurement techniques, along with measurement speed and cost [1].

There is a wide variety of techniques available for measurement of residual stresses [19]. Non-destructive measurement techniques involve measurement of stress by diffraction or some other properties, such as ultrasonic waves or magnetism. The non-destructive residual stress measurement methods have the obvious advantage of specimen preservation, and they are particularly useful for production quality control and for measurement of valuable specimens. The most commonly used non-destructive diffraction techniques include neutron diffraction, synchrotron diffraction and x-ray diffraction. The destructive and semi destructive residual stresses measurement methods use mechanical stress-relaxing methods, that is, the strain or deformation is measured as a result of stress relaxation when material is removed [6]. Generally, they require much fewer specific calibrations because they measure fundamental quantities such as displacements or strains, thus giving them a wide range of application [7]. The semi-destructive techniques remove only a small amount of material from a component leaving its overall structural integrity intact for further testing, repair and/or use. The most commonly used semi-destructive techniques include conventional hole drilling, incremental hole drilling, ring core method and the deep hole method, while the destructive techniques include slitting (crack compliance) method, layer removal and the contour method. Table A - 1 in the Appendix A provides a summary of the advantages and disadvantages of the most commonly used residual stress measurement techniques.

In the remainder of this section the destructive and non-destructive techniques used to validate the bulge error studies throughout this work, that is slitting, contour method and neutron diffraction, are discussed. Since the contour method is a main subject of this research, the method will be described in more detail in sections 2.4 to 2.7.

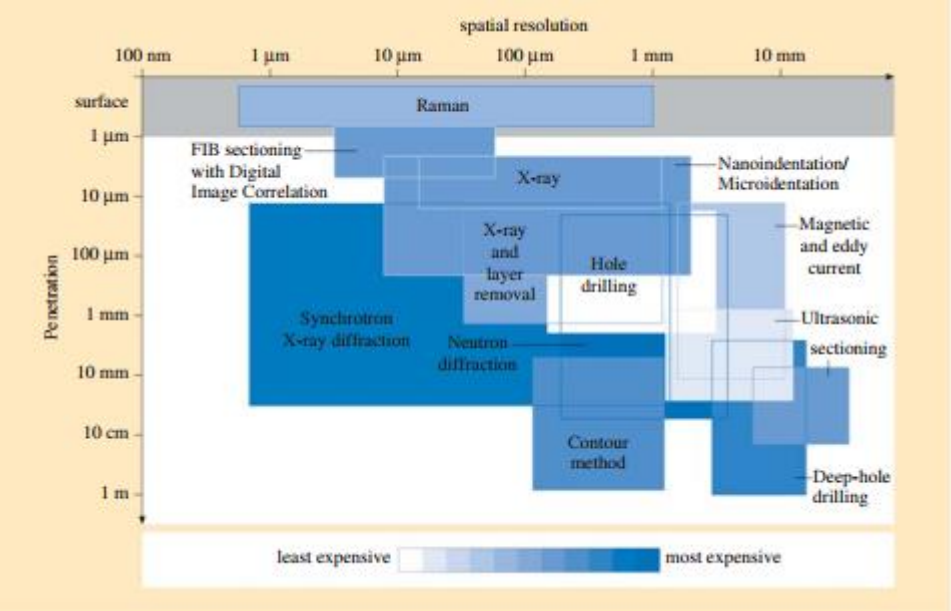

Figure 2 - 3: Measurement penetration vs. spatial resolution for various residual stress measurement methods [1]. Courtesy of Michael Fitzpatrick, Open University, UK

2.3.1 Destructive methods

Destructive or relaxation methods [5, 19] involve the removal of stressed material, allowing the residual stresses in the material to relax and redistribute which produces localized distortion. The distortion is measured experimentally as strain or displacement and used to back calculate the original stresses in the material. These techniques are preferred because they can penetrate deeper in thick components and are not sensitive to microstructural variations. In addition, they are applied with commonly available equipment, such as strain gauges or conventional machining [20]. However, the cutting process used should not introduce plasticity or heat, so that the original residual stress can be measured without the influence of plasticity effects on the cutting planes' surface.

Slitting Method

The slitting method [1, 20] involves incrementally cutting a slot into a component which releases the residual stress at the cut face and deforms the part. The resulting strains are measured as a function of slot depth using surface strain gauges and used to solve for the

distribution of stresses along the cut surface. In typical practice for metallic materials, the slit is cut using a wire electric discharge machine [1]. Strain gauges attached on the top surface shown in Figure 2 - 4, are used for near surface stress measurements, whereas strains recorded on the back face can measure stresses all the way through the thickness.

The residual stress is computed from the measured strains through a linear system called the compliance matrix, which is determined from finite element analysis, for example [1]. The technique is capable of measuring a single in-plane normal component of residual stress through the thickness of a material [1]. Limitations of the slitting technique are its destructive nature as well as the fact that residual stresses are averaged over the cut width, so this needs to be considered when choosing the cutting variables. The spatial resolution is inherently limited by the distance between the strain measurement and the location of the desired interior stresses. To resolve stress variations over a distance of say 1 mm, you must make cuts with increments of less than 1 mm. However, just making cuts in finer depth increments is not necessarily sufficient [20]. While this method can be used for a wide range of materials, the sub-millimetre spatial resolution cannot be matched [6] compared to diffraction techniques. Furthermore, the slitting method cannot determine the stresses over the last few percent of the specimen thickness because the weight of the specimen and yielding will affect the strain readings. However, one benefit of the slitting method is when the stress intensity factor (SIF) is of interest, then this method can calculate the SIF directly and precisely without prior knowledge of the residual stresses [21].

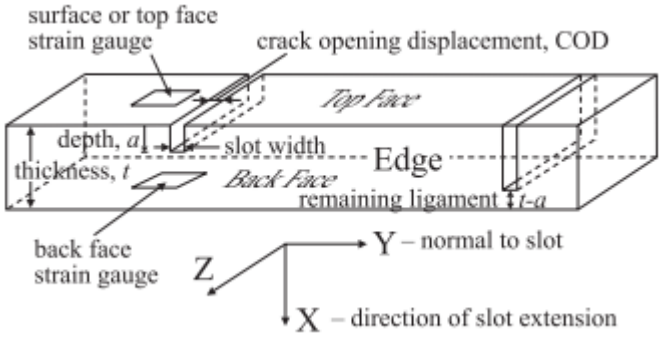

Figure 2 - 4: Slitting method coordinate system and terminology [20].

2.3.2 Non-destructive methods

Neutron, X-ray and synchrotron diffraction involve directing a beam of a specific wavelength on the sample material containing residual stresses and measuring the angular distribution of the diffracted beam from the material [1]. X-ray diffraction can measure residual stresses

very near the surface of the specimen, whereas neutron and synchrotron diffraction have the advantage that they can measure residual stress with depths of a few centimetres. These techniques provide the average stress over a small gauge volume (1 to 2 mm^3) and are therefore useful for measuring stress gradients. However, the accuracy of diffraction techniques is greatly affected by the grain size and texture and require careful surface preparation.

Neutron Diffraction

The diffraction technique, including neutron diffraction, is based on Bragg's Law (see Figure 2 - 5) which relates the atomic lattice spacing for crystallographic planes to a particular angle at which the peak of these planes are observed [22]. The Bragg relationship can be generalised in Equation 2 – 1 to apply to multiple different crystal planes,

$$n\lambda = 2\, d_{hkl}\, \sin\theta_{hkl} \qquad \text{Eqn. 2 - 1}$$

where the subscripts (hkl) are the Miller indices that define the crystallographic planes. θ_{hkl} is the Bragg scattering angle, d_{hkl} is the atomic lattice spacing, λ is the radiation wavelength and n is a positive integer.

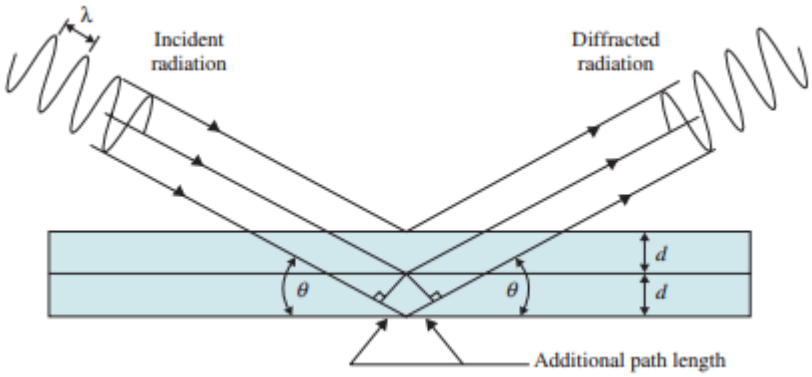

Figure 2 - 5: Radiation diffraction within a crystal structure d = spacing between lattice planes, θ = Bragg angle, and λ = wavelength of the radiation [1].

Residual stress measurement by the neutron diffraction technique involves performing a lattice parameter measurement for both stressed and stress-free material, followed by data analysis for diffraction peak fitting and strain-stress calculations.

The accuracy of the neutron diffraction residual strain calculations is highly dependent on obtaining reliable measurement of a stress-free reference material (d_0) specially on effect

of microstructure. The reference samples may have the form of thin plates, combs or small cubes cut with the expectation that the stress normal to the surface in a thin section is zero [23].

The lattice parameter (*d*-spacing) can be determined by two methods, monochromatic 2θ strain scanning and the time of flight technique [5, 22]. The monochromatic 2θ strain scanning technique is commonly found at a reactor source. Since the technique is based on a monochromatic (i.e. single wavelength) neutron beam , Equation 2 – 1 can be differentiated to Equation 2 – 2 which can be applied for strain calculation.

$$\varepsilon = \frac{d - d_0}{d_0} = \frac{\Delta d}{d_0} = -\cot\theta\,\Delta\theta \qquad \textit{Eqn. 2 - 2}$$

where Δd is the change in lattice spacing and d_0 is the stress-free lattice spacing.

The residual strains can then be converted into stresses by using the material's diffraction elastic constants (such as bulk Young's modulus and Poisson's ratio of isotropic materials) and by applying the classical Hooke's law in Equation 2 – 3.

$$\sigma_{xx} = \frac{E}{(1+\nu)(1-2\nu)}\left[(1-\nu)\varepsilon_{xx} + \nu\left(\varepsilon_{yy} + \varepsilon_{zz}\right)\right]$$

$$\sigma_{yy} = \frac{E}{(1+\nu)(1-2\nu)}\left[(1-\nu)\varepsilon_{yy} + \nu(\varepsilon_{xx} + \varepsilon_{zz})\right] \qquad \textit{Eqn. 2 - 3}$$

$$\sigma_{zz} = \frac{E}{(1+\nu)(1-2\nu)}\left[(1-\nu)\varepsilon_{zz} + \nu\left(\varepsilon_{xx} + \varepsilon_{yy}\right)\right]$$

were σ_{xx} is the relevant stress direction and E and ν are the crystallographic Young's modulus and Poisson's ratio, respectively.

Neutron diffraction has the advantage that it can measure bulk residual stresses for up to 100 mm in aluminium or 25 mm in steel [1]. With high spatial resolution, the neutron diffraction method can provide complete three-dimensional maps of the residual stresses in material [6]. An important complication in the application of neutron diffraction is the introduction of apparent strains when internal or external surfaces are encountered. This arises because of shifts in the centre of gravity of the diffracting volume when it is only partially filled [5]. Also, compared to other diffraction technique such as X-ray diffraction, the relative cost of application of neutron diffraction method, is much higher, mainly because of the equipment cost. It is too expensive to be used for routine process quality control in engineering applications [6].

2.4 The contour method

The contour method, first published by Mike Prime in 2000 [2], is unique in its ability to measure a 2-D cross-sectional map of residual stresses on a plane of interest [1]. In its application, a specimen is cut into two halves and residual stresses in the part are allowed to relax causing the cut surfaces to distort. The cut surface profile (contour) is then measured and used to back calculate the 2-D map of original residual stresses normal to the plane of the cut [1].

In this section the ideal theory of the contour method and assumptions required for practical implementation are presented. The steps of the experimental procedure of the contour method is discussed in the next section.

2.4.1 Theory of the contour method

The theory of the contour method is based on a variation of Bueckner's elastic superposition principle [24] as shown in Figure 2 - 6.

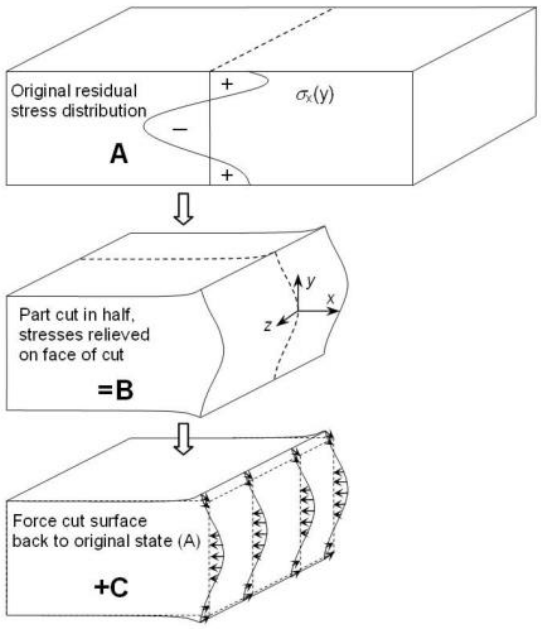

Figure 2 - 6: Superposition principle to calculate residual stresses in the contour method [25].

Step A represents the undisturbed part containing residual stresses. In step B, the part has been cut in two halves on the plane x = 0 and the cut surface has deformed due to the relaxing residual stresses along the cut plane. In step C, the deformed cut surface is forced back to its original shape and the resulting change in stress is determined [1].

Superimposing the stress state in B with the change in stress from C gives the original residual stresses throughout the part [2]. Therefore,

$$\sigma^{A}(x,y,z) = \sigma^{B}(x,y,z) + \sigma^{C}(x,y,z) \qquad \textit{Eqn. 2 - 4}$$

where σ refers to the entire stress tensor and the superscripts refer to the various steps of Figure 2 - 6.

However, the remaining stresses throughout the part in step B is unknown, but the normal and shear stresses on the cut surface (σ_x, τ_{xy} and τ_{xz}) must be zero to satisfy the free surface boundary condition.

$$\sigma_x^{(B)}(0, y, z) = 0$$

Therefore, step C by itself will give the correct original stress distribution (σ_x) along the plane of the cut in step A [25].

$$\sigma_x^{(A)}(0,y,z) = \sigma_x^{(C)}(0,y,z) \qquad \textit{Eqn. 2 - 5}$$

2.4.2 Assumptions and approximations

The three main assumptions for the practical application of the superposition principle are:

- The material behaves elastically during stress relaxation.
- The material removal process does not introduce significant stresses that affect the measured displacements.
- The width of the cut is constant, when measured relative to the state of the body prior to cutting.

The first two assumptions are common to most mechanical stress relaxation techniques but the third assumption is unique to the contour method.

From a theoretical point of view, the superposition principle can determine the full stress tensor on the cut surface. But because practically one can only measure out of plane deformations, shear stresses cannot be measured. However, this is not going to have effects on normal stress measurement because the FE calculation also correctly reveals how the shear stress component has changed in step C [26]. The effect of shear stress on the surface deformation can be evaluated by considering the surface tractions equivalent

to the releasing stresses on the cut plane as shown in Figure 2 - 7. The normal traction, $T_{x,}$ is symmetric with respect to the cut plane, whereas the transverse traction, T_y, is antisymmetric [2]. Averaging the contours of the two halves removes the transverse shear stress effect to uniquely provide information about the normal stresses. This is a necessary step for the correct implementation of the contour method. It is worth noting that if one could measure in-plane displacements on the cut surface, the superposition theory would be complete [1].

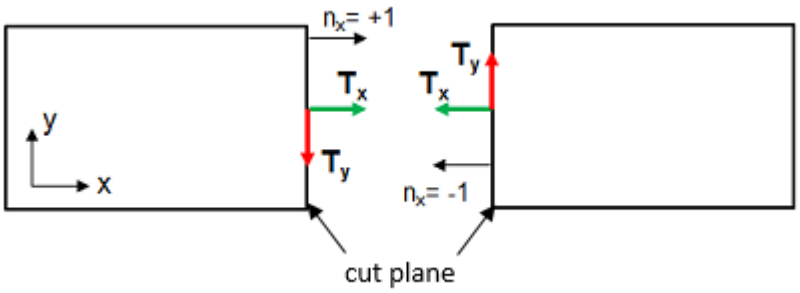

Figure 2 - 7: Surface tractions equivalent to releasing residual stress on the cut surface [2].

Averaging requires the assumption that the cut occurs on a symmetric plane were the material stiffness is the same on both sides of the cut. This assumption is satisfied for homogenous materials that are cut precisely in half but challenges exist for dissimilar materials and making asymmetric cuts. However, in practice, the part only needs to be symmetric about the cut within the region where the stress release has a significant effect. The length of this region is about 1.5 times the Saint Venant's characteristic distance, usually taken as the thickness of the component [3].

One approximation to the theory is implemented to make the finite element analysis simpler. The component is initially modelled with a flat surface along the cut plane and the opposite of the measured deformations are applied as boundary conditions to force the surface into the deformed shape. Prime [2] showed that because the deformations are small for engineering components and the stress analysis is elastic and linear, this approximation will not have significant influence on the accuracy of the results.

2.5 Experimental procedure of the contour method

The four stages of the contour method include: (1) cutting the specimen into two halves, (2) measuring the out of plane surface deformations of the cut surfaces, (3) processing and smoothing the data and (4) back-calculating the residual stresses using finite element

analysis. This section describes the equipment necessary to implement the contour method and requirements for each step to ensure that accurate results are achieved.

2.5.1 Specimen cutting

Cutting the specimen into two halves is the most important step in the contour method, as all subsequent steps are dependent on the precise information from the cut surfaces after stress relaxation. The ideal cutting technique should produce a straight cut of minimal cut width and low surface roughness, not introduce significant stresses or recut surfaces that have already been cut and avoid local cutting irregularities.

Wire electro-discharge machining (EDM) is the most effective cutting technique to satisfy the requirements for the contour method. This limits the application of the technique to metals and a few other materials that can be cut with EDM [1]. However recent studies have found other cutting methods to be effective to produce accurate contour cut, such as water-jet cutting [27]. In wire EDM shown in Figure 2 - 8, a wire is electrically charged with respect to the workpiece, and spark erosion causes material removal. The best results for the quality of cut have been obtained using wire made of brass.

Conventional EDM usually performs a rough cut followed by several finish cuts, however the contour method requires a single cut with good surface finish and accuracy. Therefore, “finishing or skim” cut settings in a single pass should be performed for contour cutting. The high temperature involved in wire EDM introduces a heat affected zone HAZ that contains a thin layer of recast [28], shown in Figure 2 - 9. When skim cuts are used, much less energy is applied to the surface which has negligible effect on the material properties [29], provides low surface roughness and greatly reduces the recast layer [28]. During cutting the spark erosion generally leaves a path slightly wider than the wire depending on the intensity of the spark energy. Also, the part is submerged in temperature controlled deionized water during cutting, which minimizes thermal effects [30].

Since the cutting procedure for the contour method deviates from the conventional EDM cutting technique, special consideration must be given when selecting the cutting wire size and operating parameters for each component. Using a smaller wire size (typically 100-150µm) is favourable to remove minimum material, however this can result in undesirable wire breakage and long cutting times. Using a larger wire size (typically 200-250µm) and an orientation that minimises the wire contact length [1], will minimise the risk of wire breakage especially in the presence of defects.

An important practice, to ensure that the cut plane does not move during stress relaxation, is to clamp the specimen on both sides, preferably symmetrically, and as close to the cut as is practicable [31].

The use of sacrificial layers is advisable when determining near-surface residual stresses with the contour method [32] and to minimize very-near-surface cutting irregularities along the perimeter of the cut [33]. Good practice guidelines are available in the literature on how best to cut the specimens for contour residual stress measurement [30].

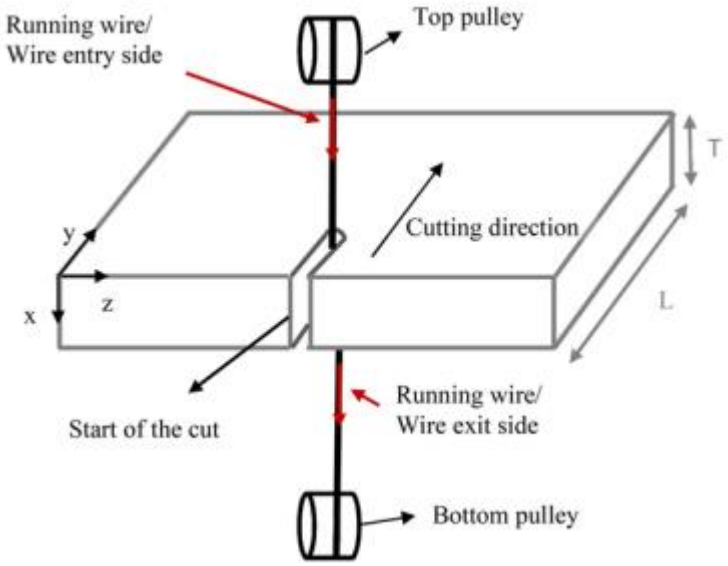

Figure 2 - 8: Schematic drawing of a component being cut by wire electro-discharge machining [30].

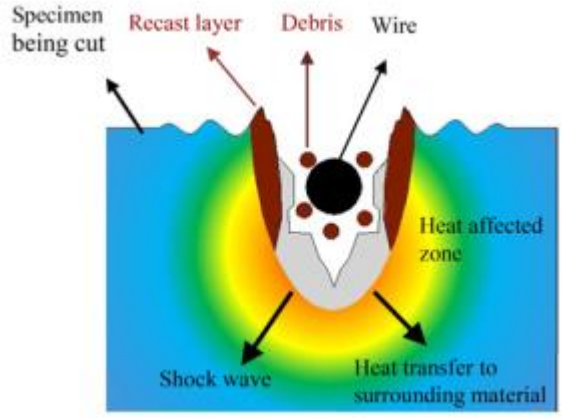

Figure 2 - 9: Schematic drawing of the EDM process showing the moving wire, debris, re-cast layer and HAZ [30].

2.5.2 Surface contour measurement

The contour method requires accurate measurement of the cut surface deformations and lateral location on the surface. Surface measurements in the contour method generally have a peak-to valley magnitude of approximately 10 to 100 µm [1] which requires the use of precision metrology equipment. Data about the deformation along the cut surface contours is gathered using a coordinate measurement machine or laser profilometer [1]. The most common technique for the contour method is a coordinate measurement machine (CMM) shown in Figure 2 - 10. A CMM is a commonly found device for measuring geometrical characteristics of an object with sub-micrometre precision. Measurements are defined by a probe, usually tactile or laser, attached to a moving axis of the machine and recorded using a mathematical grid form. For the contour method measurement process, both cut surfaces are measured using the same point locations. The CMM is usually programmed to measure the perimeter of the specimen first and then move across the cut surface to record the cut surface deformations.

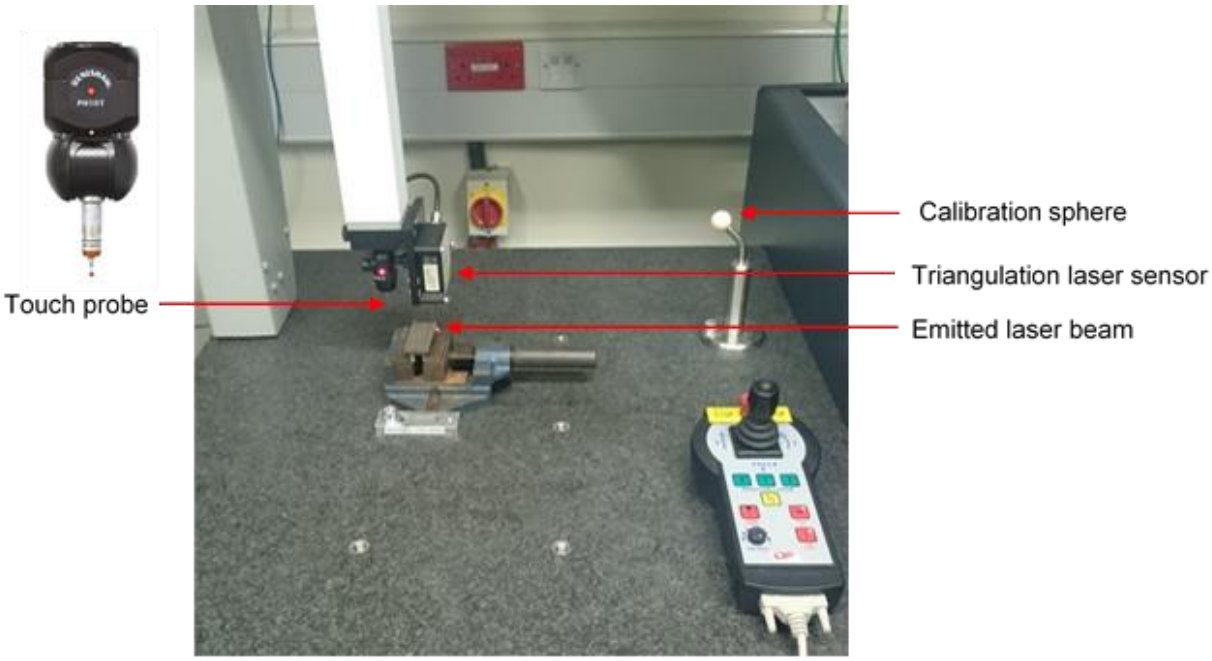

Figure 2 - 10: Hybrid Coordinate Measurement Machine at the Open University.

Tactile or touch probes generally have good resolution of 0.5 µm [30] and do not suffer from large quantities of background noise. Using a large probe diameter reduces the effect of the surface roughness on the measurement being taken. However, they do encounter problems close to the specimen edges and may also record false points (‘air-trigger’) when the force threshold is set too low [31]. Because the probe is in contact with the surface during

measurement, there is a risk that the specimen may be locally deformed by the contact force. The peak-to-valley amplitude of the contour method typically decreases as the stress magnitude or sample size decreases because the surface contour is a displacement not a strain. The laser CMM offers better resolution less than 0.1 µm [30] which is suitable for smaller specimens and specimens with low stress levels. The technique has quicker sampling times compared to touch probes. However, the measurements are often very noisy throughout and large data sets can be problematic and usually require some sort of reduction process. The method is also very sensitive to surface roughness and defects which can cause unwanted points to be recorded in the contour method [31] and the surface contour map can be uncertain near edges because, especially with noncontact scanners, it can be difficult to know exactly where the edge of the surface is. It is recommended that, for thin samples, the sacrificial layers be carefully removed before the contour measurement as the subsequent removal of the data from the sacrificial layers and the interface is challenging [32] . For high-precision measurements, temperature stability is important and the CMM is usually isolated from thermal fluctuations [1]. The component is left to reach the room temperature before performing the measurement.

2.5.3 Data processing

The measured data obtained from the cut surface is usually a combination of surface deformations due to the releasing stresses and noise from cutting artefacts or surface roughness caused by the EDM and inherent errors in the measurement process. Therefore, it is essential to process the measured data to minimize the errors and extract the underlying surface deformation that is purely due to the relaxation of residual stress. In the contour method the data is processed in several steps. At the Open University the data processing is done in MATLAB and the Spline Toolbox using specifically developed scripts [1]. This section gives a brief description of these steps.

1. Aligning: As discussed in section 2.4.2, the measured data of the two cut halves needs to be averaged and this requires that they be on the same coordinate system. However, during the CMM measurement each cut half is measured in its own local coordinate system. To align the two sets shown in step (a) of Figure 2 - 11 so that the points correspond to each other, one surface is mirrored about the y-axis as shown in step (b), then one of the two data sets is reoriented by translating and rotating the coordinate system in the x–y plane as shown in step (c) [30]. The perimeter trace can be used to assist the alignment [1].

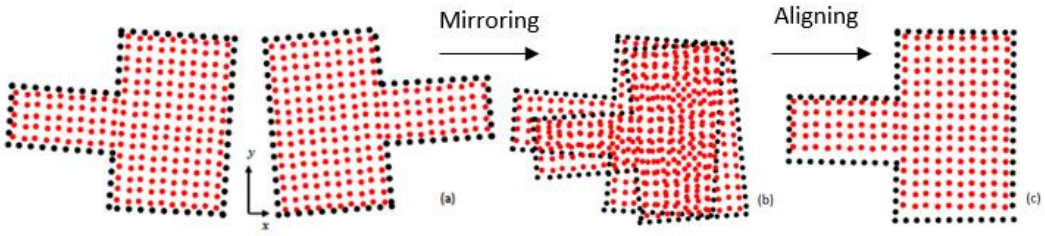

Figure 2 - 11: Schematic of the different steps of the data alignment process. The black and red dots represent the perimeter and cut surface deformation data respectively [34].

2. Interpolating: After alignment, the grid point coordinates of the two surfaces might not be the same, due to lateral misalignment errors during the measurement process [26]. Also, the smoothing process requires that the data be on a rectangular grid. To resolve this, data sets are linearly interpolated to a common grid with approximately the same size density as the original data [26].

3. Extrapolating: For the subsequent finite element analysis, displacement information for all nodes on the cut surface must be applied including those regions on the perimeter of the cut surface [30]. However, the measurement process does not give accurate or complete displacement information at the perimeter and the missing data must be filled in by extrapolation.

4. Averaging: It is a standard practice in the contour method to average the data of the two contour halves to remove the effects of the releasing shear stresses and some cutting artefacts. The data sets, now on a common grid, are averaged point by point to generate a single x, y data set used for further processing [30].

5. Cleaning: At this stage, the surface data can be plotted to identify and remove any obvious outliers from the overall surface. These may exist because of measurement or cutting irregularities, for example, the CMM probe slipping at the edge of the specimen, wire breakage during cutting or over burning of EDM at some foreign particle [30].

6. Flattening: It is necessary to calculate the zero position for the out-of-plane measurement direction because the reference plane for the surface contour is not clearly defined from the measurement process. This is done by taking an average of the whole data set, which is effectively placing the zero point in the middle of the data set [30].

7. Smoothing: Different fitting methods can be used for smoothing and removing any noise in the data, such as fitting to a Fourier series, polynomial smoothing and bivariate spline fitting [26, 31]. It has been reported that the Fourier series method cannot always capture all the important features of a surface contour [26]. Spline fitting is currently the most widely used approach and is typically accomplished by fitting the displacements to a cubic spline (piecewise polynomial). The piecewise polynomials are joined at given locations called "knots" which define the domain of each polynomial. The main factor that determines the amount of smoothing is the knot spacing, which is the spacing between the points where the piecewise polynomials are joined as shown in Figure 2 - 12.

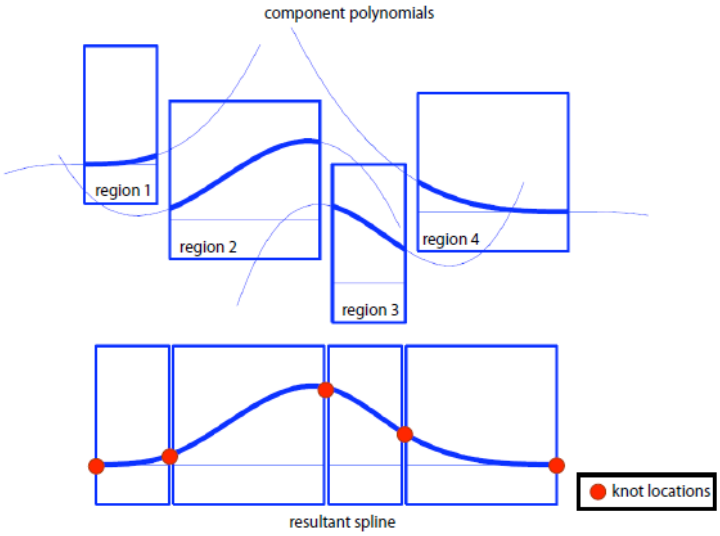

Figure 2 - 12: Construction of a spline - piecewise smooth combinations of polynomials [31].

Uncertainties in the smoothing process arise from using a too large knot spacing which may not accurately capture the features on the surface or a too small knot spacing which can capture noise in the data. However, the amount of smoothing can be objectively chosen by minimizing the estimate of uncertainty in the calculated stresses. This is done by incrementally refining the knot spacing and calculating the stresses for each increment [26]. The standard deviation technique, equation 2 - 6, is then used to estimate the uncertainty between the new stress at a given node and the previous stress having coarser knot spacing. Then an average over the whole stress map is calculated by the root mean square of all the nodal uncertainty using equation 2 - 7. The optimum smoothing is then achieved by minimising the uncertainty in the calculated stress [30].

$$\partial\sigma(i,j)=\frac{1}{\sqrt{2}}[\sigma(i,j)-\sigma(i,j-1)] \qquad \text{Eqn. 2 - 6}$$

where σ(i,j) is the stress at node i on the FE model cut surface for the smoothing spline solution designated j, and j-1 refers to the previous, coarser smoothing-spline solution.

$$\partial\sigma(j)=\frac{1}{\sqrt{n}}\sqrt{\sum_{i=1}^{n}[\partial\sigma(i,j)]^2} \qquad \text{Eqn. 2 - 7}$$

where n is the number of FE nodes on the cut surface in the model.

8. Evaluating the data for the FE model: To prepare the data for the subsequent finite element (FE) analysis, the z coordinates of the smoothed data are evaluated at the x, y locations of the nodes of the FE model and the sign of the deformations reversed. The final displacements are then written into the FE input deck as displacement boundary conditions [26].

2.5.4 Residual stresses back calculation

Calculating the residual stresses in the contour method is possible to do analytically for simple rectangular geometries with homogenous material properties [35]. However, for most engineering components a numerical technique is required and finite element (FE) modelling using ABAQUS software is suitable.

For the FE analysis, a 3D model of one half of the component is constructed to reveal the cross section of the cut plane. For simple geometries the perimeter trace from the CMM measurement is used to sketch the perimeter of the part and is then extruded in the third dimension to create the model. In general, detailed features of the part far from the measurement plane are unlikely to influence the stiffness properties at the cut region and can typically be ignored [1].

Linear elastic material properties, that is, Young's modulus and Poisson's ratio, are then defined to represent the stiffness behaviour of the material under investigation. However, Bueckner's principle and the contour method do not require any assumption that the material is elastically isotropic or homogeneous, only that the linear elastic behaviour is accurately reflected in the FE model used to calculate stress [1]. Therefore, for cases of heterogeneous elasticity, such as weld clad components or dissimilar welded alloys, it is important to apply the appropriate elastic properties for each material of the component.

A mesh is then generated on the model using first or second order hexahedral elements and is usually bias for higher refinement at the measurement surface and near the edges. This can help to produce a converged solution in an efficient manner [1]. Three restraining

boundary conditions, shown in Figure 2 - 13, are applied at the measurement surface to prevent rigid body motion, that is, translation in the y and z directions [1]. The boundary conditions used are only translational BC's and not rotational. Finally, a list of nodes and their coordinate positions on the measurement surface are generated and used to apply the smoothed and reversed displacements as boundary conditions. A linear elastic stress analysis is performed and the model is allowed to reach equilibrium. Information about the stresses normal to the cut surfaces at each node on the measurement surface is the result for the contour method and represents the residual stresses that were originally on the cut plane prior to cutting.

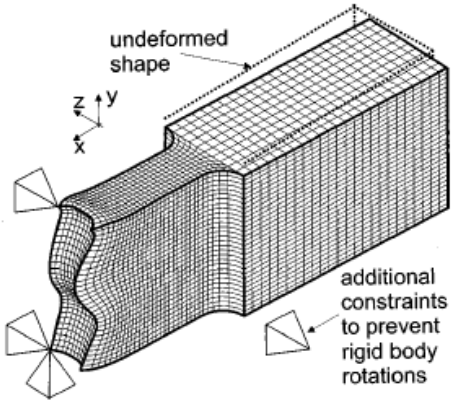

Figure 2 - 13: Additional constraints to prevent rigid body motion [2].

2.5.5 Contour method versus common measurement techniques

The contour method has the ability to provide a 2D map of residual stresses through the cross section of a component. The only methods that can measure similar 2D stress maps are neutron diffraction and sectioning methods but these have significant limitations [2]. The contour technique is relatively simple and can be applied with equipment that is generally available in workshops and inspection laboratories [2]. Another advantage is that the residual stresses can be obtained directly from localized deformations on the cut surface, therefore no inverse procedure or assumptions about the stress variations are necessary [2]. While the conventional contour method can determine one component of residual stress (i.e. normal to the cut plane), several approaches have been developed to access multiple stress components, such as application of the eigenstrain theory [36-38], the multiple cuts contour method which allows for stress components to be determined on different cross sections of the part [39-41] and the surface superposition contour method which makes use of additional measurement techniques, namely X-ray diffraction and hole-drilling, to determine the remaining surface stresses [42-45].

The contour method has proven useful for studying various manufacturing processes such as bent beams [2], quenched steel [46-48], impacted plates [49, 50] and more recently additive manufacturing [51, 52]. One particular advantage compared with diffraction techniques is for measuring welding residual stresses as it is insensitive to microstructural variations [53-55]. The method has been used to achieve 2D stress maps in specimens with different welding methods including arc welding [56, 57], variable-polarity plasma-arc welding [58, 59], friction welding [60-63], and electron beam welding [64-67].

The contour measurement method has been validated with several other measurement techniques [68-70] and compares well with the conventional and more established methods of neutron and synchrotron x-ray diffraction [31]. It is also a powerful tool for informing and validating FE-based weld residual stress analyses [6, 71]. The contour method generally shows good agreement with diffraction techniques for non-welded specimens such as railway rails [72], laser deposited Waspaloy [73] and laser peened plates [44, 74]. Some contour measurements can show poor agreement with diffraction techniques for materials with severe microstructural gradients in the weld regions [31, 75, 76] or in the heat affected zone [77], but diffraction techniques can have issues to obtain reliable d_0 measurements for welds [78]. Also, high stress gradients [64, 79] and localized stress fields found in weld specimens can be difficult to resolve using the contour method [80]. Although contour weld residual stress results still show good agreement with diffraction techniques considering the problem of innate scatter in multiple measurements [81, 82]. The method shows good agreement with diffraction techniques for measuring complicated geometries [83-85] and novel approaches have been developed to obtain excellent agreement for bearing rings [86] and welded cylinders [31, 45].

The contour method can be used to measure residual stresses in large components [45, 87, 88]. There are some difficulties for thin samples which are very sensitive to data analysis parameters [32, 89]. High resolution measurements can be performed with the contour method if careful measures are taken [6, 30], however performing measurements on parts smaller than 5 mm by 5 mm in cross-section requires extreme precision [1].

One limitation of the method is that near-surface residual stresses are challenging to obtain owing to cutting and measurement artefacts as well as the challenge of accurately measuring surface deformations near the edges of the cut surfaces [3, 90]. However, reliable near-surface residual stress measurements are possible with careful work on contour measurements as shown for laser peened plates [44, 74, 89] and electron-beam welded specimens [91]. Some contour measurement errors are caused by cutting

difficulties, for example wire breakage can lead to re-cut surfaces in welded specimens [92], incorrect EDM wire selection for case hardened disks [93], edge effects such as the barrelling shape in friction stir welded parts [61] or artefacts on the cut surface for non-uniform cross-sections [86] or dissimilar metal specimens [66]. Contour method results are also influenced by post-processing procedures [94] and over-smoothing the contour data can result in under-measured peak stresses [66, 95] or less variation in the results [96], particularly for weld specimens.

Two systematic errors which can cause significant measurement inaccuracies are plasticity and/or bulge error, discussed in more detail in section 2.7. These errors manifests as reduced magnitude stresses and a phase shift in the results obtained from the contour method [17, 97]. Plasticity errors are possible for measurements of very high magnitude stresses often found in welding and surface treatment processes [62, 70, 98, 99] and bulge error can occur when specimens are only clamped on one side for simultaneous slitting and contour measurements [4, 100]. For example, Figure 2 - 14 shows the longitudinal stresses on a through wall line, identified as line BD, at the centre of an austenitic three-pass slot welded plate [70] measured using the contour method, incremental deep hole drilling technique and several diffraction-based measurements. The first contour method measurement, on specimen 2-1B, clearly deviates from the other measurement results. The authors attributed this to occurrence of plasticity during the measurement. Plasticity error is plausible since high magnitude residual stresses were present and the asymmetric and lower than expected peak stresses measured by the contour method are features suggesting that significant plasticity has occurred during cutting. The second measurement was optimised to minimise cut plasticity (using a novel embedded cutting strategy [101]) and achieved extremely good agreement with the diffraction consensus [102]. Similar lower than expected peak stresses were observed in contour method residual stress measurements in a ferritic weld bead-on-plate sample [103], when compared with the results from neutron diffraction, see Figure 2 - 15. At – 4 mm from the weld centre line the peak stress from the contour method of 350 MPa is substantially lower than the neutron peak of 450 MPa [103]. The reduced tensile stresses measured by the contour method were related to the onset of local tensile plasticity at the weld centre line, despite the special measures taken to minimise plasticity effects (embedded cutting configuration, symmetric clamping and using a large diameter EDM wire). That being the case, bulge error could also be present in the contour method results.

Prime et al. [3] examined the bulge error on a bent beam specimen with a low magnitude (< 150 MPa) residual stress profile where the initial stress results measured by the contour

method showed both a reduced peak stress magnitude and a spatial shift of the peaks compared with the stresses predicted in the bend test, see Figure 2 - 25. A novel FEM procedure, discussed in detail in section 2.7.3, was applied to correct for bulge error and the revised contour method results were in closer agreement with the bend test prediction. For specimens that are only clamped on one-side, the main feature is an apparent shift in the location of the peak stress region. For example, Traore et al. [4] examined the transverse residual stresses in an Esshete 1250 C(T) specimen containing an electron beam weld by neutron diffraction, slitting, and the contour method, shown in Figure 2 - 16, where the results are shown at mid-thickness of the specimen. A shift in the stress profile measured by the contour method under asymmetric clamping arrangement can be seen. The possible sources of error in the contour method technique was explained by development of compressive plasticity during cutting associated with the lack of restraint applied to the specimen during the measurement or wire cutting artefacts which were observed at a cut depth of about 5 mm [34]. The potential significance of cutting plasticity on the accuracy of the slitting stresses was assessed [34] and estimated to be about 15 % for the parent material and 2 % in the region of the electron beam weld. Nonetheless, the one-sided clamping will make for a larger bulge error and correcting for this systematic error in contour method measurements will give more reliable comparison with independent techniques.

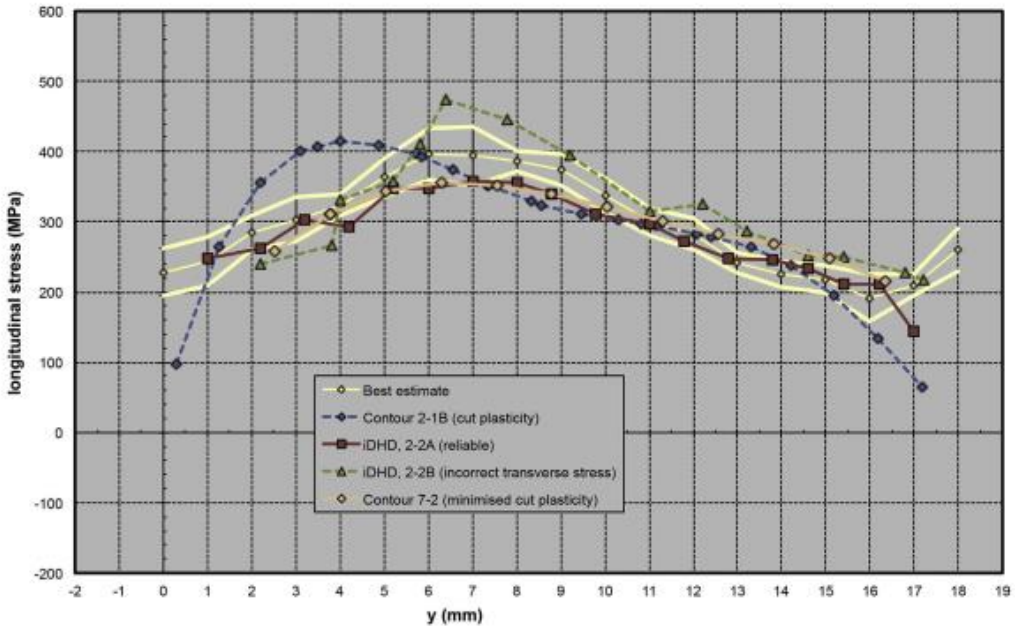

Figure 2 - 14: Comparison of measured longitudinal stresses on line BD using strain-relief methods with diffraction-based best estimates. Best estimate (with symbols and lines) and ± 1 sd (lines) shown in yellow [70].

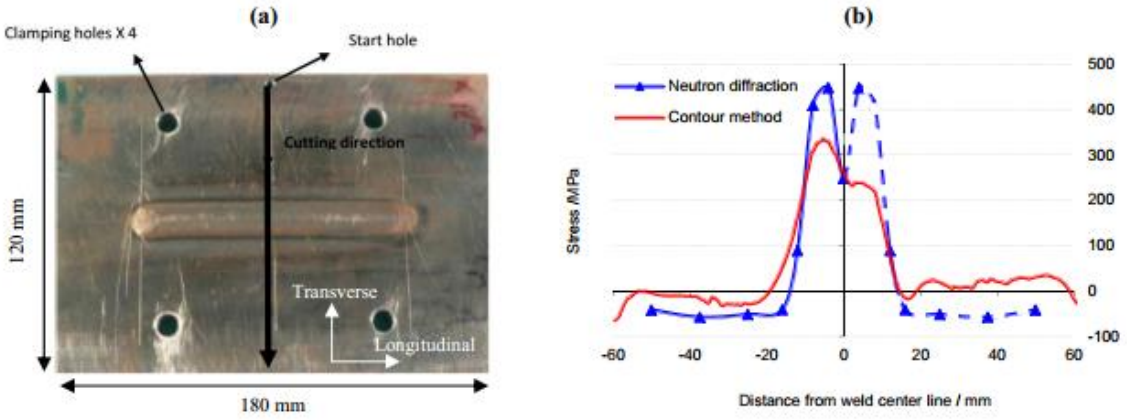

Figure 2 - 15: Photograph of the 20 mm thick weld bead-on-plate specimen showing the holes for clamping and the location of the contour cut (a). In (b) the measured longitudinal contour results at 17.5 mm from the plate back face are compared with neutron diffraction measurements (made on one side of the plate and mirrored about the weld centre-line) [104].

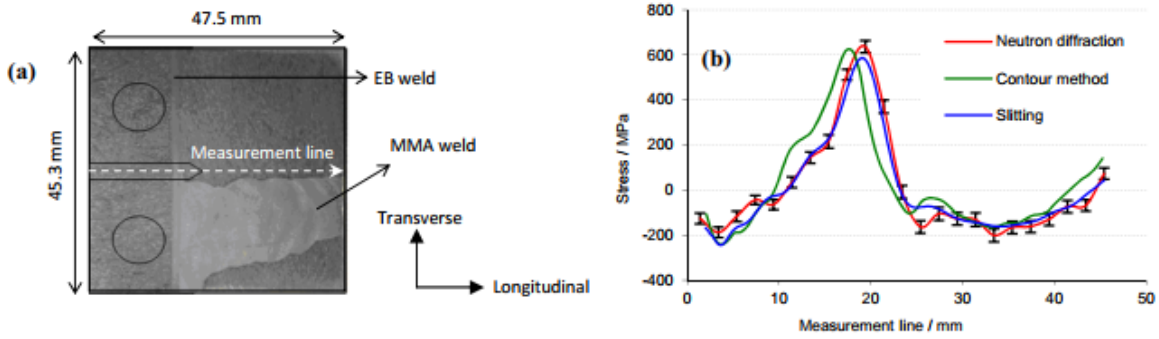

Figure 2 - 16: Schematic drawing/photograph showing the 16 mm thick compact tension specimen blank studied, with the measurement line marked up. In (b) transverse residual stresses measured by the contour method are compared with neutron diffraction results at mid-thickness and slitting results (averaged over the thickness) [104].

Repeatability studies have demonstrated that the contour method is in reasonable agreement with that found in other residual stress repeatability studies [105]. The repeatability of results obtained from the contour method performed for a range of specimens was found to be relatively good in the specimen interior but poor along the perimeter [106, 107]. For instance the repeatability standard deviations over much of the cross section ranged from 5 MPa for an aluminium T-section to 25 MPa for a nickel disk forging [107]. In another study of a stainless steel plate containing a weld, the repeatability standard deviation was under 20 MPa over a large portion of the cross-section, but was

near 30 MPa in the weld region [108]. A method to estimate the uncertainties in contour stress results caused by the noise in the measured displacement surface (displacement error) and smoothing used in the data processing (model error) has been proposed [26, 109]. The uncertainty estimator shows the contour method to have larger uncertainty near the perimeter of the measurement plane [109]. For example the uncertainty due to the post-processing procedure in a bent notched specimen was about 55 MPa at the edges and 20 MPa in the rest of the specimen [94]. The average uncertainty based on the model error described above was 41 MPa for the contour method results for a 2 mm thick aluminium alloy laser peened plate but was significantly lower, only 10 MPa, for a 28 mm thick laser-peened aluminium alloy sample [89]. The stress uncertainty estimated considering both errors for contour measurements in an 80 mm thick weld was about ±30 MPa [76] and at least ± 50 MPa for the rings of a through hardened inner bearing race [86].

Nevertheless, the contour method is the youngest technique to measure residual stresses and there are some challenges to improve the accuracy and reliability of the measurement results. In the next section the cutting errors in the method are discussed.

2.6 Cutting errors in the contour method

As with any measurement process, errors and uncertainties exist due to limitations and inaccuracies in implementation of the technique. In the contour method, errors occur at all stages: cutting the specimen, measuring the cut surfaces, processing the data and calculating the stresses. These errors will accumulate during the different stages but a number of good practices have been established to minimize these errors during each step of the process [3, 30, 31]. Nonetheless, cutting errors are the most significant as all subsequent processes are dependent on the quality of the cut surface. This section focuses on sources of cutting errors and ways to minimise these errors in the contour method. Bulge errors, which is the main subject of this research, is described in detail in section 2.7.2.

Cutting errors in the contour method can be characterised by their effect on the cut surfaces, namely anti-symmetric and symmetric effects. Figure 2 - 17 provides a summary of cutting error sources and methods that have been successfully applied to correct for these errors in the contour method.

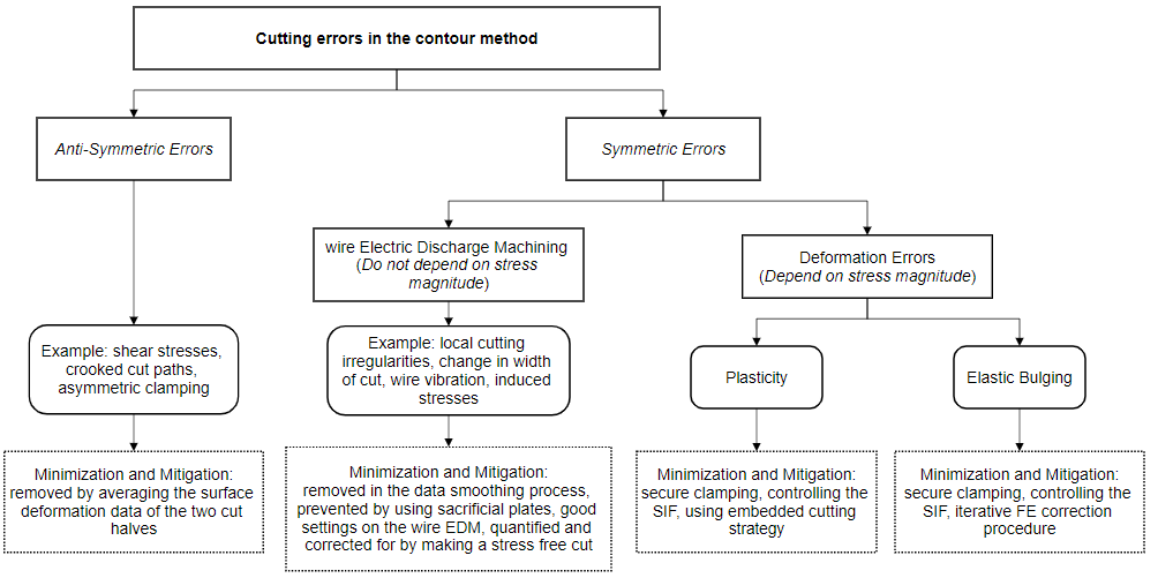

Figure 2 - 17: Summary of cutting error sources and correction methods in the contour method.

2.6.1 Anti-symmetric errors

Anti-symmetric errors are usually from the release of shear stresses, warped cut paths or when the part is only clamped on one side or clamped non-symmetrically during cutting [3]. These effects form opposite features on the two cut surfaces as shown in Figure 2 - 18 and are consequently removed by averaging the cut two halves. The effect of a wandering cut i.e. crooked cut, is shown in Figure 2 - 19.

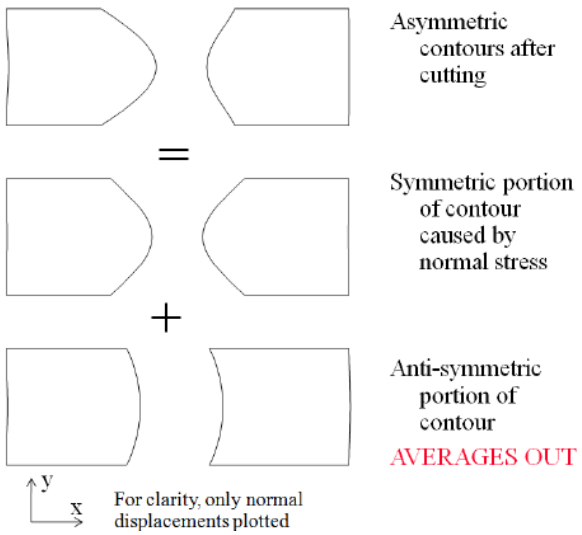

Figure 2 - 18: Asymmetric contours after cutting and effect of averaging [3].

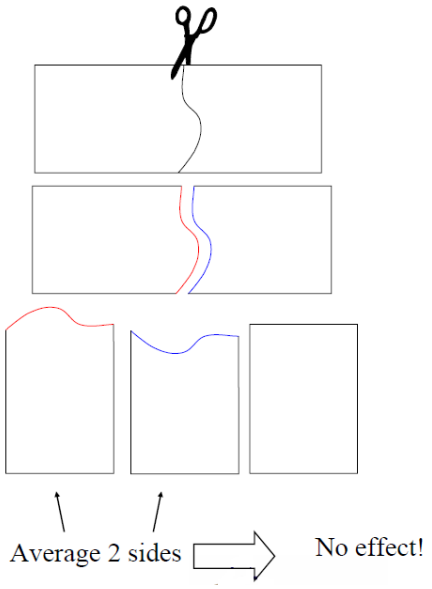

Figure 2 - 19: The effect of a crooked cut removed by averaging the two contour surfaces [3].

2.6.2 Symmetric errors

The elastic relaxation of normal stress causes symmetric deformations on the cut surfaces. It is these symmetric features that have to be measured and used to back calculate the stresses in the contour method. However, there are sources of errors that could cause symmetric features on the cut surfaces. These sources of errors are either dependent or independent on the stress state in the material.

Stress independent errors

Stress independent errors are caused by local cutting irregularities. These errors originate from surface roughness, wire entry and exit artefacts (such as flared edges), bowed surfaces, wire breakages or hot-spots [83], varying cut width for components with different materials or thickness [3] etc. These effects are usually small and are removed when smoothing the measured deformation data [3]. However, topographic artefacts having a length-scale, across the cut plane, greater than the wire diameter are not removed when processing the data [110]. Other effects, such as wire vibration can be minimized by performing cutting trials to determine suitable wire EDM settings or estimated by making a cut in a stress-free material. For errors near the edges of the component, using sacrificial plates on the top and back faces of the component and at the start and end of the cut has been shown to reduce these effects [64, 83, 89].

Stress dependent errors

Stress dependant errors are caused by the changing stress state in the material at the cut tip as the cut proceeds and have effects that do not average away. These deformation errors can cause significant bias errors in the contour method residual stress results. Since the two resulting effects, namely plasticity and bulge errors, are the focus of this research they are explained in detail in the next section.

2.7 Deformation errors in the contour method

As previously explained, in practice, errors can be introduced from imperfect cutting and measurement processes. Some errors can be removed by processing the measured data or minimised by means of good cutting practices. But two errors that are difficult to predict, control or avoid are: plasticity and elastic bulging. Both are dependent on the continually changing stresses in the material during cutting. In this section plasticity and bulge effects are described and published work reviewed relating to the influence of these errors in the contour method.

2.7.1 Plasticity induced errors

The contour method, like other mechanical stress relaxation techniques, is based on the elastic relaxation of stresses by removing material. However, during the cutting process the magnitude of stress in the material may approach the material yield strength and plastic yielding can occur. The residual stresses are not allowed to relax completely and this would cause errors in the measured results. In the contour method, the cut created by wire EDM can be seen as a moving blunt crack which causes a redistribution of stresses in the material ahead of the cut. In the region around the cut tip a stress concentration develops which may cause high magnitude redistributed stresses that yield the material. The stress concentration at the cut tip depends on the cut length and magnitude of the stresses along the cut path [34, 101]. For this reason, welded components can be challenging for contour measurements because the stresses can be quite high and the local yield strength may be lowered by the thermal process, both effects increasing plasticity errors [1].

Plasticity errors often manifests itself by asymmetric stress profiles and reduced peak stresses in the contour method results. Several practitioners have investigated the influence of plasticity in contour method measurements and showed that clamping the component on both sides of the cut and all along the cut length helps to minimize the stress concentration at the cut tip and reduce plasticity effects [46, 97, 111, 112].

More in depth research on plasticity in the contour method was performed by Yeli Traore at the Open University [34, 101, 104]. The severity of the stress field around the cut tip can be characterised by the mode I stress intensity factor (SIF) [113]. Therefore, the SIF distribution along the cut path could be used to evaluate the likelihood of plasticity-induced errors during the contour cut. The conclusion from this study was that plasticity-induced errors in the contour method can be mitigated by controlling the stress intensity factor along the cut length.

The SIF can be controlled by designing optimum cutting and restraint strategies. It is recommended to restrain the component using rigid clamping close to the cut plane; however, this can be difficult to achieve in practice and the chosen clamping arrangement should not disturb the stresses in the material. Using a larger wire diameter for the cutting process can also help to minimise plasticity-induced errors by the removal of the plastic wake zone behind the crack front [34]. Different cutting strategies can be investigated to reduce plasticity effects by carefully choosing the orientation and direction of the cut. One proposed cutting strategy is to create an embedded cut, to impose self-constraint during sample cutting, providing an effective way to reduce plasticity induced errors in contour method measurements [101]. The conventional contour cut is like an edge crack and the SIF of an edge crack is larger than the SIF of an embedded crack, hence the embedded cut configuration has the benefit of less risk of plasticity. This can be achieved by initiating the cut within the test component by using pilot holes positioned away from the edge [101].

To assist with controlling and evaluating plasticity effects, a procedure was developed to estimate plasticity-induced errors in contour method measurements [34]. The inputs require defining the initial residual stresses, specimen dimensions and material properties. Then the stress intensity factor for a particular cutting and restraint strategy is determined using either numerical tools or analytical solutions. From the obtained SIF data, the material yield stress and the specimen dimensions; the normalised average plastic zone size ahead of the crack tip is analytically calculated using a first order approximation. Finally, a set of key graphs was developed that links the normalised plastic zone size to the stress errors introduced in the contour results. The plasticity-induced error is estimated as a percentage and the procedure can be repeated for different cutting and restraining configurations until the average error is less than 5% and hence plasticity effects is minimal [34].

The procedure for estimating and mitigating plasticity-induced errors was applied to a plate containing a 3-pass slot weld, shown in Figure 2 - 20, were the transverse component of stress was measured in a notionally identical test specimen using neutron diffraction and

the contour method [114]. Figure 2 - 21 compares the transverse component of residual stress along a measurement line parallel to the weld and located 7.5 mm below the plate top surface. The 'old contour cut' stress measurement deviated from the neutron results in two regions which were possibly associated with cutting process plasticity: a tensile peak just before the weld start and constant increase of tensile stresses in the weld metal. To mitigate plasticity-induced errors the cutting and restraint strategy was optimised by using an embedded cut and firm clamping with fitted bolts. Figure 2 - 20 shows the two pilot holes to create the embedded cut and holes for the bolts. The position of the pilot holes was chosen using finite element analysis to minimize excessive plasticity in the ligaments. The measured stresses from the optimized 'new contour cut', in Figure 2 - 21, showed a tensile region that was more uniformly distributed over the weld region and lower compressive stresses towards the specimen top surface [101].

More recent work has extended the self-constraint approach by employing a double-embedded cutting configuration and demonstrated experimentally and numerically how optimised cutting directions and clamping strategies can be employed to minimise the amount of plasticity-induced stress errors in the contour method [71, 102, 115]. Although numerical studies for certain weld residual stresses have shown that a self-equilibrating cutting strategy [116] did not perform significantly better than a conventional cutting approach and the mechanical restraint was the primary variable influencing cutting-induced plasticity development [117].

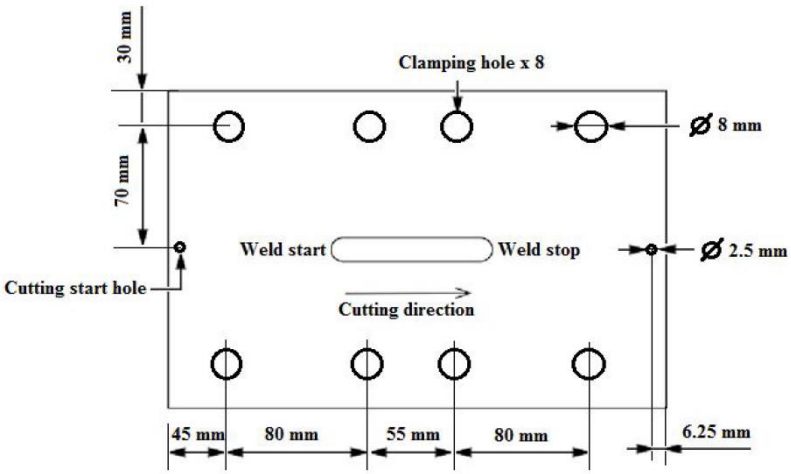

Figure 2 - 20: Schematic of the 3-pass specimen showing the cutting holes and clamping holes [101].

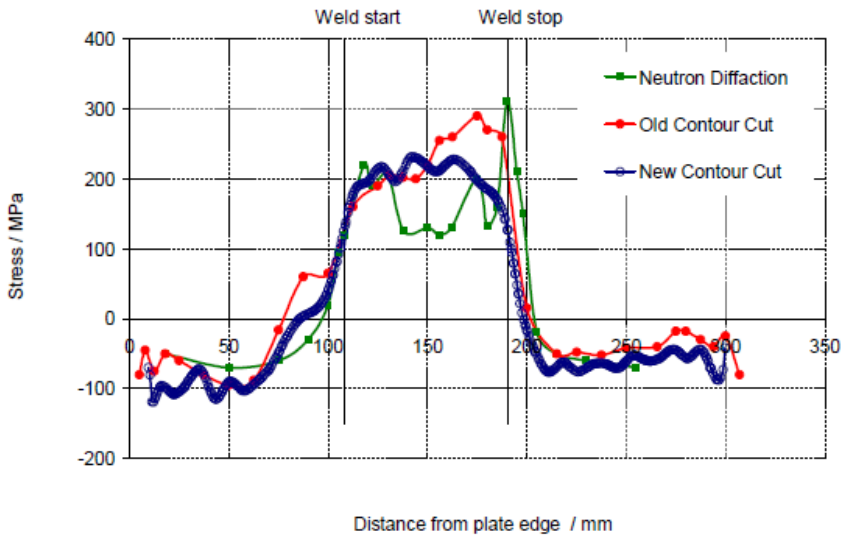

Figure 2 - 21: Comparison of transverse residual stress measurements for the 3-pass specimen along a line parallel to the weld at 7.5mm below the top surface determined by the contour method and neutron diffraction [101].

2.7.2 Bulge induced errors

One of the main assumptions of the contour method is that a constant width of material is removed during cutting when measured relative to the original state of the body. In practice a deviation from the cutting requirement, referred to as the bulge error or elastic bulging [3], causes the width of material removed to vary along the cut length. Bulge errors occur as cutting proceeds, the stresses relax and the stresses in the material ahead of the cut continually change to satisfy equilibrium. This causes the material at the cut tip to elastically deform. The physical EDM cut width is fixed, which means that the width of material removed has changed as shown in Figure 2 - 22. A tensile force at the cut tip will cause the cut tip to stretch and a reduced amount of material removed, whereas a compressive force will cause the cut tip to contract and an increased amount of material removed. Since the fundamental assumption is that step C of Figure 2 - 6 returns the material points to their original flat configuration, this causes an error that will not be averaged away [3]. In practice, the measured contours of the cut surfaces will contain effects from the varying cut width and produce errors in the stress results.

The ideal contour cut would be zero width for which there would be no bulge error. The magnitude of the bulge error depends on the change in stress state at the cut tip relative to the original stress state and this effect scales with the width of the cut. Prime and Kastengren [3] proposed that the bulge error is approximately proportional to the stress

intensity factor (SIF) at the cut tip from the accumulated effect of releasing residual stress. Since plasticity and bulge errors are both dependent on the change in stress state at the cut tip they both potentially add to each other [3]. However, because they cause similar effects in the results, any efforts to minimize the bulge error should also reduce plasticity errors. Similar to controlling plasticity effect, the bulge effect can be minimised by securely clamping the component on both sides of the cut during the EDM process. Firmly clamping the component, minimizes the crack opening and closing during cutting and helps to control (reduce) the concentration of redistributed stress at the cut tip [111]. Using a smaller wire diameter also helps to reduce bulge errors but using a wire diameter below 100µm may introduce other difficulties (such as wire breakage) in the cutting process [3].

Bulge errors tend to show the same effects as plasticity, a shift in stress distribution towards the start of the cut along with reduced peak stresses. Most studies attribute asymmetric stress results to plasticity. But some studies indicate possible bulge error, particularly were the specimen was only clamped on one side. [4, 46, 65, 97, 100] and when the measured stresses were far below the yield stress [3, 31].

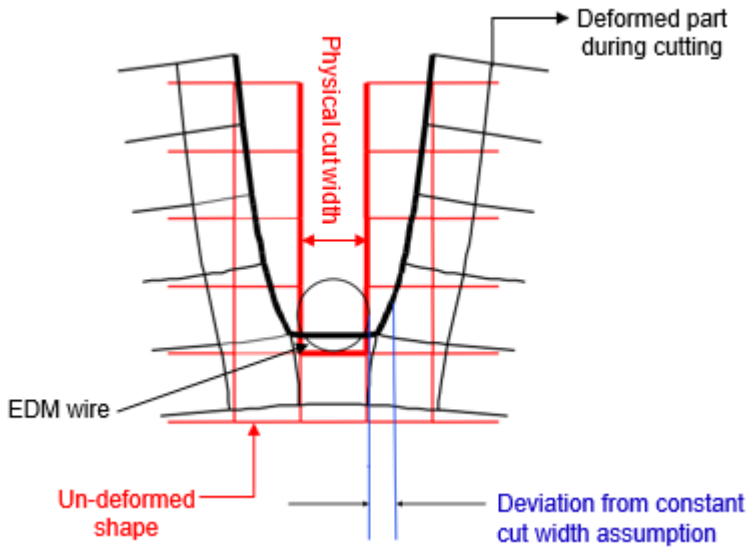

Figure 2 - 22: Schematic of the bulging effect during the cutting process due to tensile stress relaxation [31].

2.7.3 Iterative FE procedure for bulge correction

Prime and Kastengren [3] proposed an iterative ABAQUS finite element correction procedure to estimate the elastic deformation at the cut tip, which is referred to as the 'bulge error', by modelling of the cutting process. Removing this from the measured displacement

data would be a valuable improvement [31]. This correction procedure of Prime and Kastengren has been implemented for a small number of published contour method measurements [46, 65] but is not described in detail and standard procedures for correction have not been established. This section attempts to fully describe the steps of the iterative FE procedure to correct contour method measurements for bulge error. This procedure has been created with information from the published procedure [3] and additional information from private discussions with Mike Prime [118].

Assumptions for the cutting simulation

Several assumptions are used for the cutting simulation [3], (a) isotropic, linear elastic material behaviour is assumed throughout the analysis, (b) the cut is perfectly planar in space; hence, the deviations come only from deformation of the material, (c) for meshing convenience, a square slot bottom is used.

For the square slot bottom assumption, the deviation from the constant cut width is given by the out of plane displacement of the material point where cutting is about to occur, i.e. the bottom corner of the slot as shown in Figure 2 - 23. However in practice the contour method EDM cutting procedure creates a semi-circular bottom slot, therefore this may introduce errors [3]. For the semi-circular bottom EDM slot, the final slot width is cut at the outer edge of the EDM wire diameter (i.e. lateral tangent of the cutting wire), shown in Figure 2 - 23. Prime [118] suggested that this location might be a better position to estimate the slot width error.

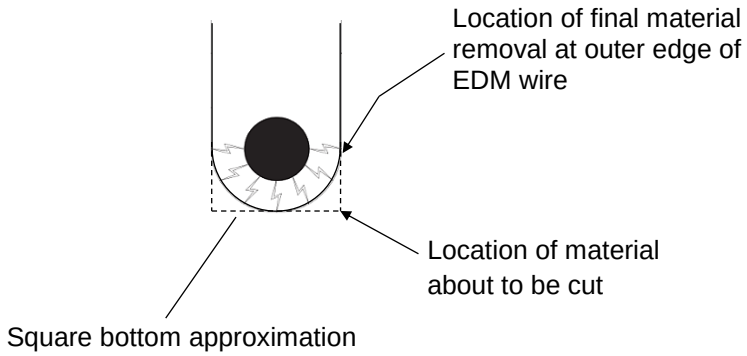

Figure 2 - 23: Schematic of the semi-circular bottomed EDM slot and square bottom assumption used in the FE cutting simulation [118].

Steps of the FE correction procedure

Step 1: Complete an experimental contour method measurement and calculate the residual stresses in the specimen.

Step 2: Create a finite element model of the specimen in ABAQUS to perform a linear elastic simulation of the EDM cutting procedure. Guidelines for selecting the correct model and parameters are given below.

Analysis Type: A simplified 2D cutting simulation can only correct a line profile of the stresses whereas 3D modelling is a more robust approach. For rapidly varying stress distributions the bulge error may vary through the thickness of the specimen requiring 3D FE analysis [1]. Furthermore, for an ideal contour method cut, clamped symmetrically on both sides of the cut, only one-half of the specimen needs to be modelled due to symmetry. If the specimen was clamped on one side only, a model of the entire specimen (i.e. no half symmetry) is required to accurately predict the bulge error on each side of the cut surfaces.

Defining the coordinate system: The global coordinate system (x, y and z axes) should be defined so that a cut tip stretch is associated with a positive out of plane displacement whereas a cut tip compression is negative. Nevertheless, for a model of the entire specimen, a stretch or contraction at the cut tip will cause the nodal points on each side of the cut surfaces to move in opposite directions in the global coordinate system. This will be dealt with in the subsequent data processing step 6. Also, the origin of the coordinate system should be defined at a point located along the cutting start edge to easily obtain the results at each cut increment because the nodal output is written to the results file in the global system in ABAQUS (since this is more convenient for postprocessing) [87].

Material properties: For a linear elastic material model, Young's modulus, E, and Poisson's ratio, ν, are defined.

Mesh type and size at the cut: For 2D analysis, plane stress or plane strain quadrilateral elements, of types CPS and CPE respectively, are required at the cutting location in the model. For a 3D model, bricks elements of type C3D are used at the cut. The size of the elements that are removed to simulate cutting should represent the final cut width created during the EDM cutting procedure. For a half symmetry model this would be half of the cut width. For the square slot bottom assumption (see Figure 2 - 23), linear (first

order) elements are suitable to estimate the bulge displacement at the bottom corner of the slot. Whereas for the semi-circular bottom slot (see Figure 2 - 24), square quadratic (second-order) elements are necessary to estimate the bulge displacement at the mid side node or outer position of the slot.

Cutting increment: The material removal and relaxation process is assumed to be elastic, which is then rate and path independent [118]. Therefore, several elements can be removed at a time to manage the number of cut increments in the model.

Step 3: Introduce the contour method residual stresses in the model and perform a general step to allow the stresses to reach equilibrium. Since bulge errors in the contour method are relatively small, and the measured surface deformation profile closely parallels the actual surface deformation profile (i.e. without bulge errors), the calculated stress profile can be used as an initial guess in the FE model [3].

The initial stress condition can be defined in the FE model via the subroutine SIGINI or the MAP SOLUTION function in ABAQUS software [119]. One assumption, to obtain correct bulge error estimates, is that the initial stresses do not contain any effects of plasticity which may contribute to the error in the calculated stresses. Because the bulge error and plasticity show the same effects in the stress results, it would be difficult to determine if the effects of plasticity at the cut tip may have contributed to the error results and give inaccurate bulge estimates [3].

Step 4: Apply restraints to represent the clamping condition during EDM cutting and to prevent rigid body motion. The purpose of clamping is to minimize the opening and closing of the cut, that is to prevent the movement in the normal direction to the cut i.e. x-direction motion in Figure 2 - 24. The constraint applied during the FE simulation is representative of the perfect constraint, that is $U_x = 0$, which is not likely to be applied in practice and may influence the bulge estimation if applied very close to the cut surface. Modelling clamping with perfect displacement constraint is only an approximation and more realistic simulation of clamping forces and locations may help to quantify the bulge error more accurately [3].

Step 5: Sequentially remove elements to simulate the cutting step and record the local normal displacement at the cut tip for each cut increment as described below.

The bulge error is the out of plane displacement of the material at the cut tip. In the FE analysis, this is given by the displacement variable U in the x direction shown in Figure 2 - 24. The proposed material positions at the cut tip to estimate the bulge error (see Figure 2

- 23) are represented in the FE model by the corner node (bottom of slot) and mid side node (outer edge of slot) as shown in Figure 2 - 24. For a model of the entire specimen, the displacement of the nodes on both sides of the slot is required and for 3D cases, the displacements through the thickness of the specimen should be measured.

An additional measurement is required to obtain an accurate estimation of the bulge error. Since the assumption is that the cut width is constant when measured relative to the state of the body prior to cutting, this would essentially be after the stresses reach equilibrium in step 3. Therefore, the displacements after the equilibrium step should also be obtained in order to deduct these from the bulge displacements measured during cutting [118].

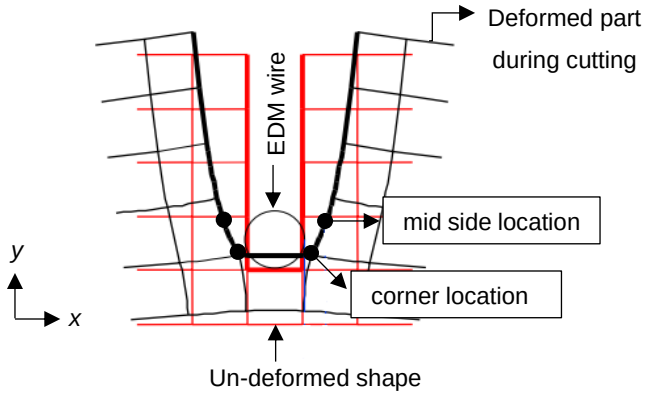

Figure 2 - 24: Schematic of the corner and mid side locations for bulge error measurement.

Step 6: Extract and process the bulge displacement data to correct the averaged smoothed surface deformations measured from implementing experimental contour. Firstly, subtract the bulge displacements after the equilibrium step from those measured during cutting. The value after subtraction is final the bulge displacement error given by Equation 2 - 8.

$$U_{final\ bulge\ error} = U_{bulge\ during\ cutting} - U_{bulge\ after\ equilibrium\ step} \qquad \textit{Eqn. 2 - 8}$$

For a full model, calculate the final bulge displacement error for each cut half and then average the displacements using Equation 2 - 9. In the finite element analysis, each side of the cut tip is moving in opposite directions to the reference coordinate system, therefore the sign of the displacements from one side should be reversed before averaging.

$$U_{averaged\ final\ bulge\ error} = \frac{U_{final\ bulge\ side\ 1} + \left(-U_{final\ bulge\ side\ 2}\right)}{2} \qquad \textit{Eqn. 2 - 9}$$

Then, interpolate the final bulge displacement error data for the positions required to correct the initial experimentally measured surface deformations.

Step 7: Correct the initial measured averaged smoothed surface deformations by subtracting the averaged final bulge displacement error using Equation 2 - 10.

$$U_{\substack{corrected\ surface \\ deformations}} = -\left(U_{\substack{initial\ surface \\ deformations}} - U_{\substack{averaged\ final \\ bulge\ error}}\right) \qquad \textit{Eqn. 2 - 10}$$

where the negative sign outside the bracket represents the reversed deformations used to calculate the stresses [3].

Step 8: Calculate the new stresses using the conventional contour method procedure, by creating a finite element model of one half of the specimen in ABAQUS and applying the corrected displacements as boundary conditions on the cut surface and allowing the model to reach equilibrium.

Step 9: An iterative solution is required to solve for the new stresses since the first estimate of the bulge error is based on stresses calculated assuming no bulge error. The process is repeated until successive stress estimates converge. That is, repeat steps 3 to 8 by initializing the new stresses to re-estimate the bulge displacements. For each iteration, the re-estimated bulge error is used to correct the initial averaged smoothed surface deformations and not the corrected displacements from the previous iteration. Since the bulge errors are usually relatively small, no more than two or three iterations are required for reasonable convergence.

Step 10: Finally, the new stresses are evaluated for a converging solution. No criteria have been specified in the literature but the chosen criteria for convergence is a variance of less than 5 percent (≤ 5 %) for the peak stresses.

Application of the iterative FE bulge correction procedure

Prime and Kastengren [3] experimentally validated the finite element bulge correction procedure for a stainless steel four point bent beam were the correction was not large but moved the contour result closer to the bend test prediction as shown in Figure 2 - 25. Since then it has only been implemented for two contour measurements. The first is a 2D analysis for a stainless steel quenched cylinder contour measurement [46] to assess the possibility of bulge error. However, no significant influence was observed after the correction shown in Figure 2 - 26 and the non-symmetry distributions of residual stresses was mainly attributed to plasticity effects. More recently the procedure was applied for an EB welded C(T) specimen contour measurement [65] using three dimensional (3D) cutting simulations to estimate the bulge error which is a more robust approach. In the corrected stress results

shown in Figure 2 - 27, the peak tensile stress was moved towards the mid-width of the specimen, which was the expected weld position, and there was a slight increase in the magnitude of the tensile residual stress. These studies showed that the bulge effect in the contour method residual stress results can cause errors of 5% to 10% in magnitude and spatial misalignment by a small amount, even when the part is securely clamped during cutting [3, 65]. Any effort to minimize or correct for these errors will improve the accuracy of measurements made by the contour method.

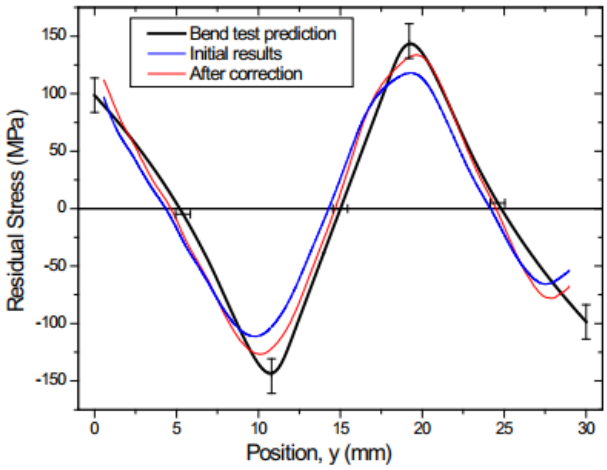

Figure 2 - 25: Contour method residual stresses along mid-thickness of a stainless steel four-point bend beam, before and after bulge correction compared with the prediction from the bend test [3].

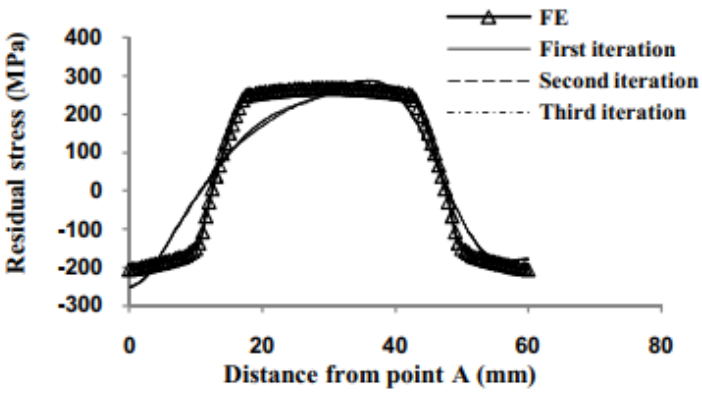

Figure 2 - 26: Residual stresses for a stainless steel quenched (at 850^{o}C) cylinder after bulge correction for the first, second and third iterations compared with FE prediction along cylinder centreline [46].

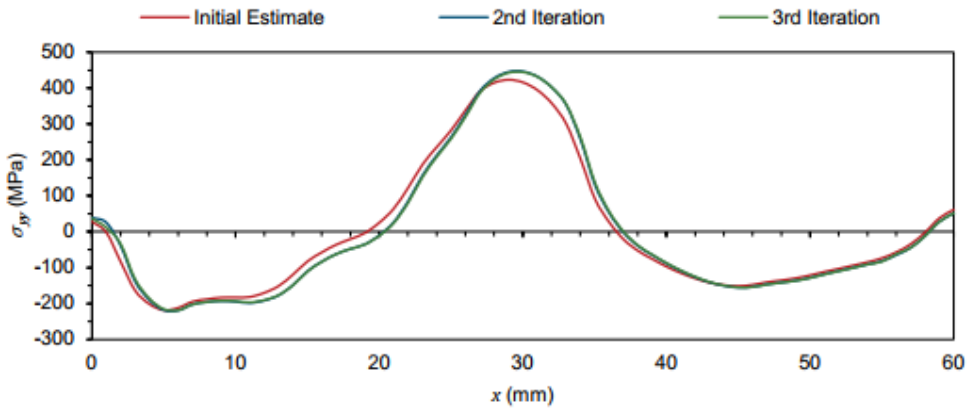

Figure 2 - 27: Contour method longitudinal weld residual stresses, along mid-thickness of EB welded C(T) blank, before and after bulge correction for the second and third iterations [65].

2.8 Fracture mechanics concepts

In the contour method, the cut created by wire EDM can be seen as a moving blunt edge crack which causes a redistribution of residual stresses in the uncut material that are concentrated at the cut tip. In the field of Linear Elastic Fracture Mechanics (LEFM), the magnitude of the stresses and displacements surrounding the tip of a crack can be characterised by the stress intensity factor. In this section the principles and expressions of fracture mechanics analysis are presented and the existing methods to obtain the stress intensity factor is discussed with a focus on numerical solutions which are employed in this work.

2.8.1 Linear Elastic Fracture Mechanics

LEFM is the basic theory of fracture that deals with the growth of sharp cracks in elastic bodies controlled by the stresses and deformations around the crack tip. The surfaces of a crack are the dominating influence on the distribution of stresses near and around the crack-tip, as they are the nearby stress-free boundaries of the body [120]. There are three modes of crack surface displacement shown in Figure 2 - 28, mode I is identified as the opening mode, in which the crack surfaces move opposite and perpendicular to each other. This mode has been studied more extensively than modes II and III, which involve sliding and lateral tearing respectively. The crack surface displacements can be conveniently characterised by the stress intensity factor [121], which is a function of the specimen dimensions and loading conditions. The general form of the stress intensity factor is $K =$

$\sigma\sqrt{\pi a}$, where σ is the remote load and a is the crack length, which is expressed as $MPa\sqrt{m}$. When K is known, the stresses and displacements near the crack tip can be calculated using standard equations. As mentioned, K is taken as positive when the crack surfaces move apart but a negative K only has meaning if the crack is regarded as a narrow slit because if the crack surfaces are pressed together the crack has no effect on the stress distribution [121].

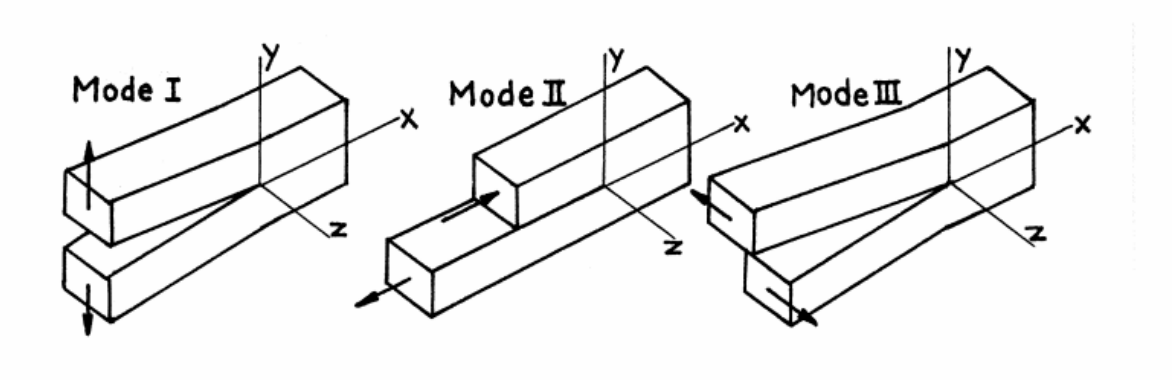

Figure 2 - 28: Basic modes of crack surface displacements [120].

Closed-form expressions to determine the stress and displacement fields associated with each mode were first published by Irwin [122], which is based on the method of Westergaard [123]. The stresses and deformations around a sharp crack tip can be expressed in terms of stress intensity factors K [124-126] in Equations 2 – 11 to 2 – 16 respectively, where r and θ are polar coordinates from the crack tip shown in Figure 2 - 29 [127]. As r approaches zero, the leading $1/(r)^{1/2}$ term approaches infinity, but the other higher-order terms, such as uniform stress parallel to cracks, σ_{x0}, and terms of the order of square root of r, $O(r^{1/2})$, remain finite or approach zero and are normally omitted [120]. Thus, stress near the crack tip varies with r, regardless of the configuration of the cracked body [124].

The equations for the stresses and displacements near a crack tip are derived for a crack in an infinite plane subjected to remote biaxial tension a shown in Figure 2 - 30. However, these expressions hold for any cracked body undergoing mode I deformations. The difference is only the value of the stress intensity factor [128]. All elastic analysis is for static problems in linear elastic, isotropic, homogeneous materials. Small-scale non-linear effects, such as small amounts of plasticity or microstructural irregularities in the crack surface, do not affect the general character of the stress field and are regarded as being within the crack tip stress field and can therefore be neglected in a reasonable approximation [121].

For mode I, the displacement must be symmetric with respect to the crack direction. The equation implies that for mode I the crack opens into a parabola shape, and because a crack is regarded as a mathematical 'cut', θ must lie in the range $\pm\pi$. The displacements at a crack tip are non-singular and proportional to $K_I\sqrt{r}$ and depend on the stress state [129]. The displacements are a factor $(1 - \nu^2)$ less for plane strain than for plane stress.

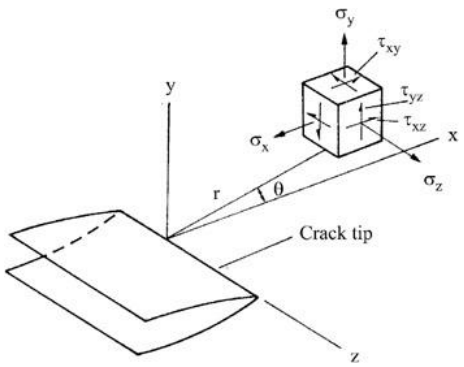

Figure 2 - 29: Coordinates measured from leading edge of a crack and stress components in the crack-tip stress field [127].

The following equations present stress field for mode I crack opening,

$$\sigma_x = \frac{K_I}{(2\pi r)^{1/2}} cos\frac{\theta}{2}\left[1 - sin\frac{\theta}{2}sin\frac{3\theta}{2}\right] + \sigma_{x0} + O(r)^{1/2} \qquad \textit{Eqn. 2 - 11}$$

$$\sigma_y = \frac{K_I}{(2\pi r)^{1/2}} cos\frac{\theta}{2}\left[1 + sin\frac{\theta}{2}sin\frac{3\theta}{2}\right] + O(r)^{1/2} \qquad \textit{Eqn. 2 - 12}$$

$$\tau_{xy} = \frac{K_I}{(2\pi r)^{1/2}} sin\frac{\theta}{2}cos\frac{\theta}{2}cos\frac{3\theta}{2} + O(r)^{1/2} \qquad \textit{Eqn. 2 - 13}$$

The following equations present displacement fields for mode I crack opening (with higher-order terms omitted),

$$v = \frac{K_I}{G}[r/(2\pi)]^{1/2} cos\frac{\theta}{2}\left(1 - 2\nu + 2sin^2\frac{\theta}{2}\right) \qquad \textit{Eqn. 2 - 14}$$

$$u = \frac{K_I}{G}[r/(2\pi)]^{1/2}\ sin\frac{\theta}{2}\left(2 - 2\nu - 2cos^2\frac{\theta}{2}\right) \qquad \textit{Eqn. 2 - 15}$$

$$w = 0 \qquad \textit{Eqn. 2 - 16}$$

where v and u are the horizontal (x-direction) and vertical (y-direction) displacements, G is the shear modulus and ν is the Poisson's ratio. Equations 2 – 11 to 2 -16 have been written

for the case of plane strain (i.e., $w = 0$) but can be changed to plane stress by replacing Poisson's ratio, ν, in the displacements with $\nu/(1+\nu)$.

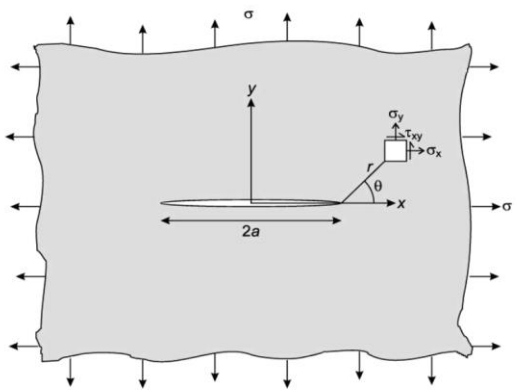

Figure 2 - 30: Schematic drawing showing a biaxial loaded infinite plate containing a crack [130].

As previously mentioned, a blunted crack tip is introduced by wire EDM. The field equations are only valid for "mathematically sharp" plane crack. The elastic stress field equations for blunt cracks [131], defined by Equations 2 – 17 to 2 - 19, were derived by shifting the origin of the co-ordinate system a distance $\rho/2$ away from the crack tip, were ρ is the blunt crack tip radius shown in Figure 2 - 31.

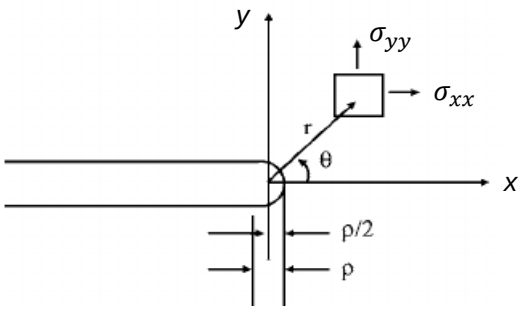

Figure 2 - 31: Coordinates for the local stress distribution at a distance r, ahead of a blunt crack tip radius ρ.

The following equations present mode I crack opening stress fields for blunt crack,

$$\sigma_x = \frac{K_I}{(2\pi r)^{1/2}} cos\frac{\theta}{2}\left[1 - sin\frac{\theta}{2} sin\frac{3\theta}{2}\right] - \frac{K_I}{(2\pi r)^{1/2}}\frac{\rho}{2r} cos\frac{3\theta}{2} \qquad \textit{Eqn. 2 - 17}$$

$$\sigma_y = \frac{K_I}{(2\pi r)^{1/2}} cos\frac{\theta}{2}\left[1 + sin\frac{\theta}{2} sin\frac{3\theta}{2}\right] - \frac{K_I}{(2\pi r)^{1/2}}\frac{\rho}{2r} cos\frac{3\theta}{2} \qquad \textit{Eqn. 2 - 18}$$

$$\tau_{xy} = \frac{K_I}{(2\pi r)^{1/2}} sin\frac{\theta}{2} cos\frac{\theta}{2} cos\frac{3\theta}{2} - \frac{K_I}{(2\pi r)^{1/2}} \frac{\rho}{2r} sin\frac{3\theta}{2} \quad \textit{Eqn. 2 - 19}$$

For a blunt crack or slender notch, there is no singularity in stress at the crack tip ($\theta = 0,\ r = \rho/2$) and for mode I type loading the maximum stress may be found by [120, 132],

$$\sigma_{Y\,max} = \frac{2K_I}{\sqrt{\pi\rho}} \quad \textit{Eqn. 2 - 20}$$

2.8.2 Stress Intensity Factor Solutions

The crack-tip stress intensity factor (SIF) values, which characterize the magnitude of the stress fields surrounding the crack-tip, depends linearly on the applied external load, on the length of the crack, and on the geometry of the crack and the geometry of the component. Consequently formulas for their evaluation come from a complete stress analysis of a given configuration and loading [120]. Closed-form solutions for K have been derived for a number of simple configurations. It can be written in the form [130],

$$K_I = Y(a/W)\,\sigma\,\sqrt{\pi a} \quad \textit{Eqn. 2 - 21}$$

where $Y(a/W)$ is a dimensionless geometric factor that depends on the geometries of the specimen and crack, and σ is the (remotely) applied stress.

Two common geometries for which closed-form solution exists [130] are shown in Figure 2 - 32. For the infinite plate with a central crack with length $2a$, $Y(a/W) = 1$ and thus $K_I = \sigma\sqrt{\pi a}$. A related solution is that for a semi-infinite plate with an edge crack the stress intensity factor is given by $K_I = 1.12\,\sigma\sqrt{\pi a}$. The 12% increase in K_I for the edge crack is caused by different boundary conditions at the free edge but has diminishing effect as the crack extends deeper into the material.

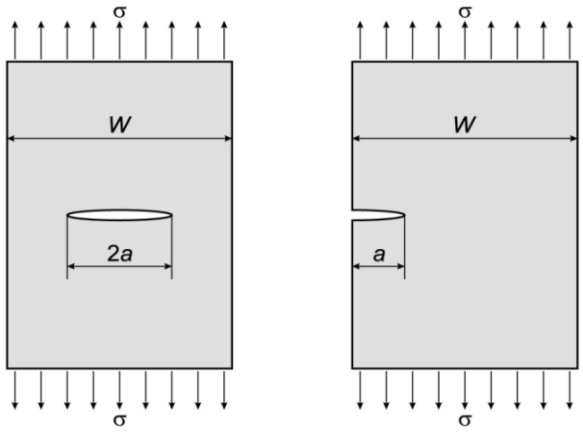

Figure 2 - 32: Schematic drawing showing two common cracked-plate configurations: centre crack (left) and single edge notched (right) [130].

Expressions such as this for other types of cracks and loading geometries have been obtained for numerous structural configurations. Methods to determine the stress intensity factor can be broadly categorised into analytical, numerical and experimental methods. In general, analytical methods are restricted to idealized problems where the geometrical configuration of cracks and the boundary conditions are rather simple. The numerical method is useful for determining the stress intensity factor where the geometry and loading are complex and not available from simple analytical solutions. Experimental methods cannot directly measure the stress intensity factor, but it is determined from its relationship to measurable quantities such as strain or displacement, therefore they are approximate solutions. SIF solutions for numerous geometries and loading conditions have been compiled in published handbooks [120, 133, 134]. Some solutions include analytical methods such as closed form solutions [120, 130] and weight functions [135, 136]. Numerical methods include finite element methods (ABAQUS software [119]), boundary collocation methods [137, 138] and software (R-Code [139] or CRACKWISE [140]). Common experimental techniques include the compliance method [20], photoelastcity and moire interferometry [141].

The numerical finite element method and boundary collocation method (BCM) are considered to determine the stress intensity factors in this research, that is to characterise the stresses at the cut tip during finite element simulation of the EDM cutting process and relate this to the bulge error. Therefore, the FE and BCM methods to estimate K will be described next.

K Estimates from Finite Element Method (FEM)

Fundamentals of the finite element method

ABAQUS software is a powerful engineering simulation program, based on finite element method, that can analyse a wide range of complex geometric configurations, boundary conditions and loads. The finite element method is a procedure for obtaining approximate solutions to continuum problems. It involves conceptually dividing the body under consideration into elements that are connected to associated nodes and assuming an approximate form for the solution within each element. For each typical element, there exist dependent variables at the nodes such as displacement. An interpolation function is defined relative to the values of the dependent variables at the nodes associated with the element. For one element, the equation including these variable can be expressed by [119],

$$[K]_e\{U\}_e = \{F\}_e \qquad \textit{Eqn. 2 - 22}$$

where $[K]_e$ is the elementary stiffness matrix, which is determined by geometry, material property and element property, $\{U\}_e$ is the elementary displacement vector, which describe the motion of nodes under force and $\{F\}_e$ is the elementary force vector, which describe the force applied on element.

The functions of all the elements are assembled into global matrix equation $[K]\{U\} = \{F\}$ (governing algebraic equations) to represent the object.

After applying boundary condition, the governing algebraic equation can be solved for the dependent variable at each node. The strain and stress can be calculated based on the displacement of nodes associated with the element.

Calculating K by the finite element method

There are a few methods for evaluating the stress intensity factor by FEM, such as the crack tip displacement extrapolation, the J-integral approach and the strain energy approach using the virtual crack extension technique. For ABAQUS linear elastic analysis, a simple and accurate method to obtain the stress intensity factor at the crack tip is by a contour integral evaluation related to the *J*-integral [119]. The finite element method to calculate the stress intensity factor requires conforming the mesh to the cracked geometry, to explicitly define the crack front, and to specify the crack extension direction. Special contour elements are required to manage the stress singularity at the sharp crack tip in order to obtain correct stress intensity factor solutions. Generally, second-order elements are used and the crack

tip is modelled with a ring of collapsed elements with the mid side nodes connected to the crack tip moved to the 1/4 point nearest the crack tip, as shown in Figure 2 - 33. Each contour is a ring of elements completely surrounding the crack tip or the nodes along the crack line. The rings of elements are defined recursively to surround all previous contours and each ring provides an evaluation of the contour integral [119]. The accuracy of these contours is determined by evaluating the value of the contour integral that appears approximately constant from one contour to the next. In linear elastic problems the first and second contours may be inaccurate and should be ignored.

The number of contours to be used in calculating contour integrals must be specified as well as the type of contour integral to be calculated. By default ABAQUS calculates the *J*-integral [119]. For an elastic crack, the *J*-integral is calculated by ABAQUS, and then K is determined by a conversion.

$$J_e = \frac{{K_I}^2}{E'} \qquad \textit{Eqn. 2 - 23}$$

where the Young's Modulus $E' = E$ for plane stress and $E' = E/(1-\nu^2)$ for plane strain.

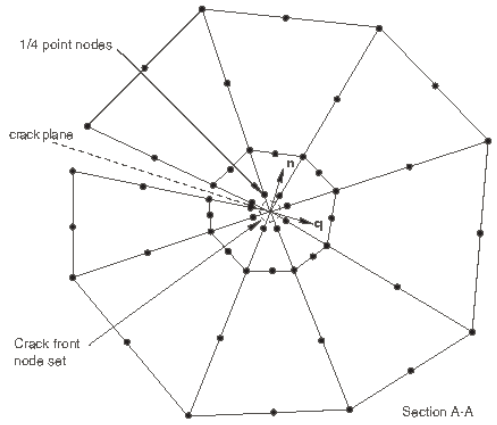

Figure 2 - 33: Typical focused mesh for modelling the crack-tip singularity [119].

K Estimates from the Boundary Collocation Method

Another numerical modelling method is the boundary collocation method, which only the boundaries of the region of interest need to be modelled. The method of boundary collocation consists in finding certain coefficients of the elastic crack solution by satisfying the boundary conditions at a finite number of points along the boundary of the body. A boundary value collocation procedure was employed to determine the elastic stress distribution in the immediate vicinity of the tip of an edge crack in a finite-width specimen

subjected to uniform tensile and bending loading [137, 138]. The analytical results were expressed so that the stress intensity factor may be determined from known conditions of specimen geometry and loading.

Stress intensity factors K for the case of a freely deformable single edge-cracked plate of width W, height $2H$, containing a crack of depth a, were determined using the boundary collocation method (BCM) for pure tension (Figure 2 - 34 (a)) and pure bending (Figure 2 - 34 (b)) and input into Table 2 - 1 and Table 2 - 2 in the form of the geometric function F' defined by Equation 2 -24 for several H/W ratios [135, 142].

$$K = \sigma\sqrt{\pi a}\, F\left(\alpha, \frac{H}{W}\right), \qquad F' = F(1-\alpha)^{3/2}, \qquad \alpha = a/W \qquad \textit{Eqn. 2 - 24}$$

where σ is the constant stress in the tensile case or the outer fibre bending stress σ_0 under bending load $\sigma_{(x)} = \sigma_0(1 - 2x/W)$

The numerical values of $F(a/W)$ using collocation method are based on results which is accurate to within 1% for all $H/W \geq 1.0$ and $a/W \leq 0.6$ [120, 134]. The effect of H/W is practically negligible for $H/W \geq 1.0$ [120]. Since no restriction on free deformation is made, bending of the cracked specimen is possible due to the homogeneous stresses at the specimen ends.

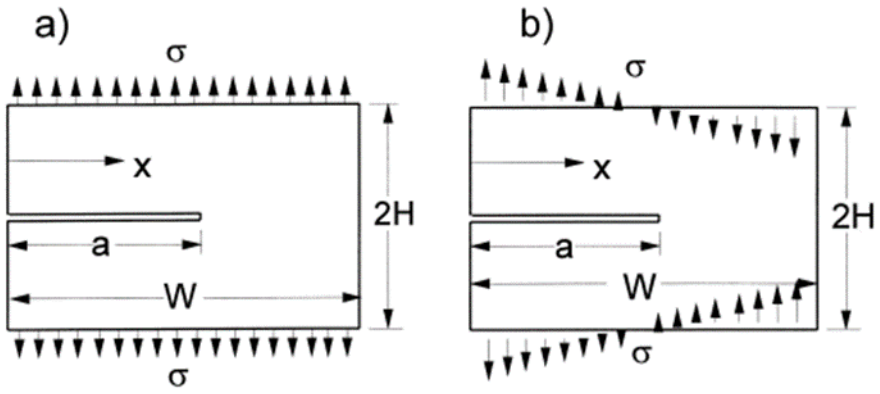

Figure 2 - 34: Edge-cracked rectangular plate under (a) tensile and (b) bending loading.

Table 2 - 1: Geometric functions F' for tension, in Equation 2 – 15, to determine the stress intensity factor using the boundary collocation methods (BCM) [142].

Geometric function F' for tension, Eq. (1)

α	$H/W = 1.5$	1.25	1.00	0.75	0.5	0.4	0.3	0.25
0	1.1215	1.1215	1.1215	1.1215	1.1215	1.1215	1.1215	1.1215
0.1	1.0170	1.0172	1.0174	1.0182	1.0352	1.0649	1.1455	1.2431
0.2	0.9800	0.9799	0.9798	0.9877	1.0649	1.1625	1.3619	1.5358
0.3	0.9722	0.9723	0.9729	0.9840	1.0821	1.2134	1.4892	1.7225
0.4	0.9813	0.9813	0.9819	0.9915	1.0819	1.2106	1.5061	1.7819
0.5	0.9985	0.9986	0.9989	1.0055	1.0649	1.1667	1.4298	1.7013
0.6	1.0203	1.0203	1.0204	1.0221	1.0496	1.1073	1.2898	1.5061
0.7	1.0440	1.0441	1.0441	1.0442	1.0522	1.0691	1.1498	1.2685
0.8	1.0683	1.0683	1.0683	1.0690	1.0691	1.0734	1.0861	1.1201
1.0	1.1215	1.1215	1.1215	1.1215	1.1215	1.1215	1.1215	1.1215

Table 2 - 2: Geometric functions F' for bending, in Equation 2 – 15, to determine the stress intensity factor using the boundary collocation methods (BCM) [142].

Geometric function F' for bending, Eq. (1)

α	$H/W = 1.5$	1.25	1.00	0.75	0.5	0.4
0	1.1215	1.1215	1.1215	1.1215	1.1215	1.1215
0.2	0.7561	0.7561	0.7562	0.7628	0.8279	0.9130
0.3	0.6583	0.6583	0.6589	0.6677	0.7444	0.8475
0.4	0.5861	0.5861	0.5865	0.5930	0.6567	0.7505
0.5	0.5293	0.5293	0.5296	0.5332	0.5717	0.6388
0.6	0.4842	0.4842	0.4842	0.4852	0.5022	0.5367
0.7	0.4481	0.4479	0.4478	0.4478	0.4514	0.4621
0.8	0.4203	0.4188	0.4191	0.4185	0.4180	0.4185
1.0	0.374	0.374	0.374	0.374	0.374	0.374

2.9 The contour method needs and gaps

The contour method is gaining increasing use in characterising residual stresses in a wide range of engineering structures due to its unique advantages. These include (a) providing a two-dimensional map of the residual stress distribution over the entire material cross-section, (b) not being restricted by the size and geometry of the component and (c) being insensitive to microstructural changes in the material. Nevertheless the contour method is the youngest residual stress measurement technique and is not as well established as other methods [1].

One limitation to apply the contour method is that the part is symmetric about the cut plane and measuring stresses where the two halves are not the same shape or size would require creating asymmetric cuts which will may introduce large errors. However, recent work has

been done to advance the contour method for asymmetric cuts [143, 144]. Another challenge for the contour method is when near-surface residual stresses are desired to be determined and often the near surface stresses results in contour measurements are not reported. Some studies [31, 55, 70, 72] have been performed to try to minimize the edge effects during cutting using sacrificial plates or improve the measured results near the surfaces but standard practices to deal with near surface measurements has not been established.

Errors and uncertainties in the contour method can be introduced at all experimental measurement and data processing stages. Some errors can be removed by processing the measured data or minimised by means of good cutting practices. But two errors that are difficult to predict, control or avoid are: plasticity and elastic bulging. These phenomena do not average away and can cause significant bias in residual stress measurements. There are many published studies on plasticity in the contour method [34, 46, 97, 101, 104, 111, 112] but the procedure for estimating plasticity-induced errors in contour method measurements [34, 101, 104] was developed for 2D plane stress and plane strain analysis and elastic-perfectly plastic materials. Further work is needed to develop procedures to estimate plasticity errors in strain hardening materials and for 3D cases.

Bulge error can have a significant effect on the accuracy of stress measurement made by the contour method as it causes decreased magnitude and a spatial misalignment of the stress predictions. This can be very important, for example in structural integrity assessment when the SIF is calculated from contour method results. However, bulge error has only recently been addressed and little knowledge exists about the influence of bulge errors in contour method measurements. Prime and Kastengren [3] proposed an iterative ABAQUS finite element procedure to estimate and correct contour measurements for bulge error. However, the procedure can be cumbersome and time consuming and 3D modelling is required in most engineering cases. Some improvement is required to automate the finite element procedure or develop a simpler approach whereby bulge correction can be easily integrated into the data analysis procedure of the technique. And to improve the fidelity of the simulations at the beginning and end of the cut and applied constraint to represent the actual clamping condition used during the cutting process. Besides the correction procedure of Prime and Kastengren has been implemented for a small number of published contour method measurements [28, 42] and standard procedures for bulge correction have not been established. Furthermore, the interaction between bulge and plasticity deformation errors is unknown.

Understanding how to control and correct deformation errors that occur during the cutting step of the technique will help to improve the accuracy and reliability of measurements made by the contour method. Details of the aim and objectives are explained in the following section.

2.10 Aims of the research

This research will be working towards improving the understanding of bulge errors in the contour method. The main aim is to understand when the bulge error arises, estimate the magnitude of that error, develop procedures to correct for it, and where feasible, eliminate or control it. The hypothesis put forward was that a simple approach could be developed to be integrated in the standard data analysis of the contour method in order to correct for bulge error.

Based on this, the objectives of this research are as follows:

- Develop an analytical solution to describe the deformation at the cut tip using LEFM and predict the onset of bulging.
- Evaluate the 2D iterative FE procedure proposed by Prime and Kastengren [3] to estimate and correct for the bulge error in residual stress measurements made with the contour method and advance the method for application to 3D models (i.e. contour measurements of real components).
- Develop an alternative quantitative approach to replace the cumbersome iterative FE procedure to estimate and correct for the bulge error in contour method measurements. This research will also investigate the influence of parameters on the bulge error such as plane stress and plane strain conditions, material properties and cut width.
- Develop approaches to estimate the level of error in residual stress measurement that can be introduced by bulging to enable the practitioner to decide whether to correct for it.
- Develop guidelines for correcting for bulge errors in residual stress measurements made with the contour method.

2.11 Methodology

The research method in this thesis consists of two main approaches, analytical solution and finite element analysis. This section describes the individual methods that will be used for the objectives outlined in the previous section and includes any proposed specimens where applicable.

A part of this study is focused on the fundamental theory of the contour method to understand the origin of the bulge error and factors that influence the magnitude of deformation at the cut tip. This part of the research is focused on using the principles of linear elastic fracture mechanics to explore an analytical solution to relate the displacements at the crack tip to the local stress distribution [120]. That is to develop a criterion to predict the onset of bulging error for the contour method.

The study to investigate the finite element bulge correction procedure proposed by Prime and Kastengren [3] is achieved by applying the procedure for a stainless steel (Esshete 1250) C(T) cross-weld specimen where residual stresses were measured using neutron diffraction, incremental slitting and the contour method [4] and the bulge error was suspected to be present in the contour method measurement. This study evaluates the capability of the bulge correction procedure for complex (varying) residual stress, first using 2D FE modelling in ABAQUS to correct the C(T) specimen contour method stresses at mid-thickness and then 3D modelling to correct the stresses across the cut surface.

An alternative quantitative method to estimate the bulge error in contour method measurements may be possible as Prime and Kastengren [3] proposed that the bulge error is approximately proportional to the mode I stress intensity factor (SIF). To demonstrate the relationship between the SIF and the bulge error or “varying cut width”, extensive finite element simulations for a series of different parameters i.e. stress conditions, plate geometries, material properties and cut width sizes, were chosen to develop robust correlations. Then an analytical solution to estimate the bulge error is derived based on the standard LEFM displacement field equations for a crack in a body found in the literature. The analytical approach is implemented for two contour method measurements, first the cross-weld C(T) specimen which was investigated previously and then a bent beam specimen which was the first published work to correct for the bulge error using the iterative FE procedure [3].

The final study is to develop correlations of the normalised stress error with the mode I stress intensity factor. The stress error due to bulging is evaluated using Fourier based SIF solutions [145] and finite element analysis for the simple case of a self-equilibrated cosine residual stress profile and then for a more real case of a complex weld stress profile in the plane stress and plane strain conditions. Systematic studies were performed for different parameters to develop the stress error correlations.

Based on this research, guidelines are proposed for correcting contour method measurements for the bulge error.

Chapter 3: Investigating the iterative FE bulge correction procedure

One of the main assumptions of the contour method is that a constant width of material is removed during cutting when measured relative to the original state of the body. Bulge errors occur as cutting proceeds because the stresses relax and the material at the cut tip elastically deforms. This causes the width of material removed to vary along the cut length. To estimate and correct for the bulge error Prime and Kastengren [3] proposed an iterative ABAQUS finite element correction procedure which has been described in the literature review chapter. This correction procedure of Prime and Kastengren has been implemented for a small number of published contour method measurements [46, 65] but is not described in detail and standard procedures for correction have not been established.

The primary objective of this chapter is to set out the steps of Prime and Kastengren bulge correction procedure in detail and understand its ability and limitations with respect to correcting contour measurements with complex (varying) residual stress fields. The iterative FE procedure proposed by Prime and Kastengren [3] is based on two-dimensional (2D) plane stress finite element analysis. There is only one publication extending the bulge correction procedure to a 3D case [65]. A secondary objective of this chapter is to develop the 2D iterative FE procedure for application to 3D cases (i.e. real contour method measurements). The objectives are achieved by applying the corrective procedures to a case study that is a welded compact tension, C(T), specimen where the bulge error was suspected to be present in a previous contour method measurement.

First, the case study C(T) specimen details and previous contour measurement results are given. Next Prime and Kastengren bulge correction procedure is implemented using a 2D FE analysis to correct the C(T) specimen stresses at mid-thickness previously measured using the contour method. Then the procedure is extended to a full 3D FE analysis for the same sample to correct the stresses across the cut surface. Based on this investigation, an alternative simpler procedure to calculate the corrected stresses is presented and applied for the C(T) specimen. Finally, a discussion and the main conclusions are given.

3.1 Case study : cross-weld C(T) specimen

The previous work on this C(T) specimen was performed by Yeli Traore at the Open University [4, 34] and involved characterising the distribution of residual stress by neutron

diffraction, incremental slitting and contour method measurement techniques. In the contour method result, a small shift in the position of the tensile peak in the stress distribution was found when compared with the slitting and neutron results. The hypothesis put forward to explain this result was the possible occurrence of plasticity during cutting or elastic bulging error, or both types of error. The influence of plasticity was previously studied for this sample [4] but no work has been done to evaluate the bulge error. In this work the iterative FE procedure is implemented to correct the previously measured contour method stresses for bulge error.

The aim is to investigate two different bulge correction approaches, the first using the 2D FE approach proposed by Prime and Kastengren which assumes stresses are uniform across the thickness and then a more robust 3D FE approach to correct the stresses across the entire cut surface. A secondary aim is to explore which displacements in the FE idealised model of the slot geometry should be used to estimate the bulge error. This includes the model positions for the bottom corner of the slot described in the literature review chapter (see Figure 2 - 23), that have been proposed by Prime [118], and the outer edge of the slot not yet examined (see Figure 2 - 24).

This section first describes the specimen details and previous measurement results. Then the 2D bulge correction procedure and the results are presented. After that the 3D procedure is presented following with the results. Finally, the corrected contour method stress results are compared with those previously obtained by neutron diffraction and the slitting methods.

3.1.1 Specimen details

The cross-weld test sample of interest was extracted from an austenitic stainless steel (Esshete 1250) pipe butt weld that had previously experienced prolonged exposure to high temperature service conditions. The multi-pass butt weld was made using a manual metal arc (MMA) process, see Figure 3 - 1.

In order to create a geometry that resembles a C(T) test specimen of standard dimensions, an extension piece also made from Esshete 1250, was attached to the outer surface of the sample by electron beam (EB) welding [34] as shown in Figure 3 - 1. A rectangular block 47.5 mm wide, 45.3 mm deep and 21mm thick was then extracted from the welded sample by wire EDM. A 5 mm thick slice was also removed from the face labelled A, by wire EDM to determine the stress-free lattice parameter measurements for the neutron diffraction

technique. This reduced the thickness of the specimen to 16 mm. Finally, the cut face was polished and etched to reveal the MMA weld fusion boundary.

The elastic properties of the service-exposed parent materials and weld metal were assumed to be isotropic with a Young's modulus of 204.5 GPa and a Poisson's ratio of 0.29 at room temperature [146].

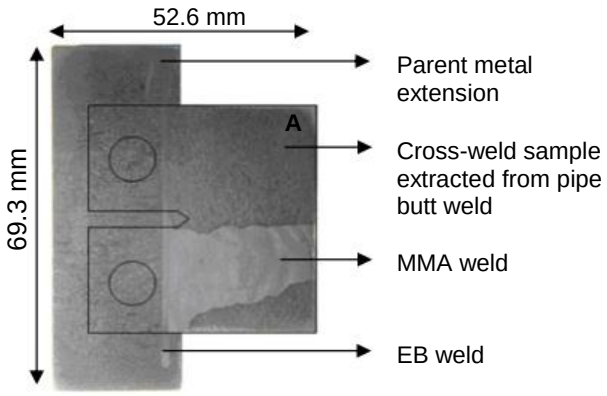

Figure 3 - 1: Photograph of the T-shaped welded specimen prior to machining the C(T) specimen.

3.1.2 Previous measurement results documented in [4, 34]

The final geometry of the C(T) specimen that has been measured in this study is shown in Figure 3 - 2 (i.e. a rectangular unnotched sample). The xy measurement plane for all three residual stress measurement techniques is also shown in Figure 3 - 2. This plane is located 2 mm from the deepest point of penetration of the MMA weld passes. First, neutron diffraction was applied to measure the full residual stress tensor along a line at mid-thickness. Then the contour and slitting methods were conducted in tandem to measure the transverse stresses on the measurement plane.

The neutron diffraction residual strain measurements were carried out on the L3 spectrometer of the Canadian Neutron Beam Centre. The gauge volume used for all measurements was (2 x 2 x 2) mm^3. The measurement points were spaced at 2 mm intervals with the first point located 1.41mm from the C(T) specimen front face giving a total of 23 points. The stress-free lattice parameter was measured using several stress-free reference cubes of dimensions (5 x 5 x 5) mm^3.

Then the slitting technique was implemented by introducing a slit using the incremental wire EDM process. A relatively large wire diameter 250 µm was used to help to minimise the risk

of wire breakage and plasticity during cutting. The specimen was 'finger' clamped on one side during cutting to allow the sample to deform and strains to be monitored at the back face shown in Figure 3 - 2. The gauge length of all strain gauges was 1 mm. Cutting was performed using two different cut increment settings: 0.1 mm increment from 0 up to 8 mm and from 46 mm up to 47.4 mm and 0.2 mm increment from 8 mm to 46 mm. The weight function approach, for a single edge crack within a finite width rectangular plate, was applied to determine the averaged residual stress distribution across the thickness of the sample. A plane strain condition was assumed based on the C(T) specimen dimensions.

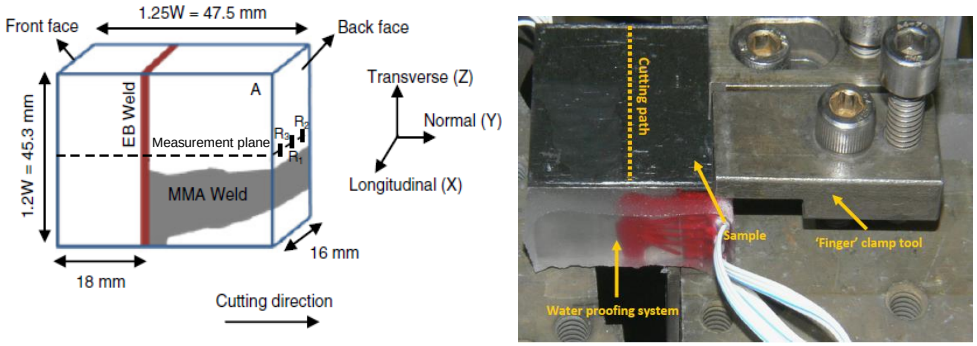

Figure 3 - 2: Schematic drawing showing the final dimensions of C(T) sample and the 'finger' clamp arrangement on one side during wire EDM cutting, from [34]

On completion of cutting for the slitting technique, the created cut surfaces were analysed using the contour method. Ideal restraint conditions to produce a high-quality contour cut requires rigidly clamping the specimen on both sides of the cut. The non-ideal restraint condition (clamping on one side) used for slitting will increase the likelihood of getting non-symmetric surface deformations and increase the risk of plasticity. The cut surfaces profiles were measured using a CMM with a 3 mm diameter touch probe and a measurement spacing of 0.5 mm in the x and y directions in Figure 3 - 2. The data from the two cut surfaces were averaged to eliminate antisymmetric errors and the effect of shear stress. Two approaches were evaluated to smooth the data: cubic spline fitting with different knot spacings and an alternative second order polynomial smoothing technique. To back-calculate the residual stresses, the finite element model of one half of the specimen was meshed with linear hexahedral elementals of type C3D8R and a mesh size of 0.5 mm. The polynomial smoothing approach [147] was found to be more robust in dealing with the extrapolation of data to specimen edges compared to the spline fitting. Therefore, the results obtained from the polynomial smoothing approach were used when comparing measurements from the three techniques.

The distribution of transverse stress for a line profile at mid-thickness of the sample measured using neutron diffraction, slitting and contour method techniques is presented in Figure 3 - 3. All three stress profiles follow the same trend with a tensile region located around the electron beam weld balanced by compressive stress fields in the parent material extension piece and in the HAZ of the MMA weld. The peak transverse residual stress measured by the contour method and slitting were lower than the neutron diffraction measurement (~ 640 MPa) by 19MPa (3%) and 50 MPa (8%) respectively. In the contour method result, a slight shift (2 mm) in the location of the tensile peak towards the C(T) specimen front face is observed. The 2D map of transverse residual stress on the cut surface measured by the contour method is also shown in Figure 3 - 3.

For neutron diffraction, the uncertainty in the calculated stresses, based on the measurement of both lattice parameters was no greater than ± 25 MPa. The significance of plasticity error in the slitting measurement was assessed using the approach of Prime [148] and found to be about 15 % for the parent material for a yield stress of 241 MPa and 2 % in the region of the electron beam weld for a yield stress of 430 MPa. Upon further investigation the author found that the small shift in location of the contour method peak tensile stress can be explained by the development of compressive plasticity during cutting caused by the lack of restraint applied to the specimen during the measurement [34]. Nevertheless, bulge error has the same symptoms as plasticity error and therefore cannot be discounted.

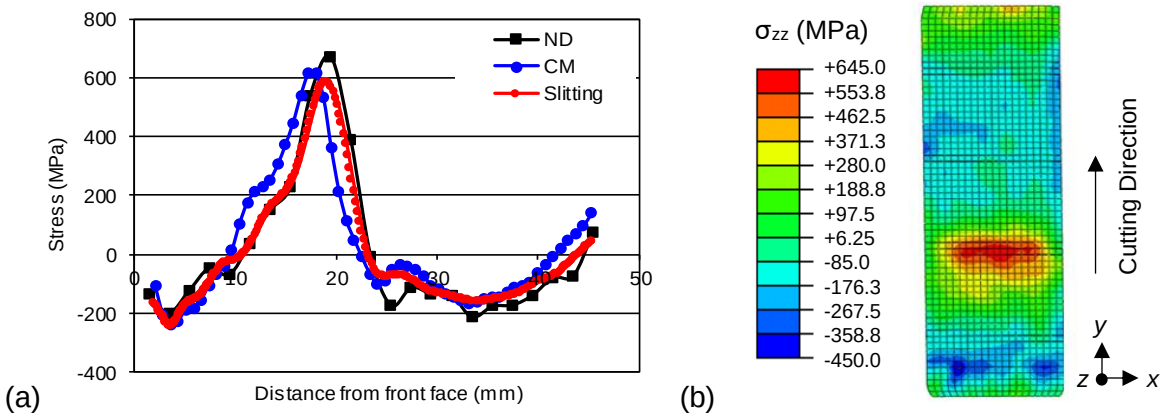

Figure 3 - 3: (a) Comparison of the transverse residual stress distribution at mid-thickness of a C(T) sample measured by neutron diffraction, slitting and the contour method (b) 2D map of transverse residual stresses measured using the contour method, from [34]

3.1.3 2D bulge correction procedure

The hypothesis put forward was that the slight shift in the location of the maximum tensile stress and the marginally lower tensile stress magnitude obtained in the contour method measurement results could be associated with bulge error. To investigate this conjecture 2D iterative bulge correction procedure, described in section 2.7.2 of the literature review chapter, was implemented to correct the contour method stresses at mid thickness.

In this procedure, the transverse residual stress profile at mid thickness from the contour measurement was applied as an initial condition in a 2D FE model of the C(T) sample. The entire sample cross section was modelled (i.e. no half symmetry) to correctly represent the asymmetric restraint condition, clamping on one side, used for the slitting measurement. The weld metal and homogenous parent materials were assumed to be isotropic. The cutting process was then simulated by sequentially removing elements. At each cut increment, the normal displacement of the material points originally on the cut plane were recorded to estimate the bulge error. After bulge estimation, a line profile of measured contour surface deformations was corrected for bulge error and used to back calculate corrected stresses at mid thickness using the conventional contour method. The procedure was iteratively repeated until the stress distributions converged, that is a variance of less than 5 percent (≤ 5 %) was achieved for the peak tensile stress. The details of the steps used to perform the 2D bulge correction are described next.

Step 1: **Experimental contour method measurement**

The transverse residual stresses at mid thickness of the C(T) sample has been previously calculated using the contour method (see Figure 3 - 3).

Step 2: **Creating the finite element model**

To perform the cutting analysis a 2D model of the specimen was created in ABAQUS, as shown in Figure 3 - 4. A linear elastic homogenous material model was used with Young's modulus, E, and Poisson's ratio, ν, of 205 GPa and 0.29 respectively. A final cut width of 0.3 mm was chosen to represent the material removed by the 250 µm diameter wire used for cutting. An element size of 0.3 mm in the x and y directions was chosen. A plane strain condition was assumed based on the specimen dimensions. The model was meshed with 43 766 quadratic plane strain elements of type CPE8R and contained 132 169 number of nodes. The mesh was refined at the cut and biased by a factor of 4 to the opposite edges.

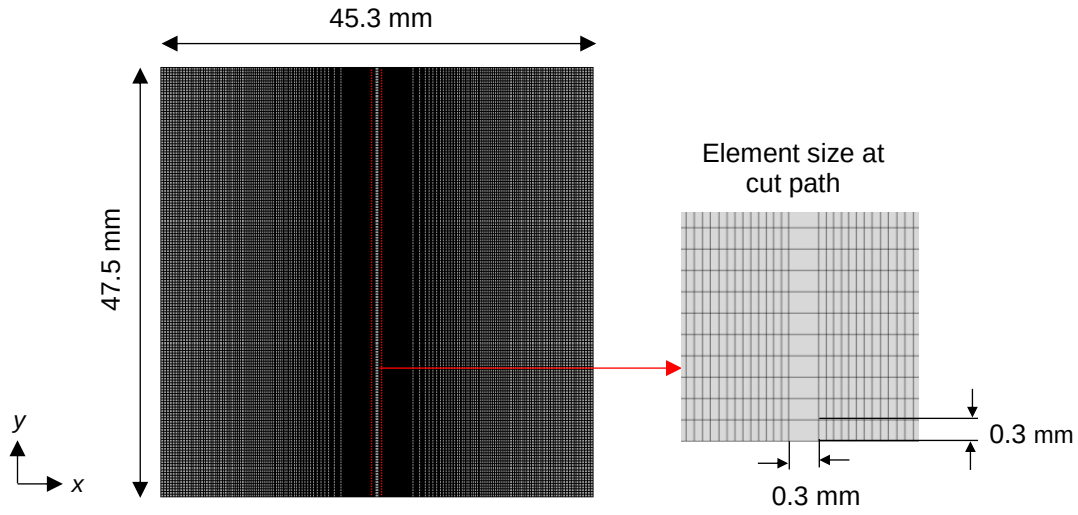

Figure 3 - 4: The 2D FE mesh used to estimate the bulge error in the contour measurement of the C(T) sample.

***Step 3:* Initiating the residual stresses**

An initial residual stress field was defined in the model by using an ABAQUS user subroutine (SIGINI) provided by Prime [118]. This subroutine defined the initial stresses at material points along the cut path as functions of model coordinates. The initial stresses were then introduced in the remainder of the sample using interpolation, i.e. the method assumes a uniform stress distribution along the length of the sample normal to the cut path. This interpolation is performed using an embedded FORTRAN polynomial interpolation subroutine which in general takes a set of data associated with successive values of a parameter and produces an interpolating function which can be evaluated over a continuous range of the parameter [149].

When initial stresses are introduced into an ABAQUS mechanical model, the initial stress state may not satisfy equilibrium. A subsequent static step is applied to allow ABAQUS to check for equilibrium and iterate, if necessary, to achieve equilibrium [119]. A map of the initial residual stress field defined in the model and stresses after reaching equilibrium is shown in Figure 3 - 5 (a) and Figure 3 - 5 (b) respectively. A line profile of the stresses along the cut path at mid thickness of the model is shown in Figure 3 - 6. During the subsequent step, the stress field was modified to satisfy force and moment equilibrium and the boundary conditions ($\sigma_x = 0$ and τ_{xy} = 0 at the edges of the specimen). The peak tensile stress at mid thickness decreased by ~100 MPa. For a complex (varying) stress field, as for the C(T) welded specimen, a line profile of stresses at mid thickness of the specimen is not likely to

be in equilibrium, instead the stresses would be balanced through the thickness of the sample.

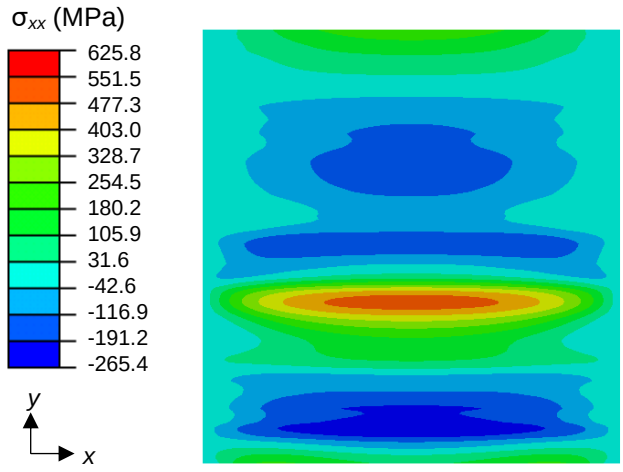

Figure 3 - 5: Map of the contour method residual stresses defined in the 2D FE model (a) before and (b) after equilibrium to be used for iterative bulge correction for the C(T) sample.

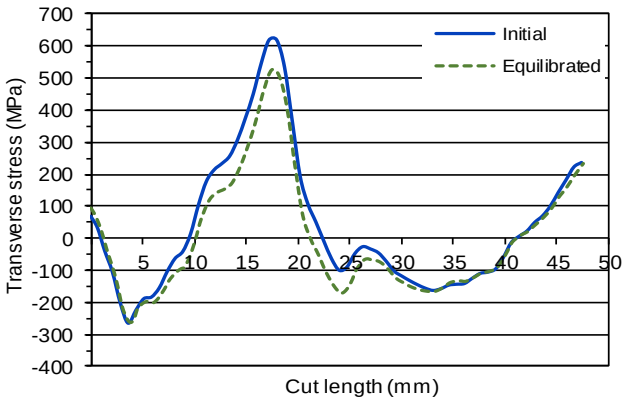

Figure 3 - 6: Line profile of the contour method residual at mid thickness in the FE model before and after equilibrium to be used for iterative bulge correction for the C(T) sample.

Step 4: Applying the restraints for clamping

The restraints applied to represent the asymmetric (one-sided) 'finger' clamping condition used for the slitting technique is shown in Figure 3 - 7. In practice finger clamps prevent the part from moving by applying sufficient vertical clamping force and to some extent the lateral movement is restricted by friction. Since the purpose of the clamping for the contour method is to minimize the lateral movement or opening and closing of the cut, only movement in the x direction is prevented. To implement this, a set of nodes 5 mm from the left edge and all along the cut line were fixed in the x direction. To prevent rigid body motion during cutting

the model was fixed in the y direction at the left top corner node. For this analysis, the left half of the model is referred to as the ‘clamped side’ and the right half the ‘unclamped side.

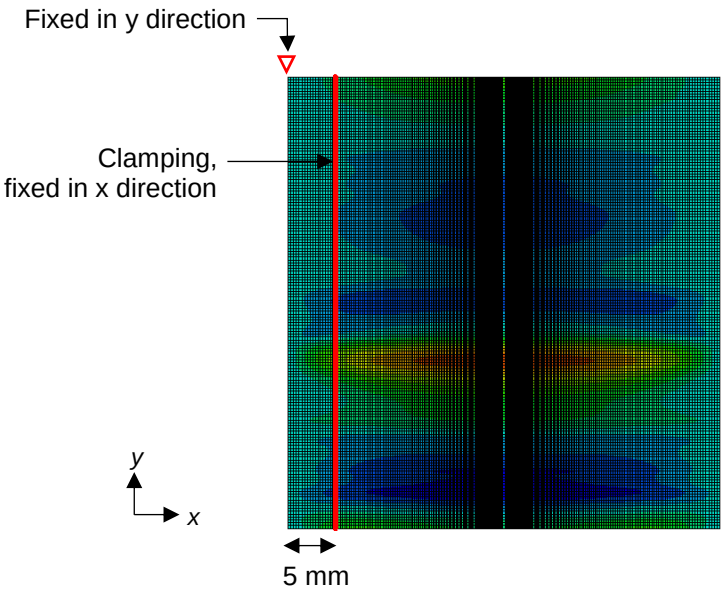

Figure 3 - 7: The FE model used for the bulge error correction of the C(T) sample showing the restraint applied to represent one sided clamping strategy implemented for the slitting measurement.

***Step 5:* Performing the contour cut simulation**

To simulate the cutting step of the contour method the MODEL CHANGE function in ABAQUS was used to sequentially remove elements representing the cut width (see Figure 3 - 4) giving 158 cut increments in total. After each increment the normal displacements at the cut tip (bulge error), U_x, for the clamped and unclamped sides were recorded as history output data. The displacement was measured at two node locations, the corner and mid side entry nodes, shown in Figure 3 - 8. Initially the deviation from the flat cut assumption was suggested by Prime and Kastengren [3] to be the out of plane displacement of the material point where cutting is about to occur, i.e. the bottom corner of the slot. However, Prime later suggested [118] that the wire mid side entry node, which represents the outer position of the EDM wire diameter, is a better location to estimate the bulge error. The final slot width is created at the outer wire diameter position; therefore, the mid side node is a better representation of the slot width and could provide a more accurate estimation of the slot width error.

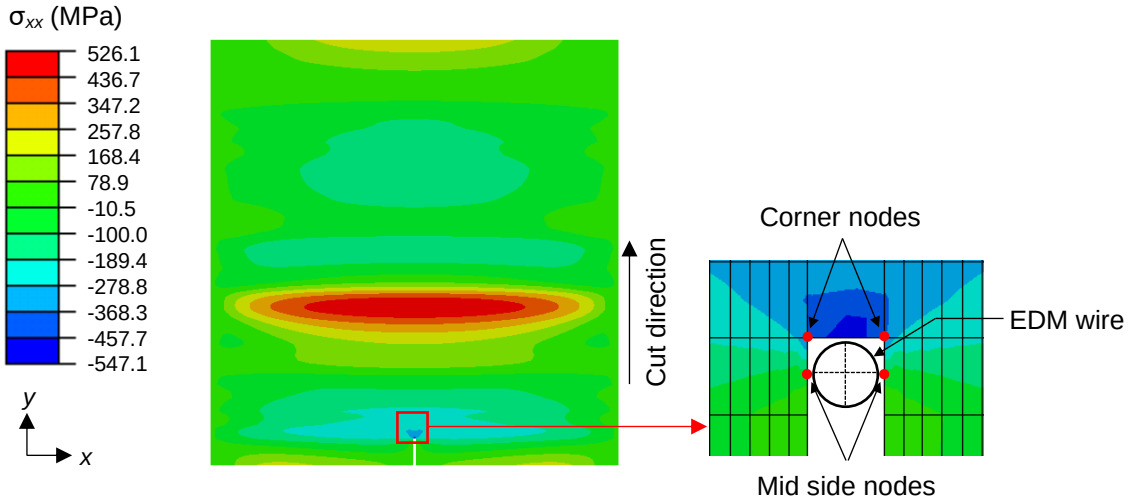

Figure 3 - 8: Redistributed stresses ahead of the cut for the C(T) sample cutting simulation and positions for determining the bulge error at 5 mm cut increment.

Mesh sensitivity study:

The results obtained using the finite element method are dependent on the mesh size and a mesh refinement study must be carried out. Using smaller elements can result in much longer computation times and it is usually a compromise between mesh size and the accuracy of results. Consideration should be given to the optimum element size, that is the smallest element size necessary to obtain converged results, and a practical element size which can be used to ensure a reasonable simulation time and accuracy of the results.

For the mesh sensitivity study, the mesh next to the cut path was incrementally refined to evaluate its influence on the displacement being measured at the cut tip. The element width in the x-direction was evaluated for mesh sizes 0.3, 0.15, 0.075 and 0.0375 mm. The maximum bulge displacement at cut length 19 mm for the mid side location and the first iteration was taken as a reference. It can be seen in Figure 3 - 9 that the magnitude of the bulge displacement increases with mesh refinement. The optimum element size would be 0.0375 mm as the difference between the last two mesh sizes was only 1.5 percentage (%). However, to reduce the simulation time the second to last element size of 0.075 mm was chosen for the cutting analysis.

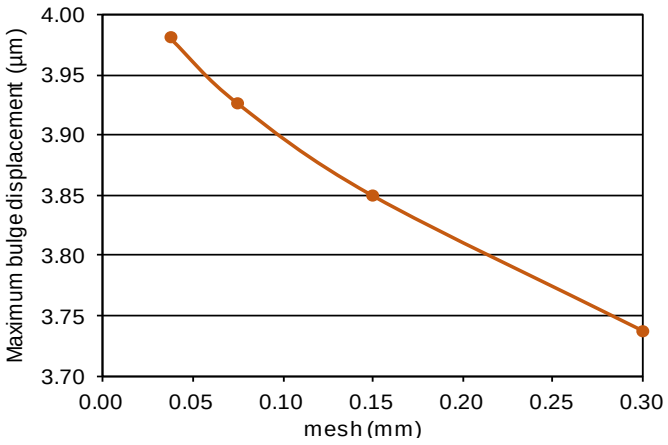

Figure 3 - 9: Variation of the maximum bulge displacement at the mid side location for different mesh sizes next to the cut path.

Step 6 to 10: **Correcting for the bulge error**

When a specimen clamped non-symmetrically is cut for an experimental residual stress measurement, large differences can be seen between the surface deformation measured on the two halves after cutting. However, the stresses calculated using the average surface deformation can provide good stress results [3]. Similarly, the final bulge displacement was first calculated for the clamped and unclamped sides separately using Equation 2-8 in section 2.7.2. Then the displacement data from both sides were averaged using Equation 2-9. The average bulge displacement profile was interpolated to correspond with the 0.5 mm grid spacing used for the experimental surface deformation data processing. This was done in MATLAB with the cubic spline interpolation [150] function.

Then a line profile of the experimentally measured surface deformations at mid thickness of the specimen were corrected for bulge using Equation 2-10. However, the surface deformations are not corrected at the start and end of the cut since there is no bulge error measured at the free edges of the specimen. This may lead to large discrepancies in the corrected surface deformation profile and result in erratic stresses near the edges of the specimen. Therefore, the corrected surface deformations were extrapolated to the start and end edges of the specimen using the MATLAB cubic spline extrapolation function.

To back-calculate the corrected stresses a 2D model of one half of the C(T) specimen was created in ABAQUS, shown in Figure 3 - 10. A linear elastic material model was used with Young's modulus, E, and Poisson's ratio, ν, of 205 GPa and 0.29 respectively. A mesh sensitivity study, also depicted in Figure 3 - 10, showed that an optimum element size of 0.15 mm next to the cut surface was suitable to calculate the stresses. The mesh was

concentrated at the cut face and biased toward the opposite edge. The mesh was created with 3780 linear plane strain elements of type CPE4 and 3904 nodes. The top corner node was fixed in the y direction to prevent rigid body motion. The corrected surface deformation was applied as a boundary condition to the nodes on the cut surface and an elastic stress analysis was performed.

Finally, to perform the next iteration, the new corrected stresses were defined in the cutting model (Figure 3 - 4) as an initial condition and the contour cut simulation and bulge correction procedures repeated until a converged solution was reached for the stresses. The corrected stresses converged after the third iteration. The results for the 2D bulge correction are presented next.

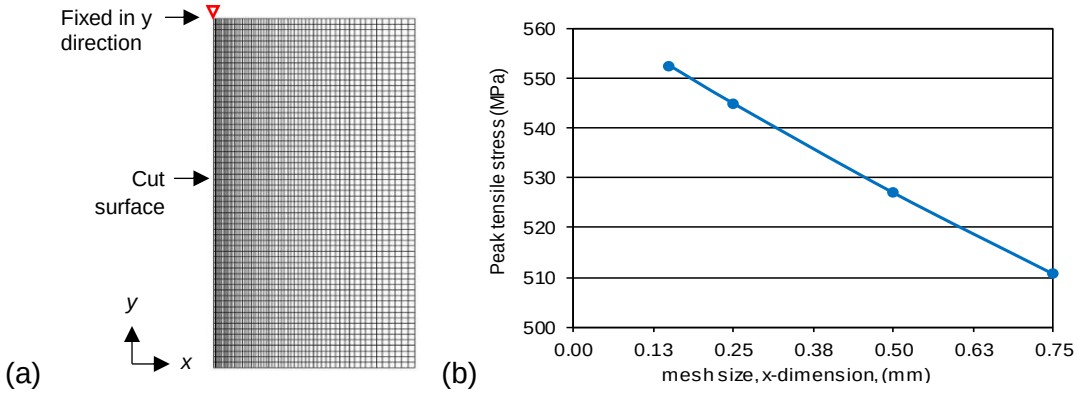

Figure 3 - 10: (a) The mesh of the FE model used to back calculate the corrected contour stresses for the C(T) sample, also shown is the boundary condition applied to prevent Rigid Body Motion. (b) Mesh sensitivity analysis showing the variation of the peak stress for the C(T) sample for different mesh sizes (x-dimension) at the cut surface.

3.1.4 Results and discussion of 2D bulge error correction

For the 2D bulge error analysis, it was important to first understand how using a line profile of the experimentally measured surface deformations at mid-thickness to correct the stresses would differ from using the surface deformations on the entire cut surface as in the experimental contour procedure (3D analysis). To do this the initial surface deformation at mid-thickness, i.e. before bulge correction, was applied as a boundary condition in the 2D model of one half of the C(T) specimen (see Figure 3 - 10) to back calculate the stresses. Figure 3 - 11 compares the initial stresses obtained using 2D FE analysis with the contour method measured stresses at mid-thickness based on 3D analysis (see Figure 3 - 6). The stresses using 2D FE analysis did not give the same magnitude stresses as the 3D analysis. The peak tensile stress at 18 mm decreased by 10 % (to 552.5 MPa) and the peak

compressive stress at 3.75 mm increased by 17 % (to -314.3 MPa). The stresses most likely changed to satisfy equilibrium as described previously.

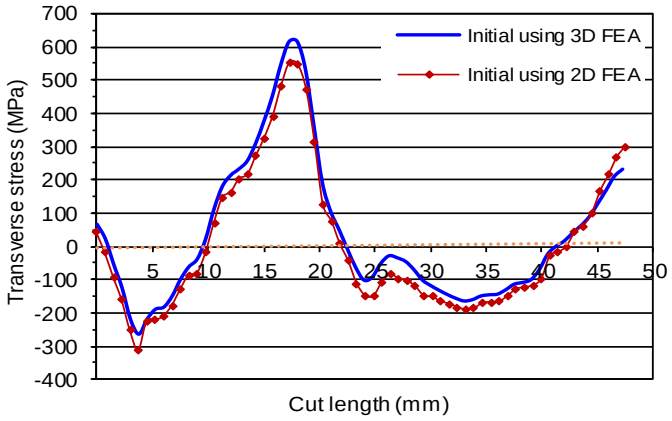

Figure 3 - 11: Comparison of the initial experimental contour method measured stresses at mid-thickness based on 3D FE analysis and the initial stresses obtained using 2D FE analysis.

The average bulge displacement for each iteration is shown in Figure 3 - 12. A negative bulge displacement corresponds to cutting through compressive stresses causing the cut tip to contract and a positive displacement to tensile stresses causing the cut tip to stretch. The maximum mid-side bulge correction (3.7 µm) is almost 3 x greater than the corner bulge correction (1.3 µm), though both are located at roughly 20 mm cut length. This is close to the tensile region located around the electron beam weld at 18 mm. The initial surface deformation and corrected surface deformation at mid-thickness after iteration is shown in Figure 3 - 13. For the initially measured surface deformation range of ± 17 µm (ignoring the first 5 mm cut length), the maximum corner bulge correction is ~8 % of the displacements and the mid side bulge correction is ~22 % of the displacements. The shift in the contour profile is more significant for the mid-side correction.

The corrected contour stresses after each iteration are shown in Figure 3 - 14. For the third iteration, the peak tensile stress decreased by 12 % for the corner correction and 5 % for the mid side correction. Both results showed a slight shift (0.754 mm) in peak tensile stress position towards the cut end.

As demonstrated earlier using a line profile of the experimental measured surface deformations at mid-thickness to back-calculate the stresses at mid-thickness gave stresses that were initially not in equilibrium. ABAQUS modified the stress field to achieve equilibrium in a subsequent step. Consequently, this gave unreliable corrected stresses

after bulge correction. For a specimen with a complex (varying) residual stress field, 3D bulge correction is probably necessary. This will be investigated for the C(T) welded specimen in the next section.

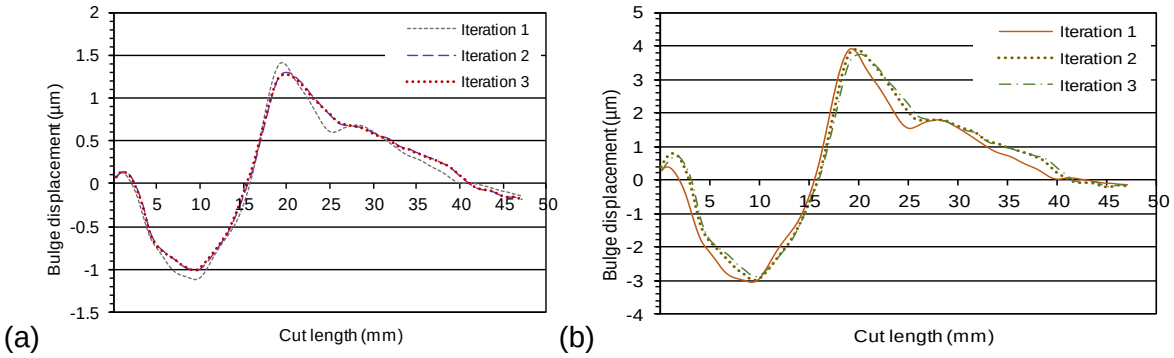

Figure 3 - 12: Average bulge displacement for the C(T) sample at the (a) corner and (b) mid-side locations for each iteration using 2D correction procedure.

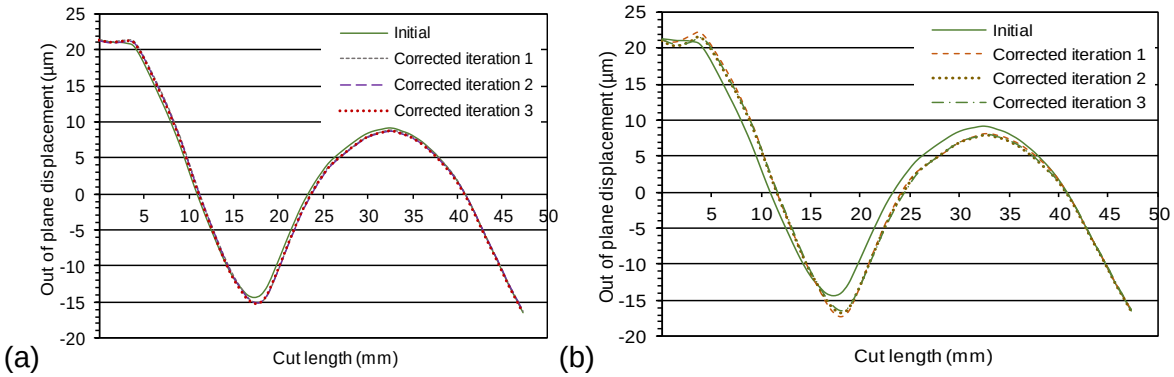

Figure 3 - 13: Initial average out of plane displacement for the C(T) sample along the mid thickness of the contour cut plane and the corrected displacement for bulge error for each iteration using 2D correction procedure for the (a) corner and (b) mid-side bulge measurement.

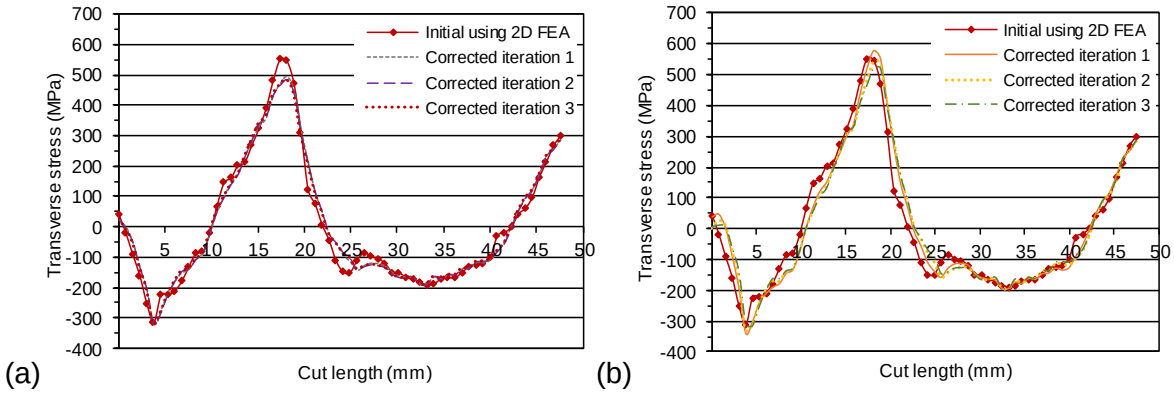

Figure 3 - 14: Initial stresses at mid-thickness of the C(T) sample using 2D FE analysis and the corrected stresses for bulge error for each iteration using the (a) corner and (b) mid side bulge measurements.

3.1.5 3D bulge correction procedure

The previous section implemented a 2D bulge correction procedure based upon the mid thickness stress profile measured in the C(T) sample using the contour method. Here the bulge correction procedure, described in section 2.7.2, is extended to a 3D analysis to correct the previously measured contour method stresses on the entire cut surface.

In this procedure, contour method measured residual stresses across the cut surface were applied as an initial condition in a 3D FE model of the C(T) entire sample including constraints for one-sided clamping. The cutting process was then simulated by sequentially removing rows of elements to predict the displacements along the length of the cut tip at each cut increment. After the bulge displacements were estimated, the measured displacements on the cut surface were corrected and used to back calculate the corrected stresses using the conventional finite element procedure performed for the contour method. The procedure was iteratively repeated until the stress distributions converged, that is a variance of less than 5 percent (≤ 5 %) was achieved for the peak tensile stress. The details of the steps used to perform 3D bulge correction are described next.

***Step 1:* Experimental contour method measurement**

The transverse residual stresses at mid thickness of the C(T) sample has been previously calculated using the contour method (see Figure 3 - 3).

Step 2: Creating the finite element model

In order to embed measured residual stresses into a FE model of the C(T) sample, a 3D model of one half of the specimen was created in ABAQUS. The cross section of the cut surface was built based on the measured perimeter from the contour method measurement and then extruded in the length, z, direction to create a 3D model of one half of the C(T) sample, shown in Figure 3 - 15. A linear elastic material model was used with Young's modulus, E, and Poisson's ratio, ν, of 205 GPa and 0.29 respectively. The model was meshed with 100 170 quadratic hexahedral elements of type C3D20R and 427 318 nodes. The cut width was 0.3 mm for the 250 µm diameter wire used for cutting. The mesh size at the cut was 0.75 mm x 0.3 mm x 0.15 mm in the x, y and z directions respectively. The mesh through the length, i.e. in the z direction, was kept uniform for 5 mm and then biased by a factor of 4 to the opposite edge to reduce the computation time.

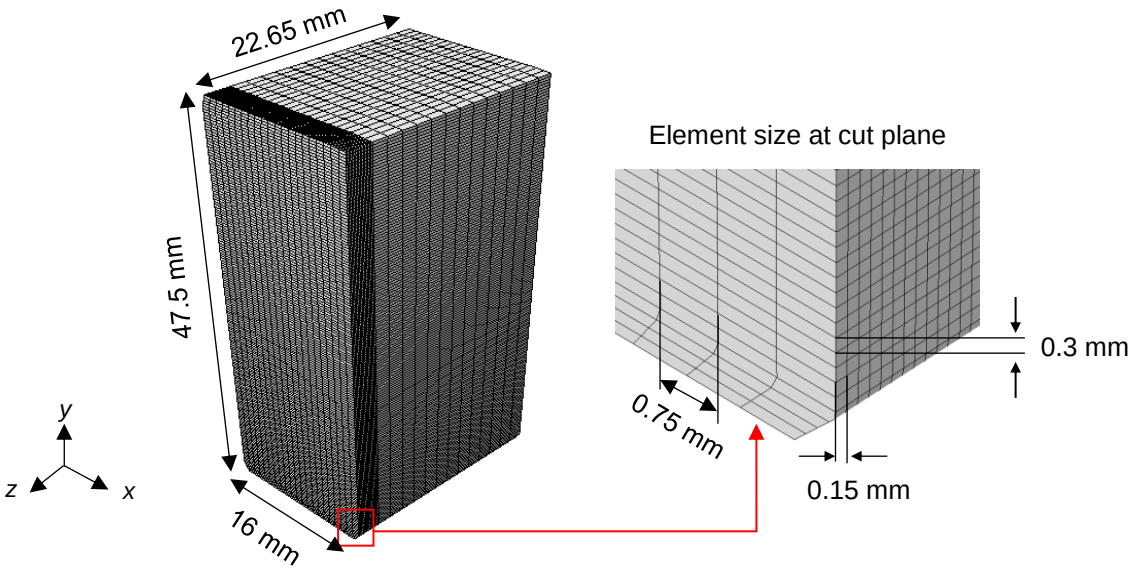

Figure 3 - 15: 3D FE model of the C(T) sample used for bulge error estimation.

Step 3: Introducing initial residual stresses

To define the initial stress field in the model Prime and Kastengren [3] have proposed employing a user-defined SIGINI subroutine and assuming a uniform stress distribution across the entire sample length. For 3D modelling, this would require a complex SIGINI subroutine to be scripted. An alternative method is to map the stress results from the experimental contour FE model directly in a new 3D model for the cutting simulation. However, in the contour calculation, the stresses away from the cut surface equilibrate to

satisfy the stress-free condition at the edges of the specimen i.e. the stresses diminish with increasing distance from the cut surface. Though only the stresses at the cut surface are expected to have a significant effect on the local bulge displacement required to be measured at the cut tip.

Therefore, the residual stresses from the contour method measurement (Figure 3 - 3) were defined in the model for bulge estimation as an initial stress field using the MAP SOLUTION function in ABAQUS. A static step was included to allow the model to equilibrate. There was only a slight change (< 10 MPa) to the mapped stress field shown in Figure 3 - 16 which results from the ABAQUS interpolation for the new mesh size.

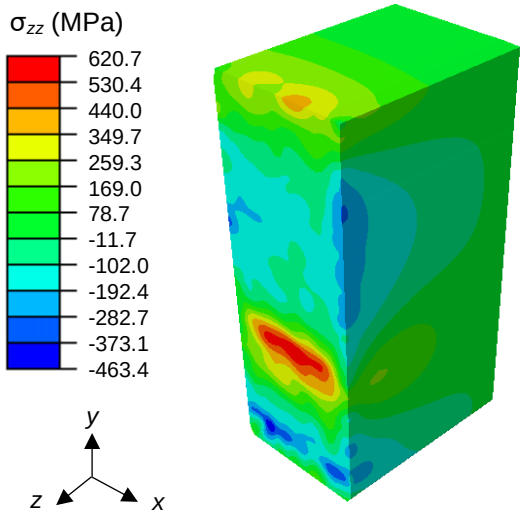

Figure 3 - 16: Contour method stresses mapped onto the new 3D FE model to be used for iterative FE bulge correction for the C(T) sample.

***Step 4:* Applying restraints for clamping**

Due to the specimen being clamped on one side during EDM cutting, a model of the entire specimen (no half symmetry) is required to correctly represent the clamping condition so that the bulge error can be estimated for the clamped and unclamped sides during the cutting analysis. To create a full model of the C(T) specimen, the SYMMETRIC MODEL GENERATION and SYMMETRIC RESULTS TRANSFER functions in ABAQUS were used to transfer the stresses to a full 3D model for the cutting analysis shown in Figure 3 - 18. The restraints applied to represent the asymmetric (one-sided) clamping condition used for the slitting technique is also shown in Figure 3 - 17. A set of nodes at the top and bottom left edge were fixed in the z direction to prevent lateral movement on one side of the

specimen during cutting. For this analysis, the left half of the model is referred to as the 'clamped side' and the right half the 'unclamped side'.

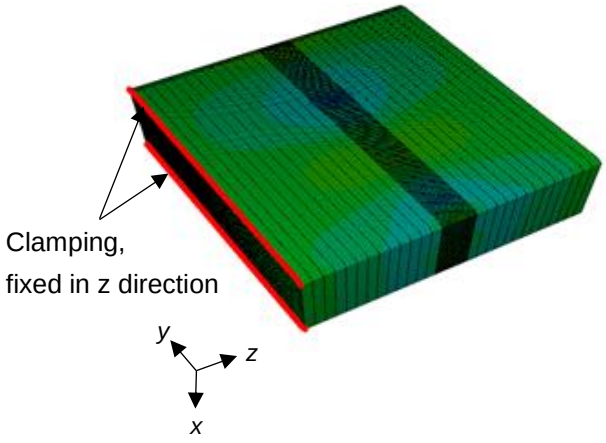

Figure 3 - 17: Full 3D model used for bulge error correction for the C(T) sample and restraint applied to represent the one sided clamping implemented for the slitting measurement.

Step 5: **Performing a contour cut simulation**

The MODEL CHANGE function in ABAQUS was used to sequentially remove two rows of elements for each of 79 cut increments. After each increment the displacements at the cut tip (bulge error), U_z, must be recorded for the clamped and unclamped sides through the thickness of the specimen. The error evaluation positions for the 3 mm cut increment are shown in Figure 3 - 18.

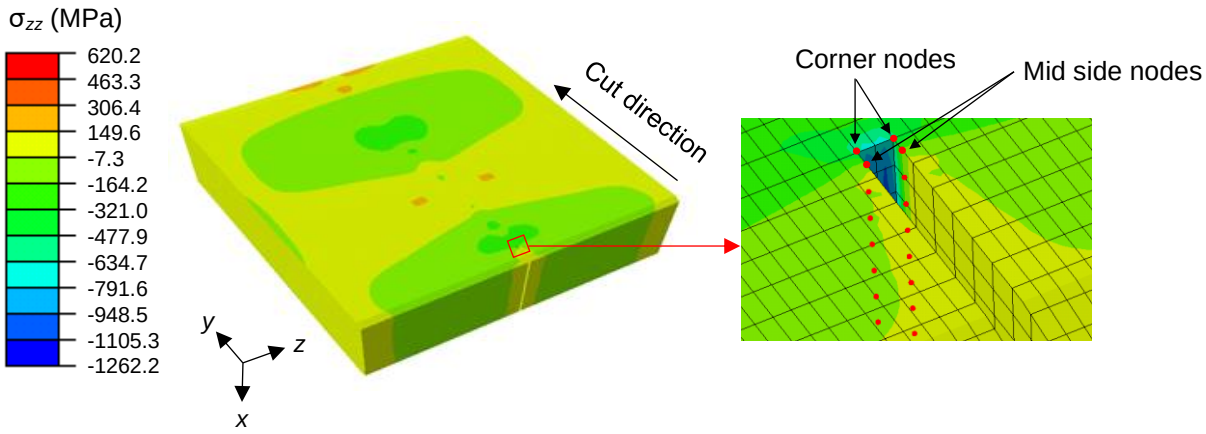

Figure 3 - 18: Redistributed stresses ahead of the cut for the C(T) sample cutting simulation and positions for evaluating bulge error displacements at the 3 mm depth cut increment.

An ABAQUS Python script was created to extract the displacements at each cut increment and subtract the displacement after the equilibrium step to give the final bulge displacement for the clamped and unclamped sides separately using Equation 2-8 in section 2.7.2. Then the final bulge corrections from both sides were averaged using Equation 2-9. Lastly, the average bulge correction was interpolated for the grid spacing used for the experimental surface deformation data processing that is 0.5 mm spacing, in the x and y directions. This was done in MATLAB with the scatter interpolation function using natural neighbour interpolation which gave the least number of outliers through the thickness compared with the linear and nearest neighbour interpolation.

Step 6 to 10: **Correcting for the bulge error**

The initial averaged surface deformations on the cut surface experimentally measured for the contour method were then corrected using Equation 2-10. As explained in the 2D correction procedure, the corrected displacements should be extrapolated to the free edges of the specimen to avoid erratic stress results in this region. This was done in MATLAB with the scatter interpolation [150] function by specifying nearest neighbour extrapolation.

To back-calculate the corrected stresses, the original FE model of one half of the C(T) specimen (Figure 3 - 3) was used to apply the corrected averaged displacement as a boundary condition to the nodes on the cut surface and an elastic stress analysis performed.

For the iteration step the new corrected stresses were introduced into the cutting model (Figure 3 - 16) as an initial condition and the contour cut simulation and bulge correction procedures repeated until a converged solution was reached for the stresses. The corrected stresses converged after the second iteration. The 3D bulge corrected results are presented next.

3.1.6 Result and discussion of 3D bulge error correction

The average bulge displacements after one iteration is shown in Figure 3 - 19. A negative bulge displacement corresponds to a reduced cut width and a positive displacement to a stretched cut width. The maximum mid side bulge correction (4.1 µm) is 2.5 x greater than the corner bulge correction (1.6 µm) and both are located at roughly 19 mm cut length. This is quite close to the electron beam weld located at 18 mm. The initial surface deformation at mid thickness and corrected surface deformation at mid thickness after iteration is shown in Figure 3 - 20. For the initially measured contour range of ± 17 µm (ignoring the first 5 mm cut length), the maximum corner correction is 9 % of the displacements and the mid side

correction is 24 % of the displacements. These results are remarkably close to the bulge correction obtained for the 2D FE analysis considering the uncertainties in the changing stresses.

A 3D map of the corrected stresses on the cut surface after the first iteration is shown in Figure 3 - 21 and the results at mid-thickness after iteration in Figure 3 - 22. After iteration, the peak tensile stress at mid-thickness of the specimen (616.9 MPa) increased by 7.1 % (to 660.70 MPa) for the corner correction and 20.4 % (to 742.80 MPa) for the mid side correction. Though both results showed a negligible shift (0.001 mm) in peak tensile stress, a slight shift in the stress profile towards the cut end can be seen. Special care has been taken to extrapolate the displacements near the edges of the cut which has given reliable stress results in this region.

Further work is needed to understand how the applied restraint conditions influence the bulge prediction and whether the stress distribution in the remainder of the model has an important influence.

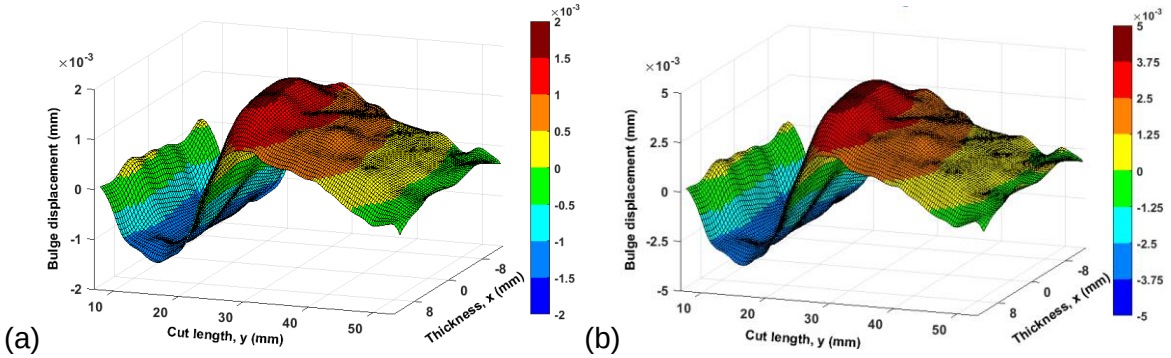

Figure 3 - 19: Average bulge displacement for the C(T) sample at (a) the corner node and (b) the mid-side node locations using the 3D correction procedure after the second iteration.

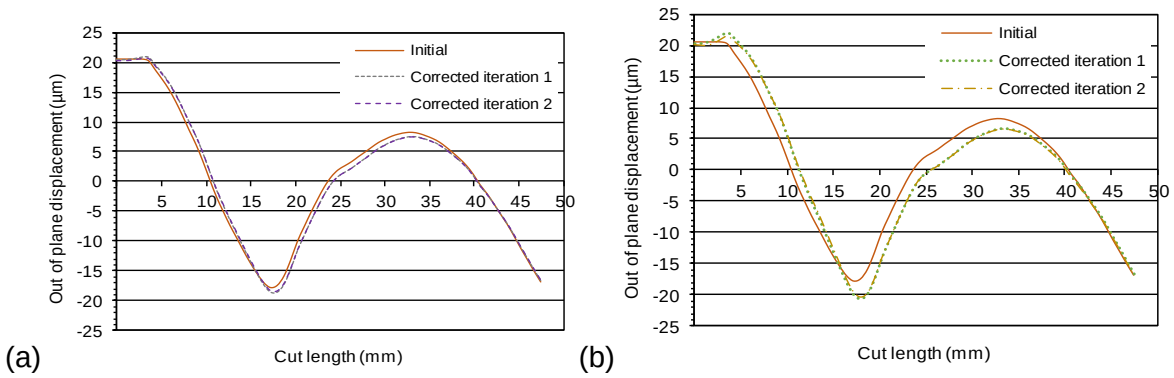

Figure 3 - 20: Initial average out of plane displacement for the C(T) sample along the mid thickness of the contour cut plane and the corrected displacement for each iteration using the 3D correction procedure and (a) the corner node and (b) the mid-side node bulge error estimates.

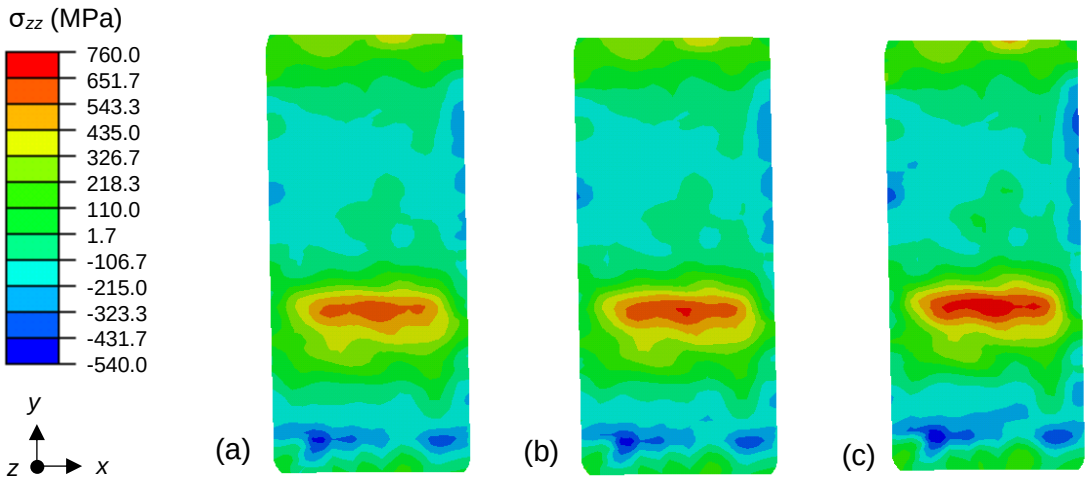

Figure 3 - 21: (a) Initial transverse stress map on the cut surface of the C(T) sample measured using the contour method and the map of corrected stresses for the bulge error using 3D FE analysis based on (b) the corner node and (c) the mid-side node bulge error estimates after the first iteration.

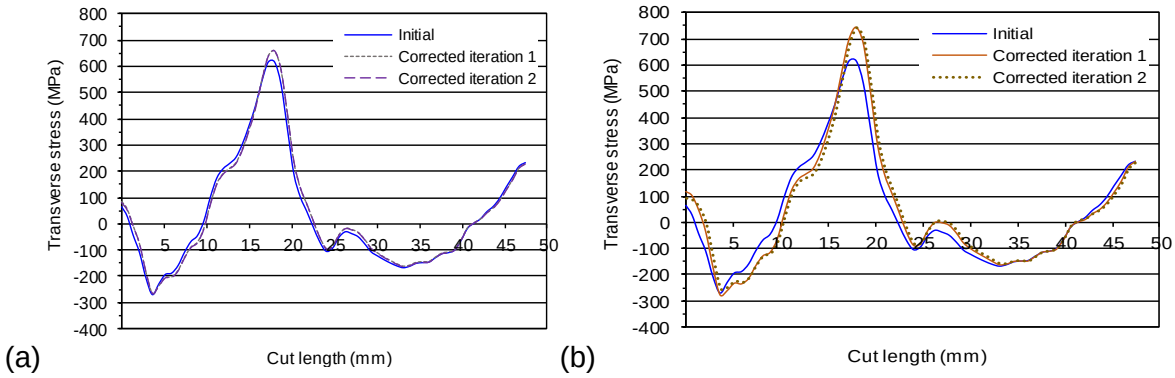

Figure 3 - 22: Line profile distribution of transverse stress along the mid thickness of the contour cut plane showing the initially measured stresses and stresses corrected for bulge displacements obtained from (a) the corner node and (b) the mid-side node locations using 3D FE analysis.

Comparison of neutron, slitting and contour method results:

The graph comparing the initially measured stresses using neutron diffraction, slitting and contour method techniques (Figure 3 - 3), is revised in Figure 3 - 23 to include the corner and mid-side position corrected contour method stresses from the 3D bulge correction analysis. It is evident that the 3D bulge corrected results correlate more closely with the neutron diffraction and slitting measurements with the mid-side correction giving significantly better results.

The peak tensile stress from the mid side corrected contour method measurement (743 MPa) was greater by 103 MPa and 153 MPa than the neutron diffraction and slitting measurements respectively. The slitting technique measures the average stresses across the thickness of the specimen; therefore, these stresses are expected to be lower in magnitude. The neutron diffraction stresses are also averaged over the gauge volume. If the uncertainty in the neutron diffraction results (± 25 MPa) is included, then the difference is reduced to 78 MPa. The corrected contour method profile was shifted slightly (negative y-direction) towards the neutron diffraction and slitting measurements. This supports the author's conjecture that the shift is potentially a result of the presence of compressive plasticity associated with non-ideal (one-sided) restraint condition used during cutting [4, 34].

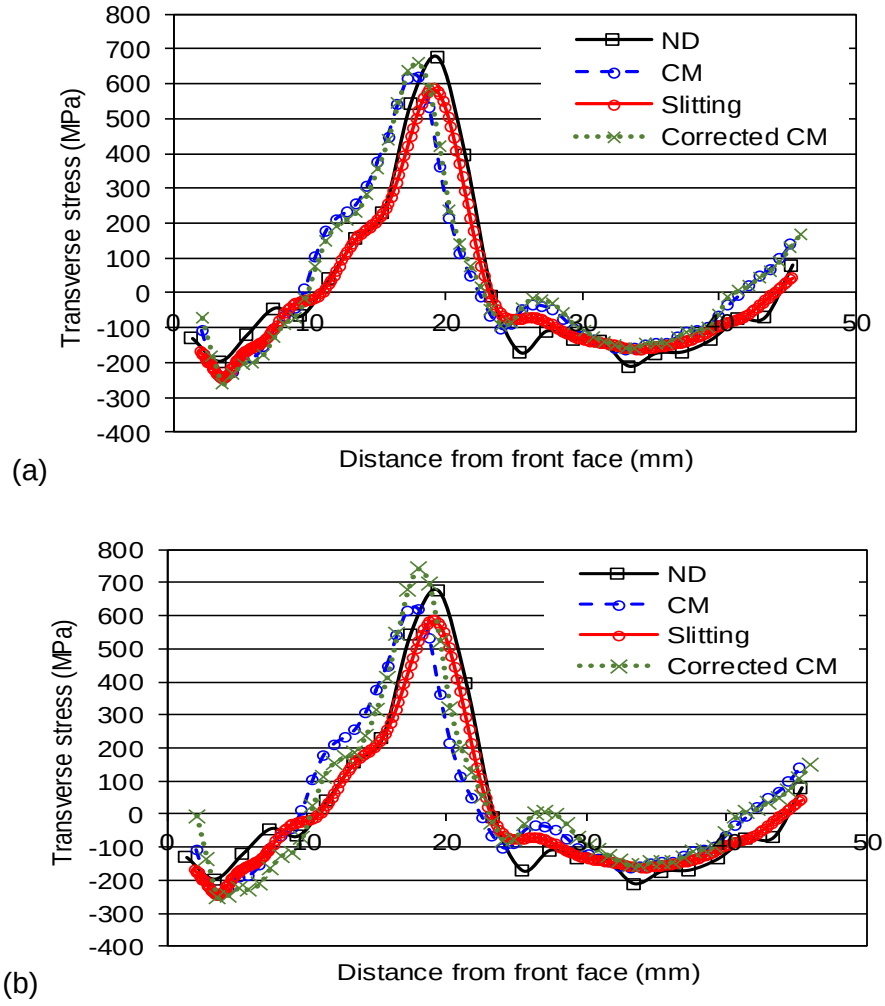

Figure 3 - 23: Comparison of the transverse residual stress distribution at mid-thickness of a C(T) sample measured by neutron diffraction, slitting and the contour method and the corrected contour method results using 3D FE analysis with bulge displacements obtained from (a) the corner and (b) mid side locations.

3.2 Alternative stress correction procedure

In this section an alternative approach to calculate corrected stresses from estimated bulge displacements is proposed. The proposed approach is less cumbersome than the procedure discussed previously. It involves using estimated bulge displacements directly in a contour type of elastic FE analysis to calculate the stress error. The obtained stress error is then used to correct the initial contour method measured stresses. The approach is valid because the solid mechanics analyses are linear elastic. The advantage of this procedure is that the complexity of the bulge correction is reduced, and the initially measured surface deformations are not required for determining the bulge error.

In this section the steps of the iterative FE bulge correction procedure, explained in section 2.7.2, are revised for the proposed approach. Then the procedure is implemented for the C(T) specimen case study to correct the contour method stresses for the bulge error using 2D and 3D analysis. The results from the original and alternative stress correction approaches are then compared.

3.2.1 Revised bulge correction procedure

The initial steps to perform the cutting analysis and estimate the bulge displacements (steps 1 to 5 below which are described in more detail in section 2.7.2) are the same, therefore the revised procedure starts from step 6 below.

Step 1: Complete a contour method measurement to determine the residual stresses in the specimen.

Step 2: Create a finite element model of the specimen in ABAQUS to perform a linear elastic simulation of the EDM cutting procedure.

Step 3: Initialize the contour method stresses in the model and perform a general stress analysis step to allow the stresses to reach equilibrium.

Step 4: Apply restraints to represent the clamping condition during EDM cutting and to prevent rigid body motion.

Step 5: Sequentially remove elements to simulate the cutting step and record the local bulge displacements at the cut tip for each cut increment.

Step 6: Process the bulge displacement data to correct the initial measured stresses from implementing the contour method procedure.

Step 7: Calculate the stress error using the conventional contour method procedure, by creating a finite element model of one half of the specimen in ABAQUS and applying the opposite of the bulge displacements as boundary conditions on the cut surface and performing an elastic stress analysis. The back calculated stresses are the stress error ($\sigma_{stress\ error}$) due to the bulge.

Step 8: Add the stress error calculated in step 7 to the initially measured stresses ($\sigma_{initial\ CM\ stress}$) to obtain the corrected contour stresses.

$$\sigma_{corrected\ CM\ stress} = \sigma_{initial\ CM\ stress} + \sigma_{stress\ error} \qquad \textit{Eqn. 3 - 1}$$

Step 9: Iteration is necessary since the first estimate of the bulge error is based on the stresses calculated assuming no bulge error. To perform the iteration, steps 3 to 8 are repeated by initializing the corrected stresses in the cutting simulation and re-estimate the bulge displacements. For each iteration, the new stress error is added to the initially measured stresses and not the corrected stresses from the previous iteration.

Step 10: Finally check whether the corrected stresses have converged. An incremental change of ≤ 5 % of the peak tensile stress has been used in the present study to indicate convergence.

3.2.2 Application of the alternative approach

In this section the alternative approach is implemented using 2D analysis to correct the C(T) welded specimen stresses at mid-thickness and then using 3D analysis to correct the stresses on the entire cut surface. In both analyses, the bulge displacements for the first iteration have already been predicted in section 3.1.3 and 3.1.5. Therefore, this section only describes the alternative procedure used to calculate the stress error and correct the stresses. Only the mid side bulge location is evaluated since this gave a better bulge error correction and was selected as the final result in the previous study.

(1) 2D bulge correction

To calculate the stress error, step 7 in section 3.2.1, the opposite of the final average bulge displacements for the first iteration, shown in Figure 3 - 12, was applied as a boundary condition to the cut surface of the 2D FE model shown in Figure 3 - 10. Before doing this, it was necessary to extrapolate the bulge displacements to the edges of the specimen since there is no bulge displacement measured at the start and end of the cut. This was done in MATLAB using the cubic spline extrapolation function.

The stress error was then combined with the initial contour method stresses at mid thickness to give the new stress results using Equation 3-1 in step 7. Iteration was performed according to steps 8 and 9 and a converged stress solution was reached after two iterations.

The corrected stresses after each iteration are shown in Figure 3 - 24. After the second iteration, the peak tensile stress increased by 19.6 % (to 738.03 MPa) and a slight shift in the stress profile towards the cut end can be seen. The corrected stresses are very similar to the previous 3D results at mid-thickness (Figure 3 - 22). This is a very promising result considering the bulge estimation is based on the stresses which decreased after equilibrating (Figure 3 - 5 (b)). In Figure 3 - 25 the corrected stresses at mid thickness are

compared with the corrected stresses using the original procedure where the corrected tensile stresses decreased after iteration.

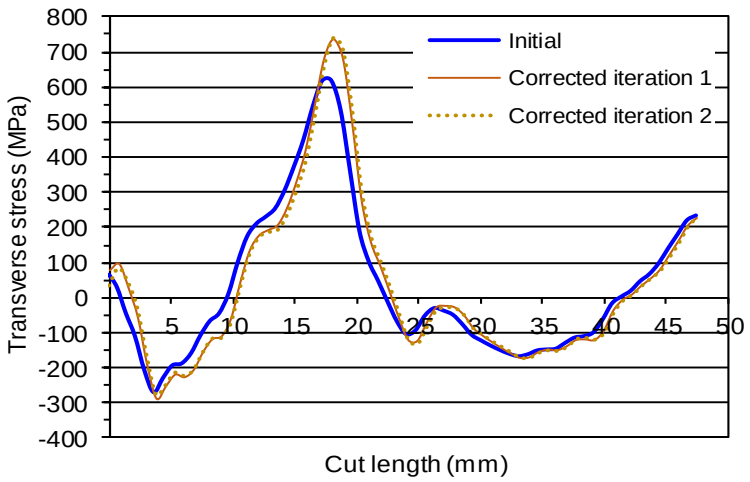

Figure 3 - 24: Line profile distribution of transverse stress along the mid thickness of the contour cut plane showing the initial measured stresses and stresses corrected for bulge error using the proposed alternative procedure for bulge displacements obtained from the mid side node location using 2D iterative FE analysis.

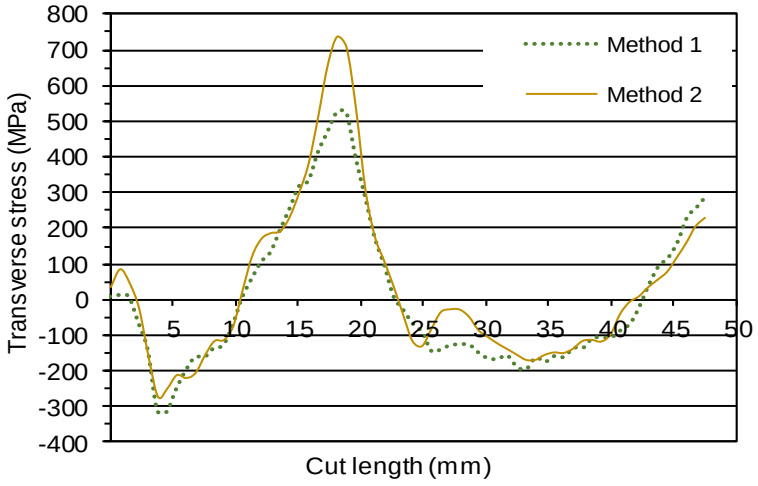

Figure 3 - 25: Comparison of the 2D corrected stresses for the C(T) sample at mid-thickness using the original bulge error correction procedure (method 1) and the proposed alternative approach (method 2).

(2) 3D bulge correction

To calculate the stress error, step 7 in section 3.2.1, the opposite of the 3D map of bulge displacements, shown in Figure 3 - 19, were applied as boundary conditions to the FE model

of half of the C(T) sample (see Figure 3 - 15) and elastic stress analysis was performed. As previously explained, the bulge displacements were first extrapolated to the edges of the specimen in MATLAB with the scatter interpolation function by specifying nearest neighbour extrapolation.

The stress error was then combined with the initial contour method stresses on the cut surface to give the corrected stress results using Equation 3-1 in step 7. Iteration was performed according to steps 8 and 9 and a converged stress solution was reached after two iterations. The corrected stresses on the cut surface for the first iteration were visualized in MATLAB using a contour plot, shown in Figure 3 - 26. The corrected stresses at mid thickness are compared with the corrected stresses using the original procedure in Figure 3 - 27. As expected, the results from both approaches are in excellent agreement due to the nature of linear elastic stress analysis.

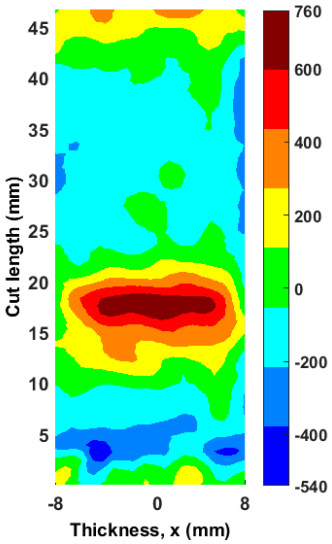

Figure 3 - 26: Map of the corrected transverse stresses on the contour cut plane after iteration using the proposed alternative correction procedure and the bulge displacements obtained from the mid side node location using 3D FE analysis.

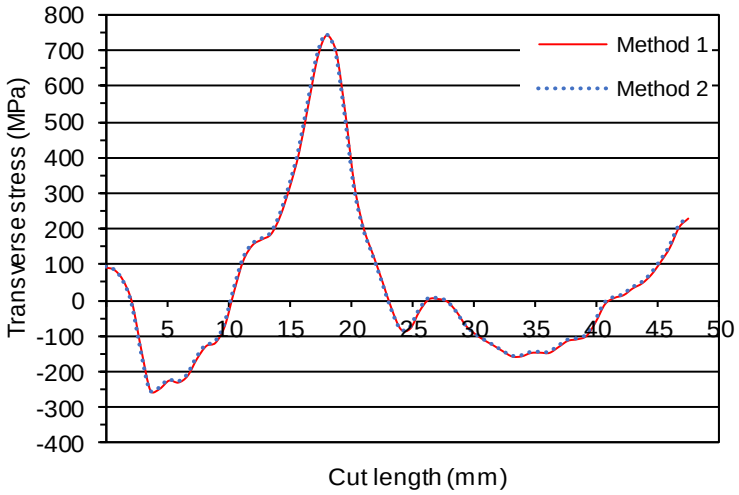

Figure 3 - 27: Comparison of the 3D corrected stresses for the C(T) sample at mid-thickness using the original bulge error correction procedure (method 1) and the proposed alternative approach (method 2).

(3) Comparison of 2D and 3D bulge correction

For the 2D correction the stress error was estimated for the mid-thickness stresses based upon a 2D FE model of the cutting process and the correction was applied to the measured mid thickness stress profile from the 3D contour measurement. Whereas for the 3D correction the stress error was estimated for the stresses across the cut surface based upon a 3D FE model of the cutting process and the stress correction was applied to the entire 3D contour measurement.

A comparison of the 2D and 3D corrected contour stress profiles at mid-thickness using the alternative procedure for each iteration is shown in Figure 3 - 28. The corrected stresses for both iterations agree very well. This result is promising as it shows that, even for a complex (varying) contour residual stress map, the bulge error can be corrected for along a line by using simplified 2D analysis, thus avoiding the need to perform complex 3D analysis.

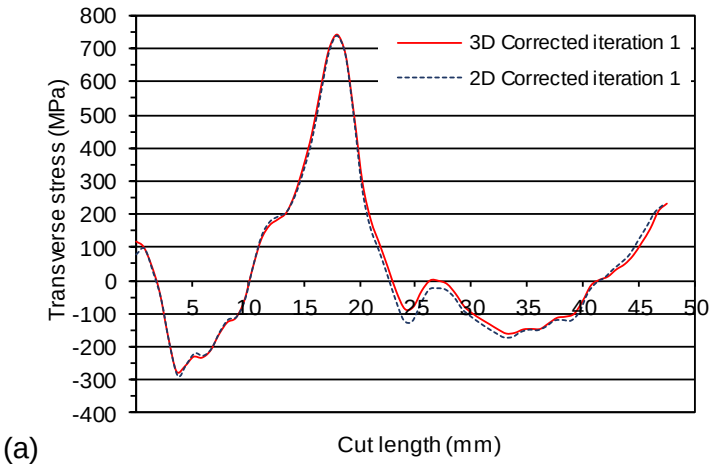

(a)

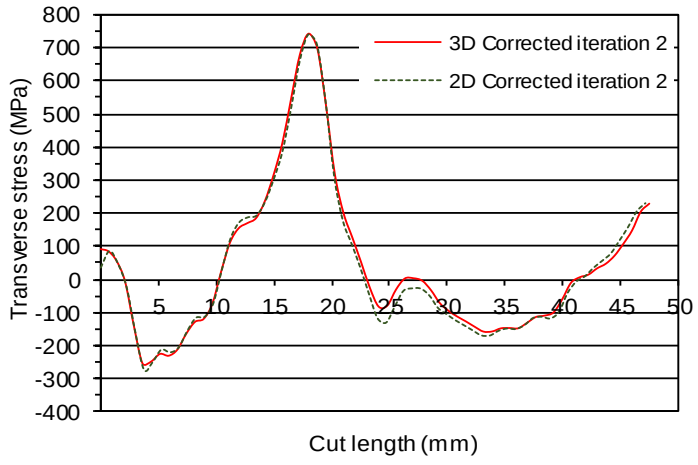

(b)

Figure 3 - 28: Comparison of corrected contour stresses at mid thickness based on 2D and 3D FE bulge stress error correction analyses for (a) the first and (b) the second iteration.

3.3 Discussion

In this chapter the published iterative FE bulge error correction procedure [3] of Prime and Kastengren was applied to a C(T) weld specimen that appeared to show symptoms of bulge error in the measured residual stress results made by the contour method. The capability of the bulge correction procedure to correct the complex (varying) residual stress field was investigated using a simplified 2D approach and a more robust 3D approach.

In the 2D approach a line profile of the contour method stresses at mid thickness were corrected for the bulge error. The experiment measured stress profile at mid thickness was used as an initial condition in a two-dimensional finite element contour cutting simulation in ABAQUS to estimate the bulge error. The magnitude of the tensile stresses in the model reduced by 16 % during the first analysis equilibrium step prior to cutting but the stress profile remained sufficiently representative to give a reasonable estimate of the bulge

displacement error. A line profile of the experimental contour displacements at mid thickness were corrected for bulge error and used to back calculate corrected contour stresses at mid thickness. After three iterations the corrected stresses showed reduced tensile stresses relative to the equilibrated 2D FE model and increased compressive stresses which is not consistent with published contour method measurements corrected for bulge error [3, 65]. Using the contour method stresses that are averaged across the thickness of the specimen is more likely to be balanced but varying residual stress fields will change significantly. Therefore, for a specimen with a complex (varying) residual stress field, 3D bulge correction is probably necessary.

In the 3D approach the contour method stresses on the entire cut surface were corrected for the bulge error. The stresses on the cut surface would be physically self-balanced and provide a more accurate finite element bulge estimation and correction procedure in ABAQUS. A converged stress solution was reached after two iterations. The peak tensile stress was increased from 617MPa to 743MPa (~20%) and slightly shifted towards the end of the cut . These changes in the stresses are expected after bulge correction and confirmed that the 3D approach is robust. The increase in magnitude of the corrected contour stresses demonstrated that the bulge error can significantly compromise the accuracy of measurements made using the contour method.

The geometric/nodal positions used to estimate the displacement at the cut tip in the FE analysis was also examined and found to be important. The magnitude of the estimated displacement errors at the cut tip were found to be up to 9 % of the measured surface deformations for the corner node position and up to 24 % for the mid side position. For the corner node, this agrees with a similar study, for an electron beam (EB) welded C(T) specimen, which found the displacements at the cut tip to be 10 % of the average displacements on the surface [65]. The estimated displacements at the mid side position were much larger and produced a larger correction (~20%) in the peak tensile stress, compared to the corner position (~7%). The mid side position is a better location to estimate the displacements since this represents the physical location of where the EDM wire creates the final slot width. The estimated cut tip displacements for the 2D and 3D procedures were in close agreement considering the differences in the stress fields used as an initial condition for the contour cutting simulation.

The practices established in this work to ensure reliable estimation and correction of the bulge error using the iterative finite element procedure are discussed next,

- As there is no bulge error at the start and end of the cut, extrapolating the corrected surface deformations near the edges of the cut using MATLAB software gave reliable stress results in this region.
- A mesh sensitivity study showed the size of the mesh close to the cutting path had a significant effect on the displacements and stresses calculated at the cut. The results showed that the width of the mesh close to the cut should be at least half the size of the mesh used along the cutting path.
- The effect of the asymmetric clamping (required for the slitting measurement) was removed by averaging the bulge displacements from both cut halves before correcting the measured averaged contour displacements. In the finite element analysis, each side of the cut tip is moving in opposite directions to the reference coordinate system, therefore the sign of the displacements from one side should be reversed before averaging.
- An incremental change of ≤ 5 % of the peak tensile stress has been used in the present study to indicate convergence.

The factors that have not been explored in this work to determine their influence on the bulge prediction are the applied restraint to represent the clamping condition, the stress distribution in the remainder of the model and using a semi-circular slot bottom.

Based on this investigation, a simpler correction procedure for full field contour measurement is proposed. Estimated bulge displacement errors at the cut tip are used directly in an elastic contour type FE analysis to calculate the associated stress error. The stress error is then used to correct the initially measured stresses. This procedure has been applied for the C(T) specimen case study using 2D and 3D finite element analysis. The corrected stresses showed excellent agreement with the original procedure due to the nature of linear elastic stress analysis. The alternative procedure can be used to correct a line profile of contour method residual stresses using the estimated bulge displacements from a simplified 2D contour cutting simulation. And a complex 3D bulge correction procedure is not necessary, even for a complex (varying) residual stress profile.

3.4 Conclusion

- A 2D FE approach proposed by Prime and Kastengren [3] to correct complex (varying) stress fields for the bulge error is unreliable and 3D analysis is necessary.

- A 3D FE approach can be applied to correct complex stress fields for the bulge error, but this procedure is very complex and time-consuming requiring bespoke scripts to extract the bulge error through the thickness of the specimen.

- The displacement at the wire mid side entry node is a better position to estimate the bulge error as the correct contour method measurement for the case study explored in this chapter showed a closer correlation with the neutron diffraction and slitting measurements.

- The bulge error can be significant for contour measurements. The peak tensile stress increased by ~20 % for the case study explored in this chapter.

- A simpler procedure, which calculates directly the stress error offers a more robust approach to correcting contour results.

- The simple procedure allows stress line profiles from a contour measurement map to be corrected based upon stress errors estimated from a 2D FE model of the cutting process.

The work in this chapter has shown that the bulge error can have significant effects on reliable measurements made by the contour method. An iterative FE correction procedure is time consuming and 3D modeling is required in most engineering cases. Furthermore, the position at the tip of a contour cut to estimate the bulge error has so far only been explored using finite element analysis and there is a need for experimental validation (see future work section 7.2). In the next chapter an analytical approach to estimate and correct for the bulge error is investigated.

Chapter 4: An analytical approach for bulge error estimation

In the contour method, the cut created by wire electric discharge machining (WEDM) can be interpreted as a slow-moving blunt crack which causes a redistribution of residual stresses in the uncut material that are concentrated at the cut tip. The bulge error arises when the stress field near the cut tip causes the material at the cut tip to elastically deform resulting in a varying amount of material being removed. Linear Elastic Fracture Mechanics (LEFM) characterises the magnitude of the stresses and displacements surrounding the tip of a sharp crack by the stress intensity factor (SIF), associated with the cut length and the redistributed residual stress field. The hypothesis explored in this chapter is that bulge error opening and closing displacements, are dependent on the local stress state at the cut tip which can be characterised by the mode-I SIF. If true, the SIF for a sharp crack can be used to predict the elastic displacements for a blunt crack or slot [125, 126].

The main aim of this chapter is to develop an analytical method to predict the bulge error using the SIF as an alternative to the finite element procedures presented in Chapter 3. The initial objective is to demonstrate the relationship between bulge error and SIF by FE analysis, then to investigate using the LEFM displacement field equations to estimate the bulge displacements (bulge error), and finally to establish the suitability of the equations for idealised stress distributions and real residual stress measurements made with the contour method. In each study the analytical bulge displacement solution is compared with the FE predictive procedure to evaluate its accuracy.

This chapter first describes the design of the simulation matrix to develop the SIF correlations and results. Then the analytical solution to estimate the bulge error is derived based on standard LEFM displacement field equations for a crack in a body found in literature. Following this, the derived bulge displacement equations are verified for two idealised cases; first an edged cracked plate under tension loading in plane stress and plane strain conditions and secondly a quenched cylinder to evaluate the bulge displacements through the thickness of the specimen. Finally the analytical bulge correction approach is implemented for two contour method measurements; first the cross-weld C(T) specimen which was investigated in Chapter 3 and then the bent beam test specimen example where an iterative FE bulge correction procedure [3] was first applied. A discussion of the results and conclusions are given at the end.

4.1 Stress Intensity Factor Correlations

The purpose of this work was to examine the relationship between the stress state at the tip of a contour cut and the cut width. Extensive FE simulations were carried out for a series of different parameters i.e. stress conditions, plate geometries, material properties and cut width sizes, to develop robust correlations. The underlying assumption in this work is that the LEFM stress intensity factor (SIF) characterises the stress state at the tip of a blunt notch.

First the specimen and simulation matrix comprising a total of 36 different test conditions to produce the correlations is described. Then the FE simulations are presented including a mesh convergence study and validation of the FE SIF. The correlation results, that is graphs of bulge displacement versus SIF, and the study findings are given at the end.

4.1.1 Specimen Design and Parameters

A benchmark case was designed to vary the SIF, cut length and cut width. An important consideration is the extent to which the SIF value is affected by the specimen design. SIF solutions, and expressions for the near-tip stresses and displacements, of edge-crack problems in finite width plates are widely available [120, 133, 134]. The solutions are generally for isotropic linear elastic material containing a mathematical or sharp crack positioned symmetrically with respect to the specimen geometry and applied loading.

For this reason, a single edge “crack” with a finite width geometry in a flat plate was chosen. A series of 2D linear-elastic finite element simulations were performed in ABAQUS for an edge-notched plate subjected to far field uniform tension and pure bending loadings. A schematic of the plate is shown in Figure 4 - 1 identifying the length (L), width (W), cut length (a) and cut width (b). The uniform tension and bending stresses that are applied at the far edge of the plate are also shown.

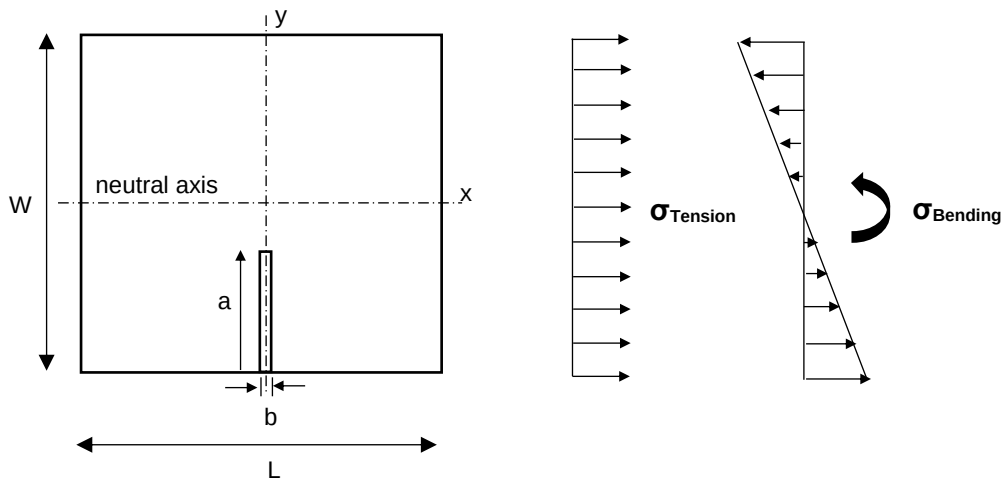

Figure 4 - 1: Schematic of a single edge-cracked plate and far field loading used to develop the stress intensity factor correlations.

SIFs depend on the geometry of the component, crack shape and loading condition. Taking this into consideration, the main parameters varied in the simulation studies were the plate geometry, plane stress and plane strain state, the elastic material properties and the cut width. The initial plate dimensions were chosen to be 50 mm for the length and width, aspect ratio L/W = 1, based on a standard compact tension, C(T), specimen size. The elastic material properties, Young's modulus or Modulus of Elasticity (E) and Poisson's ratio (ν), were defined for aluminium 7050 which has a low modulus of elasticity with E = 71.1 GPa and ν = 0.33. The initial cut width size (b) was 250 µm which is representative of a wire EDM cut. A uniform tensile stress ($\sigma_{Tension}$) of 10 MPa was chosen to create sufficient load in the plate to identify the bulge displacements and SIF at the cut tip.

Following this, the length of the plate was varied for aspect ratios L/W = 0.5 and 2, to include short and long plates. The elastic material properties were changed to stainless steel 316H having a higher modulus of elasticity with E = 195.6 GPa and ν = 0.294. The cut width size for the initial plate geometry was varied and six sizes were evaluated based on the range of wire diameters typically used for EDM cutting and the final slot width: 50 µm, 150 µm, 250 µm, 350 µm, 450 µm and 550 µm. And finally, the different cut width sizes were re-assessed for a bending load having a bending moment of 200 Nm. For each study, plane stress and plane strain analysis were performed. One factor was varied for each study to develop the stress intensity factor correlations giving a total of 36 cases. The complete simulation matrix is shown in Table 4 - 1 in the appendix.

4.1.2 FE Models and Mesh Sensitivity Studies

This section first describes the FE models used to develop the SIF correlations. Mesh sensitivity studies were performed to evaluate the significance of the element size and shape at the cut tip for the square slot assumption. The FE stress intensity factor was verified using the Boundary Collocation Method (BCM) [135, 142]. The correlation results, that is graphs of bulge error versus SIF, are presented in section 4.1.3.

FE Models and Procedure

To simplify the FE analysis, a 2D model of one half of the plate was created in ABAQUS with a symmetry boundary condition, shown in Figure 4 - 2. A linear elastic material model was used with the Young's modulus, E, and Poisson's ratio, ν, defined. The tensile and bending loads were defined at the far edge of the plate. The model was allowed to freely deform (unconstrained) and only one additional constraint was applied to avoid rigid body motion.

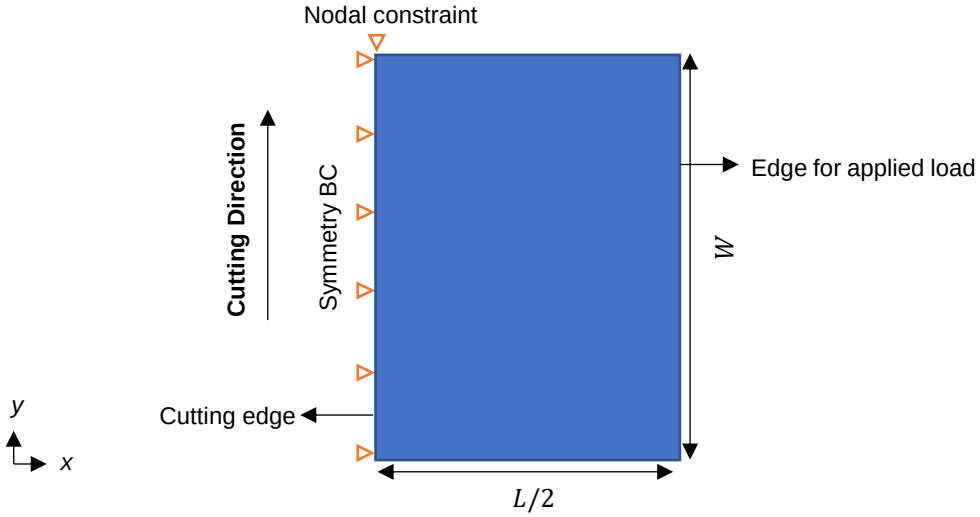

Figure 4 - 2: The FE model of a single edge-cracked plate used for the stress intensity factor correlations showing the loading edge and boundary condition to prevent rigid body motion.

Two models were required, one with a sharp crack to evaluate the SIF and the other with a square slot for bulge quantification. Figure 4 - 3 shows the mesh used to evaluate the stress intensity factor and bulge displacement for the different plate geometries. For a 0.25 mm cut width size, the element size at the cut was 0.125 mm and 0.25 mm in the x and y directions respectively. Figure 4 - 4 shows the mesh to evaluate the different cut width sizes using a plate with aspect ratio L/W = 1. The element size at the cut was chosen so that an

increasing number of elements could be removed as the cut width size increased without needing to re-mesh the model. The element size at the cut was 0.025 mm and 0.05 mm in the x and y directions respectively. Therefore, to create the smallest cut width one element was removed and for the largest cut width 11 elements were removed in the x-direction.

For both configurations, the models were meshed with quadratic elements and plane stress and plane strain conditions were applied by selecting plane stress and plane strain elements of type CPS8R and CPE8R respectively. The models in Figure 4 - 3 with plate aspect ratios 0.5, 1 and 2 were meshed with 14 000, 16 000, 21 000 elements and contained 42 541, 48 561, 63 611 nodes respectively. The model in Figure 4 - 4 was meshed with 95 624 elements and contained 287 627 nodes. The global element size for both was 1 mm and biased away from the cutting edge in stages.

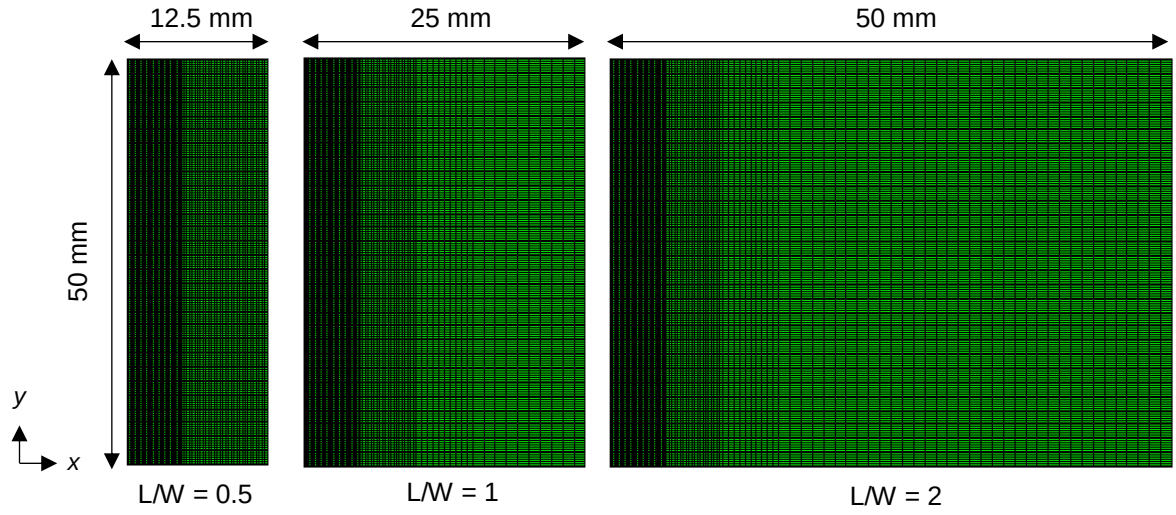

Figure 4 - 3: The 2D mesh and dimensions for the FE modelling of different plate geometries used for determining the stress intensity factor and bulge displacements.

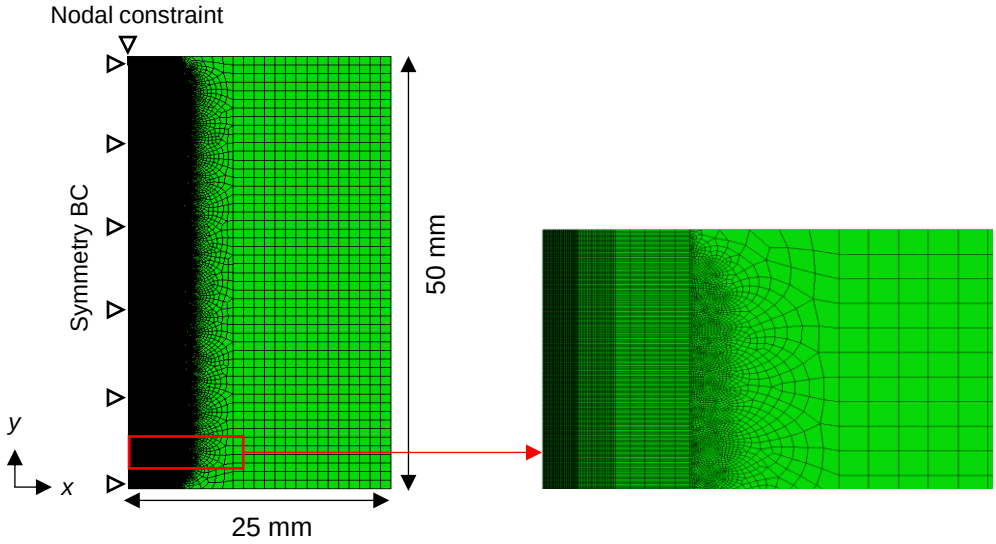

Figure 4 - 4: The 2D mesh and dimensions for the FE modelling of different cut width sizes used for determining the bulge error.

The tensile load was created by defining a constant pressure of 10 MPa on the far edge of the plate. The bending load was applied as a distribution of stresses that are tensile at the bottom of the plate and compressive at the top. The stress at any point along the y axis can be calculated using Equation 4 – 1. The resulting stress distribution for the 200 Nm bending moment, shown in Figure 4 - 5, was applied on the far edge of the plate, using the analytical expression field in ABAQUS.

$$\sigma_{Bending} = \frac{-My}{I_x} \qquad \textit{Eqn. 4 - 1}$$

where M is the bending moment, y is the distance from the neutral axis to the top or bottom of the plate and I_x is the second moment of area of the cross section about the x-axis that can be calculated by,

$$I_x = \frac{1}{12} LW^3 \qquad \textit{Eqn. 4 - 2}$$

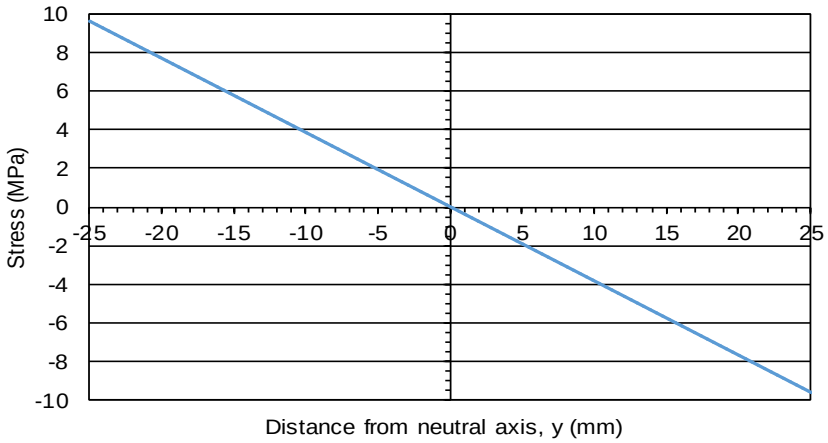

Figure 4 - 5: Distribution of bending stresses as a function of distance from the neutral axis.

To evaluate the SIF, a sharp crack was created by sequentially removing the symmetry boundary condition along the cut line. The crack was modelled by defining the crack tip and crack propagation direction. The stress singularity at the crack tip was controlled by defining quarter point node positions at the crack tip. The mode I stress intensity factor, K_I, was calculated using the J-integral method in ABAQUS. The J-integral calculation is performed over several contours to check for contour independency. To evaluate the bulge displacements, a square slot was created by sequentially removing elements along the cut line. The normal displacement at the cut tip (bulge error), U_x, was estimated at the wire mid side entry node as confirmed in Chapter 3. For both analyses cutting was simulated in 1 mm increments giving 50 cut increments in total. At each cut length, the bulge displacement and stress intensity factor were recorded.

Crack Tip Mesh Sensitivity Studies

The first study evaluates the sensitivity of bulge displacements to the mesh refinement used to represent the cut width. The second study evaluates the effect of the cut tip shape. For mesh convenience, a square slot bottom has been used to simulate cutting. However, in practice the wire EDM cut has a semi-circular bottom and this may introduce errors in the predicted bulge displacements [3]. The conclusions from both mesh studies are given at the end of this section.

(a) Mesh size

A comparison is made between one, five and ten elements used to represent a cut width size of 0.25 mm, shown in Figure 4 - 6. The following parameters were specified for all analyses, a remote uniform tensile stress of 10 MPa, a linear elastic material model with

Young's Modulus 71.1 GPa and Poisson's ratio 0.33 and a plane stress condition. The bulge displacements, U_x, were recorded at 1 mm cut increments at mid side node shown in Figure 4 - 6. The results, shown in Figure 4 - 7, show no change in the measured bulge displacements when the mesh used to represent the cut width is refined. Equation 4 – 3 was used to calculate the percentage error between the predictions of the bulge displacements for one element (x_1) and five or ten elements (x_2). The percentage error was found to be less than 1 % along the entire cut length.

$$Percentage\ Error\ (\%) = \left|\frac{x_1 - x_2}{x_2}\right| \times 100 \qquad \textit{Eqn. 4 - 3}$$

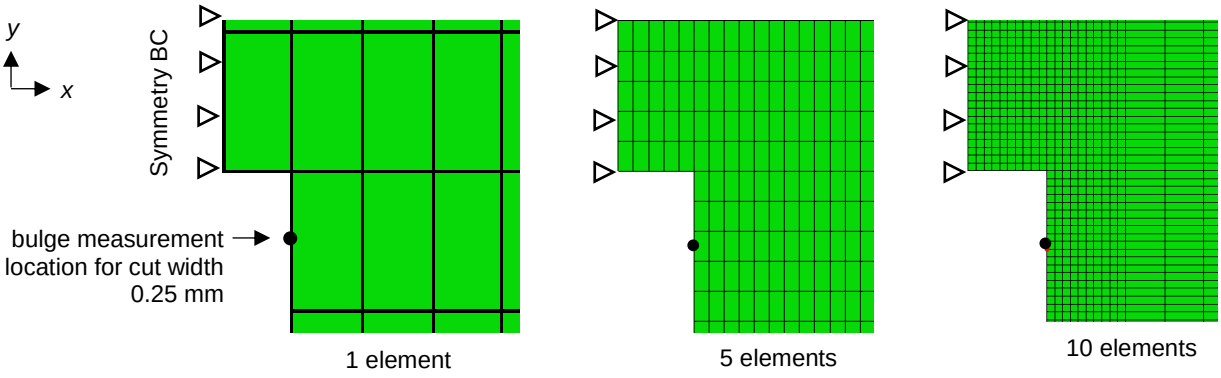

Figure 4 - 6: The mesh at the cut using one element (Figure 4 – 4, L/W = 1) compared to 5 and 10 elements (Figure 4 – 5) to represent a cut width size 0.25 mm and the bulge monitoring locations.

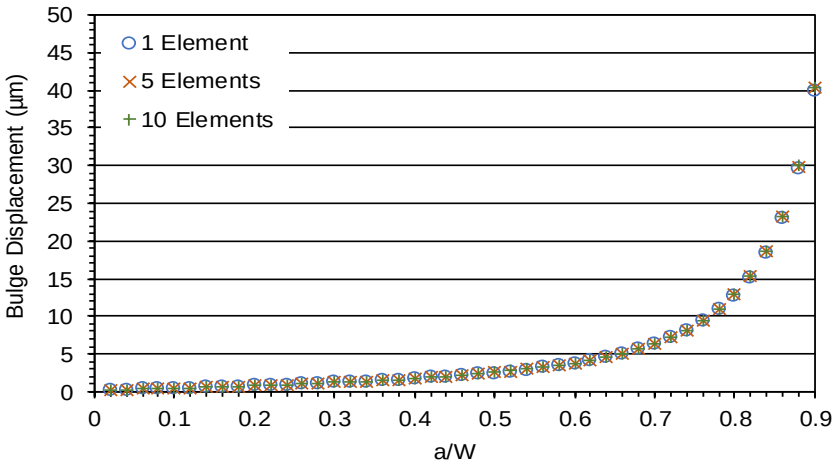

Figure 4 - 7: Comparison of the bulge displacements as a function of cut length for the mesh using one, five and ten elements to represent a cut width size 0.25 mm for a plate with a remote tensile stress of 10 MPa, Young's Modulus 71.1 GPa and Poisson's ratio 0.33, aspect ratio (L/W) of 1 and plane stress condition.

(b) Mesh shape

In this study a new FE model of the plate with L/W = 1 was created with a semi-circular shaped slot to represent a cut diameter of 0.25 mm. The parameters specified in the previous mesh study (a), were defined in the new model. Figure 4 - 8 shows the refined contoured elements at the cut tip and bulge measurement location. Since a new FE model is required for each cut length only five locations were selected at 5 mm, 15 mm, 25 mm, 35 mm and 45 mm.

Figure 4 - 9 compares the bulge displacements as a function of cut length for the semi-circular slot with the results from the previous study for the square slot. The difference increases as the cut length increases. Equation 4 – 4 was used to calculate the percentage error between the two numerical predictions of the bulge displacements for the square slot (x_1) and semi-circular slot (x_2). Figure 4 - 10 shows the error is up to 10 percent with the square idealisation overestimating bulge displacements.

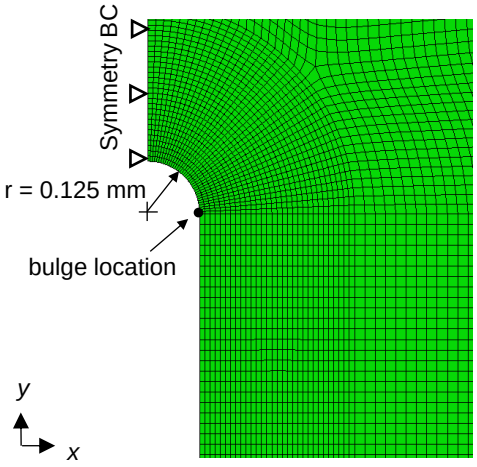

Figure 4 - 8: The mesh at the cut for the semi-circular slot bottom analysis using a slot diameter of 0.25 mm to estimate the bulge displacement at the outer edge of the radius.

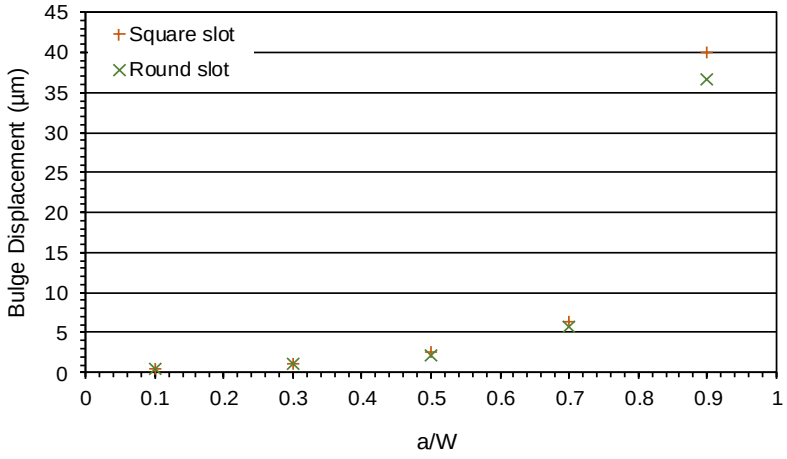

Figure 4 - 9: Comparison of the bulge displacements at selected cut lengths for the mesh using a square versus semi-circular shaped slot of diameter 0.25 mm to represent the EDM cut.

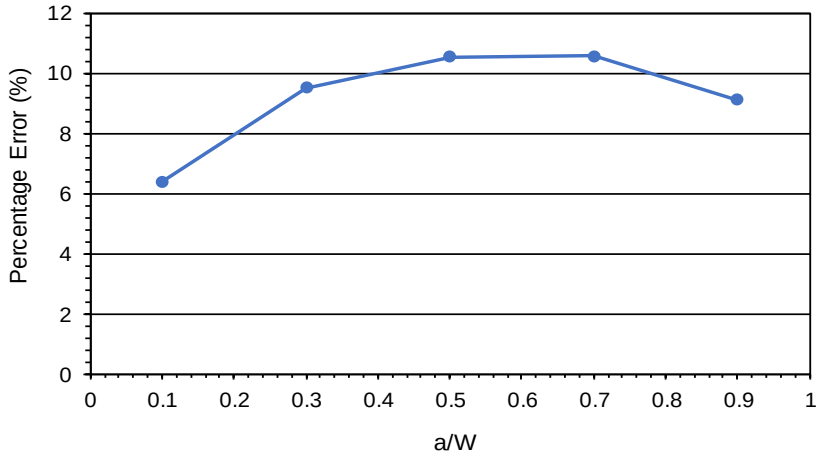

Figure 4 - 10: Percentage error in the bulge displacements using a square versus semi-circular shaped slot of diameter 0.25 mm to represent the EDM cut.

Conclusions

- Using a more refined mesh to represent the cut width has no effect on the measured bulge displacements. Therefore, both models can be used to predict the bulge error.

- A fairly significant error (up to 10 % over prediction) was found using the square slot assumption compared with the semi-circular slot created by the EDM cutting process. Since the meshing for a semi-circular slot would greatly increase the complexity of the FE analysis, it was decided to continue with the square slot idealisation to predict the

bulge error. Therefore, the square slot idealisation is likely to overestimate the bulge error.

Validation of the FE Stress Intensity Factor

Two studies are presented to check the SIFs obtained using FE simulations in ABAQUS. In the first study the FE SIF for a single edge cracked plate with tension loading is verified using the BCM solution [135, 142] explained in the literature review chapter. In linear elastic fracture mechanics, SIF solutions are typically derived for sharp cracks which assume that the stresses become infinite at the crack tip. The hypothesis is that the SIF for a sharp crack can be used to accurately predict the bulge displacements for a blunt crack or slot. Blunt cracks, which have a finite width, reduce the severity of the stress field around the crack tip and have no stress singularity. Therefore, the second study is to evaluate how the SIF for a finite width crack deviates from a sharp crack. The conclusions from both SIF studies are given at the end of this section.

(a) Comparison of the FE SIF with the Boundary Collocation Method

First the FE mode I SIF, K_I, was calculated for the different plate lengths shown in Figure 4 - 3 for a sharp crack. The following parameters were specified for all analyses, a remote uniform tensile stress of 10 MPa, a linear elastic material model with Young's Modulus 71.1 GPa and Poisson's ratio 0.33 and a plane stress condition. Then the stress intensity factors were calculated with the BCM solution for a single edge-crack plate under tension loading. The SIF solution for this case is given by the formula $K_I = \sigma\sqrt{\pi a}\, F_t$ where σ is the tension load, *a* is the crack length and *F* is the geometric function compiled in Table 2 - 1 in the literature review chapter [142] for several plate aspect ratios and cut lengths. The BCM solution is based on results which is accurate to within 1% for all $L/W \geq 1.0$ and $a/W \leq 0.6$ [120, 134].

Figure 4 - 11 shows the FE SIF as a function of cut length for the uniform tension loading compared with the BCM solution. The SIF for the sharp crack was stable after 5 contours. The SIF differs for the short plate (L/W = 0.5) but remained the same for longer plates. This is consistent with the findings in literature that the effect of L/W is practically negligible for L/W ≥ 1 [120]. This figure also shows the FE SIF with the BCM solution. Both matches fairly closely for the different plate lengths. The percentage error between the FE solution (x_1) and reference BCM solution (x_2) were calculated using Equation 4 - 4. Uncertainties in the stress intensity factor evaluation are of the order ± 5% [151]. Figure 4 - 12 shows the error, which is slightly larger for the short plate, but very good agreement is shown for the longer

plates for values of a/W between 0.2 and 0.6. Although the errors varied as a function of cut length, the overall accuracy was acceptable as all the errors were lower than 5 %.

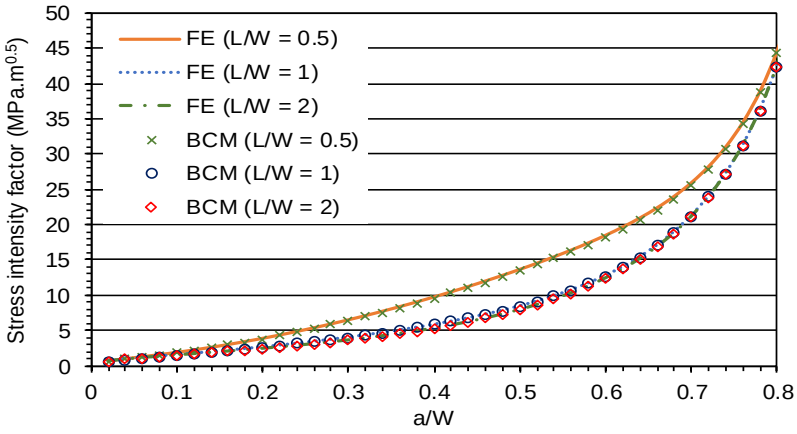

Figure 4 - 11: Comparison of the FE mode I stress intensity factor with the boundary collocation method for a single edge-cracked plate under tension loading for different plate lengths.

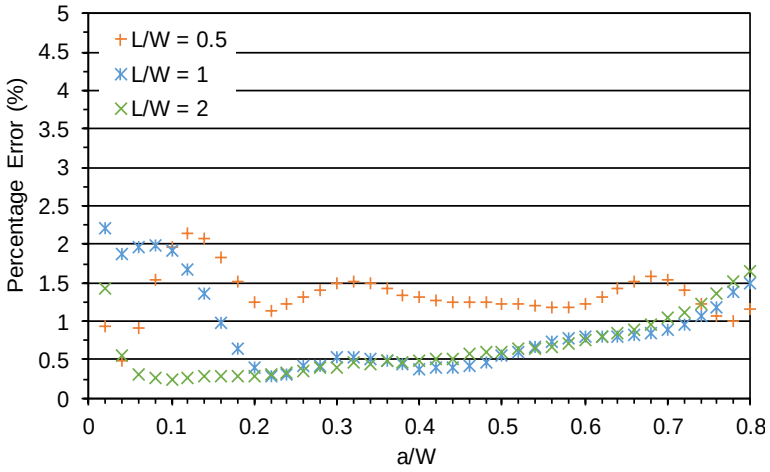

Figure 4 - 12: Percentage error between the FE SIF and boundary collocation method for a single edge-cracked plate under tension loading for different plate lengths.

(b) Evaluation of the FE SIF for a sharp crack versus finite width slot

This work evaluates how the SIF for the smallest and largest square slot sizes, i.e. 0.05 mm and 0.55 mm, deviates from the SIF for a sharp crack. Only the pure tension loading was evaluated using model shown in Figure 4 - 4 with a square slot and a remote uniform tensile stress of 10 MPa, a linear elastic material model with Youngs Modulus 71.1 GPa and Poisson's ratio 0.33 and a plane stress condition.

Figure 4 - 13 compares the SIF for the finite width slots with the results from the previous study for the sharp crack. The SIF for the slot was stable after 10 contours. The percentage error between the square slot (x_1) and sharp crack (x_2) was calculated using Equation 4 – 4 and the results are shown in Figure 4 - 14. As expected, the deviation in SIF for a square slot increases as the cut width increases. The error also increases as the cut length increases. The percentage error in SIF between the sharp crack and smallest slot (0.05 mm) was negligible mostly below 0.5 %. The error for the largest cut width size (0.55 mm) was slightly more but mostly below 1.5 %.

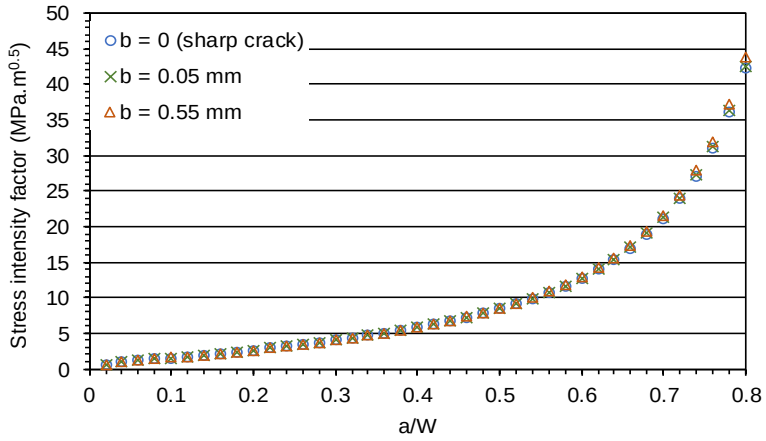

Figure 4 - 13: Comparison of the FE mode I SIF for a sharp crack and slot widths 0.05 mm and 0.55 mm for a single edge-cracked plate under tension loading.

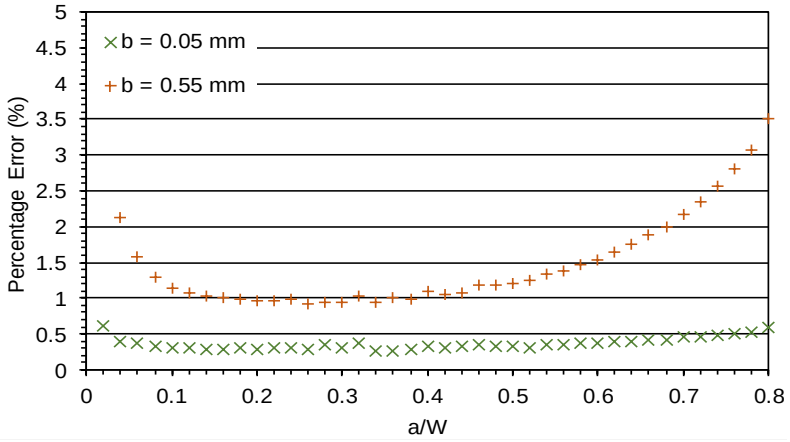

Figure 4 - 14: Percentage error between the FE SIF for a sharp crack versus slot widths 0.05 mm and 0.55 mm for a single edge-cracked plate under tension loading.

Conclusion

- There is good agreement between the FE SIF for a sharp crack and BCM solution for values of a/W ≤ 0.6. Therefore, the correlations are presented in this range.
- The SIF for a sharp crack deviates as the slot width increases but even for the largest slot width 0.55 mm this variance is small, below 1.5 percent. To avoid any uncertainties in the SIF for the correlations it was decided to use the SIF results for the sharp crack.

4.1.3 Correlation Results and Findings

In this section the relationships between bulge displacements at the cut tip and the mode I SIF are investigated for the case of an edge-cracked plate. The main parameters considered are the plate geometry, plane stress and plane strain state, elastic material properties, cut widths and loading (pure tension and bending). Graphs of the raw data and the study findings are presented under each heading.

Plate Geometry

Figure 4 - 15 shows the results for cases 1 to 6, presented in the Appendix B, Table B - 1, to evaluate the influence of different plate lengths and the plane stress and plane strain stress states.

- There is a linear relationship between the bulge displacement and SIF.
- The bulge displacement is larger for the plane stress state than the plane strain state as indicated by the steeper slope of the lines. For a Young's Modulus of 71.1 GPa the difference between the plane stress and plane strain state is 11 %.

Elastic Material Properties

Figure 4 - 16 shows the results for cases 7 to 12 for larger Young's Modulus and Poisson's ratio values.

- The bulge displacement is inversely proportional to the elastic stiffness.
- The difference between the plane stress and plane strain states reduced slightly. For a Young's Modulus of 195.6 GPa the difference is 9 %.

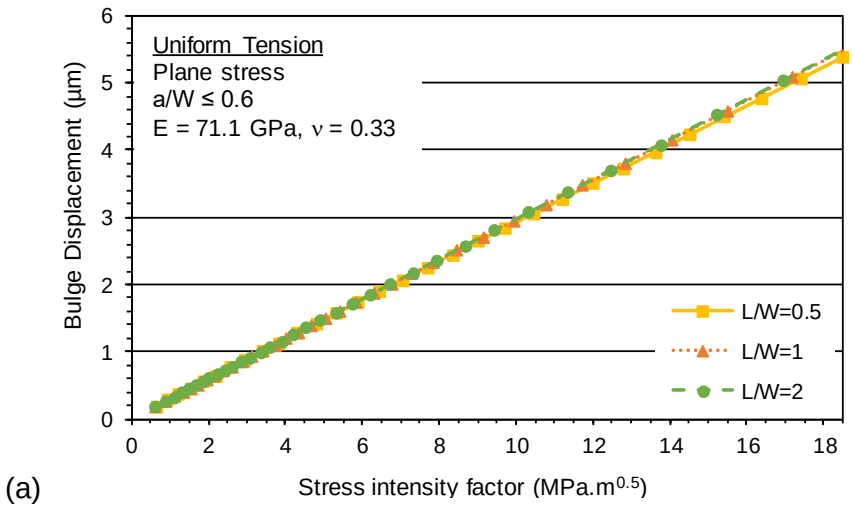

(a)

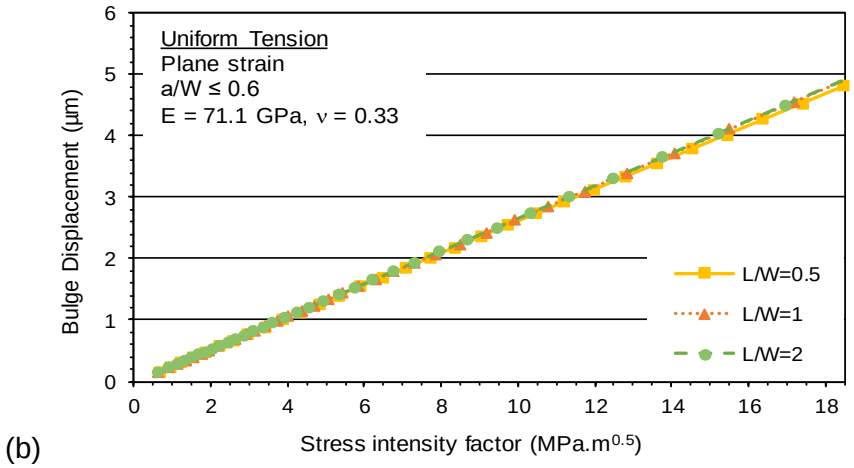

(b)

Figure 4 - 15: SIF correlations for a single edge-cracked plate under tension loading for different plate lengths and the (a) plane stress and (b) plane strain stress states (i.e. cases 1 to 6 presented in the Appendix B, Table B - 1).

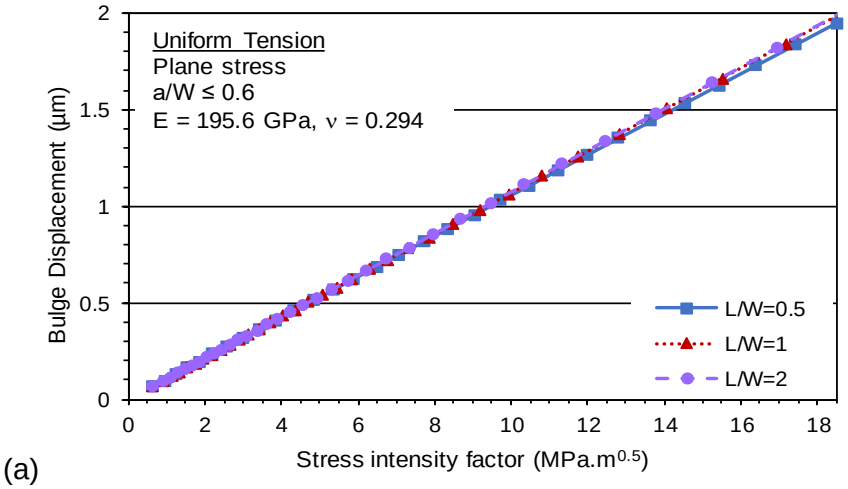

(a)

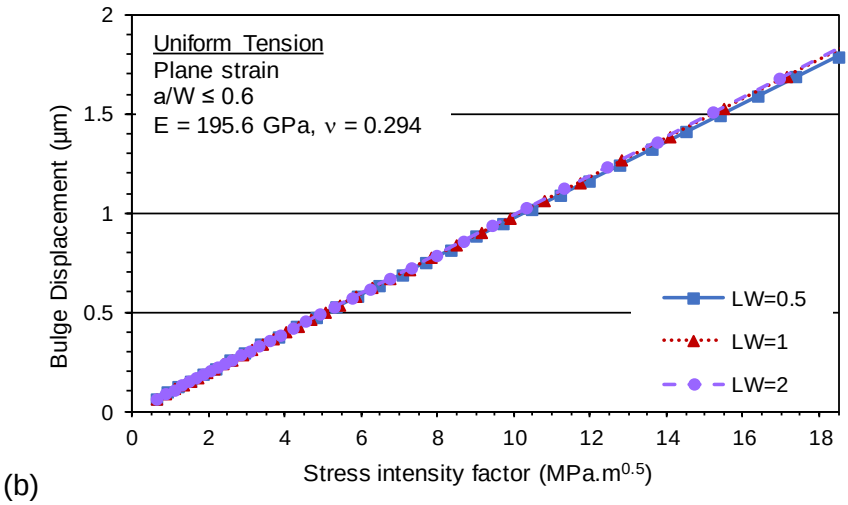

(b)

Figure 4 - 16: SIF correlations for a single edge-cracked plate under tension loading with larger elastic stiffness properties and the (a) plane stress and (b) plane strain stress states (i.e. cases 7 to 12 presented in the Appendix B, Table B - 1).

Cut Width Size

Figure 4 - 17 and Figure 4 - 18 show the results for cases 13 to 36, presented in the Appendix B, Table B - 1, to evaluate different cut width sizes for the pure tension and bending loading respectively.

- The bulge displacement is proportional to the SIF for any cut width in the range 50 µm to 550 µm for both tension and bending loads.
- The bulge displacement increases with increasing cut width.

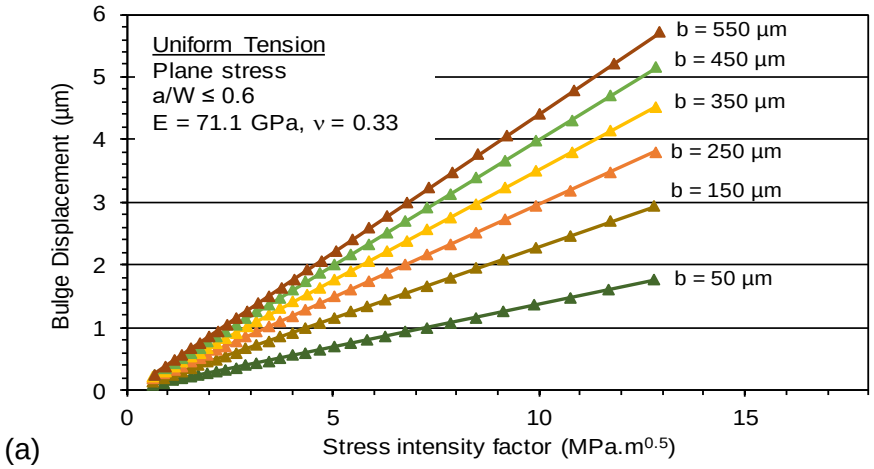

(a)

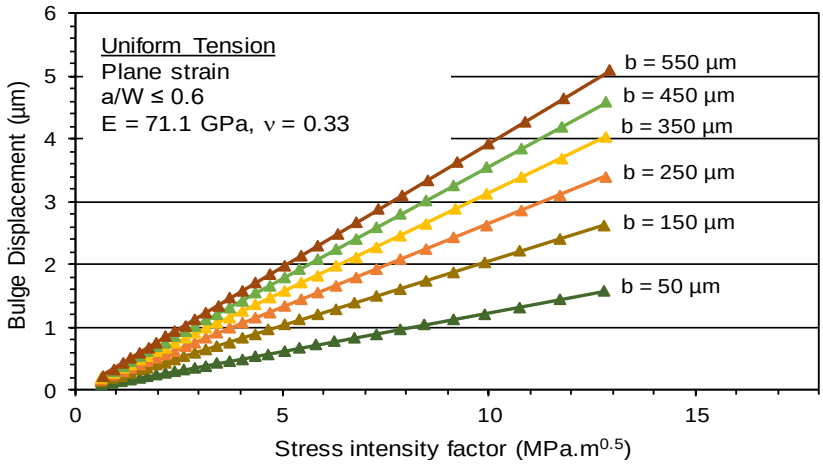

(b)

Figure 4 - 17: SIF correlations for a single edge-cracked plate under tension loading for different cut width sizes and the (a) plane stress and (b) plane strain stress states (i.e. cases 13 to 24 presented in the Appendix B, Table B - 1).

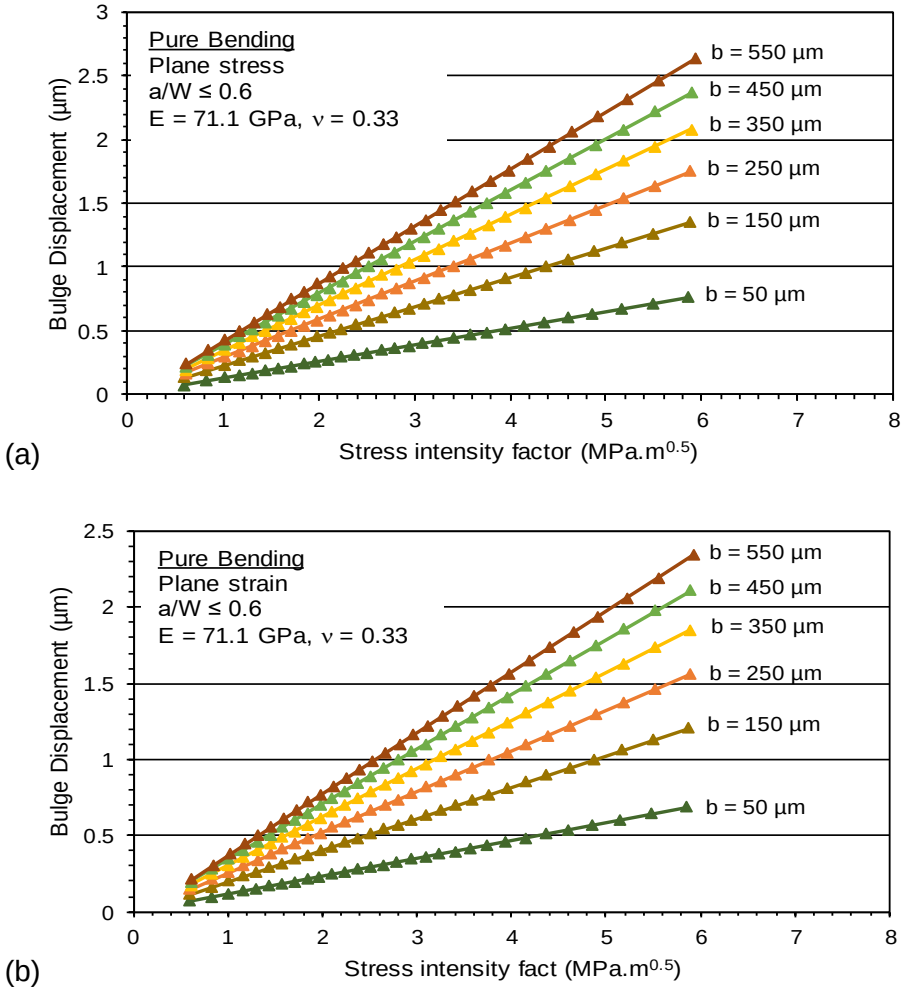

Figure 4 - 18: SIF correlations for a single edge-cracked plate under bending loading for different cut width sizes and the (a) plane stress and (b) plane strain stress states (i.e. cases 25 to 36 presented in the Appendix B, Table B - 1).

To quantify the increase in bulge displacement with cut width, the bulge displacements were extracted at specific SIF values. Figure 4 - 19 shows the displacement for increasing cut width at 10 MPa.m$^{0.5}$ and 5 MPa.m$^{0.5}$ for the tension and bending loads respectively. The increase in bulge displacement was greater for narrower cut widths. The results gave the exact relationship described below.

- The bulge displacement is proportional to the square root of the cut width.

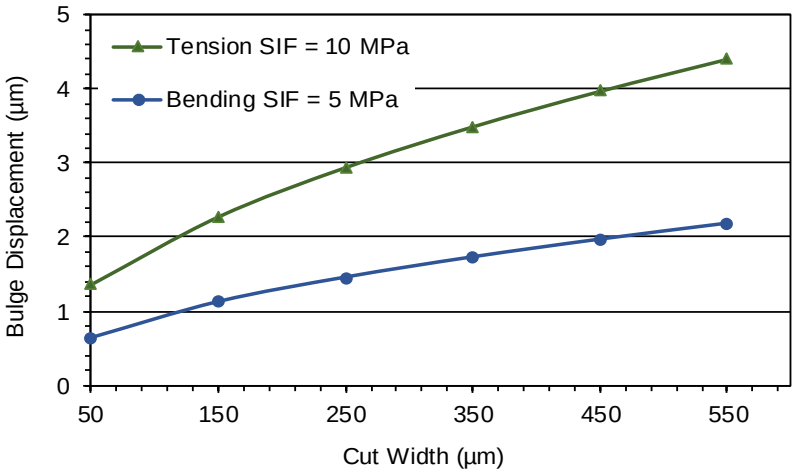

Figure 4 - 19: Bulge displacements (bulge error) with increasing cut width at specific values of SIF for a single edge-cracked plate under tension and bending loading.

4.2 Analytical Solution for Bulge Error

The previous section has shown that the bulge effect is dependent on the stress state at the cut tip, which can be characterised by the SIF at the cut tip. In LEFM when the SIF is known, stresses and displacements near a crack tip can be calculated using standard equations. In this section a LEFM based displacements solution is explored to predict bulge errors in contour method measurements for cases of plane stress and plane strain.

LEFM deals with the growth of sharp cracks in elastic bodies controlled by the stresses and deformations around the crack tip. There are three modes of fracture, mode I is identified as the opening mode, in which the crack surfaces move opposite and perpendicular to each other. This mode has been studied more extensively than modes II and III, which involve sliding and lateral tearing respectively. The displacement field ahead of a sharp crack in an infinite plane under remote tension can be expressed as an infinite series. However, only the first term is usually considered because the higher order terms have negligible influence on the solution.

The Near-Tip Solution

The near-tip solution for a sharp crack describes the stresses and deformations around the crack tip, were r and θ are polar coordinates from the crack tip shown in Figure 4 - 20 [127]. The mode I displacement field ahead of a crack which can be expressed in terms of the SIF, K, is shown in Equation 4 – 4 [124]. The equations for plane strain differ for plane stress because of the different versions of Hooke's Law, i.e. the displacements are a factor $(1 -$

ν^2) less for plane strain than for plane stress [152]. The crack opens into a parabola, and because a crack is regarded as a mathematical 'cut', θ must lie in the range $\pm\pi$. The displacements at a crack tip are non-singular and proportional to $K_I\sqrt{r}$ and depend on the stress state [121].

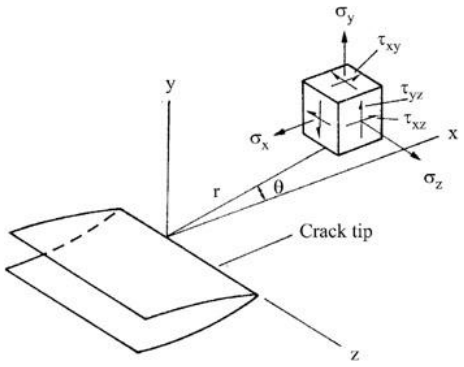

Figure 4 - 20: Crack tip coordinates and the stress field components [127].

$$u = \frac{K_I}{G}[r/(2\pi)]^{1/2} cos\frac{\theta}{2}\left(1 - 2\nu + 2sin^2\frac{\theta}{2}\right) \qquad \textit{Eqn. 4 - 4 (a)}$$

$$v = \frac{K_I}{G}[r/(2\pi)]^{1/2}\ sin\frac{\theta}{2}\left(2 - 2\nu - 2cos^2\frac{\theta}{2}\right) \qquad \textit{Eqn. 4 - 4 (b)}$$

where u and v are the x-direction and y-direction displacements in mode I, G is the shear modulus and ν is Poisson's ratio. Equation 4 - 4 has been written for the case of plane strain but can be changed to plane stress by replacing Poisson's ratio, ν, in the displacements with $\nu/(1+\nu)$.

Crack Surface Displacement

Under mode I deformation conditions, the crack surfaces open up, which is quantified by the surface displacement component u_y [128]. The upper crack surface, shown in Figure 4 - 21, corresponds to $\theta_x = \pi, \theta_y = 0$ and the lower surface is $\theta_x = -\pi, \theta_y = 0$. Using $\theta = \pi$ in Equation 4 – 4 (b), the displacement of the upper crack surface is thus given by,

For plane stress,

$$v = \frac{4K_I}{E}\sqrt{\frac{r}{2\pi}} \qquad \textit{Eqn. 4 - 5 (a)}$$

And similarly, for plane strain,

$$v = \frac{2K_I(2-2\nu^2)}{E}\sqrt{\frac{r}{2\pi}} \qquad \textit{Eqn. 4 - 5 (b)}$$

For the special case of $\theta = \pi$, it can be deduced from these equations that the displacements for plane stress are independent of Poisson's ratio ν, and that the displacements for plane strain are equal to $(1 - \nu^2)$ times those for plane stress [153].

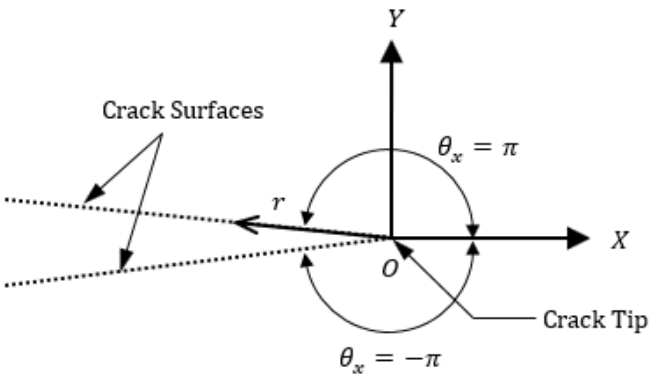

Figure 4 - 21: Definition of the coordinate system for the crack surface displacement field.

Application for bulge error estimation

The bulge error, or deformation of material at the cut tip, is a result of the slot created during the wire EDM process. Assuming a narrow slot, linear elastic fracture mechanics can represent a slot as a mathematically sharp crack. Cheng and Finnie compared a square-bottom slot with mathematical cracks and concluded that, for elastic behaviour, a slot could be considered a crack without significant errors (> ~10%) when the depth was more than five times the width [154]. The slot width created by wire EDM cutting is typically quite small (< 0.5 mm), therefore the error would only be significant for the first few millimetres (< 2.5 mm) of a contour cut. Furthermore, FE mesh sensitivity studies were performed in section 4.1.2 to evaluate how the SIF for a finite width crack deviates from a sharp crack. This work demonstrated that the SIF for a sharp crack deviates as the slot width increases but even for the largest slot width 0.55 mm this variance is small, below 1.5 percent.

In the FE procedures used to predict the bulge error (see Chapter 3) a square slot is incrementally introduced by removing elements and measuring the displacement of the wire entry node shown in Figure 4 - 22. This represents the tangent point of the EDM wire which creates the final slot width, b. This location relates to the crack surface ($\theta = \pm\pi$) where the displacements can be described by Equation 4 -5.

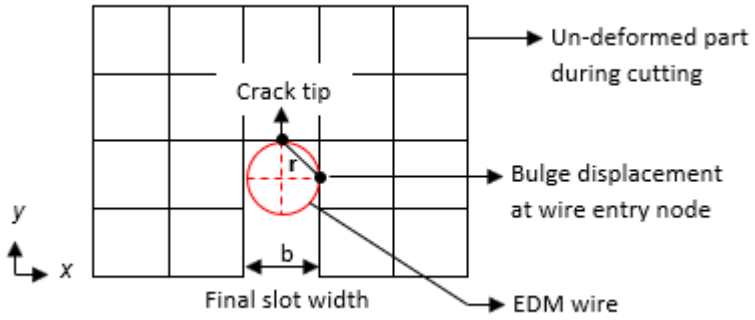

Figure 4 - 22: Schematic diagram of an undeformed body discretised for FE simulation of the wire EDM cutting process. The distance from the cut tip node to the wire entry node is shown.

The tangent distance, r, to the wire entry position node can be calculated using Pythagoras theorem,

$$r = \sqrt{\left(\frac{b}{2}\right)^2 + \left(\frac{b}{2}\right)^2} = \frac{b\sqrt{2}}{2}$$

where b is the final slot width

Substituting this into Equation 4 – 5 for the crack surface displacement where $\theta = \pi$, the bulge displacements can be determined by,

For plane stress,

$$U_{Bulge\ Error} = \frac{4K_I}{E}\sqrt{\frac{b\sqrt{2}}{4\pi}} \qquad \textit{Eqn. 4 - 6 (a)}$$

And plane strain,

$$U_{Bulge\ Error} = \frac{2K_I(2-2\nu^2)}{E}\sqrt{\frac{b\sqrt{2}}{4\pi}} \qquad \textit{Eqn. 4 - 6 (b)}$$

In the following sections the proposed analytical solution, Equation 4 – 6, is investigated to determine if and to what extent it can estimate the bulge error for idealised stress distributions and real residual stress measurements made with the contour method.

4.3 Validation studies for idealised stress distributions

In this study the displacement field equations are validated using numerical SIFs obtained for idealised stress distributions. First for a finite plate subjected to remote tension loading in the plane stress and plane strain conditions. Then for a quenched cylinder to investigate if the analytical solution can be applied for 3D cases to estimate the bulge displacements along the crack front through the thickness of the specimen.

4.3.1 2D edge crack in a plate under tension

A single edge-cracked plate under tension loading has been evaluated for the SIF correlations presented in the previous section (Figure 4 - 1). FE analysis was used to obtain the SIF and calculate the bulge displacements for different cut width sizes (i.e. 0.05 mm, 0.15 mm, 0.25 mm, 0.35 mm, 0.45 mm, 0.55 mm). Therefore, the data are available to compare the analytical and numerical bulge displacement predictions.

The input required to be defined in the analytical solution, Equation 4 – 6, is the mode I SIF, elastic material properties and final cut width size. The SIF profile as a function of cut length for the edge-cracked plate under a tension load of 10 MPa is shown in Figure 4 - 11. To avoid any effect of the plate length, a constant plate length to width aspect ratio, L/W = 1, was chosen. The elastic material properties were Young's modulus, E, and Poisson's ratio, ν, of 71.1 GPa and 0.33 respectively. The analytical bulge displacements were estimated for the different cut width sizes, b, and the plane stress and plane strain stress states.

The FE bulge displacements used to verify the analytical solution are shown in Figure 4 - 17. The error in displacements as a function of cut length (i) for the analytical solution $(\boldsymbol{x_1})$ and reference numerical FE prediction $(\boldsymbol{x_2})$ were evaluated using,

$$Percentage\ error = \left|\frac{x_1(i)-x_2(i)}{x_2(i)}\right| \times 100\% \qquad \textit{Eqn. 4 - 7}$$

The percentage error for the different cut width sizes is shown in Figure 4 - 23. The error is less than 5 percent between 5 and 80 percent of the cut length ($0.05 \leq a/W \leq 0.8$). The finite element stress intensity factor was validated with the BCM solution in section 4.1.2 and found to be in very good agreement between $0.2 \leq a/W \leq 0.6$. In this region the error is less than 1.5 percent. Beyond this the error rises sharply most likely due to the lack of restraint close to the cut end. The error also increases as the cut width increases. This is to be expected as section 4.1.2 showed that the SIF for a slot starts to deviate from a sharp crack

assumption as the slot width increases. However, the low error within the identified range is reasonable considering that the analytical solution is derived for a sharp crack.

The average percentage error by which the different cut width sizes differ was evaluated using,

$$Mean\ Percentage\ Error\ (MPE) = \frac{1}{n}\sum_{i=1}^{n}\left(\frac{x_1(i)-x_2(i)}{x_2(i)}\right) \times 100 \qquad \textit{Eqn. 4 - 8}$$

Where *i* is computed for cut length range 0.05 ≤ a/W 0.8 and n is the total number of cut increments within this range.

The mean percentage error for the different cut width sizes is shown in Figure 4 - 24. The error is less than 2 percent even for the largest cut width size 0.55 mm. The apparent inconsistency for the smallest cut width size in the plane stress state was carefully checked by refining the mesh but this did not improve the result.

The small error for all cut width sizes indicates that the analytical solution is likely to be able to estimate the bulge displacements in residual stress measurements made by the contour method if the stress intensity factor is obtained.

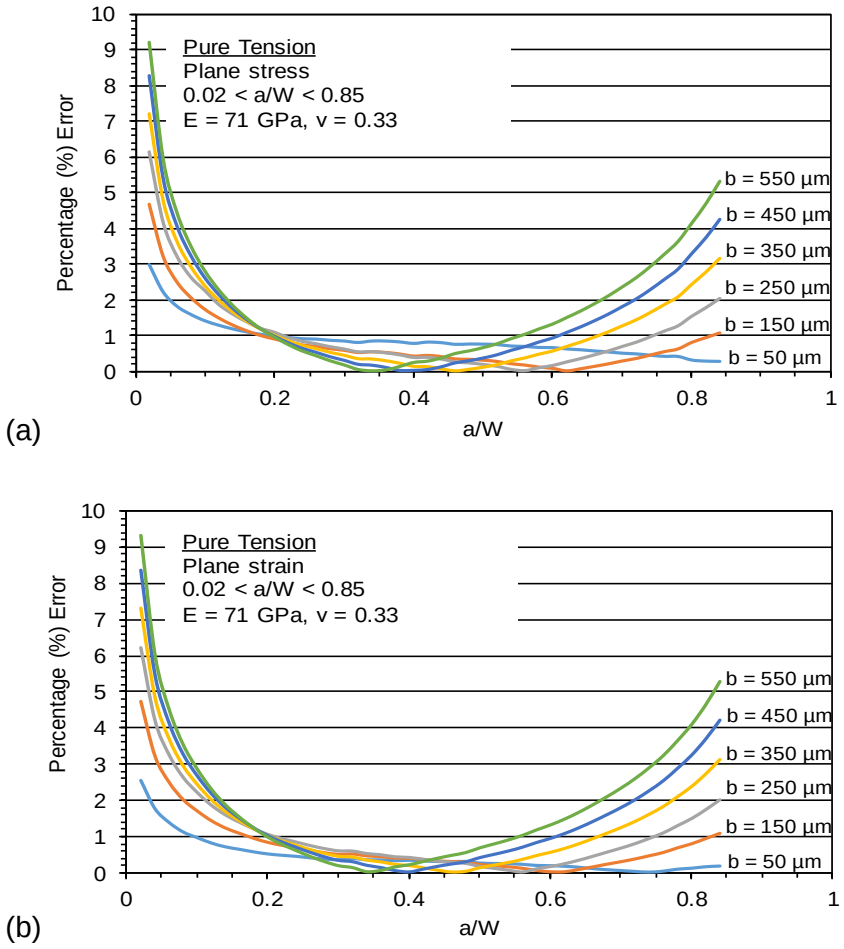

Figure 4 - 23: Percentage error between the analytical and FE bulge displacements for a single edge-cracked plate under tension loading for different cut width sizes in the (a) plane stress and (b) plane strain stress states.

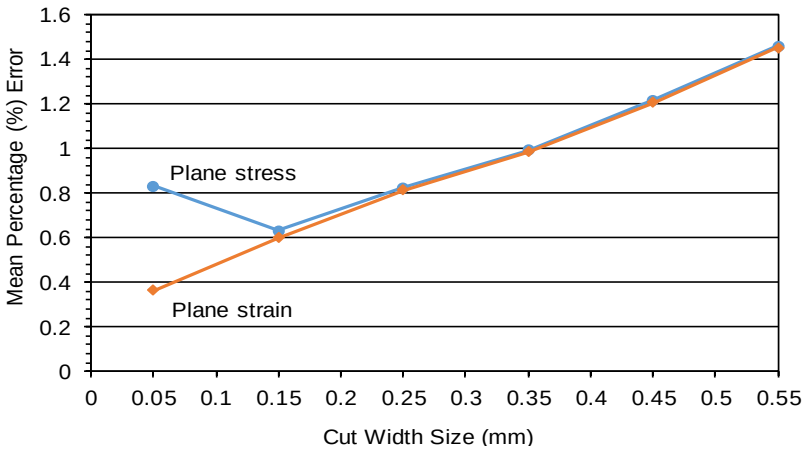

Figure 4 - 24: Mean percentage error between the analytical and FE bulge displacements for a single edge-cracked plate under tension loading for cut length range 0.05 ≤ a/W 0.8 and different cut width sizes.

4.3.2 3D edge crack in a quenched cylinder

A residual stress field was introduced into a cylinder made of stainless steel by simulating the quenching process using a sequentially coupled thermal-stress FE analysis. First a heat transfer analysis was performed to calculate the temperature history in the specimen during quenching. This temperature-time history was then used as input to an elastic-plastic mechanical analysis where the deformation and stress histories leading to the final residual stress state were determined.

Subsequent to this, diametral edge cracks of various lengths were introduced to determine the mode I SIF through the thickness of the specimen. Special J-integral contour elements had to be introduced in each FE model at the sharp crack tip. Therefore, only a few cut lengths were selected to evaluate the stress intensity factor across the cylinder diameter at depths of 5 mm, 15 mm, 30 mm, 45 mm and 57 mm. A separate analysis simulating wire EDM cutting using a slot was performed to predict the numerical bulge displacements for comparison with the analytical solution.

In this section the FE modelling is explained in more detail: (a) heat transfer analysis, (b) mechanical analysis, (c) SIF analysis and (d) bulge error analysis.

(a) Heat Transfer Analysis

A full model of a solid cylinder with diameter 60 mm and length 60 mm was created in ABAQUS as shown in Figure 4 - 25. Initially a mesh convergence study was performed for global mesh sizes 3 mm and 1.5 mm. The models consisted of quadratic heat transfer elements of type DC3D20 and a total number of elements 7 660 and 63 720 and total number of nodes 33 814 and 267 304 for models (a) and (b) respectively. The refined mesh in model (b) was the smallest possible element size for a practical solution time.

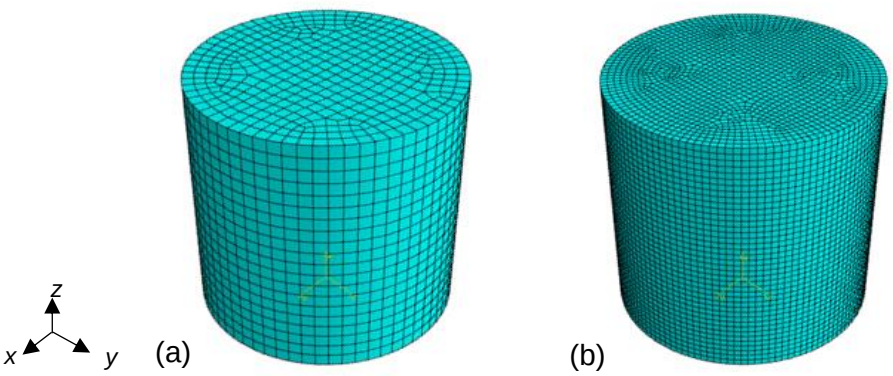

Figure 4 - 25: FE mesh for a solid cylinder, diameter 60 mm, length 60 mm, modelled with global mesh size (a) 3 mm and (b) 1.5 mm.

The heat transfer analysis required the specific heat capacity, C_p, thermal conductivity, k, and density, ρ, to be defined for the material. There are several studies in literature that have performed quenching analysis for austenitic 316H stainless steel samples and provide the temperature dependent physical and mechanical material properties [155-157] shown in Table 4 - 1 and Table 4 - 2. A temperature invariant density of 7970 kg/m^3 was specified together with a temperature invariant Poisson's ratio of 0.294. The outer surface of the cylinder was heated to 850°C and cooled to room temperature 20°C. A heat transfer coefficient of 7 000 W/m^2 K was used in the analysis [155].

To ensure sufficient accuracy in the transient solution, a maximum allowable nodal temperature change of 5 °C and time period 4 x 10^6 seconds was prescribed. The initial increment size was set to 0.01 seconds and maximum number of increments to 4000. When second-order elements are used there is a relationship between the minimum usable time increment Δt_{min} and the element length Δl given by [119]

$$\Delta t_{min} > \frac{\rho C_p}{6k} \Delta l^2 \qquad \textit{Eqn. 4 - 9}$$

In this case the smallest element length is 1.5 mm, using material properties for 850°C in Table 4 - 1, this formula suggests a minimum time increment of at least 0.06785 seconds. In the case where surface temperature is changed suddenly, time increments that are smaller than this can cause spurious oscillations in the solution. The heat transfer analysis required a minimum time increment of 1 x 10^{-6} seconds to reach a converged solution. However, no irregularities were seen in the solution.

The nodal temperatures were recorded in the field output data. The FE predicted temperature time curves during cooling at nodal points at the centre and surface of the cylinder are shown in Figure 4 - 26. The temperature profile showed good comparison with similar analysis in literature [155]. The results were not affected by refining the mesh.

Table 4 - 1: Thermal properties of austenitic 316H stainless steel [155-157].

Temp (°C)	Specific heat capacity (J/kg °C)	Conductivity (W/m °C)	Expansion coefficient (x 10^{-6} 1/°C)	Young's modulus (GPa)
20	488	14.12	14.56	195.6
100	502	15.26	15.39	191.2
200	520	16.69	16.21	185.7
300	537	18.11	16.86	179.6
400	555	19.54	17.37	172.6
500	572	20.96	17.78	164.5
600	589	22.38	18.12	155.0
700	589	23.81	18.43	144.1
800	589	25.23	18.72	131.4
900	589	26.66	18.99	116.8
1000	589	28.08	19.27	100.0
1100	589	29.5	19.53	80.0
1200	589	30.93	19.79	57.0
1300	589	32.35	20.02	30.0
1400	589	33.78	20.21	2.0

Table 4 - 2: True stress (MPa) as a function of plastic strain and temperature for austenitic 316H stainless steel [155-157].

Plastic strain (%)	Temperature (°C)						
	20	275	500	600	700	800	1100
0	273.1	205.4	192.8	187.7	161.5	121.5	25.3
0.2	284.2	215.0	202.1	197.1	167.5	123.5	25.7
1	328.2	253.3	239.3	234.5	191.7	131.3	27.1
2	356.7	280.1	266.2	260.0	205.2	133.5	28.0
5	420.0	342.7	327.8	310.6	223.6	134.9	29.8
10	504.6	425.3	408.2	356.8	232.7	136.1	31.4

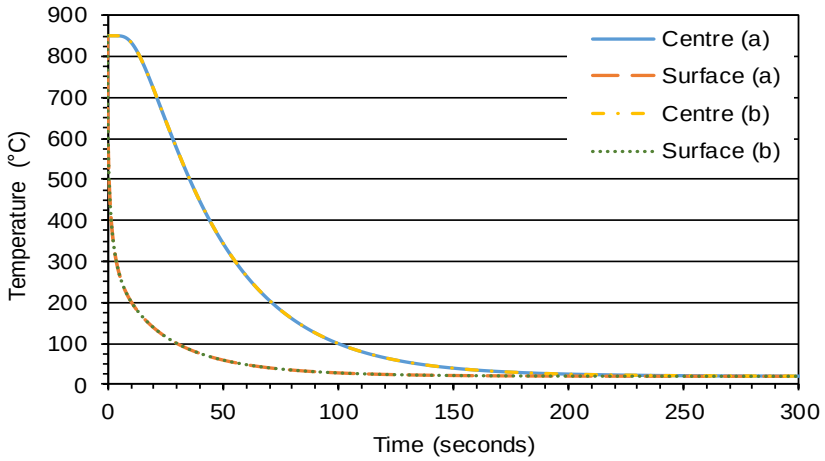

Figure 4 - 26: FE predicted temperature time curve at the centre and surface in a quenched 316H stainless steel solid cylinder, diameter 60 mm, length 60 mm, modelled with global mesh size (a) 3 mm and (b) 1.5 mm.

(b) Stress Analysis

The two mesh sizes for the solid cylinder shown in Figure 4 - 25 were used to determine the residual stresses during quenching. Quadratic hexahedral reduced integration elements of type C3D20R were required. Three nodal constraints were applied to the specimen to prevent rigid body motion shown in Figure 4 - 27. The cutting plane for the subsequent SIF analysis is also shown in this figure. The stress analysis required the temperature dependent elastic young's modulus, thermal expansion and plastic stress at zero plastic strain (0.2 %) as shown in Table 4 - 1 and Table 4 - 2.

The initial temperature of the cylinder was considered as uniform and equal to 850°C. The temperature-time history was then applied in a general step. A time period of 96 160 and minimum increment size 0.9616 was required to reach a converged solution. The initial increment size was set to 10 and maximum number of increments to 1000 000. A second general step was included to allow the stresses to equilibrate. The stresses and displacements were recorded in the field output data.

The residual stresses predicted by the mechanical model are consistent with similar quench induced stresses [155], having peak magnitude of 410 MPa and a distribution that is tensile toward the centre of the specimen and compressive around the boundary. Figure 4 - 28 shows a map of the hoop σ_x stresses on the cutting plane for the two mesh sizes. The results were not affected by refining the mesh. Figure 4 - 29 shows line profiles of all three

stress components through the thickness of the specimen at the different cut lengths chosen to evaluate the stress intensity factor in the next analysis.

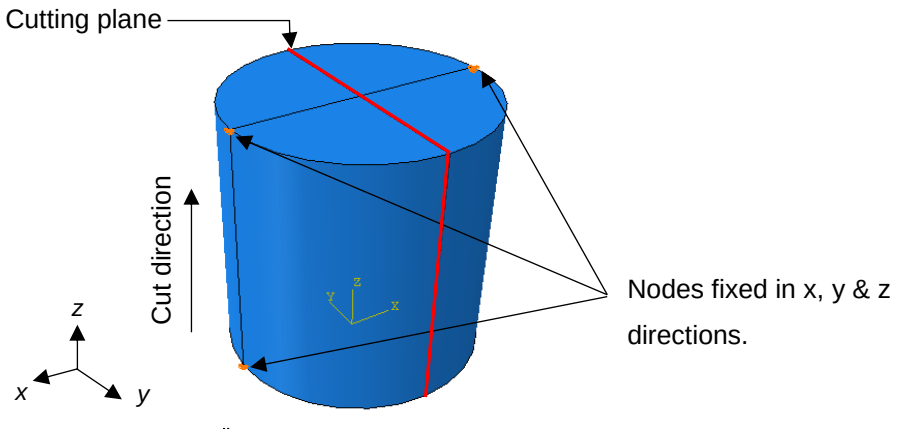

Figure 4 - 27: FE model constraints to prevent rigid body motion during the stress analysis and cutting plane for the subsequent stress intensity factor analysis.

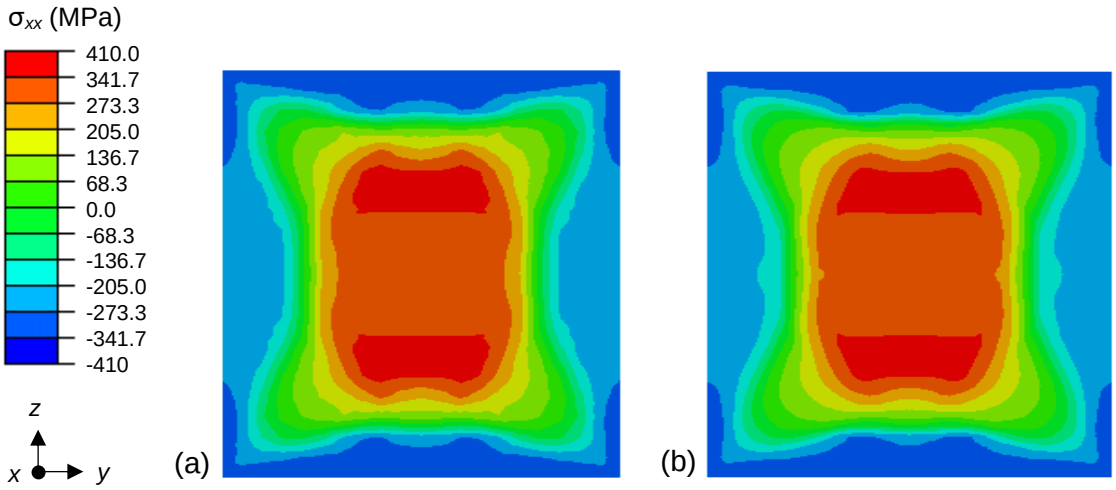

Figure 4 - 28: FE predicted residual hoop stresses in a quenched 316H stainless steel solid cylinder, diameter 60 mm, length 60 mm, modelled with global mesh size (a) 3 mm and (b) 1.5 mm.

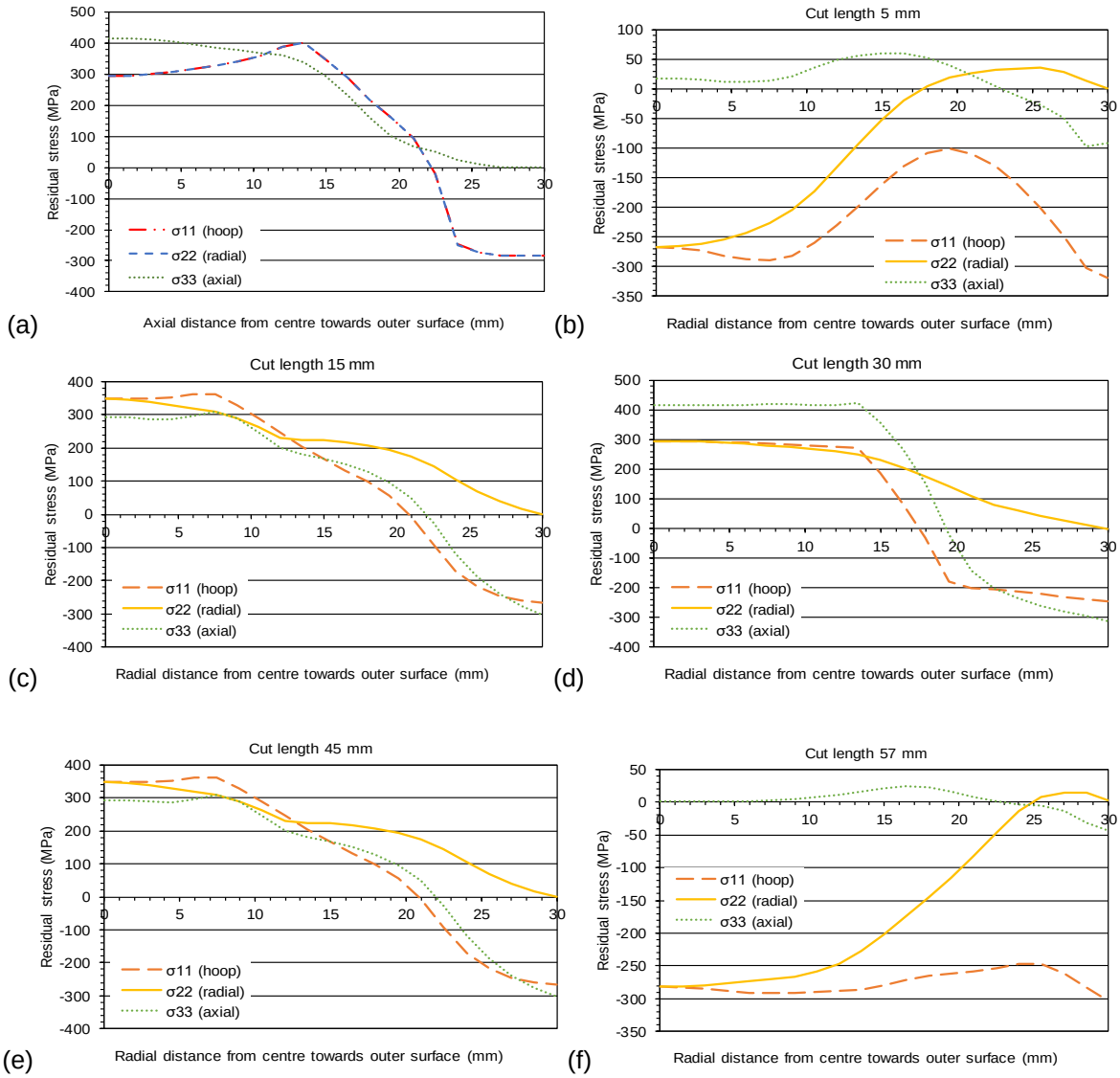

Figure 4 - 29: FE predicted residual stress distributions in a quenched 316H stainless steel solid cylinder, diameter 60 mm, length 60 mm, in (a) the axial direction at mid thickness and (b to f) the radial direction at different positions corresponding to cut lengths.

(c) Stress Intensity Factor Analysis

To simplify the FE cutting analysis, only one quarter of the solid cylinder was modelled in ABAQUS with two planes of symmetry which were located at mid thickness of the specimen and through the crack plane, i.e. the x and y planes respectively, shown in Figure 4 - 30. A linear elastic material model was used with Young's modulus, E, and Poisson's ratio, ν, of 195.6 GPa and 0.294 respectively. Only one nodal constraint was applied to prevent rigid body motion. The conventional FE method to calculate the SIF typically requires conforming the mesh to the cracked geometry, to explicitly define the crack front, and to specify the crack extension direction. For three-dimensional models, the SIFs are related to the J-

integral and require special contour elements to manage the stress concentration at the sharp crack tip. In the FE model, each contour is a ring of elements completely surrounding the crack tip or the nodes along the crack line. The rings of elements are defined recursively to surround all previous contours and each ring provides an evaluation of the contour integral [119]. The number of contours used to calculate the stress intensity factors was 10, as shown in Figure 4 - 30. The model was meshed with 78 988 quadratic hexahedral and wedge elements of type C3D20R and C3D15 respectively and a total of 330 924 nodes.

In the initial step the residual stresses from the previous mechanical analysis were mapped onto the new quarter model using the MAP SOLUTION function in ABAQUS and the stresses were allowed to redistribute to reach equilibrium. Figure 4 - 31 shows the mapped hoop σ_x stresses at the cutting plane. The crack was modelled by defining the crack tip and crack propagation direction. An edge crack was then inserted by removing the *x*-symmetry boundary condition on the crack face. The mode I SIF K_I was evaluated at 0.5 mm increments through the thickness of the specimen to allow the through thickness variation of K_I to be determined. The SIF was stable after the fifth contour, as shown in Figure 4 - 32 for a node positioned at the very centre of the cylinder. The SIF results across the thickness of the specimen at different cut lengths are shown in Figure 4 - 33.

The through thickness stress intensity factor corresponds with the redistributed quenching residual stresses at each cut increment. At the cut start the negative value of the residual SIF is due to the release of the compressive stress region and as the cut length increases the SIF distribution is due to the release of tensile stresses at the centre region and compressive stresses at the surface region. In the latter case, the calculated SIF is a minimum level from the cylinder surface region and rises to a maximum at the centre region of the cylinder. The maximum compressive stress intensity factor (~ -71.4 MPa.m$^{0.5}$ at the cut depths of 15 mm and 30 mm) is observed near the surface of the cylinder. The maximum tensile value (~ 31.7 MPa.m$^{0.5}$ at the cut depth of 45 mm) is found at the centre of the cylinder. For an edge crack and freely deformable configuration, the level of constraint gets lower as the crack length increases. Therefore, the calculated SIF at cut length 57 mm may have large errors.

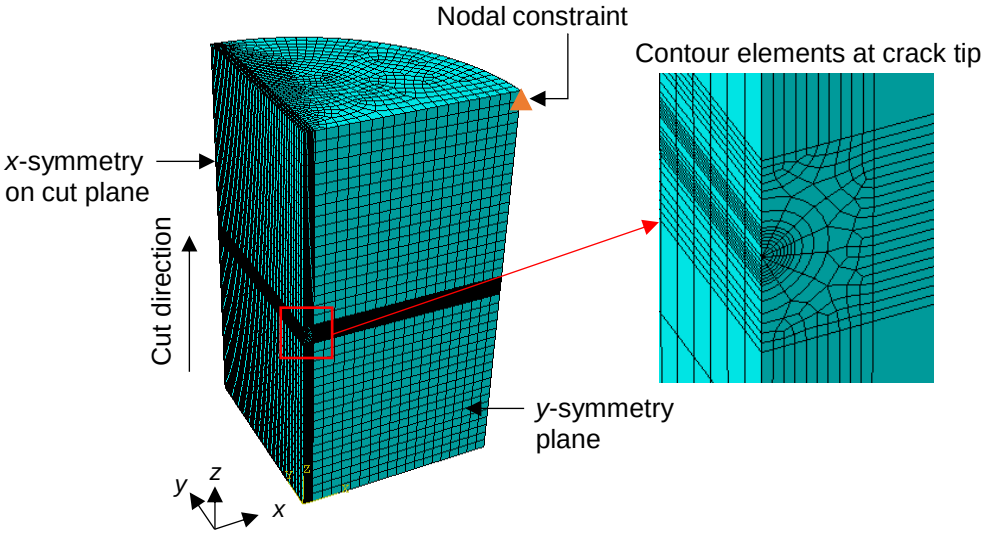

Figure 4 - 30: Quarter FE model of the solid cylinder showing the symmetry constraints and J-integral contour elements at the sharp crack tip for cut length 30 mm, to calculate the stress intensity factor through the thickness.

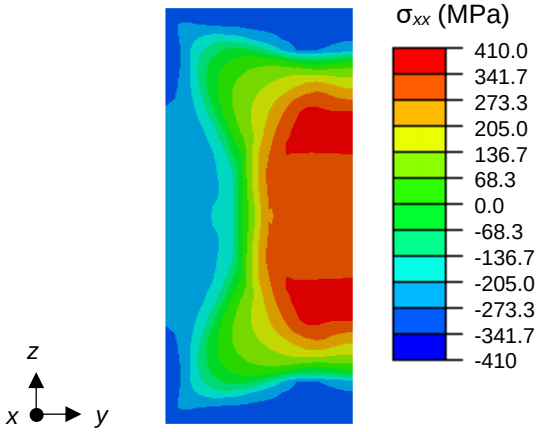

Figure 4 - 31: Mapped residual hoop stresses in a quenched 316H stainless steel solid cylinder, diameter 60 mm, length 60 mm, from a full model to a quarter model for the cutting analysis.

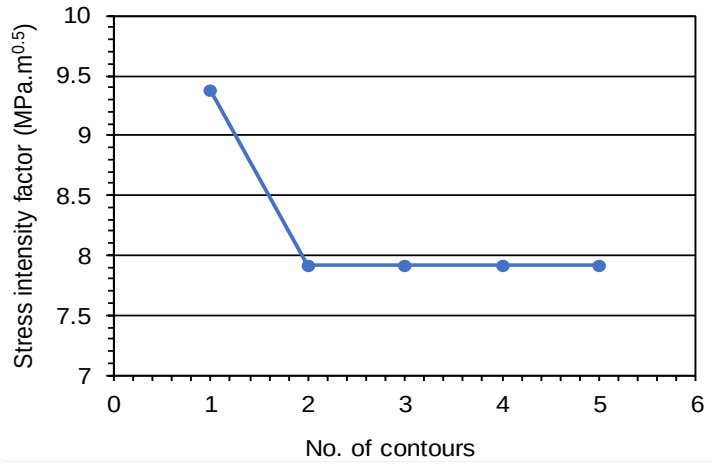

Figure 4 - 32: Variation of the FE mode I stress intensity factor for increasing number of contour regions surrounding the crack tip for a node at the centre of a quenched 316H stainless steel solid cylinder.

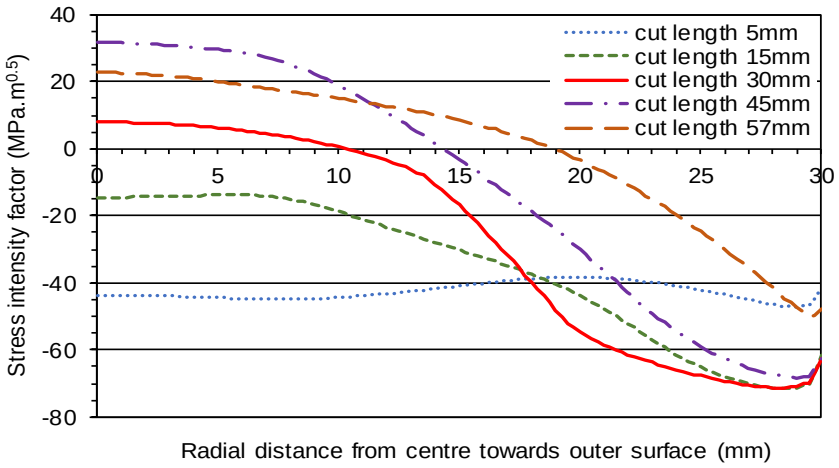

Figure 4 - 33: FE mode I stress intensity factor in a quenched 316H stainless steel solid cylinder, diameter 60 mm, length 60 mm, at different cut lengths and through the thickness.

(d) Bulge Error Analysis

Analytical method:

The analytical bulge displacement Equation 4 – 6 (a & b) is used here with the 3D stress intensity factor results (Figure 4 - 33) to estimate the plane stress and plane strain bulge estimates with a Young's modulus, E, and Poisson's ratio, ν, of 195.6 GPa and 0.294. Two cut width sizes, 0.1 mm and 0.3 mm, were evaluated for comparison with the FE method.

FE method:

One quarter of the solid cylinder, shown in Figure 4 - 34, was modelled and wire EDM cutting simulated by element removal in order to quantify bulge displacements along the crack front across the thickness of the specimen. The model was meshed with quadratic hexahedral and wedge elements of type C3D20R and C3D15 respectively. For a cut width size 0.1 mm the model was meshed with a total of 50 560 elements and 213 921 nodes. For a cut width size 0.3 mm the model had 26 560 elements and 113 681 nodes. A linear elastic material model was used with Young's modulus, E, and Poisson's ratio, ν, of 195.6 GPa and 0.294 respectively. Only one nodal constraint was applied to prevent rigid body motion.

In the initial step the residual stresses from the previous mechanical analysis were mapped onto the quarter model using the MAP SOLUTION function in ABAQUS and the stresses were allowed to redistribute to reach equilibrium. Cutting was then performed by sequentially removing rows of elements along the cut edge. The bulge displacements at the wire entry node locations were recorded at 1 mm increments through the thickness of the specimen.

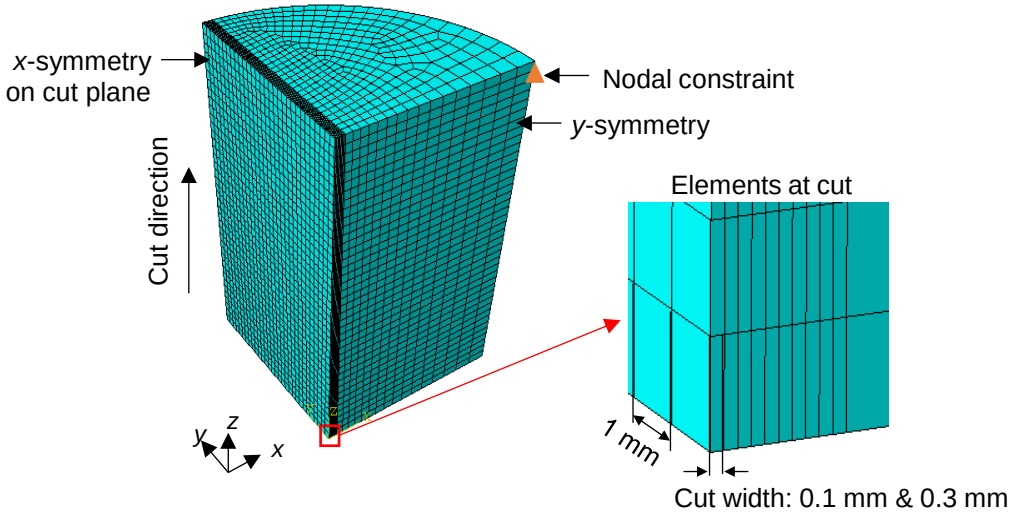

Figure 4 - 34: Quarter FE model of the solid cylinder showing the symmetry constraints and elements at the cut tip for the cutting analysis to estimate the bulge displacements across the thickness for cut width sizes 0.1 mm and 0.3 mm.

Comparison of the analytical and FE bulge displacement results:

Figure 4 - 35 and Figure 4 - 36 compare the analytical bulge displacements with the measured FE bulge displacements at different cut lengths for cut width sizes 0.1 mm and 0.3 mm respectively. It can be seen that the FE bulge displacements match more closely with the analytical plane strain solution across the thickness of the specimen. Also, the bulge displacements followed the through-thickness stress intensity factor in form and distribution. The absolute error in bulge displacements between the analytical plane strain solution (x_1) and reference numerical FE prediction (x_2) were normalised with the cut width and evaluated through the thickness using,

$$Normalised\ absolute\ error\ (\%) = \frac{|x_1 - x_2|}{cut\ width} \times 100 \qquad \textit{Eqn. 4 - 10}$$

Figure 4 - 37 shows that the error is fairly small across the thickness of the specimen and at different cut lengths. The error is the greatest at the outer surface of the cylinder. Neglecting the final 2 mm from the outer surface, the normalised error is under 0.1 % for all cases.

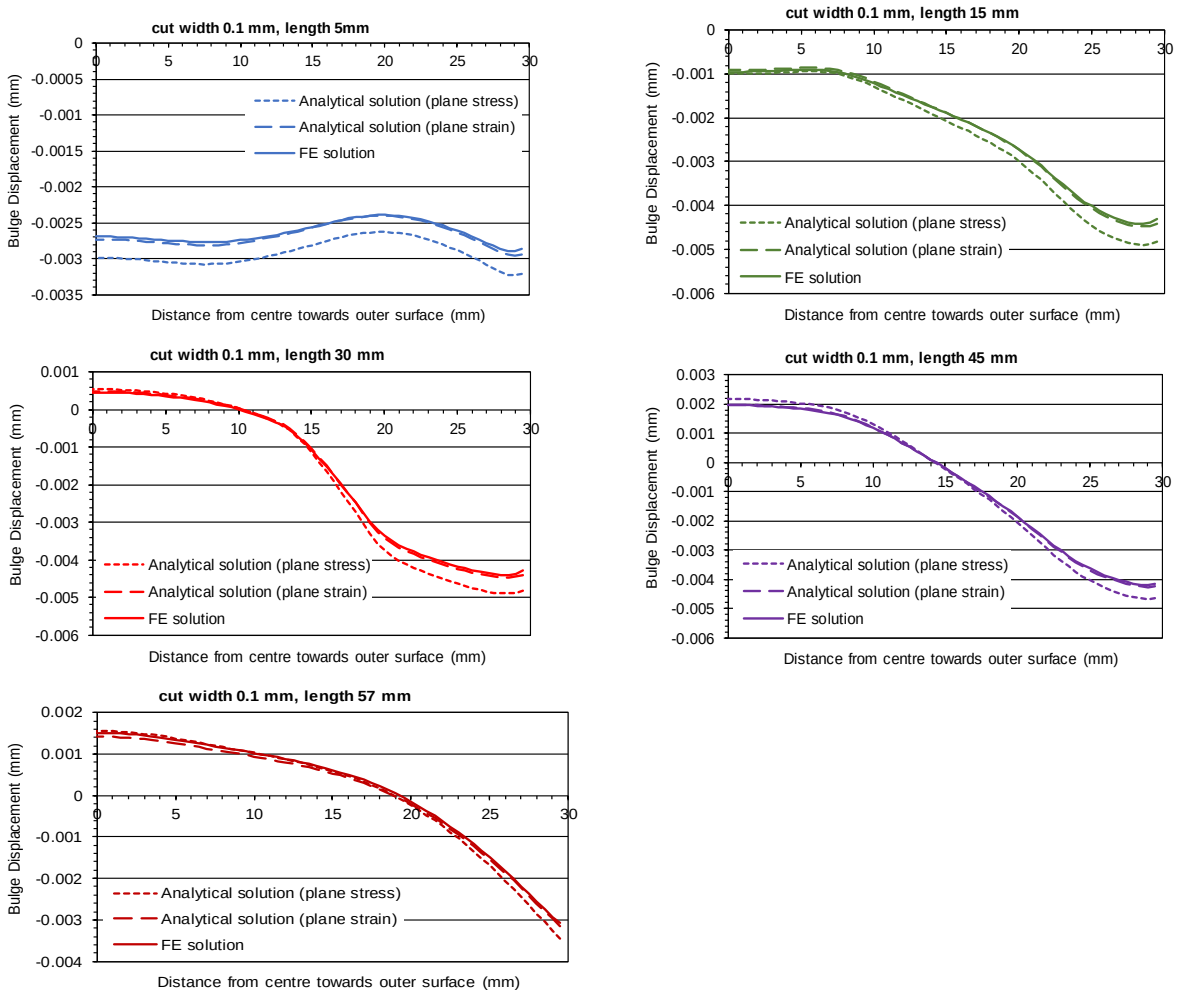

Figure 4 - 35: Comparison between the analytical plane stress and plane strain bulge displacement estimate and numerical FE calculation in a quenched 316H stainless steel solid cylinder, diameter 60 mm, length 60 mm, for cut width size 0.1 mm at different cut lengths.

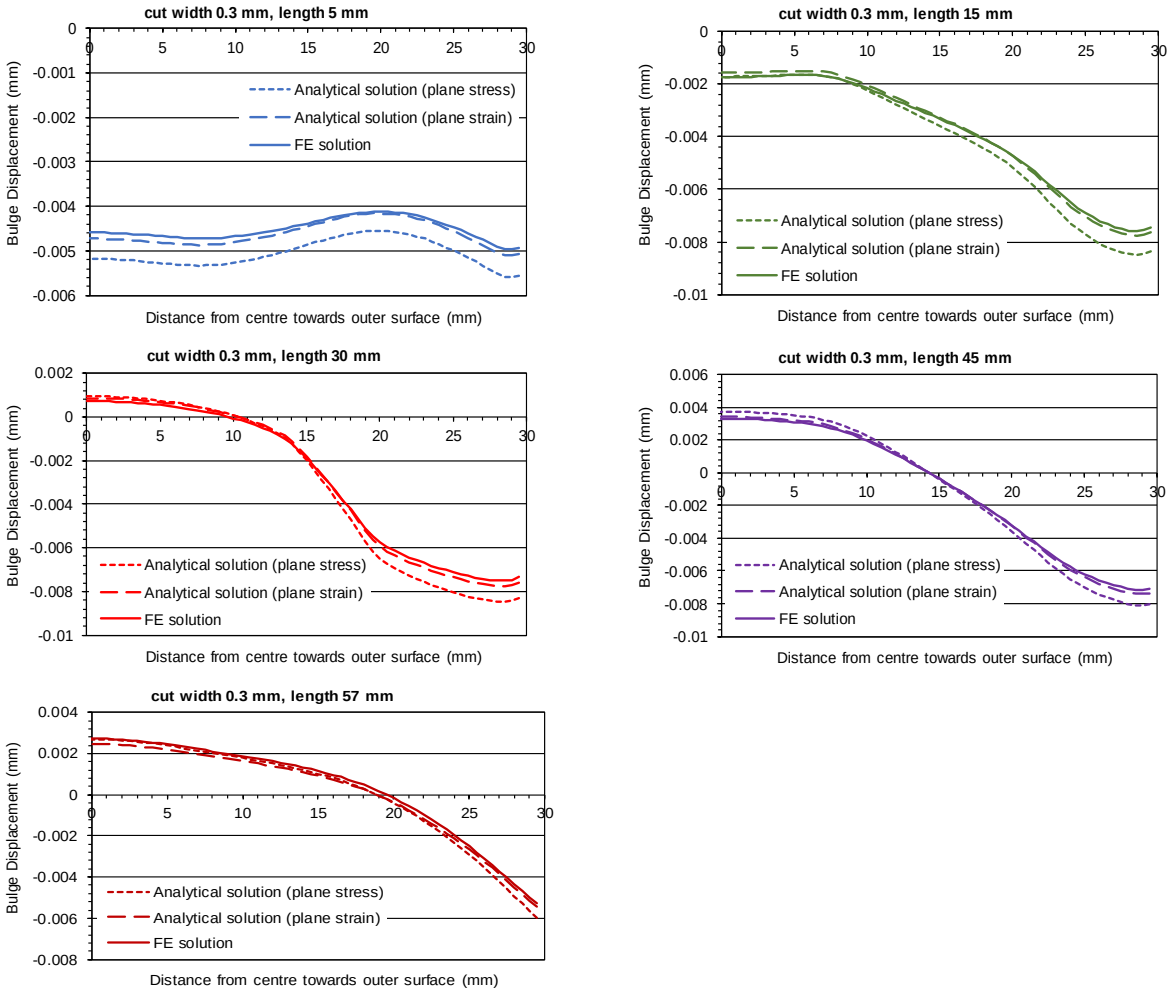

Figure 4 - 36: Comparison between the analytical plane stress and plane strain bulge displacement estimate and numerical FE prediction in a quenched 316H stainless steel solid cylinder, diameter 60 mm, length 60 mm, for cut width size 0.3 mm at different cut lengths.

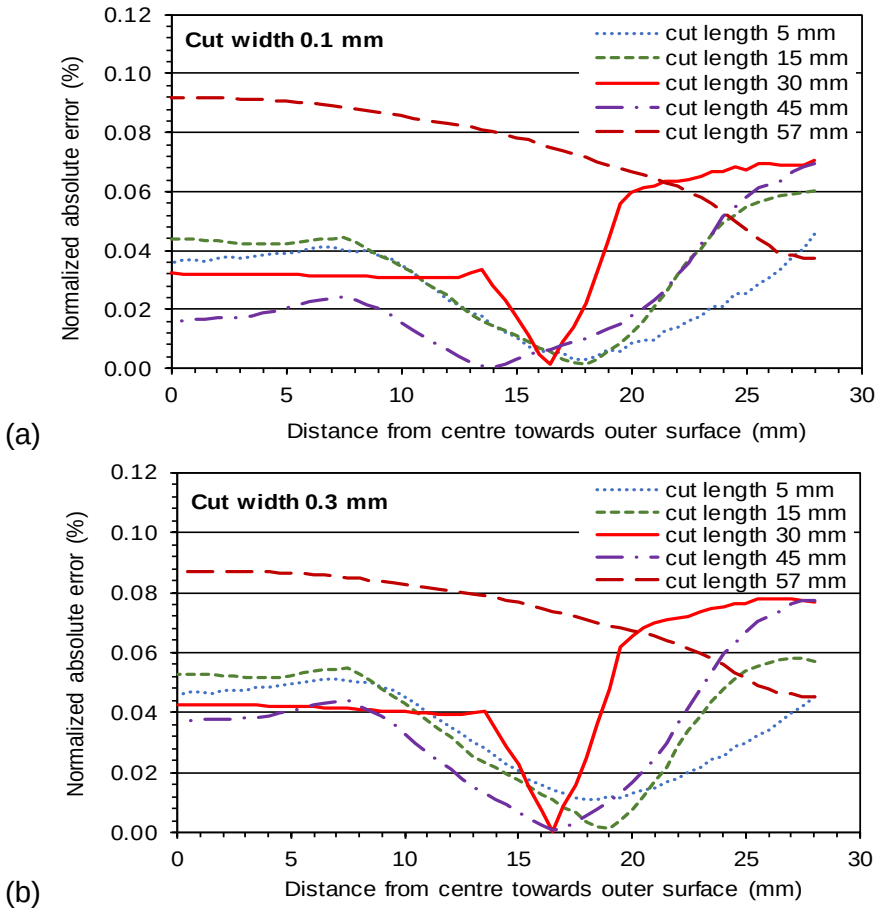

Figure 4 - 37: Normalized absolute error between the analytical and FE bulge displacement predictions in a quenched 316H stainless steel solid cylinder, diameter 60 mm, length 60 mm, for cut width size (a) 0.1 mm and (b) 0.3 mm, at different cut lengths.

4.4 Validation studies for residual stress measurements

In this section the analytical solution is implemented using SIFs for real residual stress distributions measured with the contour method. The cross-weld C(T) specimen in Chapter 3 and bent beam sample [3] were selected because the contour method stresses have been previously corrected for the bulge error using the iterative FE procedure.

4.4.1 Case study 1: Esshete 1250 cross-weld C(T) specimen

The C(T) welded specimen details and previous measurement results can be found in Chapter 3, section 3.3. The transverse residual stresses measured by the contour method were previously corrected for the bulge error using 2D and 3D iterative FE procedures in sections 3.2.3 and 3.2.4 respectively.

In this study the SIF previously measured by the slitting measurement [4] and a newly calculated FE SIF for the contour method stresses at mid thickness of the specimen is implemented in the analytical solution to estimate the bulge displacements at mid thickness of the specimen. The analytical bulge displacement solution, Equation 4 – 6 (b) with a plane strain condition was assumed based on the C(T) specimen dimensions. The elastic material properties were Young's modulus, E, and Poisson's ratio, ν, of 205 GPa and 0.29 respectively [146]. A final cut width, b, of 0.3 mm was chosen for the 250 µm diameter wire used for cutting. The contour method SIF was calculated using a 2D model of one half of the specimen with the measured stresses at mid thickness applied directly to the cut face as surface tractions during incremental cutting performed for a sharp crack. The slitting and contour method SIFs are shown in Figure 4 - 38 as a function of cut length. There is a spatial shift in the contour method SIF profile, towards the C(T) specimen front face, because the measured contour method stresses contain effects of bulging and/or plasticity. These results highlight the importance of using the SIF as it can indicate the positional error or shift in contour method measurements.

The analytical bulge displacements are shown in Figure 4 - 39 and are compared with the FE bulge displacements quantified in Chapter 3 section 3.1.4. The analytical solution provides a fairly good estimation of the bulge displacement but is slightly lower in magnitude in the tensile region and larger in magnitude in the compressive region when using the slitting SIF. In the slitting method the part is clamped on side to allow it to freely deform during the cutting (see section 3.1.2 for the previous measurement procedure). Also, the contour method SIF was calculated using a 2D model of one half of the specimen with constraints only to prevent rigid body motion. Whereas the FE procedure to estimate the bulge displacements used a full 2D model of the specimen with constraints applied to one half of the specimen to represent the clamping conditions for the slitting measurement. These inconsistencies might have influenced the magnitude of the analytical prediction.

To calculate the corrected contour method stresses, the simplified FE bulge correction procedure, described in Chapter 3 section 3.2, was implemented. The analytical bulge displacements were applied as boundary conditions to the cut surface of the 2D FE model shown in Figure 3 - 10 to calculate the stress error. The error was then combined with the initial contour method stresses at mid thickness to give the corrected stresses. Figure 4 - 40 shows the initial and corrected contour method stresses. The corrected stresses using the iterative FE procedure are also shown. Only one iteration was performed since the previously corrected stresses converged after the second iteration. The stresses corrected with the analytical bulge displacements using the contour method SIF gave a reasonably

good correction compared with the iterative FE correction. Whereas the analytical bulge displacements using the slitting SIF did not improve the stresses at mid thickness, although the stress distribution was slightly shifted away from the front face of the specimen. The unchanged peak tensile stress region (from the original profile) could be explained by the spatial shift in the slitting SIF and associated bulge correction location along the cut length.

The graph comparing the initially measured stresses using neutron diffraction, slitting and contour method techniques (Figure 3 - 3), is revised in Figure 4 - 41 to include the corrected contour method stresses using the 2D analytical approach and 2D and 3D iterative FE procedure for the first iteration. The corrected contour method stresses using the different approaches showed closer agreement with the neutron diffraction and slitting results, although detailed comparisons along the measurement line revealed some local discrepancies. Nonetheless, the proposed analytical approach using 2D FE analysis gave a reasonably good correction and is a simple method to correct complex contour method residual stress measurements for bulge error.

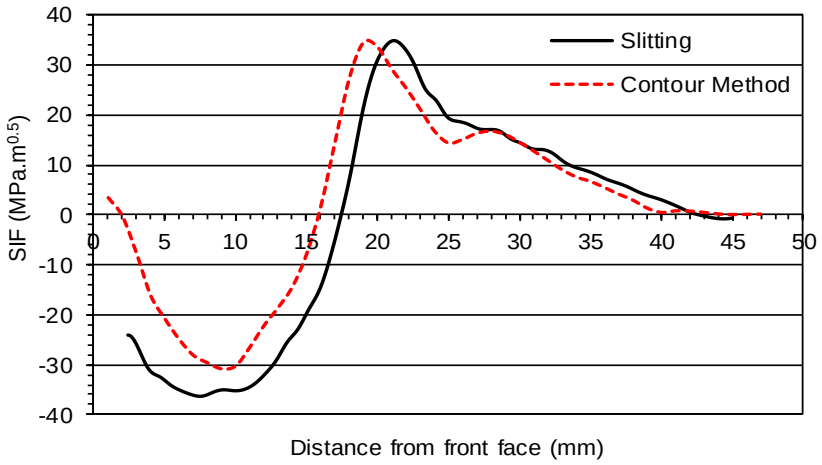

Figure 4 - 38: Mode I stress intensity factor (SIF) measured by the slitting method and the contour method SIF for the stresses at mid thickness of the specimen calculated using 2D FE analysis.

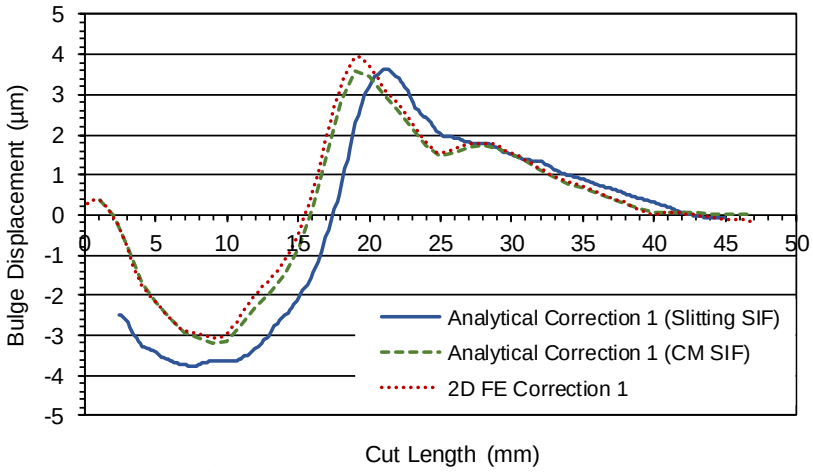

Figure 4 - 39: Comparison of the bulge displacements for the C(T) specimen estimated using the analytical solution with the slitting and contour method stress intensity factors and the previous iterative FE prediction for the first iteration.

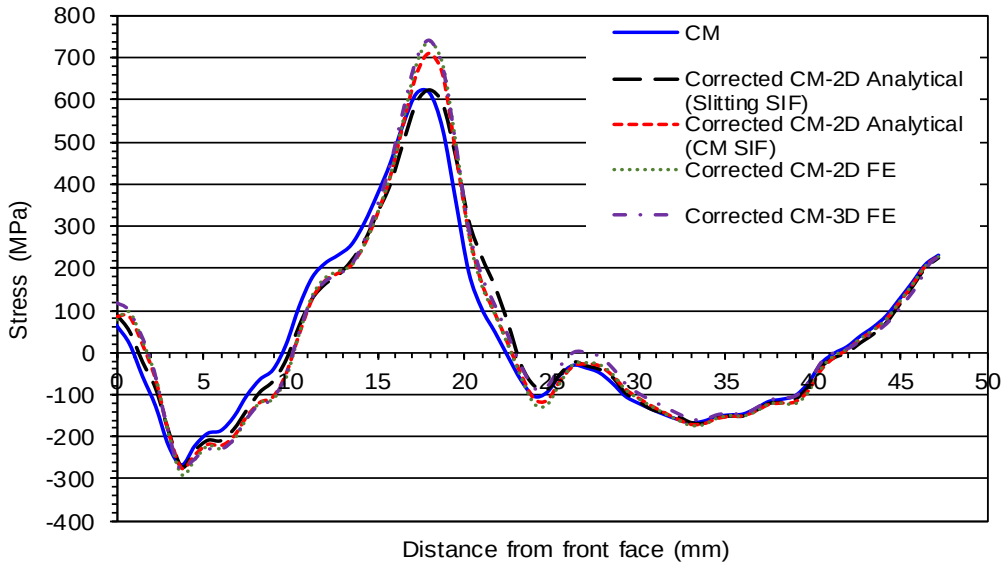

Figure 4 - 40: Line profile of the transverse stress along the mid-thickness of the contour cut plan showing the initially measured stresses, corrected stresses using the analytical solution with the contour method SIF and corrected stresses using the 2D and 3D iterative FE procedure for the first iteration.

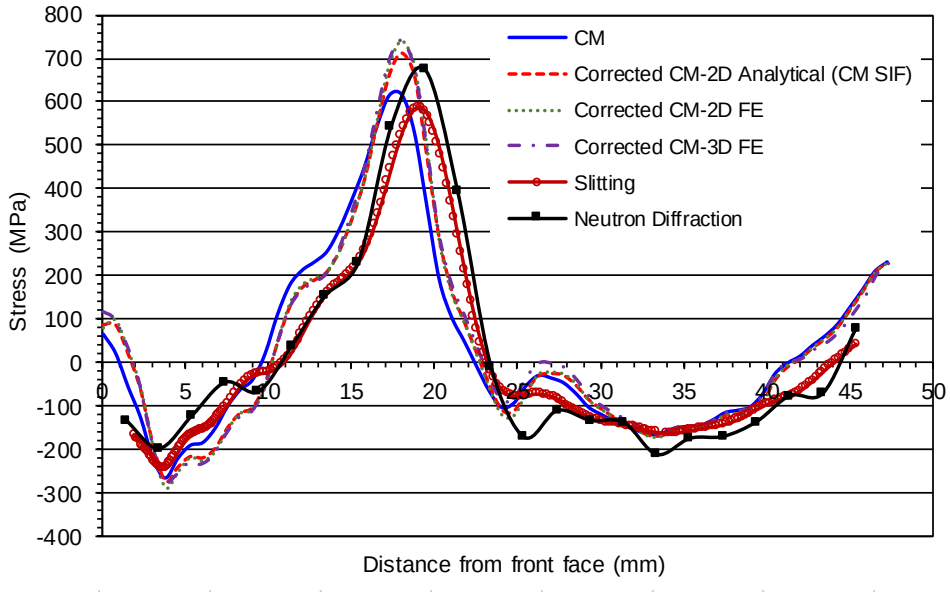

Figure 4 - 41: Line profile of the transverse stress along the mid-thickness of the contour cut plan showing the previously measured by neutron diffraction and slitting, and the corrected contour method stresses for bulge error using the 2D analytical approach and 2D and 3D iterative FE procedure for the first iteration.

4.4.2 Case study 2: Stainless steel bent beam sample

The previous work on this specimen was performed by Prime and Kastengren [3] involved characterising the residual stresses in a bent beam sample using the contour method technique and from the measured strain data. A slight shift and reduced stresses were found in the contour method results which were corrected for bulge error using 2D iterative FE procedure. The previous measurement results can be found in Chapter 2, section 2.7.2. In this section the initial contour method stresses for the bent beam are corrected for bulge error using the new analytical approach proposed.

First the specimen details and previous measurement procedure are given. Next the initial contour method results [118] are used in a 2D FE analysis to calculate the mode I SIF. Then bulge correction is performed using the analytical solution and alternative stress correction method explained in Chapter 3 section 3.2. Finally, a comparison is made between the corrected contour method stresses using the analytical approach and Prime and Kastengren's iterative FE procedure results.

Specimen details and previous measurement

The stainless-steel beam dimensions and bending setup are shown in Figure 4 - 42. The elastic material properties were Young's modulus, E, and Poisson's ratio, ν, of 194 GPa and 0.3 respectively. Residual stresses were introduced in the beam using four-point bending by loading it into the plastic range and then unloading. Strain gauges were attached on the 30mm cross-section and strain measurements recorded during bending. The residual stress profile was then calculated from the measured strain data using the stress-strain curve identification method [158].

The stresses in the beam were then measured with the contour method technique. During EDM cutting the beam was clamped on both sides of the cut. The EDM wire was a 100 µm diameter zinc-coated brass wire and gave a final cut width of 140 µm [3]. The contours of the two halves of the beam were averaged and used in a 2D FE analysis to back calculate the stresses as in the conventional contour method procedure.

The initial contour method stresses (see Figure 2 - 25) showed evidence of bulge error, i.e. reduced peak stresses and a shift towards the cut start, when compared with the stresses predicted in the bend test. Prime and Kastengren then corrected the contour method stresses for the bulge error using the 2D iterative FE procedure. The corrected stresses (shown in Figure 2 - 25) moved the contour method results closer to the bend test prediction. The initial contour method measurement data were obtained from Mike Prime [118] to estimate the SIF for analytical prediction of the bulge displacements.

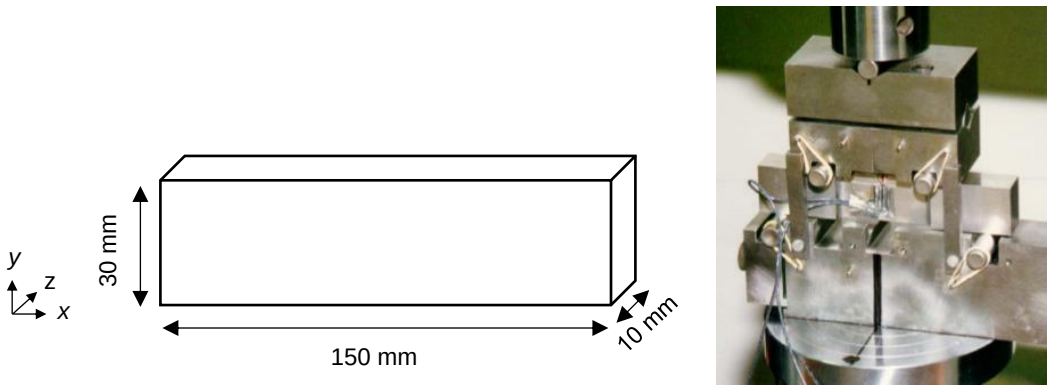

Figure 4 - 42: Stainless steel beam dimensions and four-point bending setup.

Calculating the stress intensity factor

To obtain the mode I SIF for the contour method residual stresses, a two-dimensional (2D) half symmetry model of the specimen was created in ABAQUS, shown in Figure 4 - 43. A

linear elastic material model was used with Young's modulus, E, and Poisson's ratio, ν, of 194 GPa and 0.3 respectively. The model was meshed with 44 160 quadratic plane stress elements of type CPS8 and contained 133 397 nodes. During EDM cutting, the specimen was clamped on both sides of the cut and at the top and bottom of the specimen. This was modelled by constraining the nodes at the top and bottom to prevent any lateral movement in the x-direction and one nodal constraint in the y-direction to prevent rigid body motion during cutting. The positions of the clamps were obtained via communication with Mike Prime [118].

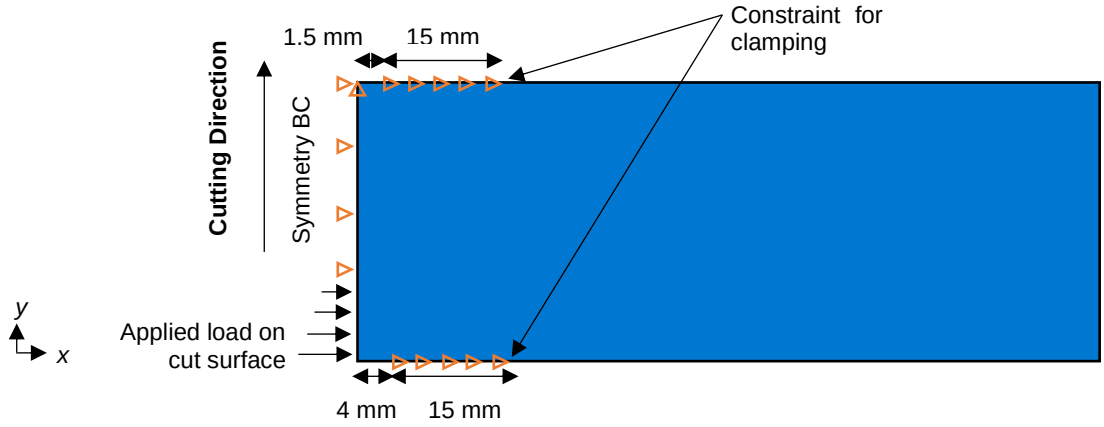

Figure 4 - 43: The 2D FE model of the beam used to calculate the mode I stress intensity factor showing the applied loading and constraints for clamping and to prevent rigid body motion.

Cutting was performed for a sharp crack by incrementally removing the symmetry boundary condition along the cut line. The measured contour method stresses were applied to the cut face as surface tractions using the analytical field function in ABAQUS. The mode I contour integral SIF was evaluated using the J-integral method. The crack was modelled by defining the crack tip and crack propagation direction. The stress singularity at the crack tip was controlled by defining quarter point node positions at the crack tip. The predicted mode I SIF, shown in Figure 4 - 44, was stable after 5 contours. The stress intensity factor is iterated every time the stresses are corrected until a converged stress solution is reached.

Correcting for the bulge error

Following this the SIF as a function of cut length was defined in the analytical bulge displacement solution, Equation 4 – 6 (a), as a plane stress condition was assumed based on the specimen dimensions. The elastic material properties were Young's modulus, E, and

Poisson's ratio, ν, of 194 GPa and 0.3 respectively. A final cut width, b, of 0.14 mm was specified for the 100 µm diameter wire used for cutting.

Once the analytical bulge displacements were obtained the alternative bulge correction procedure, described in Chapter 3 section 3.2, was used to calculate the corrected stresses. The analytical bulge displacements were applied as boundary conditions to the cut surface of the 2D FE model shown in Figure 4 - 43 to calculate the stress error. The error was then combined with the initial contour method stresses to give the corrected stresses. Only two iterations were necessary to reach a converged stress solution as the correction was small. Figure 4 - 45 shows the analytical bulge displacements for the first and second iterations. Figure 4 - 46 shows the revised graph of the contour method stress results to include the corrected stresses using the analytical bulge displacements. The stresses corrected with the analytical bulge displacement prediction showed good agreement with the iterative FE correction.

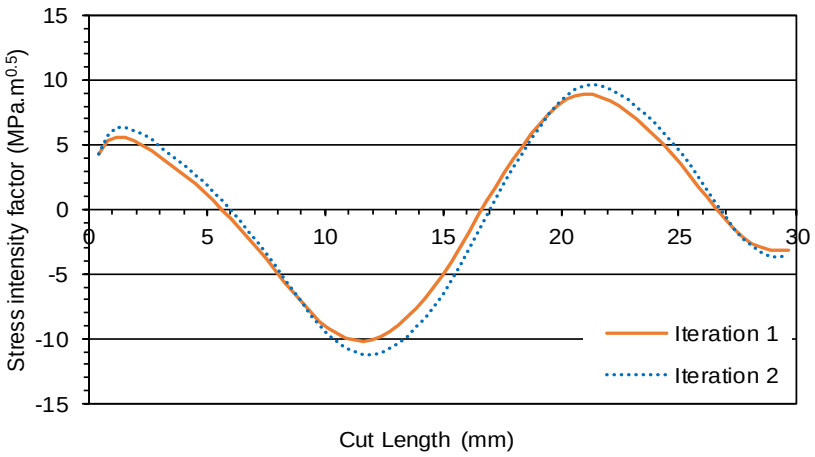

Figure 4 - 44: FE mode I stress intensity factor for the bent beam specimen calculated using the contour method stresses for first and second iterations.

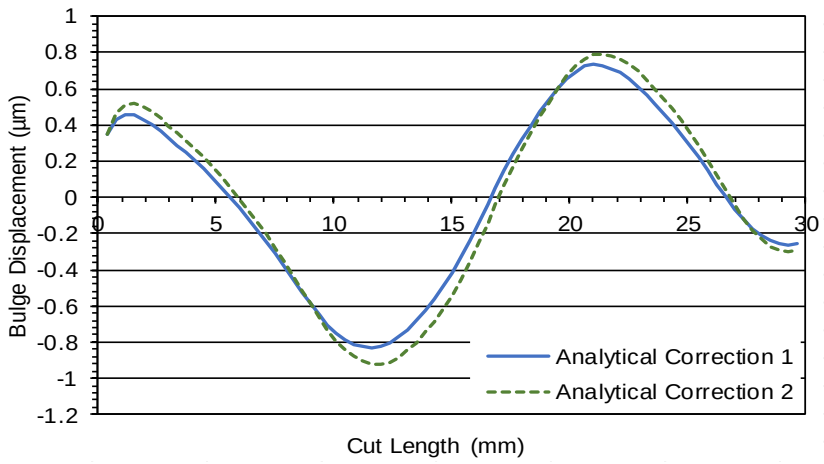

Figure 4 - 45: Bulge displacements for the bent beam specimen estimated using the analytical solution with the contour method stress intensity factor for the first and second iterations.

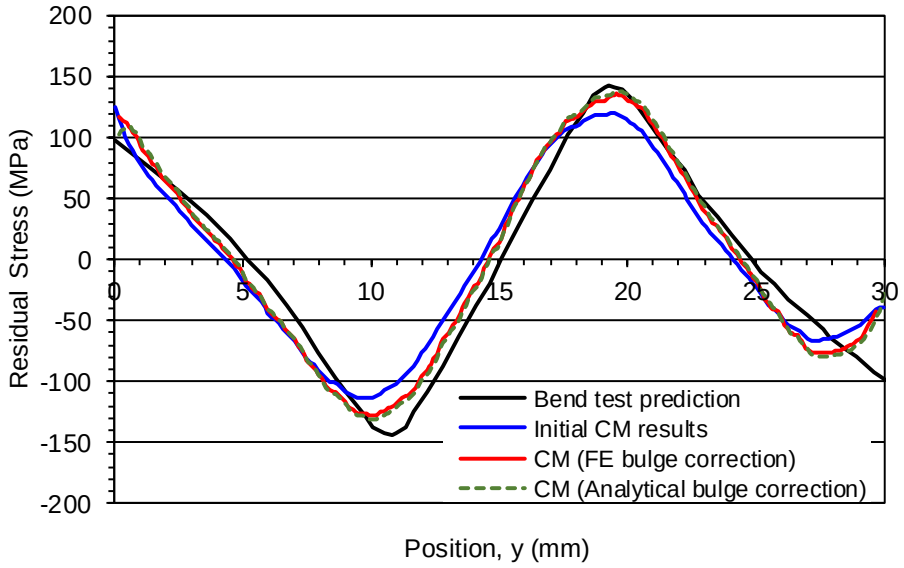

Figure 4 - 46: Contour method residual stress results showing the initially measured stresses, published correction using the iterative FE procedure and new correction using the analytical method compared with the prediction from the bend test.

4.5 Discussion

The initial work in this chapter demonstrated the relationship between the bulge error and the local stress state at the cut tip which can be characterised by the mode-I SIF. Extensive FE simulations were performed to develop SIF correlations using plane stress and plane strain analysis for a single edge-cracked plate with far field tension and bending loading.

Several parameters i.e. plate geometries, material properties and cut width sizes, were chosen to develop robust correlations.

The correlations showed a linear relationship and approximate proportionality between the bulge displacements and stress intensity factor. This confirms Prime and Kastengren suggestion that the bulge error is approximately proportional to the stress intensity factor, *K*, at the cut tip from the accumulated effect of releasing residual stress [3]. For linear elastic material behaviour, the bulge displacements were inversely proportional to the elastic stiffness. The bulge displacements for the plane stress state were approximately 10 % larger than the plane strain state. This is a fairly small difference, therefore a 2D approximation of the bulge displacements might be suitable for 3D cases (i.e. contour measurements of real components).

The bulge displacements were found to be directly proportional to the square root of the cut width. Prime and Kastengren previously examined the effect of slot width on the bulge error and found that the peak bulge error increases with slot width and the error was greater for narrow slots [3]. Using a smaller wire diameter shows a significant reduction in the bulge error although Prime has mentioned that using a smaller wire diameter below 100μm may introduce other difficulties in the cutting process such as wire breakage [3].

Additionally, the mesh size study revealed that there was no change in the calculated bulge displacements when the mesh used to represent the cut width was refined. This confirms that the current practice of using one element to represent the cut width is sufficient to estimate the bulge displacements at the cut tip. However, the mesh size close to the cut can have a large effect on the measured displacements and should be sufficiently refined (see the mesh sensitivity study in Chapter 3 section 3.1.3). A study of the geometry idealisation showed a significant error (overestimate) of up to 10 percent using a 0.25 mm square end slot rather than a semi-circular slot end: This suggests that bulge errors may be slightly overestimated using a square end idealisation. A general correction factor, example 10 percent reduction, could be applied when using a square slot, however, more work is needed because the error will depend on the local stress state at the cut tip, cut length, material properties, slot width and restraint conditions.

The parameters that have not been taken into consideration to develop the SIF correlations include additional restraint close to the cut plane, orientation and direction of the cut, non-linear effects at the cut tip such as plasticity, strain hardening etc, complex geometrical shapes and 3D cases.

Following this work an analytical solution, based on LEFM, has been presented to predict bulge displacements in contour method measurements for cases of plane stress and plane strain. The displacement equations rely on knowledge of the mode I SIF. The equations have been verified for an edge crack in a finite width plate under tension loading and showed good agreement with the numerical prediction for both the plane stress and plane strain states. The suitability of the equations to predict the bulge displacements across the thickness of a 3D body was investigated for a cylinder with residual stresses introduced by quenching. In this case, the plane strain analytical solution showed better agreement with the numerical prediction along the crack front across the thickness diameter of the cylinder.

The equations were then used to predict the bulge displacements in real contour method measurements for a C(T) welded specimen and bent beam sample. In both cases, the SIF was obtained for a line profile of stresses at mid thickness of the specimen using 2D FE analysis. The stresses corrected with the analytical bulge displacement prediction showed good agreement with the iterative FE correction method.

Accurate prediction of the SIF due to the residual stresses being measured is essential when using the analytical solution. Many SIF solutions are available in literature but are typically for two-dimensional idealizations and simple loading scenarios. Whereas, in real specimens the residual stress fields are three dimensional and more complex, such as welded specimens, and will most likely require FE analysis to obtain the SIF. When using FE analysis, it is important to apply the equilibrated contour method stresses to ensure a correct prediction of the SIF. Sometimes a slitting residual stress measurement is performed together with the contour method and this can provide direct information about the mode I SIF. However, this is for the averaged stresses across the thickness which might under predict the bulge error in specimens with large stress variances across the thickness. In such cases SIF estimates based on initial contour method measurement is required.

Since the analytical solution assumes linear elastic material behaviour, it does not account for any non-linear effects such as plasticity in contour method measurements. Also, any effect of clamping is not taken into consideration in the analytical solution. In practice the specimen is firmly clamped on both sides during cutting to prevent the cut plane from moving as the stresses relax. Depending on how close the clamping arrangement is to the cut, it may influence the magnitude of the stresses at the cut tip and should be carefully considered when determining the stress intensity factor.

4.6 Conclusion

The stress intensity factor correlations revealed the following features about the bulge error:

- There is a linear relationship between the bulge error and mode I SIF.
- The bulge error is larger for the plane stress state than plane strain state by approximately 10 percent.
- The bulge error is inversely proportional to the elastic stiffness of the material.
- The bulge error is directly proportional to the square root of the cut width size.

An analytical solution, Equation 4 – 6, derived using standard displacement field equations in LEFM, provides a simple alternative method for estimating bulge displacement errors in contour method residual stress measurements. The mode I SIF as a function of cut length (and along the cut tip) due to the residual stresses in the specimen must be known with the elastic properties of the material and the final cut width size created during the wire EDM process.

Accurate prediction of the mode I SIF is essential because it directly influences the magnitude of the bulge error. In specimens with large variances in the residual stresses across the thickness, the SIF from the slitting measurement technique may not be suitable to use in the analytical solution. In such cases, the stress intensity factor must be determined from initial contour method measurement stress results.

The analytical approach has been successfully applied to estimate the bulge error in real contour method measurements. Once the bulge displacements are obtained, the alternative method described in section 3.2 can be used to calculate the corrected stresses. The analytical solution is found to be within a few percent of the numerical predictions.

Correcting for the bulge error will help to improve the accuracy and reliability of measurements made by the contour method. The iterative FE procedure and alternative analytical solution can estimate the bulge error. In the next chapter stress error correlations are developed to set a threshold for correcting for the bulge error.

Chapter 5: Evaluating the local stress error due to bulging

The bulge error can have significant effects on residual stress measurements made with the contour method. The magnitude of the bulge displacements in contour measurements can be estimated using a contour cutting FE simulation or the proposed analytical approach that requires knowledge of the stress intensity factor. However, this cannot tell us when the bulge error becomes apparent in contour method residual stress results. Further analysis is required to correct the initially measured surface contours and calculate the new stresses using finite element analysis. The procedure is iterative and time-consuming, and the outcome of bulge correction on the measured residual stresses is only evident after a converged solution has been reached.

The aim of this chapter is to determine the stress error magnitude due to bulging in contour method results to enable the practitioner to decide whether to correct for it. To do this, the stress error due to bulging is first evaluated for the simple case of a self-equilibrated cosine residual stress profile and then for a more real case of a complex weld stress profile in the plane stress and plane strain conditions. The objective is to develop correlations of the normalised stress error with the mode I stress intensity factor. The analysis is then extended to evaluate the stress error through the thickness of a solid cylinder with a residual stress distribution introduced by quenching.

5.1 Bulge errors introduced by a cosine form residual stress profile

The stress error due to bulging was studied by considering an idealised cosine residual stress profile in the plane stress condition. The bulge error was estimated using the mode I stress intensity factor solution for a centre-crack plate in a periodic cosine residual stress distribution [145]. The corresponding stresses including the bulge error were calculated in a finite element analysis. The magnitude of the stress error was evaluated relative to the idealised cosine profile for different cut width sizes and stress wavelengths.

Idealised stress profile

A one-dimensional cosine stress profile acting across a finite width plate is self-equilibrated and can be taken to represent an idealised form of residual stress distribution most

commonly seen in quenched samples [46, 48, 159] and some types of welded specimens [160, 161].

A previous study of the data analysis parameters for the contour method showed, using a 2D FE stress analysis, that an idealised one dimensional cosine surface deformation profile (defined by Equation 5 -1) applied normal to the edge of a wide plate having a wavelength *w*, and peak amplitude *M*, results in a stress profile along the edge that has a similar cosine form [162]. Similarly, for this case the stress distribution at the surface of a finite plate is calculated for a cosine surface deformation with w = 50 mm and M = 0.02 mm (see Figure 5 - 1), using symmetric boundary conditions and assuming plane stress conditions. A linear elastic material model was defined to obtain the residual stress distribution with a Young's modulus, E, and Poisson's ratio, ν, of 71.1 GPa and 0.33 respectively.

$$y(x) = M\,cos(n\phi) \qquad \textit{Eqn. 5 - 1}$$

Where, $y(x)$ represents the surface deformation profile, M the maximum amplitude, and n is the order of the function and $\phi = \frac{2\pi x}{w}$, where w is the wavelength of the surface profile distribution.

Figure 5 - 2 shows the FE model dimensions, boundary conditions and stress results. The cosine stress empirical formula can be derived from the FE results and is defined by Equation 5 – 2 for this case. The FE predicted cosine stress profile is compared with the empirical fit in Figure 5 - 3.

$$\sigma\left(\frac{x}{w}\right) = 3.52\,E\left(\frac{M}{w}\right)cos\left(\frac{2\pi x}{w}\right) \qquad \textit{Eqn. 5 - 2}$$

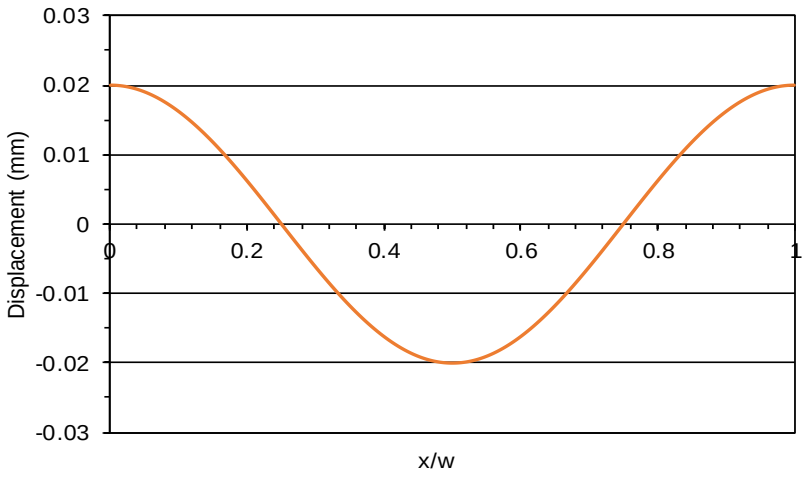

Figure 5 - 1: Idealised cosine displacement profile as a function of x/w.

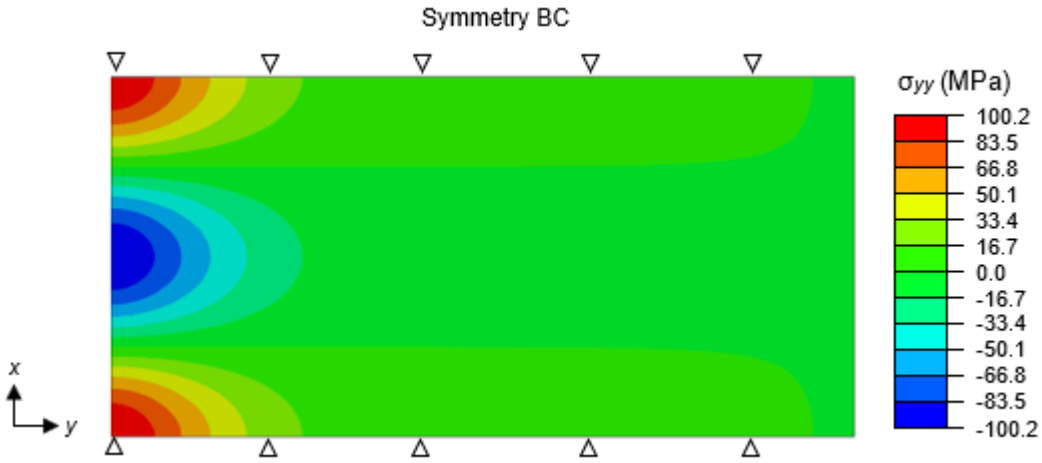

Figure 5 - 2: Finite element model of a finite plate with dimensions 50 mm x 100 mm, the boundary conditions and normal stress results along the edge (for displacement M = 0.02 mm).

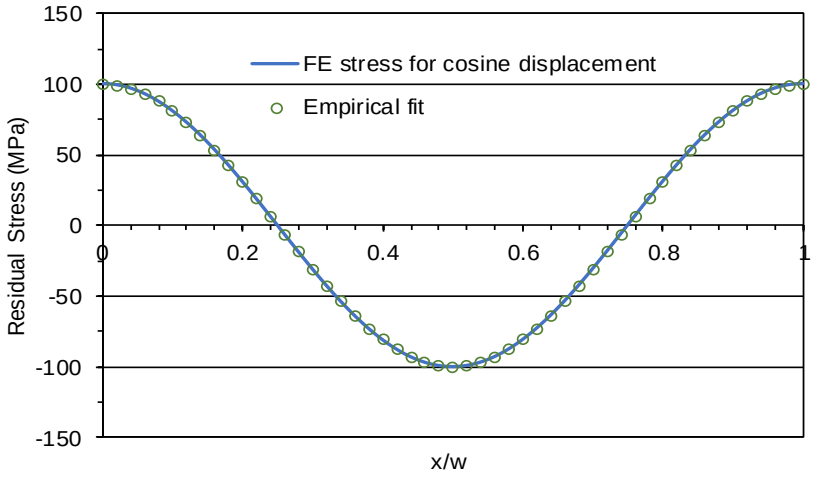

Figure 5 - 3: Predicted cosine stress profile and the derived empirical fit as a function of x/w.

Approximating the stress intensity factor

A Fourier series approach which provides a simple means of determining the stress intensity factor for an arbitrary residual stress field along a proposed crack path is available in the literature [145]. The study is based on the linear elastic analysis of stress surrounding a crack in an ideal material having isotropic elastic properties.

The mode I stress intensity factor for a centre-crack plate loaded by a periodic cosine residual stress function can be defined in terms of the Bessel function, J_0, of the first kind and order zero:

$$K_I = \sigma_0 \sqrt{\pi a}\ J_0\left(\frac{\pi n a}{w/2}\right) \qquad \textit{Eqn. 5 - 3}$$

Where $J_0(0) = 1$, σ_0 is the peak stress located at mid-length of the crack, $2a$ is the length of the crack and w is the interval over which the cosine function of order n is acting, where $w/2 > a$, see Figure 5 - 4.

This Fourier based equation is derived for the plane stress and plane strain condition and gives reliable SIF results over the entire crack length range.

The stress intensity factor as a function of crack length for the cosine stress profile (that is $\sigma_0 = 100MPa, n = 1\ \&\ w = 50\ mm$) is shown in Figure 5 - 5.

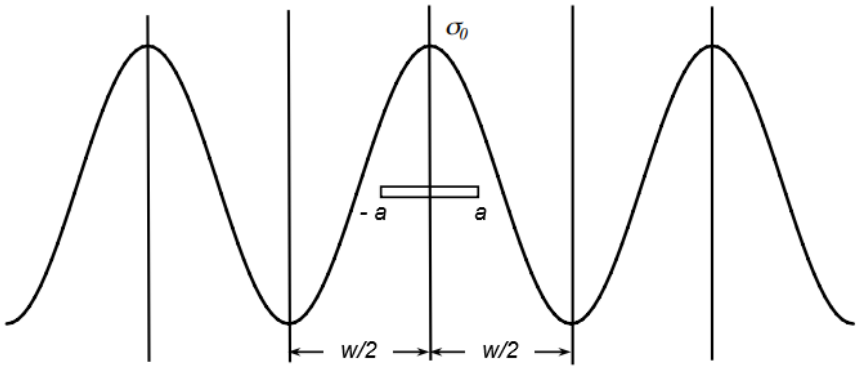

Figure 5 - 4: Single crack in a cosine residual stress field spanning length w of order n = 1.

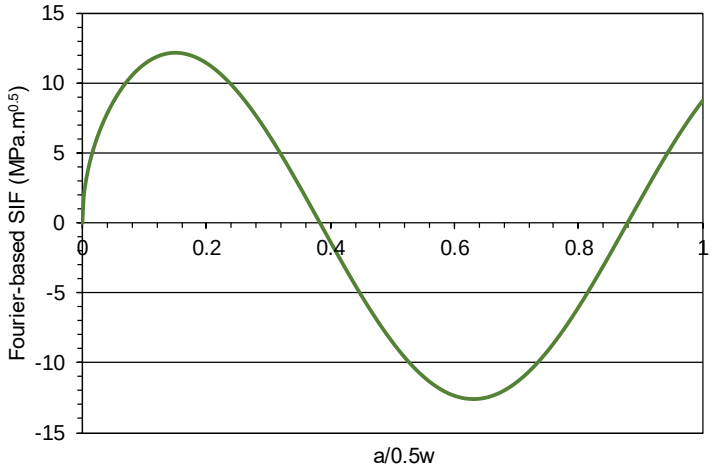

Figure 5 - 5: Mode I stress intensity factor for a centre-crack plate subjected to a cosine stress field ($\sigma_0 = 100MPa$, n = 1)

Calculating the bulge displacements

The bulge displacements due to the cosine residual stress profile were estimated using the stress intensity factor in the analytical displacement field solution, Equation 4 - 6(a) (see Chapter 4 section 4.2), for the plane stress condition and several cut width sizes (b).

Figure 5 - 6 shows the calculated bulge displacements as a function of crack length. As expected, the bulge displacements scale with the square root of the cut width.

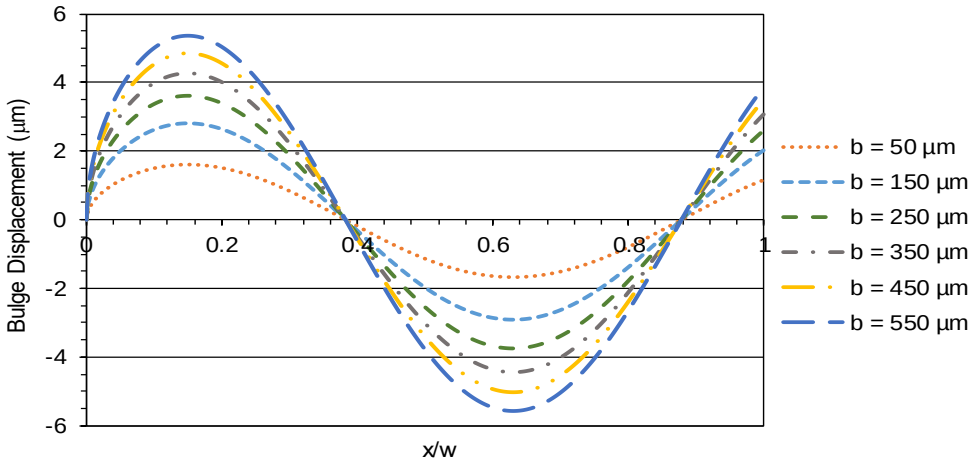

Figure 5 - 6: Analytically estimated bulge displacements for a centre-crack plate subjected to a cosine stress field ($\sigma_0 = 100MPa$, n = 1).

Furthermore, the stress intensity factor solution in terms of the Bessel function (see Equation 5 – 3) can be combined with the analytical bulge displacement solution (see Equation 4 – 6 in section 4.2) to give a general solution to calculate the bulge displacements as a function of crack half-length, a, for a centre-crack in a periodic cosine residual stress field within a large plate,

For plane stress,

$$U_{Bulge\ Error}(a) = \frac{4\sigma_0}{E}\sqrt{\frac{ba\sqrt{2}}{4}}\,J_0\left(\frac{\pi na}{w/2}\right) \qquad \textit{Eqn. 5 - 4 (a)}$$

And plane strain,

$$U_{Bulge\ Error}(a) = \frac{2\sigma_0(2-2\nu^2)}{E}\sqrt{\frac{ba\sqrt{2}}{4}}\,J_0\left(\frac{\pi na}{w/2}\right) \qquad \textit{Eqn. 5 - 4 (b)}$$

Where $J_0(0) = 1$, σ_0 is the peak stress located at mid-length of the crack, b is the final EDM slot width, $2a$ is the length of the crack and w is the interval over which the cosine function of order n is acting.

Calculating the stress including the bulge error

To calculate the stress including effects of bulge error, the bulge displacements were subtracted from the cosine surface displacements and applied in the finite element model (see Figure 5 - 2). The revised surface displacements, normalised with the peak displacement amplitude (M = 0.02 mm), are shown in Figure 5 - 7. The resultant-back calculated stresses are shown in Figure 5 - 8. The stress results towards the ends of the w domain was unstable (for the periodic stress function in an infinite plate) and therefore neglected for 2 percent (0.02 x/w) of the domain at both the ends. There is a phase difference and reduced peak amplitude in the predicted stresses including the bulge error. The maximum errors occur in three positions; 0.15, 0.63 and 0.98 x/w. Neglecting the error at 0.98, the far end of the w domain, where the stresses were more unstable, the other two positions correspond to the position of the maximum SIF (see Figure 5 - 5).

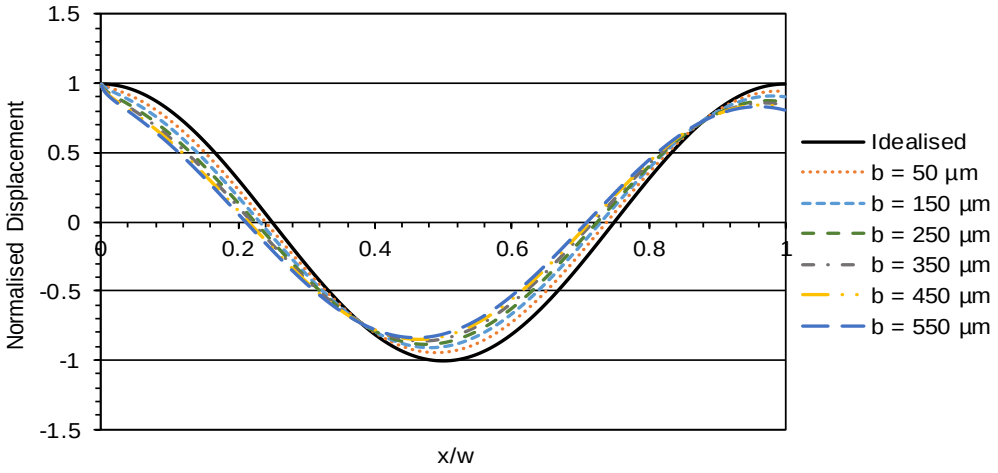

Figure 5 - 7: Normalised cosine surface displacement over domain w including the bulge displacements for various cut width sizes for a centre-crack plate subjected to a cosine stress field ($\sigma_0 = 100MPa$, n = 1).

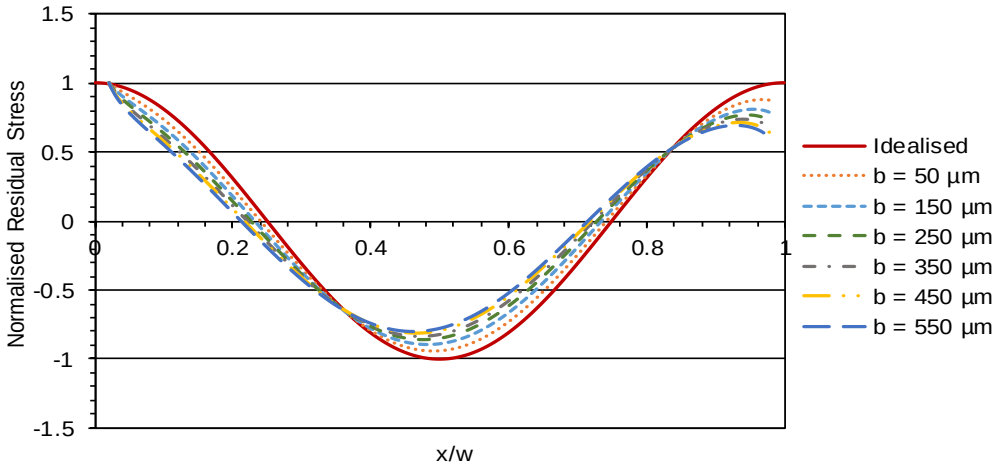

Figure 5 - 8: Normalised cosine stresses and predicted stresses including the bulge error for various cut width sizes for a centre-crack plate subjected to a cosine stress field ($\sigma_0 = 100MPa$, n = 1), acting over domain w.

Stress error correlations

The percentage stress error was calculating, using Equation 5 - 5, defined as the difference between the predicted stress including the bulge error and the known idealised cosine profile, normalised by the maximum of the known stresses.

$$\tilde{\sigma}_{error}(x) = \frac{|\sigma_{incl.\ bulge}(x) - \sigma_{idealised}(x)|}{max(\sigma_{idealised}(x))} \times 100\% \qquad \textit{Eqn. 5 - 5}$$

The root-mean-square (RMS) average stress error calculated over the entire cut, using Equation 5 - 6, quantifies the average error in the predicted stresses, where m is the total crack lengths.

$$\bar{\sigma}_{RMS\ error} = \sqrt{\frac{1}{m}\sum_{i=1}^{m}(\tilde{\sigma}_{error}(x_i))^2} \qquad \textit{Eqn. 5 - 6}$$

To develop the correlations, the normalised stress error is plotted against the absolute value of the stress intensity factor normalised with the maximum SIF. Figure 5 - 9 shows a linear relationship from 9.4 mm (x/w = 0.188) to 31.8 mm (x/w = 0.636). Outside of this range the correlation is unreliable and has been neglected. The stress error also scales with the square root of the cut width.

For the same crack length range, the normalised stress error can be plotted against the absolute value of the bulge displacements normalised with the peak displacement amplitude M. Figure 5 - 10 shows a common linear trend for the different cut width sizes.

Figure 5 - 11 shows the RMS average stress error calculated over crack length 0.05 ≤ x/w 0.95, (i.e. neglecting the first and last 5 % crack length) with the maximum normalised bulge for each slot size. Also included in this figure is the equation for a line of best fit to the data set and R^2 value indicating the accuracy of the trend line to the data points. The R^2 value is one, therefore it is a perfect fit with the line passing through all the data points. The average error in the predicted stress is up to 19 percent.

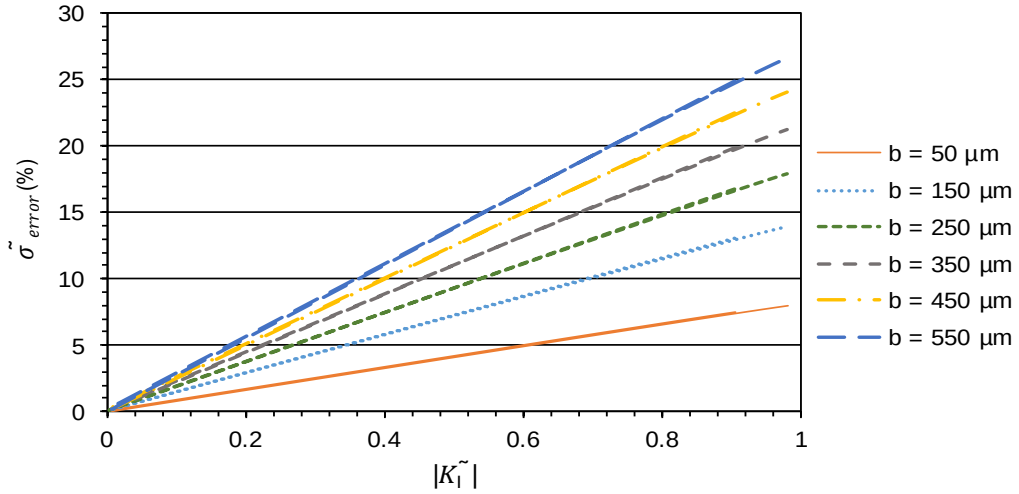

Figure 5 - 9: Correlation of the normalised stress error due to bulging with the normalised mode I stress intensity factor for a centre-crack plate subjected to a cosine stress field ($\sigma_0 = 100MPa$, n = 1) and different cut width sizes. For cut lengths 0.188 ≤ x/w ≤ 0.636.

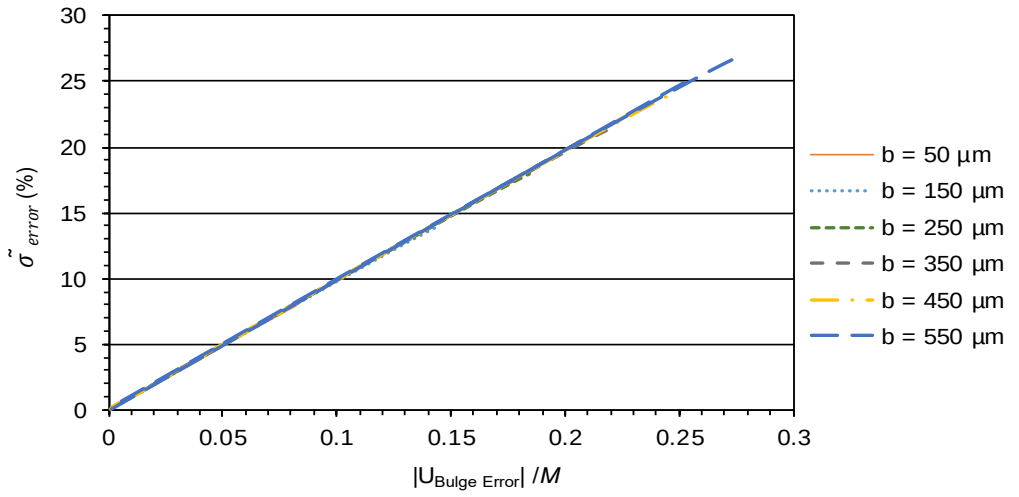

Figure 5 - 10: Correlation of the normalised stress error due to bulging and the bulge displacements normalised with the peak surface displacement M for each cut width size for a centre-crack plate subjected to a cosine stress field ($\sigma_0 = 100MPa$, n = 1). For cut lengths 0.188 ≤ x/w 0.636.

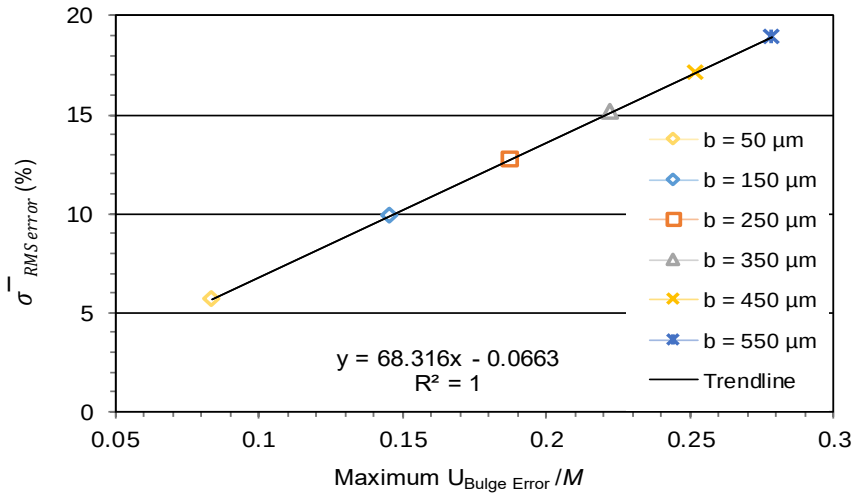

Figure 5 - 11: RMS average stress error calculated over cut lengths 0.05 ≤ x/w 0.95 and the maximum bulge displacement normalised with the peak surface displacement M for each cut width size for a centre-crack plate subjected to a cosine stress field ($\sigma_0 = 100MPa$, n = 1).

Systematic studies for varied stress parameters

This study investigates the influence of decreased stress wavelength on the stress error correlations to evaluate the bulge error in contour method measurements. The work performed in the previous analysis is repeated for a centre-crack plate loaded by an even cosine residual stress function of increasing order, *n* = 2 and 4.

Increasing the order of the cosine function, n, results in a decrease in the wavelength w. According to Equation 5 - 1, to achieve a reduced wavelength but maintain the same peak stress σ_0, the cosine surface deformation amplitude *M* must be decreased as shown in the table below.

order *n*	peak amplitude *M*	peak stress σ_0
1	0.02	100
2	0.01	100
4	0.005	100

The idealised cosine stress profiles, for, *n* = 1, 2 & 4, calculated using the empirical formula Equation 5 - 2, normalised with the peak stress is shown in Figure 5 - 12. The corresponding Fourier based stress intensity factors are shown in Figure 5 - 13. As the order of the cosine function increases, the magnitude of K_I decreases. This is in agreement with the literature

which shows that K_I decreases with the inverse of the square root of *n* and the peak SIF for any value of n can be approximated by Equation 5 - 7 [145].

$$|K_I|_{max} = 0.8\sigma_0\sqrt{\frac{w/2}{n}} \qquad \textit{Eqn. 5 - 7}$$

Figure 5 - 14 shows a similar trend for the predicted bulge displacements, for cut width size b = 0.25 mm, because the bulge error is directly proportional to the stress intensity factor. Therefore, the magnitude of the bulge error decreases with the square root of the wavelength of a cosine function.

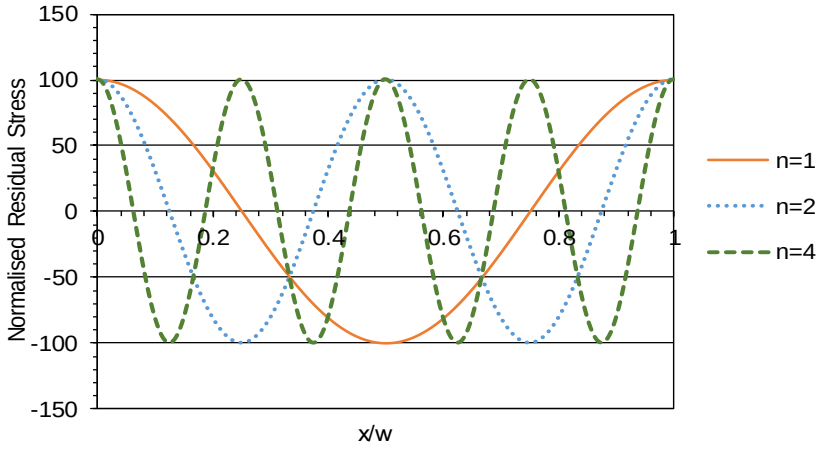

Figure 5 - 12: Predicted cosine residual stress functions of increasing order, n.

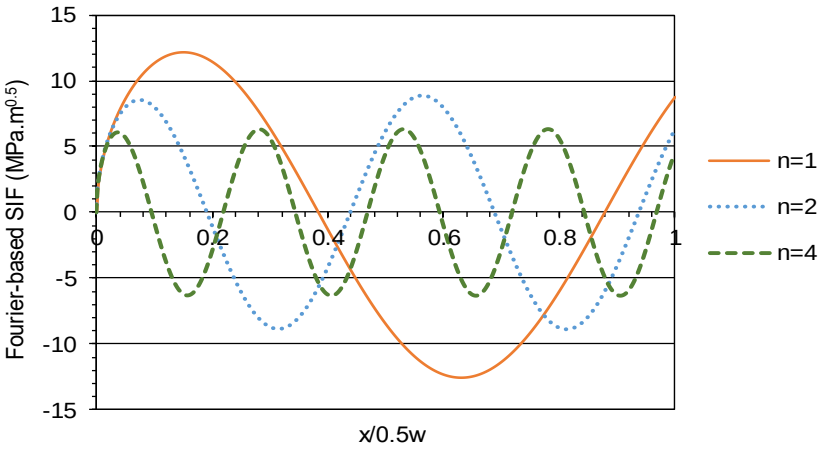

Figure 5 - 13: Mode I stress intensity factors for a centre-crack plate loaded by cosine residual stress functions of increasing order, n.

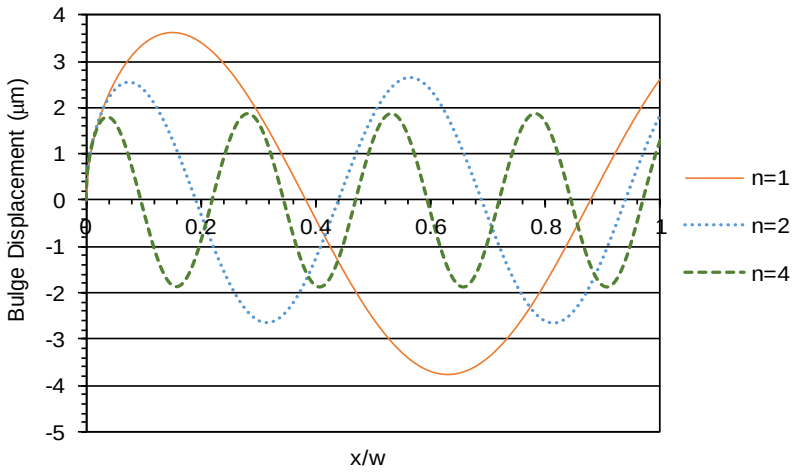

Figure 5 - 14: Analytical bulge displacements for a centre-crack plate subjected to a cosine stress field ($\sigma_0 = 100MPa$, n = 1, 2 & 4) and cut width size 0.25 mm.

The stress error correlations for a periodic cosine residual stress field of order *n* = 2 and 4 are shown in Figure 5 - 15. For the decreased stress wavelength, the correlations of the normalised stress error to the normalised absolute stress intensity factor shows a linear relationship within cut lengths 0.188 ≤ x/w ≤ 0.636. However, the level of error, that is the slope of the line, increases slightly as the crack progresses through the period cosine stress profile. That is, the stress error is slightly larger for the same value of the stress intensity factor at increased cut length.

The normalised stress error is plotted against the bulge displacements normalised with the peak displacement amplitude, M, in Figure 5 - 16. This figure shows a common linear trend for all three cosine stress fields of order *n* = 1, 2 & 4 and the different cut width sizes. The R^2 value is close to unity, therefore an acceptable fit has been made to the data. Figure 5 - 17 shows the RMS average stress error calculated over crack length 0.05 ≤ x/w 0.95 for *n* = 1, 2 & 4, with the maximum normalised bulge for each cut width. The average error in the predicted stress is up to 40 percent for *n* = 4. The decreased surface deformation wavelengths resulted in larger stress errors from bulging.

The positional error or effective shift of the peak stress was calculating, using Equation 5 - 8, defined as the difference between the location of the peak stress including the bulge error and the idealised cosine profile, normalised by the wavelength w. Figure 5 - 18 shows the positional error for *n* = 1, 2 & 4, for each cut width size.

$$x_{error} = \frac{|x_{incl.\ bulge} - x_{idealised}|}{w} \times 100\% \qquad \textit{Eqn. 5 - 8}$$

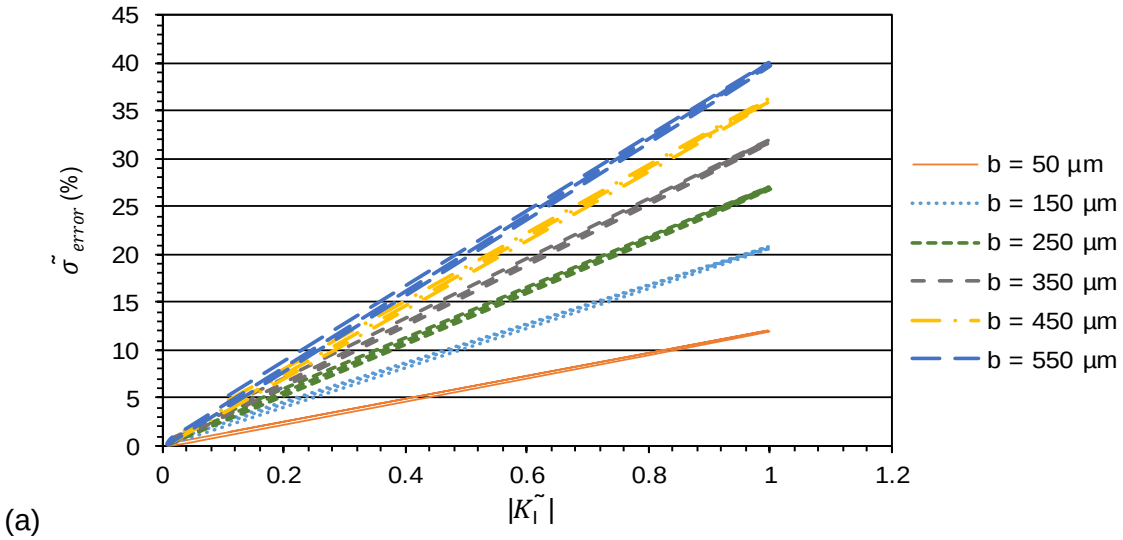

(a)

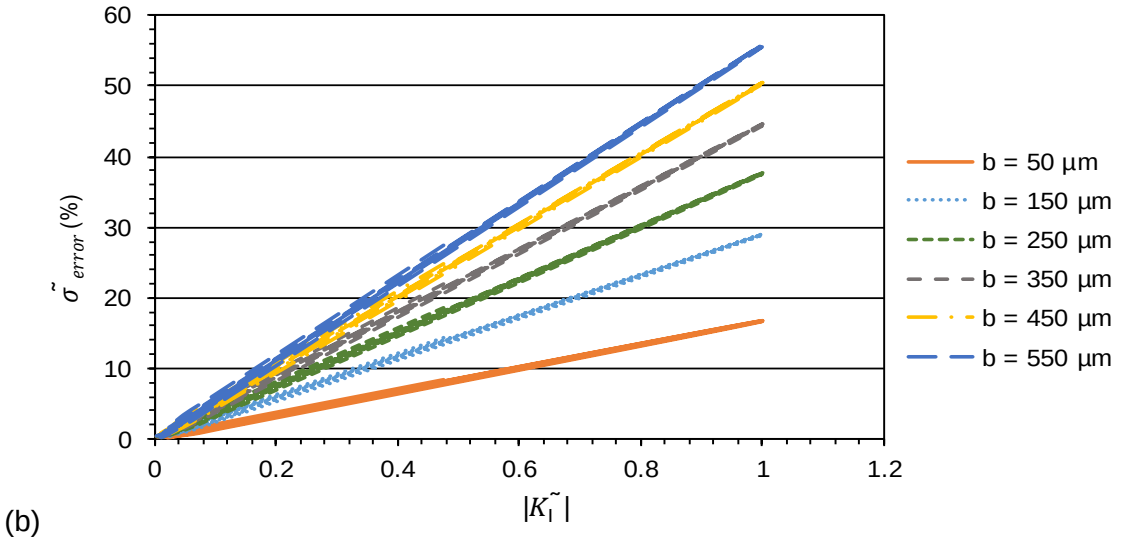

(b)

Figure 5 - 15: Correlation of the normalised stress error due to bulging and the normalised mode I stress intensity factor for a centre-crack plate subjected to a cosine stress field ($\sigma_0 = 100MPa$) of order (a) n = 2 and (b) n = 4 and different cut width sizes. For cut lengths 0.188 ≤ x/w ≤ 0.636.

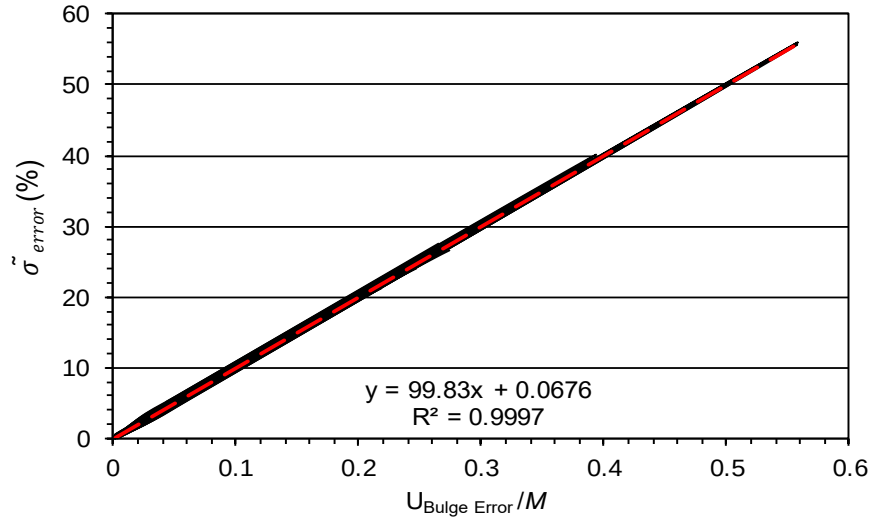

Figure 5 - 16: Correlation of the normalised stress error due to bulging and the normalised bulge displacements with the peak surface displacement M for each cut width size for a centre-crack plate subjected to a cosine stress field ($\sigma_0 = 100MPa$) of order n = 1, 2, 4. For cut lengths 0.188 ≤ x/w ≤ 0.636.

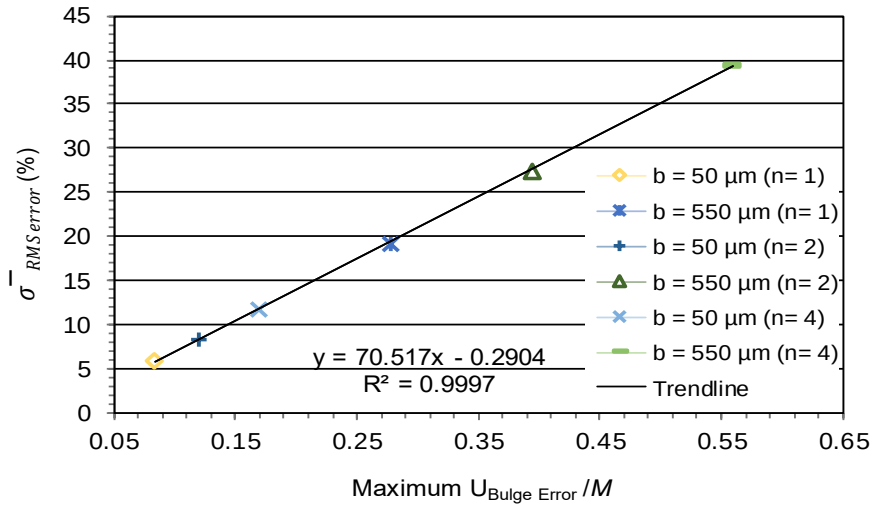

Figure 5 - 17: RMS average stress error calculated over cut lengths 0.05 ≤ x/w 0.95 and the maximum bulge displacement normalised with the peak surface displacement M for a centre-crack plate subjected to a cosine stress fields $\sigma_0 = 100MPa$ of order n = 1, 2 & 4 and slot widths 50 µm and 550 µm. A best-fit trendline is also included.

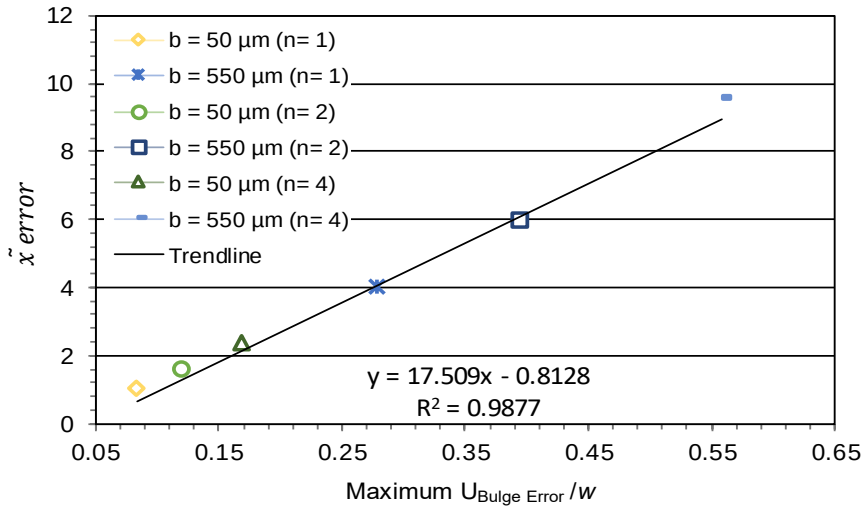

Figure 5 - 18: Positional error of the peak stress location normalised by the wavelength w and the maximum bulge displacement normalised with the peak surface displacement M for a centre-crack plate subjected to a cosine stress fields $\sigma_0 = 100MPa$ of order n = 1, 2 & 4 and slot widths 50 µm and 550 µm. A best-fit trendline is also included.

The developed Fourier correlations can be used to determine the normalised stress error due to bulging for an idealised periodic cosine residual stress distribution instead of using FE analysis to determine the stress error. Figure 5 - 9 and Figure 5 - 15 can be used to calculate the stress due to bulging for cosine stress functions of order, *n* = 1, 2 and 4 based on knowledge of the cut width 'b' and the mode I stress intensity factor, which can be determined using a simple Fourier series solution [145]. Alternatively, Figure 5 - 16 can be used to calculate the stress error due to bulging for any order of cosine stress function based on knowledge of the bulge displacement normalised with the peak displacement amplitude. A general solution, Equation 5 - 4, is provided to calculate the bulge displacement for a periodic cosine stress field.

5.2 Bulge errors in a complex weld stress profile

This work considers the stress error due to bulging for more realistic residual stress measurements. The aim is to determine if a similar linear trend in the stress error correlations, as for the centre-crack in an idealised periodic cosine stress distribution, may be found for generic residual stress fields then the stress error correlations will be valid for actual contour method residual stress measurements. The chosen case study is a butt-welded plate with complex residual stress field [58]. In the previous work, the residual stress profiles were idealised with several fitted polynomials (*n* = 1 to 20) and the associated Fourier based stress intensity factors calculated. The bulge error could therefore be

evaluated by the stress intensity factor solutions at various levels of detail. The stresses due to bulge error were calculated using finite element analysis. The magnitude of the stress error was evaluated by calculating the error relative to the fitted polynomial residual stresses and producing correlations of normalised stress error.

Fourier based residual stresses and SIF solutions

The specimen consists of two aluminium alloy butt-weld plates, approximately 140 mm wide and 240 mm long and 12 mm thick, joined by a variable polarity plasma-arc (VPPA) welding technique. The bulk longitudinal residual stress field across the mid-width cross-sectional plane of the welded plate was measured using neutron diffraction, synchrotron x-ray diffraction [58], laboratory x-ray diffraction [163] and the contour method [59]. Figure 5 - 19 shows a schematic illustration of the welded plate and cutting arrangement for the contour method. Figure 5 - 20 shows the analytical representation of the measured longitudinal stress profile from the Fourier series analysis fits for n = 1, 5, 10 and 20. The measured data cover a sub-domain [-60, 60] mm of the 278 mm wide cross-section but only one half of this is evaluated as the stress distribution is essentially symmetric about the weld centre-line. The analysis for n = 20 matched the measured data (averaged through the thickness) closely as it captured the measured peaks. The resultant SIF solution for a through-thickness crack symmetrically emanating from the centre of the weld is shown in Figure 5 - 21.

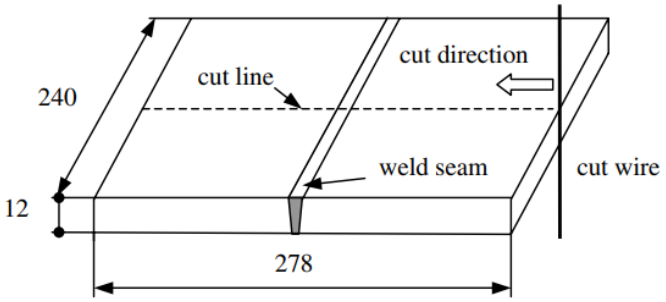

Figure 5 - 19: Schematic illustration of the aluminium alloy butt-welded plate joined by a VPPA welding technique and cut arrangement for the contour method [59].

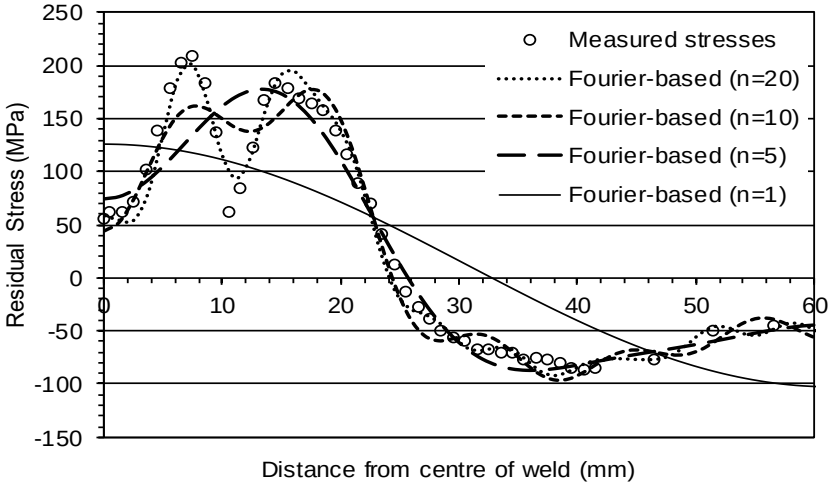

Figure 5 - 20: Four Fourier series analysis fits, for n = 1, 5, 10 and 20, of the measured longitudinal residual stress data (thickness averaged) for an aluminium alloy butt-weld plate joined by a variable polarity plasma-arc (VPPA) welding technique [59].

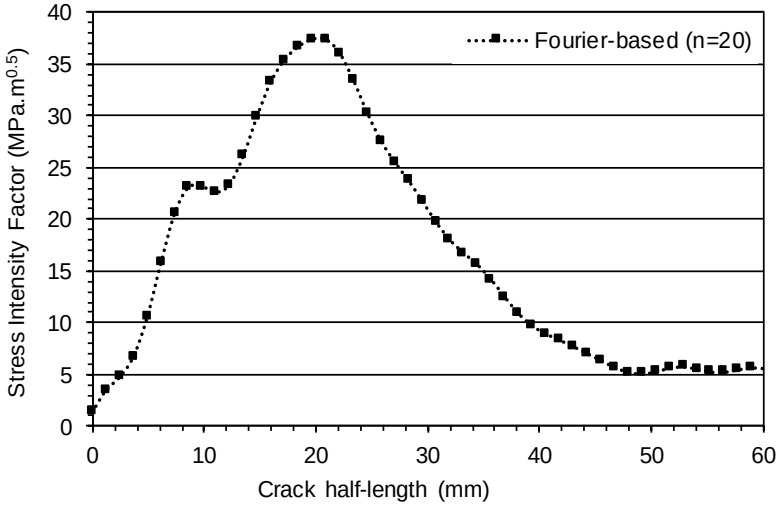

Figure 5 - 21: Associated Fourier-based SIF results, for n = 20, for the aluminium alloy butt-welded plate.

Calculating the bulge displacements

The bulge displacements for *n* = 20 Fourier series fit were estimated using the analytical solution Equation 4 - 6 (see Chapter 4 section 4.2). The Young's modulus, E, and Poisson's ratio, ν, were found from the literature to be 72.4 GPa and 0.33 respectively. For the contour method residual stress measurement, the specimen was cut into two halves using a 0.1 mm diameter brass wire. The final slot width was taken to be 0.15 mm. The predominant

stress state ahead of the cut path was evaluated using fracture mechanics criteria which states that for plane strain conditions,

$$T \geq 2.5 * \left(\frac{K_I}{\sigma_0}\right)^2$$

where T is the specimen thickness, K_I is the stress intensity factor and σ_0 is the material yield stress.

For this case, $K_{I,\,max} \approx 38$ MPa.m$^{0.5}$ and $\sigma_0 = 270$MPa, gives $T = 49.5$ mm which is greater than the 12 mm plate thickness and a plane stress state can be assumed. The bulge displacements can be evaluated using Equation 4 - 6 (a). Figure 5 - 22 shows the bulge displacements for $n = 20$.

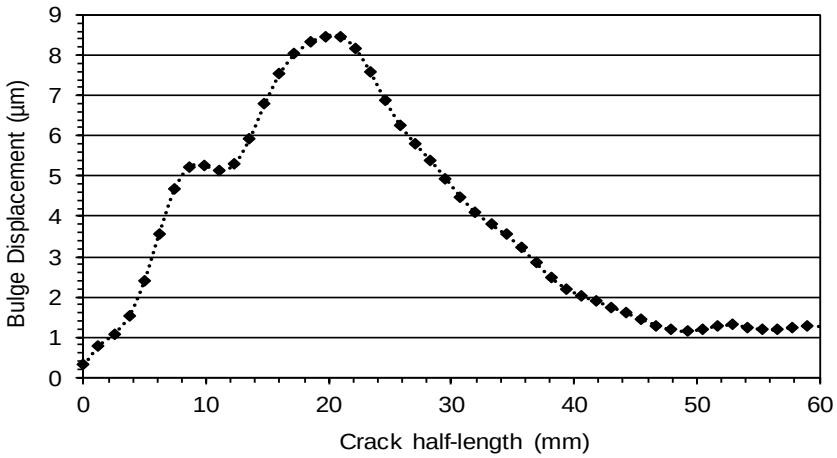

Figure 5 - 22: Analytical plane stress bulge displacements, for Fourier analysis fit with n = 20, for the aluminium alloy butt-welded plate.

Calculating the stress error due to bulge

The stresses associated with the bulge error were calculated by directly applying the bulge displacements as boundary conditions along the sub-domain region of the plate, i.e. 60 mm, in a 2D FE analysis. The resultant stresses were then subtracted from the idealised Fourier stresses to predict the residual stresses including the effects of the bulge error. Figure 5 - 23 compares the Fourier stresses and the stresses including bulge error for n = 20. As expected, the bulge error results in reduced peak stresses and a slight shift in the residual stress profile.

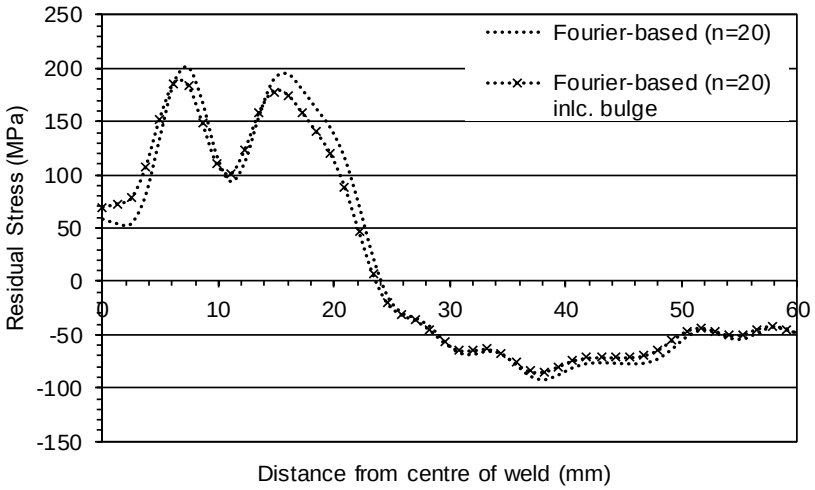

Figure 5 - 23: Comparison of the Fourier residual stresses and stresses including the effects of bulge error, for n = 20, for the aluminium alloy butt-welded plate.

Stress error correlations

Figure 5 - 24 shows correlations of the normalised stress error, calculated using Equation 5 - 5, with the absolute stress intensity factor, normalised with the maximum SIF, along the distance from the centre of the weld. The correlations show no obvious trend, however there is an apparent linear trend in the peak SIF region. The varying residual stress distribution did not provide any meaningful correlations and would be unreliable to predict the stress errors due to bulging.

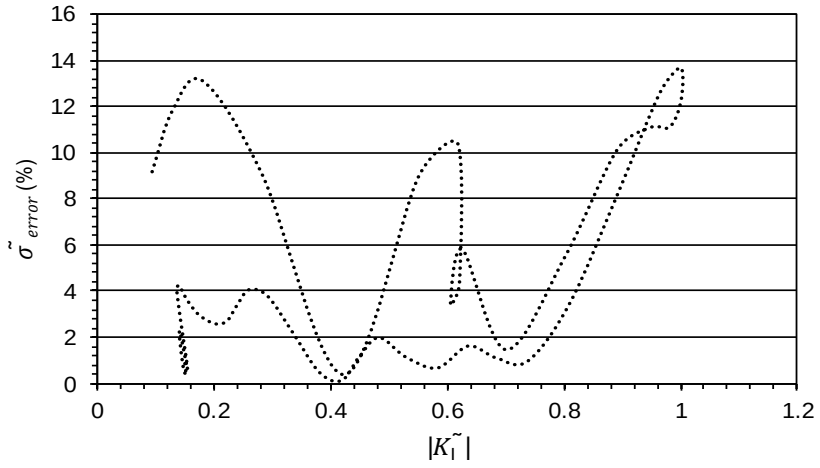

Figure 5 - 24: Correlation of the normalised stress error due to bulging and the absolute mode I stress intensity factor for Fourier analysis fit with n = 20, for the aluminium alloy butt-weld plate.

5.3 Radial thickness bulge errors in quenching stresses

This study investigates the significance of the bulge error for 3-dimensional distributions of residual stress and explores correlations for the normalised stress error with the mode I stress intensity factor. The stainless-steel solid cylinder (60mm diameter x 60mm long) studied by 3D FE analyses in Chapter 4 section 4.3.2, to validate the analytical bulge displacement solution is further examined here as the case study.

In the previous work, a residual stress distribution was introduced by simulating the quenching process using a sequentially coupled thermal-stress FE analysis. The mode I stress intensity factor was evaluated across the diameter at a few cut lengths (5, 15, 30, 45 and 57 mm) using special J-integral elements at the tip of a sharp edge crack. The analytical bulge displacements, for the plane stress and plane strain conditions, were calculated by means of the stress intensity factor and compared with the bulge displacements extracted during a contour cutting simulation for two cut width sizes, 0.1 mm and 0.3 mm. It was found that the analytical plane strain bulge solution matched closely with the FE bulge displacements across the thickness of the specimen. Also, the bulge error followed the through-thickness stress intensity factor in form and distribution.

Calculating the stress including the bulge error

To calculate the stresses including effects of bulge error, the finite element bulge displacements were applied as boundary conditions on the cut plane of a quarter model of the solid cylinder to back-calculate the associated stresses error (see Figure 4 - 34). A linear elastic material model was used with Young's modulus, E, and Poisson's ratio, ν, of 195.6 GPa and 0.294 respectively. It was necessary to first interpolate the displacements for all node locations on the cut plane as the FE bulge displacements were calculated at the wire entry node locations in the cutting simulation. This interpolation was performed in MATLAB with the scatter interpolation [150] function by specifying nearest neighbour extrapolation. Then the back-calculated stresses were subtracted from the initial simulated hoop residual stresses to give the stresses including the bulge error. Figure 5 - 24 compares the initial quenching residual stresses with the stresses including bulge error at several cut lengths. A significantly large difference (~ 100 MPa) can be seen for the 5 mm cut length where the edge crack is introduced into compressive stresses.

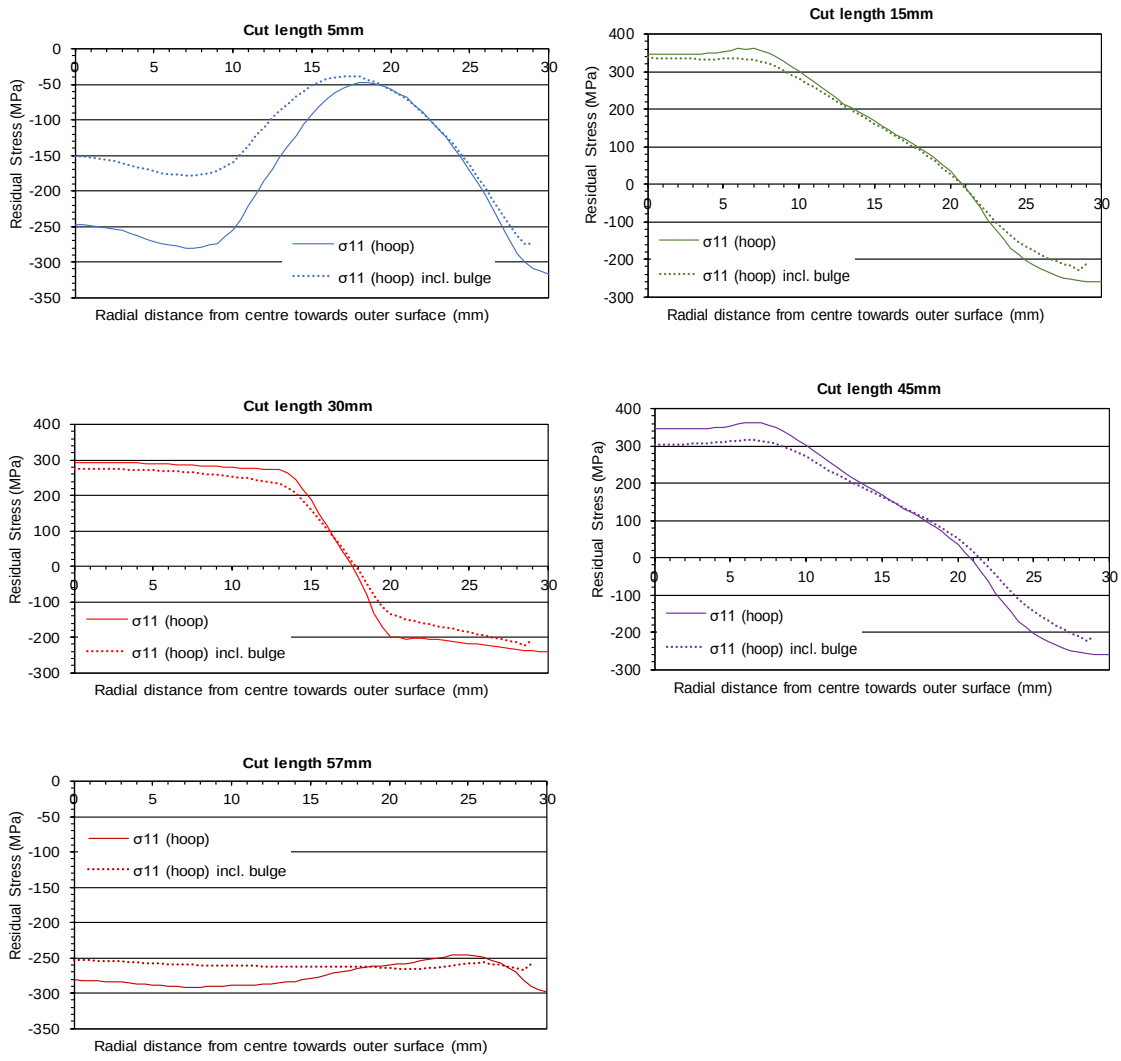

Figure 5 - 25: Comparison between the initial hoop residual stresses and stresses including bulge error for a quenched 316H stainless steel solid cylinder, diameter 60 mm, length 60 mm, for a cut width of 0.3 mm at different cut lengths.

Stress error correlations

Figure 5 - 26 shows a 2D plot of the normalised stress error across the cut surface. Significantly larger errors can be seen close to the cut start and outer surface of the cylinder. Figure 5 - 27 shows correlations of the normalised stress error, calculated using Equation 5 - 5, through the thickness of one quarter of the solid cylinder with the absolute through-thickness mode I stress intensity factor, normalised with the maximum SIF, at several cut lengths. The results near the outer surface of the cylinder (for roughly 2 mm) were unstable and therefore excluded. The correlations show no obvious trend, but the normalised stress error is less than ~ 15 % for most of the results.

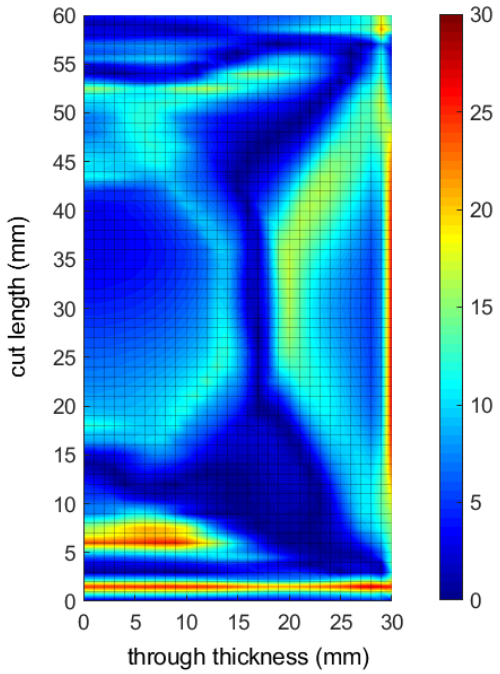

Figure 5 - 26: 2D plot of the percent normalised stress error (%) due to bulging across the cut surface of a quenched 316H stainless steel solid cylinder, diameter 60 mm, length 60 mm, for cut width size 0.3 mm.

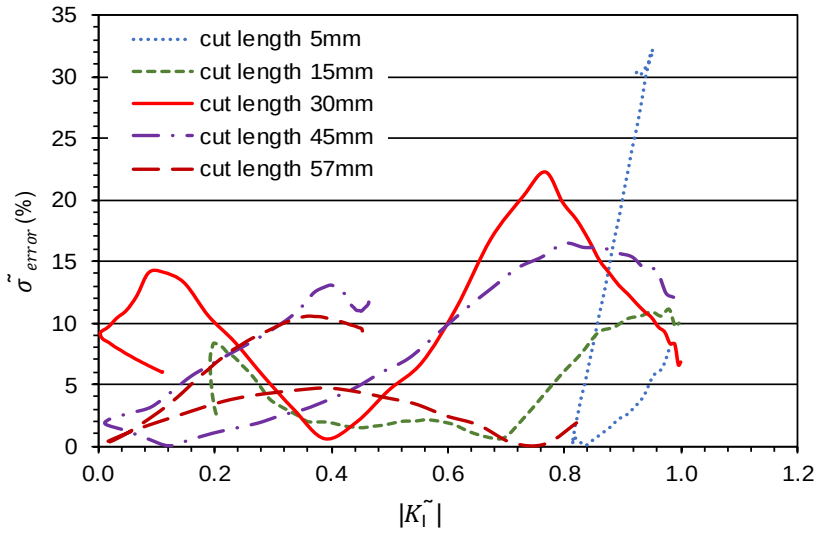

Figure 5 - 27: Correlation of the normalised stress error due to bulging and the absolute mode I stress intensity factor for a quenched 316H stainless steel solid cylinder, diameter 60 mm, length 60 mm, for cut width size 0.3 mm at different cut lengths.

The root-mean-square average stress error was calculated, using Equations 5-6, through the thickness of one quarter of the solid cylinder at 1.5 mm cut length increments. To evaluate the effect of the cut width size, the stress error analysis was repeated for cut width

0.1 mm, since the bulge displacements were also measured in the previous work. Figure 5 - 28 shows the RMS average stress error along the cut length, a, normalised with the cylinder length, L. The stress error is fairly constant (< ~ 1 % difference) between 0.2 ≤ a/L ≤ 0.7 but is larger at the start of the cut with obvious outliers. The stress error scales with the square root of the cut width which is consistent with previous findings.

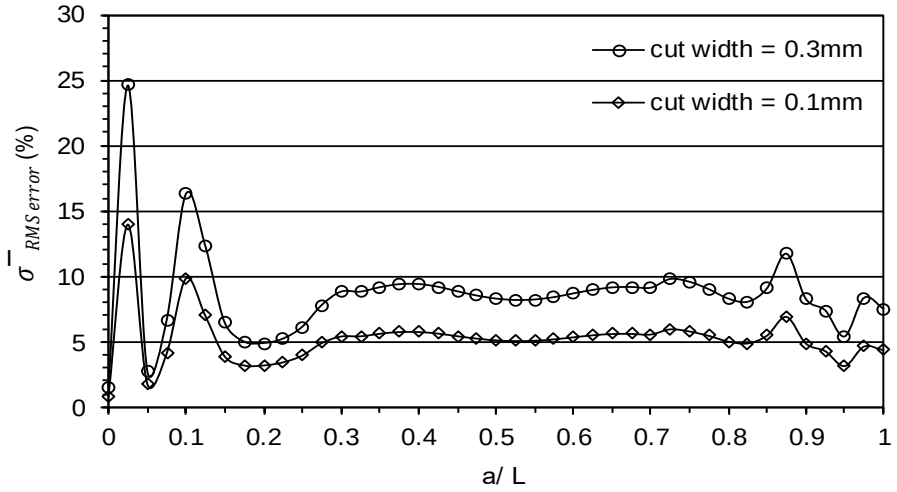

Figure 5 - 28: Diametral RMS average stress error at each cut length (a) normalised with the cylinder length (L) for a quenched 316H stainless steel solid cylinder, diameter 60 mm, length 60 mm, for cut width sizes 0.1 mm and 0.3 mm.

5.4 Discussion

In this chapter stress error correlations have been developed to predict the magnitude of stress error due to bulging in contour method measurement results using the mode I stress intensity factor. The initial correlations were based on a centre-cracked plate loaded by an idealised cosine residual stress profile in the plane stress condition. The bulge error was estimated analytically with the mode I stress intensity factor found using a Fourier-based solution for a centre-crack plate in a periodic cosine residual stress distribution [145]. The corresponding stresses including the bulge error were calculated in a finite element analysis. Systematic studies were performed for different cut width sizes and varied stress wavelength. The relationship between the normalised stress error and SIF was linear between 0.2 and 0.6 percent of the cut length but was unpredictable outside of this range. The root-mean-square average stress error in the cosine stress field ($\sigma_0 = 100MPa$) of order n = 1 was up to 19 % for a 0.55 mm cut width and up to 40 % for n = 4. Shorter surface deformation wavelengths resulted in larger stress errors from bulging. The stress error also

scales with the square root of the cut width. This implies that using a smaller wire in the cutting procedure for the contour method, will give smaller bulging errors.

Similar stress error correlations were developed for a centre-crack in a butt-welded plate with more complex residual stresses. The correlations were developed for idealised longitudinal residual stress profiles based on Fourier series analysis. The stresses due to bulge error were calculated using finite element analysis. The aim was to determine if a similar linear trend in the stress error correlations is found for rapidly varying stresses then the correlations, for the centre-crack in an idealised periodic cosine stress distribution, will be valid for actual contour method residual stress measurements. However, the stress error correlations did not show a definite linear trend.

The stress error analysis was extended to evaluate the bulge error for 3D geometries. The specimen studied was a stainless-steel solid cylinder with residual stresses introduced by quenching using finite element analysis. The bulge error and associated stresses including bulge error were calculated using finite element analysis. Correlations of the stress error along the length of the cut tip and the associated stress intensity factor did not show a definite linear trend, even for the stresses at mid thickness of the specimen which are close to a cosine profile. The one-dimensional idealised cosine residual stress profile appears to be a unique case showing a linear correlation to obtain a precise estimation of the stress error due to bulging in contour method measurements.

The 3D analysis of the quenched cylinder showed that the bulge error caused significantly larger errors in the hoop stresses close to the cut start (< 10 mm) where the edge crack was introduced into compressive stresses and near the outer surfaces (~ 2 mm). The root-mean-square diametral average stress error was roughly the same magnitude along the cut length $0.2 \leq a/L \leq 0.7$ and provides a more robust evaluation of the stress error. In this region, the error was roughly 10 % for the 0.3 mm cut width and 5 % for the 0.1 mm cut width. The stress error scales with the square root of the cut width, therefore the RMS average stress error due to bulging can be predicted for any cut width size for this case study.

5.5 Conclusion

- Stress error correlations have been developed to predict the magnitude of stress error due to bulging in contour method measurements for a one-dimensional idealised cosine residual stress profile. The correlations rely on knowledge of the mode I stress intensity

factor due to the residual stresses in the specimen and can be determined using a simple Fourier series solution [145].

- A general analytical solution based on the Bessel function, Equation 5-4, provides a simple method for estimating bulge displacement errors as a function of cut length for a centre-crack in a periodic cosine residual stress field.

- Smaller length scale surface displacements result in larger stress errors from bulging (see Figure 5 - 17). In the cutting procedure for the contour method, using a smaller wire will help to capture the smaller displacements and bulge error.

- The approach to develop correlations for stress errors due to bulging showed linear trends for the idealised cosine form of residual stress but no obvious trend was observed for the other two cases containing a more generic residual stress field.

The bulge error occurs in all residual stress measurements made with the contour method. There are different levels of complexity that can be used to correct for the bulge error. In the next chapter the bulge correction procedures are reviewed and guidelines are provided to assist practitioners of the contour method to decide on a suitable approach.

Chapter 6: Discussion and guidelines for bulge correction in the contour method

The aim of this PhD project was to understand the origins and influence of the bulge error in residual stress measurements made with the contour method. The scope of bulge error studies was to evaluate application of an iterative FE based (2D) correction procedure first published by Prime [3] and extend its application to 3D cases (Chapter 3). A new analytical bulge error estimation solution based on the linear elastic fracture mechanics mode I SIF is proposed (Chapter 4) instead of the cumbersome iterative FE procedure. This solution is used to develop a set of stress error correlations for periodic stress functions that have the potential to be used for estimating stress errors due to bulging in a contour method measurement (Chapter 5). The present chapter provides a general discussion of the methods used in this thesis and a set of guidelines to help contour method measurement practitioners estimate the magnitude of stress error due to bulging and, if necessary, correct the residual stress measurements made with the contour method.

The contour method determines residual stress by carefully cutting a component into two halves which allows the residual stresses in the material to redistribute and results in distortion of the cut surfaces. This distortion is then measured and used to back calculate the residual stresses using an elastic FE analysis. Wire electro-discharge machining (EDM) is the most effective cutting technique to satisfy the requirements for the contour method where one of the main assumptions is that the cut removes a constant width of material when measured relative to the original state of the body. However, the width of cut material removed is affected by the stress concentration at the cut tip that elastically stretches or contracts the material about to be cut. This causes the width of material removed to vary along the cut length which creates deformation errors that bias the back-calculated stresses. Bulge errors tend to shift the stress distribution towards the origin of the cut and reduce tensile peak stresses.

6.1 The iterative FE bulge correction procedure

The present study evaluated the 2D bulge correction approach of Prime and Kastengren [3] before adapting the approach to correct a 3-dimensional residual stress field in a stainless steel compact tension specimen containing a weld. A new approach is proposed for calculating the bulge stress error once the deformation error has been estimated by a contour cutting simulation using either 2D or 3D analyses. The new approach simplifies the

bulge correction procedure to some extent but still requires FE cutting simulation which can be time-consuming and complex (requiring ABAQUS scripting) for three-dimensional cases.

The most important modelling factors for the cutting simulation are the shape of the slot and the geometric locations used to estimate the bulge error. For mesh design convenience a square slot bottom was used for most of the studies. It was established that the material position at the outer edge of the slot (i.e. lateral tangent of the cutting wire), has a greater ability to correct contour method measurements. The slot corner node position (that is the material point about to be cut) gave a reasonable estimation of the bulge error but this position does not physically model the approximately semi-circular shape of the cut tip. A drawback with using the slot tangent position is that a denser mesh ideally using second order elements is required.

Nonetheless, the square slot shape assumption could cause inaccuracies in the FE prediction of the bulge error. An FE idealisation study in this work (see Chapter 4 section 4.1.2) indicated a significant decrease in the estimated bulge error (10 % for a 0.25 mm cut width) when using a semi-circular slot bottom compared with the square slot bottom assumption. The effect of the slot shape could significantly improve the accuracy of the bulge prediction but would be difficult to implement for FE analysis since re-meshing would be required at each cut increment.

Further inaccuracies in the cutting simulation could result from the assumption that the final slot width is 120 % of the EDM wire size based on advise in the literature [28]. For example, for a 250 µm wire size a 300 µm final slot width was chosen. The slot width correlations (see Figure 4 - 17 and Figure 4 - 18) have shown that the significance of the final slot width to predict the bulge displacements is more important for narrower slots.

Nevertheless, numerical predictions are based on theory and experimental validation of the elastic deformation at the cut tip, or change in slot width, as a function of cut depth could provide valuable information about the conditions and behaviour of the material at the cut tip during the cutting process. This could help to improve the assumptions used for the FE cutting simulation to more precisely predict the bulge error. Also, it has been shown that the SIF for a square slot up to 0.55 mm wide does not deviate significantly from that of a sharp crack (see Figure 4 - 14). A blunt notch is expected to reduce the stress concentration at the cut tip and therefore could show a larger deviation from the SIF for a sharp crack. These effects could be investigated using experimental methods by relating different stress conditions at the cut tip, or the associated SIF, to the deformation or change in the cut width.

However, experimentally measuring the change in cut width could be challenging due to the interference from features at the cut such as surface roughness and the recast layer.

The bulge error in a complex residual stress distribution measured by the contour method has been investigated using 2D and 3D FE simulations. The case study was a stainless steel compact tension weld specimen where residual stresses were measured using neutron diffraction, incremental slitting and the contour method [4]. Figure 3 - 3 shows the contour method results which showed possible evidence of bulge error, that is a spatial shift in the distribution towards the origin of the cut and slightly reduced peak stresses. Applying the FE correction procedure showed that bulge effects introduced a negligible spatial error (~ 1 mm) but a significant increase (20 %) in the peak tensile stress. This level of error is larger than desirable for a residual stress measurement technique and emphasizes the importance of estimating and correcting for deformation errors in the measured residual stresses to improve the accuracy and reliability of contour method measurements.

6.2 Analytical bulge error estimation

One of the aims of this research was to develop a simpler approach for bulge error correction. This has been achieved based on the hypothesis that the bulge error is dependent on the local stress state at the cut tip, which can be characterised by the mode I SIF. This was demonstrated by developing numerical correlations for a finite plate with a uniform far field tension loading in the plane stress and plane strain conditions, for a series of different geometries, material properties and cut width sizes. The correlations proved that the bulge error is approximately proportional to the SIF and the square root of the cut width size and inversely proportional to the material stiffness. The bulge error for plane stress conditions was approximately 10 % larger than for plane strain.

The effects of the bulge error can be minimised during the cutting procedure by controlling the change in the stress state at the cut tip, that is by controlling the stress intensity as cutting progresses across the component of interest. This can be achieved by restraining (clamping) the component close to the cut and by carefully choosing the cut propagation pathway [101, 102]. The same measures will minimise the amount of plasticity-induced stress errors in the contour method. The bulge error can also be reduced by using a smaller EDM wire diameter as the error scales with the square root of the slot width. This finding is of high practical significance because it tells us that bulge errors can be minimised simply by choosing the smallest diameter of wire that delivers a stable cut (i.e. minimises wire breaks) in the component of interest.

FE studies have shown that the displacements at a crack tip are non-singular and proportional to $K_I\sqrt{r}$ and depend on the stress state [121]. The magnitude of the bulge error (elastic displacement) can be estimated analytically by setting the radius, *r,* equal to the distance from the slot tip to the outer edge of the slot (tangent of a circular wire of diameter equal to the slot width) for both plane stress and plane strain stress conditions. This represents the lateral displacements of the crack faces and validates the choice of mid side node location used in FE cutting models to estimate bulge displacements. Extensive 2D and 3D modelling was performed to validate the analytical solution for idealised stress distributions and real residual stress measurements. The analytical bulge was estimated using FE predictions of the SIF and compared with the actual FE displacements at the cut tip. The bulge error followed the SIF in form and distribution, even across the thickness of the specimen. The analytical approach can replace the cumbersome FE cutting simulation stage and provides a much quicker method to estimate the bulge error. For 2D approximations and 3D cases it is recommended to estimate the bulge error using the plane strain assumption.

The difficulty in using the analytical solution is the need to know the SIF associated with the residual stress of interest for cut lengths spanning the component cross section. The SIF depends on the size and geometry of the component, crack shape, the loading condition and the boundary conditions. SIFs can be determined using analytical handbook solutions [120, 133, 134] for typical geometries but for more complicated geometry and loading, numerical methods are used which have been proven for their accuracy in establishing SIF [164-166]. However, there is still a lack of information on SIFs for irregular cracks in complex three-dimensional shapes. It is worthwhile to mention here that the concept of the SIF is applied to critical design and failure calculations in structural integrity assessments [8, 167].

An important limitation of the analytical approach is that the there is no SIF at the start of a cut (zero crack length) and end of a cut. The workaround is to extrapolate the bulge error from deeper cut lengths back to the starting and far edge. It would be valuable to determine what factors influence the discrepancies seen at the edges and whether a simple correction is possible for more accurate corrections. However, it has been shown that a shallow cut does not behave like a “sharp crack” [154] and therefore the SIF characterisation completely breaks down. A more classical stress concentration factor measure could be used to deal with the results at the edges.

Finally, the analytical solution does not account for non-linear (plasticity) effects at the crack tip. Interestingly it has been shown that the SIF can be used to indicate the risk of plasticity

errors in contour measurements [2]. This suggests the possibility of developing a common estimation method that can distinguish and combine plastic and elastic (bulge) errors in contour measurements.

6.3 Evaluation of the stress error due to bulging

A simple FE investigation of the stress error due to bulging in the contour method has been conducted in this research based on a centre crack in a finite plate subjected to a cosine residual stress profile in the plane stress state. A one-dimensional cosine stress profile is self-equilibrated, having zero resultant force and moment, and can therefore be taken to represent an idealised residual stress profile. The objective was to develop a criterion to predict the magnitude of stress error due to bulging for the contour method to help practitioners decide whether to correct for it. This work provides correlations of the normalised stress error due to bulging and the mode I SIF for several cut width sizes. The stresses including the bulge error clearly show reduced peak stresses and a spatial shift in the stress distribution. The root-mean-square (RMS) average stress errors were determined to provide a more robust comparison and were in the order of ~ 20 % (for a 550 µm cut width). A significant finding was that the stress error was larger ~ 40 % for smaller surface deformation wavelengths. Therefore, a smaller wire should be used for the cutting procedure to capture the smaller resolution surface displacements to increase the accuracy of correcting for the bulge error in contour method measurements. The stress error correlations in this work can only be used for an idealised cosine distribution of the residual stresses since the SIF depends on the applied load.

This work was extended to develop similar stress error correlations for a complex welding residual stress distribution in the plane stress state and to evaluate the variation in the stress error through the thickness of a solid cylinder with quenching residual stresses. The correlations for both varying stress profiles were random and could not be used to estimate the stress error in contour method measurements. The RMS stress errors averaged across the thickness for the quenched cylinder were < ~ 5 % (for a 100 µm cut width) and < ~ 10 % (for a 300 µm cut width). As the stress errors are normalised with the maximum stress, the errors could be more significant for stress distributions with larger magnitude peak stresses.

6.4 Guidelines for bulge error correction

As explained previously, the stress errors due to bulging in the contour method are directly related to the stress concentration at the cut tip during the specimen cutting process. In

Chapter 5 it has been demonstrated that for an idealised one-dimensional cosine stress profile the stress error due to bulging can be estimated and corrected for using knowledge of the mode I SIF. Correlations were developed to estimate the level of stress error in contour method measurements for any idealised cosine stress profile. The stress magnitude can be approximated before contour cut and the SIF estimated using a Fourier approach, weight functions, FE analysis or commercial software, for example R-code [139].

However, in contour method measurements for more generic stress fields it is necessary to estimate and correct for the bulge error. There are two methods that can be used to estimate the bulge displacement error which results from elastic deformation in contour measurements. The first is an analytical approach based on the mode I SIF and the second is an FE approach to perform simulations of the cutting procedure. Once the bulge displacements have been estimated, the associated stress error is calculated using an elastic FE analysis. The procedure is repeated until a converged stress solution is reached. Both methods can be applied using simplified 2D correction for a line profile of the contour method residual stresses on the cut plane e.g. at mid-thickness or 3D correction which is more time-consuming but provides a more robust correction for all the contour method stresses on the cut plane. Figure 6 - 1 shows a flowchart of the proposed procedure for correcting contour method measurements for bulge error.

An incremental change of ≤ 5 % of the peak tensile stress has been used in the present studies to indicate convergence. The stresses converged after only two to three iterations (see section 3.1.3, 3.1.6 and 4.4.2). Therefore, it is suggested to use a convergence criteria of ≤ 1 % variance for the peak stresses to improve the accuracy of the bulge correction.

When using the analytical approach, accurate prediction of the mode I SIF is essential because it directly influences the magnitude of the predicted elastic deformation. In specimens with large variances in the residual stresses across the cut plane, the SIF from the slitting measurement technique may not be suitable to use in the analytical solution. In such cases, the stress intensity factor must be determined from initial contour method measurement stress results.

Another important factor is the constraint applied to represent the clamping condition in the FE analysis either to perform contour cutting simulation or to determine the stress intensity factor. Depending on how close the clamping arrangement is to the cut, it may influence the magnitude of the stresses at the cut tip and the predicted results. Finally, these bulge

correction procedures can give large errors at the edges of the specimen and any unstable stress results at the edges should be neglected.

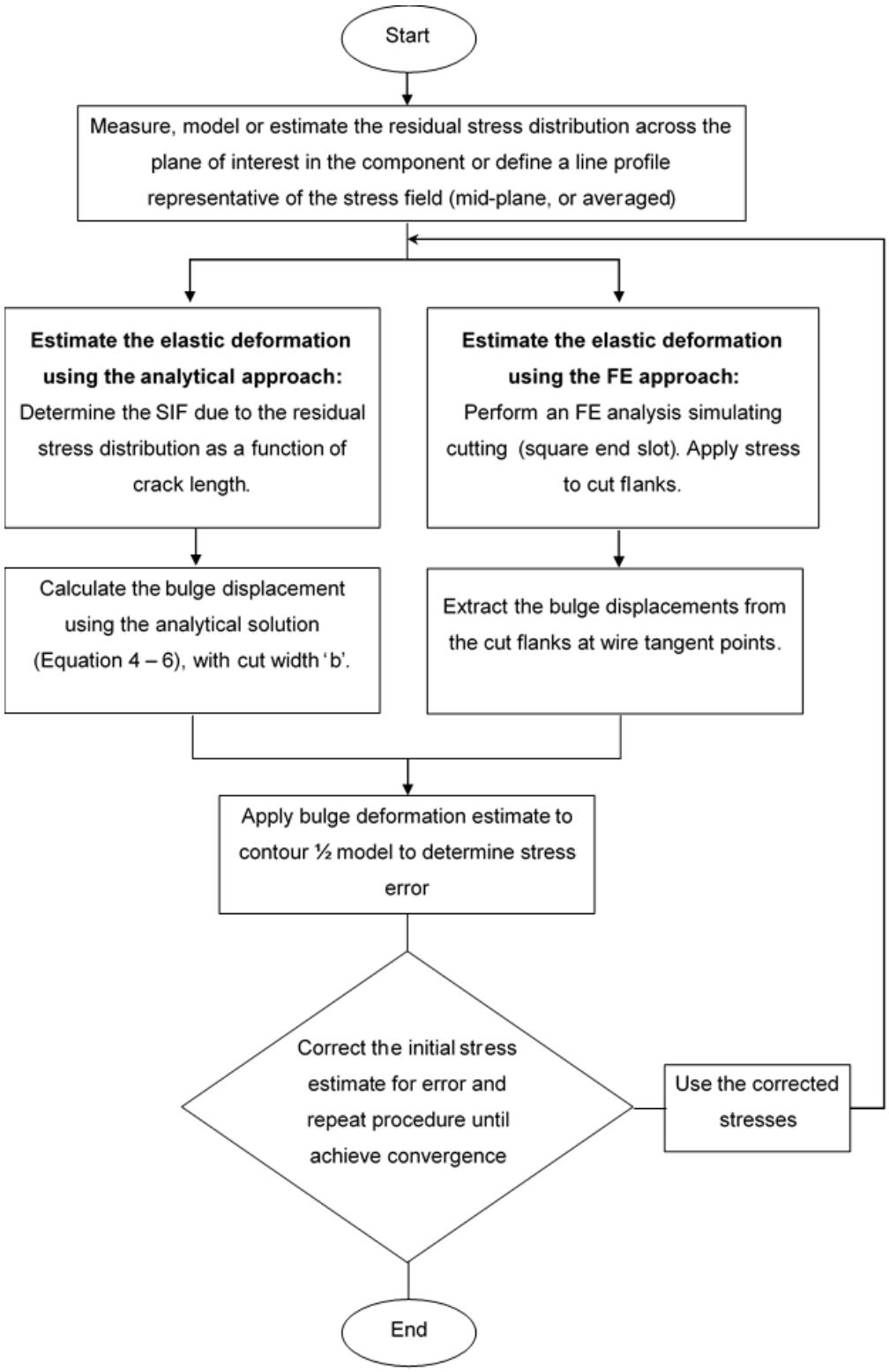

Figure 6 - 1: Flowchart illustrating the proposed procedure for estimating and correcting for bulge errors in residual stress measurements made with the contour method.

Chapter 7: Conclusions and future work

7.1 Conclusions

Bulge error can have a significant effect on the accuracy of residual stress measurements made by the contour method, as illustrated below in very recent work, but there is little published knowledge about its influence.

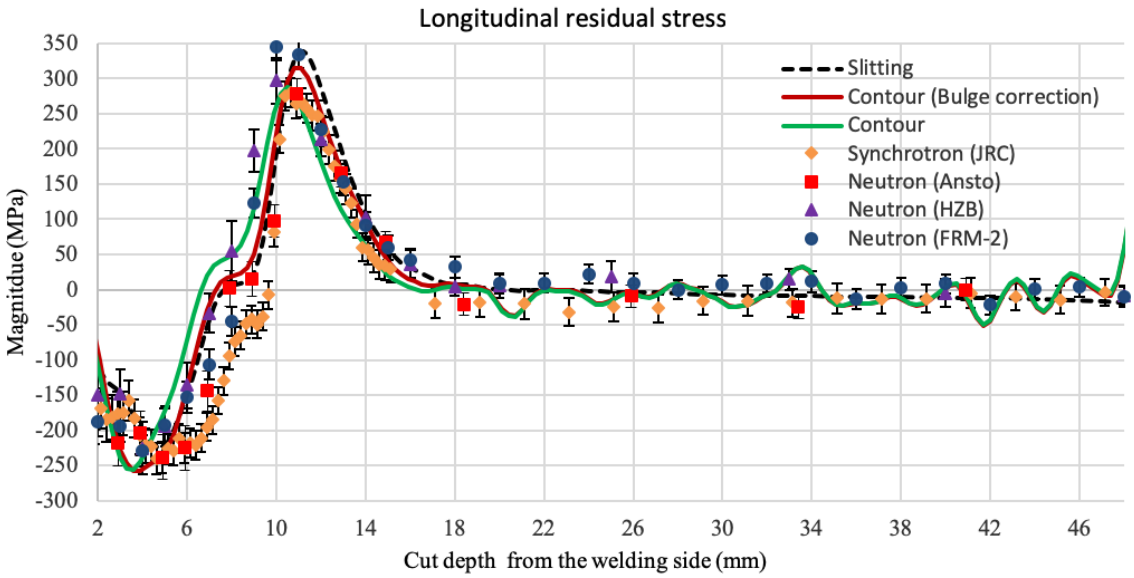

Figure 7 - 1: Contour and bulge-corrected measurements of residual stress for the NeT TG5 edge-welded ferritic steel beam round robin compared with slitting, neutron and synchrotron diffraction measurements [168].

The aim of this PhD project was to improve the understanding of bulge errors and investigate existing and new procedures to correct for it in contour method measurements. The hypothesis put forward was that a simple bulge error correction approach could be developed and integrated within the standard data analysis steps of the contour method.

In this research an alternative finite element procedure, compared to the FE procedure proposed by Prime and Kastengren [3], and a new analytical solution have been proposed to simplify the process of correcting for bulge error in contour method measurements. Finite element studies of the relationship between the stress state at the tip of a contour cut, characterised by the SIF, and the bulge error or “varying” cut width have helped improve the understanding of the factors that influence the bulge error and ways to control bulging effects during the cutting process of the contour method. Furthermore, a parametric study of the magnitude of the bulge error for a one-dimensional idealised cosine residual stress

profile has been investigated. The research has shown that there are different levels of complexity that can be used to correct for the bulge error. Therefore, guidelines have been proposed to assist practitioners of the contour method to decide on a suitable approach.

The results and conclusions for each study have been discussed in detail in the previous chapters. Therefore, this section provides the main conclusions from each study. Thereafter future work is suggested based on the challenges and improvements of the methods used in this research.

- A 2D FE approach proposed by Prime and Kastengren [3] to correct complex (varying) stress fields for the bulge error did not improve the results. A 3D FE approach has been developed and applied to correct complex stress fields for the bulge error, but this procedure is very complex and time-consuming requiring bespoke scripts to extract the bulge error through the thickness of the specimen.

- The 2D and 3D FE bulge correction approaches are based on predicted displacements near the tip of the idealised contour cut slot geometry; the sensitivity to the exact position of displacements in the model that should be used has been investigated throughout this thesis. The displacement at the outer edge of the slot, that is the lateral tangent position of the cutting wire (see Figure 2 - 23), is a better position to estimate the bulge error as it has a greater ability to correct contour method measurements.

- A simpler procedure for calculating contour stress error directly from the bulge displacements has been proposed. The new procedure allows stress line profiles from a contour measurement map to be corrected based upon stress errors estimated from a 2D FE model of the cutting process.

- Numerical mode I SIF correlations have been developed for a finite plate with a uniform far field tension loading in the plane stress and plane strain conditions, for a series of different geometries, material properties and cut width sizes. The correlations proved that the bulge error is approximately proportional to the SIF and the square root of the cut width size and inversely proportional to the material stiffness. The bulge error for plane stress conditions was approximately 10 % larger than for plane strain.

- The effects of the bulge error can be minimised during the cutting procedure by controlling the change in the stress state at the cut tip, that is by controlling the stress intensity factor as cutting progresses across the component of interest. The bulge error

can also be reduced by using a smaller EDM wire diameter as the error scales with the square root of the slot width.

- An analytical solution, Equation 4 – 6, based on LEFM, provides a new simple alternative method for estimating bulge displacement errors in contour method residual stress measurements. The mode I SIF as a function of cut length (and along the cut tip) due to the residual stresses in the specimen must be known with the elastic properties of the material and the final cut width size created during the wire EDM process. The analytical solution is found to be within a few percent of the numerical predictions. For 2D approximations and 3D cases it is recommended to estimate the bulge error using the plane strain assumption.

- Stress error correlations have been developed to predict the magnitude of stress error due to bulging in contour method measurements for a one-dimensional idealised cosine residual stress profile. A general analytical solution based on the Bessel function, Equation 5-4, provides a simple method for estimating bulge displacement errors as a function of cut length for a centre-crack in a periodic cosine residual stress field.

7.2 Suggested future work

Although the goal of the thesis has been accomplished, there are improvements that could be done in order to achieve better estimates of bulge error in contour method measurements. Also, several interesting findings could not be explored further in this research due to the time constraint. Therefore, some of these topics are given as suggested future work in this section.

7.2.1 Improvements in the iterative FE bulge correction procedure

Modelling the slot geometry: One of the assumptions to simplify the bulge correction approach by Prime and Kastengren [3] is to use an idealised square slot bottom to estimate the bulge error in the finite element cutting simulation. However, in practice the wire EDM cutting process creates a semi-circular slot bottom which could introduce errors. A study of the geometry idealisation showed a significant error (overestimate) of up to 10 percent using a 0.25 mm square end slot rather than a semi-circular slot end: This suggests that bulge errors may be slightly overestimated using a square end idealisation. A general correction factor, example 10 percent reduction, could be applied when using a square slot, however, more work is needed because the error will depend on the local stress state at the cut tip, cut length, material properties, slot width and restraint conditions.

Applying the clamping constraint: Another factor that can greatly influence the bulge error estimation during the cutting simulation is the applied constraint to represent the clamping condition used during the EDM cutting procedure. The constraint applied in the FE model is representative of the perfect constraint, that is zero lateral displacement, which could be overly restrictive. Modelling clamping with perfect displacement constraint is only an approximation and more realistic simulation of clamping forces may help to quantify the bulge error more accurately [3]. Different types of clamping arrangements, such as finger clamping and fitted bolts, and different clamping distances from the cut plane can be investigated.

Defining the initial stress: In this research two different approaches were used to define the initial stresses in the model for the cutting simulation. In the 2D analysis an ABAQUS user subroutine (SIGINI) provided by Prime [118] was used to define a uniform stress distribution along the length of the sample normal to the cut path. Whereas in the 3D analysis the contour method measured residual stresses across the cut surface were mapped directly in the model. Further investigation is required to assess how the stresses in the remainder of the model i.e. away from the cut plane influence the local bulge displacement required to be measured at the cut tip.

Automating the procedure: It would be a valuable contribution to automate the finite element bulge correction processes so that a practitioner can correct for the bulge error as a standard practice. The proposed alternative procedure to calculate the stress error directly can be applied for a simplified 2D bulge correction approach, or a 3D approach when more robust contour method results are required. Programming in the ABAQUS Scripting Interface can be used to create a finite element bulge correction procedure that can be applied in a simple and practical way for different engineering components that are measured with the contour method.

7.2.2 Experimental analysis of the bulge error:

The bulge effect has so far only been demonstrated using finite element analysis. For avoidance of doubt the bulge displacement phenomenon and its prediction should be validated using experimental methods. One proposed method is to apply different amounts of load, e.g. a stepped increasing tensile load, to a test specimen during wire EDM cutting and evaluate the deviations of the cut width afterwards with suitable measurement techniques.

The deviations in cut width are likely to be a few microns (≤ 10 μm) and the suitability of different techniques, such as digital image correlation, optical microscopes and SEM could be investigated. For example a study [33] has examined the wire EDM slot size along the cutting path on a stress-free material using an optical microscope. It would be particularly challenging to deal with interference from local features at the cut tip such as surface roughness and the recast layer, which could make the measurement particularly difficult. Ideally the test sample should be designed to magnify the deformation at the cut tip and avoid the occurrence of plasticity during cutting, this could be achieved by selecting a material with a low elastic modulus and high yield strength, such as aluminium or magnesium alloys.

7.2.3 Determining how bulge and plasticity effects influence each other:

The bulge error studies performed in this research are for linear elastic materials and have not accounted for non-linear (plasticity) effects at the cut tip. It is not known how the presence of plasticity at the cut tip will alter the bulge error estimation. Further studies are required for elastic plastic material behaviour to determine how bulge and plasticity effects influence each other. Interestingly it has been shown that the SIF can be used to indicate the risk of plasticity errors in contour measurements [2]. This suggests the possibility of developing a common estimation method that can distinguish and combine plastic and elastic (bulge) errors in contour measurements.

Appendix A – Characteristics of residual stress measurement techniques

Table A - 1: Characteristics of commonly used residual stress measurement techniques.

Technique	Advantages	Disadvantages
Neutron Diffraction	• Triaxial residual stress measurements. • Bulk residual stresses and 3D maps. • Useful for measuring stress gradients. • Non-destructive.	• Requires specialised facilities. • Sensitive to grain size and texture. • Requires reliable zero stress reference. • Not suitable for surface measurements or thick samples.
Synchrotron Diffraction	• Fast data acquisition times. • Triaxial residual stress measurements. • Bulk residual stresses and 3D maps. • Useful for measuring stress gradients. • Non-destructive.	• Requires specialized facilities. • Elongated gauge volume. • Sensitive to grain size and texture. • Requires reliable zero stress reference.
X-ray Diffraction	• Lab based and widely available. • Quick and easy to apply. • Bi-axial residual stress measurements. • Useful for measuring surface stress gradients. • Non-destructive.	• Requires good surface finish. • Sensitive to grain size and texture. • Requires material removal to get subsurface stresses and not suitable for through thickness residual stress measurements. • Requires reliable stress-free reference.
Hole Drilling	• Lab based, portable and widely available. • Quick and easy to apply. • Bi-axial residual stress measurement. • Damage is often tolerable or repairable. • Not sensitive to microstructural variation.	• Requires good surface preparation. • Limited depth capabilities. • Compromised by plasticity. • Application for complex shaped components is limited.
Deep Hole Drilling (DHD)	• Through-thickness bi-axial residual stress measurement. • Lab based and in-situ (can be portable). • Applicable for complex component shapes and large samples. • Not sensitive to microstructural variation.	• Semi-destructive. • Standard DHD compromised by plasticity. • Not applicable for very thin components.
Slitting	• 1-D normal component of residual stress measurement. • Applied fairly easily with commonly available equipment. • Can calculate the stress intensity factor directly without prior knowledge of the residual stresses. • Not sensitive to microstructural variation.	• Destructive. • Uni-axial residual stress measurements. • Analytical complexity and need for an inverse solution. • Cannot determine the stresses over the last few percent of the specimen thickness. • Limitations to measure stresses that are nonuniform across the width. • Compromised by plasticity.

Contour Method	• 2-D cross-sectional map of normal component of residual stress measurement. • Applied easily with commonly available equipment. • Not sensitive to microstructural variation. • Can be used for large and complex shaped components. • Useful for complex (varying) residual stress fields.	• Destructive. • Uni-axial residual stress measurements. • Difficult to resolve very small parts. • Difficult to resolve small magnitude and localized stress fields. • Least accurate near surfaces. • Compromised by plasticity and bulge error.
Ultrasonic	• Lab-based, portable and very quick. • Triaxial residual stress measurements possible. • Non-destructive.	• Average stress measurement over whole volume. • Requires stress free reference measurement. • Sensitive to microstructural variations. • Requires good surface finish. • Not applicable to complex shaped components.

Appendix B – Simulation matrix for SIF correlations

Table B - 1: Design of simulations to develop the stress intensity factor correlations. The parameter investigated for each group of experiments is shaded in grey.

Study No.	Plate Geometry			Material properties		Loading		Cut width [μm]	Plane stress/ strain analysis
	L [mm]	W [mm]	L/ W	E [GPa]	v	Pure tension/ bending	Magnitude		
1	25	50	0.5	71.1	0.33	Tension	10 MPa	250	Stress
2	50	50	1	71.1	0.33	Tension	10 MPa	250	Stress
3	100	50	2	71.1	0.33	Tension	10 MPa	250	Stress
4	25	50	0.5	71.1	0.33	Tension	10 MPa	250	Strain
5	50	50	1	71.1	0.33	Tension	10 MPa	250	Strain
6	100	50	2	71.1	0.33	Tension	10 MPa	250	Strain
7	25	50	0.5	195.6	0.294	Tension	10 MPa	250	Stress
8	50	50	1	195.6	0.294	Tension	10 MPa	250	Stress
9	100	50	2	195.6	0.294	Tension	10 MPa	250	Stress
10	25	50	0.5	195.6	0.294	Tension	10 MPa	250	Strain
11	50	50	1	195.6	0.294	Tension	10 MPa	250	Strain
12	100	50	2	195.6	0.294	Tension	10 MPa	250	Strain
13	50	50	1	71.1	0.33	Tension	10 MPa	50	Stress
14	50	50	1	71.1	0.33	Tension	10 MPa	150	Stress
15	50	50	1	71.1	0.33	Tension	10 MPa	250	Stress
16	50	50	1	71.1	0.33	Tension	10 MPa	350	Stress
17	50	50	1	71.1	0.33	Tension	10 MPa	450	Stress
18	50	50	1	71.1	0.33	Tension	10 MPa	550	Stress
19	50	50	1	71.1	0.33	Tension	10 MPa	50	Strain
20	50	50	1	71.1	0.33	Tension	10 MPa	150	Strain
21	50	50	1	71.1	0.33	Tension	10 MPa	250	Strain
22	50	50	1	71.1	0.33	Tension	10 MPa	350	Strain
23	50	50	1	71.1	0.33	Tension	10 MPa	450	Strain
24	50	50	1	71.1	0.33	Tension	10 MPa	550	Strain
25	50	50	1	71.1	0.33	Bending	200 Nm	50	Stress
26	50	50	1	71.1	0.33	Bending	200 Nm	150	Stress
27	50	50	1	71.1	0.33	Bending	200 Nm	250	Stress
28	50	50	1	71.1	0.33	Bending	200 Nm	350	Stress
29	50	50	1	71.1	0.33	Bending	200 Nm	450	Stress
30	50	50	1	71.1	0.33	Bending	200 Nm	550	Stress
31	50	50	1	71.1	0.33	Bending	200 Nm	50	Strain
32	50	50	1	71.1	0.33	Bending	200 Nm	150	Strain
33	50	50	1	71.1	0.33	Bending	200 Nm	250	Strain
34	50	50	1	71.1	0.33	Bending	200 Nm	350	Strain
35	50	50	1	71.1	0.33	Bending	200 Nm	450	Strain
36	50	50	1	71.1	0.33	Bending	200 Nm	550	Strain

References

1. Schajer, G.S., *Practical Residual Stress Measurement Methods*. 2013, United Kingdom: John Wiley & Sons Ltd.

2. Prime, M.B., *Cross-Sectional Mapping of Residual Stresses by Measuring the Surface Contour After a Cut.* Journal of Engineering Materials and Technology, 2000. **123**(2): pp. 162-168.

3. Prime, M.B. and Kastengren, A.L. *The Contour Method Cutting Assumption: Error Minimization and Correction*. in *SEM Annual Conference*. 2011. Indianapolis, Indiana USA: Experimental and Applied Mechanics.

4. Traore, Y., Paddea, S., Bouchard, P.J., and Gharghouri, M.A., *Measurement of the Residual Stress Tensor in a Compact Tension Weld Specimen.* Experimental Mechanics, 2012. **53**(4): pp. 605-618.

5. Withers, P.J. and Bhadeshia, H.K.D.H., *Residual Stress Part 1 - Measurement Techniques.* Materials Science and Technology, 2001. **17**: pp. 355-365.

6. Rossini, N.S., Dassisti, M., Benyounis, K.Y., and Olbai, A.G., *Methods of Measuring Residual Stresses in Components.* Materials and Deisgn, 2012. **35**: pp. 572–588.

7. Totten, G., Howes, M., and Inoue, T., *Handbook of Residual Stress and Deformation of Steel*. 2002, ASM International.

8. British Energy Generation Ltd, Assessment of the integrity of structures containing defects, R6 Revision 4, 2009.

9. Totten, G., Howes, M., and Inoue, T., *Handbook of Residual Stress and Deformation of Steel*. 2002: ASM International.

10. Withers, P.J., *Residual stress and its role in failure.* Reports on Progress in Physics, 2007. **70**(12): pp. 2211-2264.

11. Hashmi, S., *Comprehensive Materials Finishing*. 2017: Elsevier Inc. 1484.

12. Tönshoff, H.K., Kroos, F., and Marzenell, C., *High-Pressure Water Peening-a New Mechanical Surface-Strengthening Process.* CIRP Annals, 1997. **46**(1): pp. 113-116.

13. Malaki, M. and Ding, H., *A review of ultrasonic peening treatment.* Materials & Design, 2015. **87**: pp. 1072-1086.

14. Schulze, V., *Modern Mechanical Surface Treatment: States, Stability, Effects*. 2006: WILEY-VCH.

15. Withers, P.J. and Bhadeshia, H.K.D.H., *Residual Stress Part 2 - Nature and Origins.* Materials Science and Technology, 2001. **17**: pp. 366-374.

16. Kandil, F.A., Lord, J.D., Fry, A.T., and Grant, P.V., *A Review of Residual Stress Measurement Methods - A Guide to Technique Selection*, N.P. Laboratory, Editor. 2001, NPL Materials Centre: UK.

17. Withers, P.J., Turski, M., Edwards, L., Bouchard, P.J., and Buttle, D.J., *Recent advances in residual stress measurement.* International Journal of Pressure Vessels and Piping, 2008. **85**(3): pp. 118-127.

18. Bouchard, P.J., *The Appropriateness of Residual Stress Length Scales in Structural Integrity.* Journal of neutron research, 2004. **12**(1/3): pp. 18-92.

19. Lu, J., *Handbook of Measurement of Residual Stresses*. 1996, Lilburn, USA: Fairmont Press.

20. Prime, M.B., *Residual stress measurement by successive extension of a slot: The crack compliance method.* Applied Mechanics, 1999. **52**(2): pp. 75-96.

21. Schindler, H.J., Cheng, W., and Finnie, I., *Experimental Determination of Stress Intensity Factors Due to Residual Stresses.* Experimental Mechanics, 1997. **37**(3).

22. Hutchings, M.T., Withers, P.J., Holden, T.M., and Lorentzen, T., *Introduction to the Characterization of Residual Stress by Neutron Diffraction*. 2005: CRC Press.

23. Withers, P.J., Preuss, M., Steuwer, A., and Pang, J.W.L., *Methods for obtaining the strain-free lattice parameter when using diffraction to determine residual stress.* Journal of Applied Crystallography, 2007. **50**(5): pp. 891-904.

24. Bueckner, H.F., *Propogation of Cracks and the Energy of Elastic Deformation.* Trans. ASME, 1958. **80**: pp. 1225-1230.

25. Prime, M.B., *The Contour Method: A New Approach in Experimental Mechanics*, in *SEM Annual Conference*. 2009: Albuquerque, New Mexico, USA.

26. Prime, M.B., Sebring, R.J., Edwards, J.M., Darren, J.H., and Webster, P.J., *Laser Surface-Contouring and Spline Data-Smoothing for Residual Stress Measurement.* Experimental Mechanics, 2004. **44**: pp. 176-184.

27. Balan, B.J. and Achintha, M., *Assessment of Stresses in Float and Tempered Glass Using Eigenstrains.* Experimental Mechanics, 2015. **55**(7): pp. pp 1301-1315.

28. Sommer, C. and Sommer, S., *Understanding the Wire EDM Process*, in *Complete EDM Handbook*. 2005. pp. 69-81.

29. Cheng, W., Finnie, I., Gremaud, M., and Prime, M.B., *Measurement of Near Surface Residual Stresses Using Electric Discharge Wire Machining.* Journal of Engineering Materials and Technology, 1994. **116**: pp. 1-7.

30. Hosseinzadeh, F., Kowal, J., and Bouchard, P.J., *Towards good practice guidelines for the contour method of residual stress measurement.* The Journal of Engineering, 2014. **2014**(8): pp. 453-468.

31. Johnson, G., Residual Stress Measurements using the Contour Method, a thesis in the Faculty of Engineering and Physical Sciences, 2008, University of Manchester.

32. Toparli, M.B. and Fitzpatrick, M.E., *Development and Application of the Contour Method to Determine the Residual Stresses in Thin Laser-Peened Aluminium Alloy Plates.* Experimental Mechanics, 2015. **56**(2): pp. 323-330.

33. Ahmad, B. and Fitzpatrick, M.E., *Minimization and Mitigation of Wire EDM Cutting Errors in the Application of the Contour Method of Residual Stress Measurement.* METALLURGICAL AND MATERIALS TRANSACTIONS A, 2016. **47**: pp. 301-313.

34. Traore, Y., Influence of Plasticity in the Measurement of Residual Stresses by the Contour Method, a thesis in the School of Engineering and Innovation, 2014, The Open University.

35. Kartal, M.E., *Analytical Solutions for Determining Residual Stresses in Two-Dimensional Domains using the Contour Method.* Proc Math Phys Eng Sci, 2013. **469**(2159): pp. 20130367.

36. DeWald, A.T. and Hill, M.R., *Eigenstrain-based Model for Prediction of Laser Peening Residual Stresses in Arbitrary Three-Dimensional Bodies: Part 1 model description.* Journal of Strain Analysis for Engineering Design, 2009. **44**(1): pp. 1-11.

37. DeWald, A.T. and Hill, M.R., *Eigenstrain-based model for prediction of laser peening residual stresses in arbitrary three-dimensional bodies. Part 2: Model verification.* Journal of Strain Analysis for Engineering Design, 2009. **44**(1): pp. 13-27.

38. Coratella, S., Sticchi, M., Toparli, M.B., Fitzpatrick, M.E., and Kashaev, N., *Application of the eigenstrain approach to predict the residual stress distribution in laser shock peened AA7050-T7451 samples.* Surface and Coatings Technology, 2015. **273**: pp. 39-49.

39. Pagliaro, P., Prime, M.B., Swenson, H., and Zuccarello, B., *Measuring Multiple Residual-Stress Components using the Contour Method and Multiple Cuts.* Experimental Mechanics, 2010. **50**(2): pp. 187-194.

40. Liu, C., Wang, C., Cheng, X., Yan, Y., Yang, J., and Guo, Y., *Experimental Investigation on the Residual Stresses in a Thick Joint with a Partial Repair Weld Using Multiple-Cut Contour Method.* Materials, 2018. **11**(4): pp. 633.

41. Prime, M.B., Newborn, M.A., and Balog, J.A., *Quenching and Cold-Work Residual Stresses in Aluminum Hand Forgings : Contour Method Measurement and FEM Prediction.* Materials Science Forum, 2003. **426-432**: pp. 435-440.

42. Olson, M.D. and Hill, M.R., *A New Mechanical Method for Biaxial Residual Stress Mapping.* Experimental Mechanics, 2015. **55**(6): pp. 1139-1150.

43. Pagliaro, P., Prime, M.B., Robinson, J.S., Clausen, B., Swenson, H., Steinzig, M., and Zuccarello, B., *Measuring Inaccessible Residual Stresses Using Multiple Methods and Superposition.* Experimental Mechanics, 2010. **51**(7): pp. 1123-1134.

44. Toparli, M.B., Fitzpatrick, M.E., and Gungor, S., *Determination of multiple near-surface residual stress components in laser peened aluminium alloy via the contour method.* Metallurgical and Materials Transactions A, 2015. **46**(9): pp. pp 4268-4275.

45. Hosseinzadeh, F. and Bouchard, P.J., *Mapping Multiple Components of the Residual Stress Tensor in a Large P91 Steel Pipe Girth Weld Using a Single Contour Cut.* Experimental Mechanics, 2012. **53**(2): pp. 171-181.

46. Mahmoudi, A.H., *Plasticity Effect on Residual Stresses Measurement using Contour Method.* International Journal of Engineering, 2013. **26**(10): pp. 1203-1212.

47. Masoudi, S., Amirin, G., Saeedi, E., and Ahmadi, M., *The Effect of Quench-Induced Residual Stresses on the Distortion of Machined Thin-Walled Parts.* Journal of Materials Engineering and Performance, 2015. **24**(10): pp. 3933-3941.

48. Prime, M.B., *Residual Stresses Measured in Quenched HSLA-100 Steel Plate*, in *Proceedings of the 2005 SEM Annual Conference and Exposition on Experimental and Applied Mechanics*. 2005: Portland, OR, USA.

49. Prime, M.B. and Martineau, R.L., *Mapping Residual Stresses After Foreign Object Damage Using the Contour Method.* Materials Science Forum, 2002. **404-407**: pp. 521-526.

50. Martineau, R.L., Prime, M.B., and Duffey, T., *Penetration of HSLA-100 Steel with Tungsten Carbide Spheres at Striking Velocities Between 0.8 and 2.5 km/s.* International Journal of Impact Engineering, 2004. **30**(5): pp. 505-520.

51. Ahmad, B., van der Veen, S.O., Fitzpatrick, M.E., and Guo, H., *Residual stress evaluation in selective-laser-melting additively manufactured titanium (Ti-6Al-4V) and inconel 718 using the contour method and numerical simulation.* Additive Manufacturing, 2018. **22**: pp. 571-582.

52. Ahmad, B., O. van der Veen, S., Fitzpatrick, M.E., and Guo, H., *Measurement and modelling of residual stress in wire-feed additively manufactured titanium.* Materials Science and Technology, 2018. **34**(18): pp. 2250-2259.

53. Prime, M.B., Hughes, D.J., and Webster, P.J., *Weld Application of a New Method for Cross-Sectional Residual Stress Mapping*, in *Society for Engineering Mechanics Annual Conference and Exposition*. 2001: Portland, Oregon.

54. Dewald, A.T. and Hill, M.R., *Residual stress in a thick steel weld determined using the contour method*. 2001, Report on LANL contract 32390-001-01 49.

55. Prime, M.B., Gnaupel-Herold, T., Baumann, J.A., Lederich, R.J., Bowden, D.M., and Sebring, R.J., *Residual stress measurements ina thick, dissimilar aluminum alloy friction stir weld.* Acta Materialia, 2006. **54**(15): pp. 4013-4021.

56. Prime, M.B., Hill, M.R., DeWald, A.T., Sebring, R.J., Dave, V.R., and Cola, M.J., *Residual Stress Mapping in Welds Using the Contour Method*, in *Proceedings of the Sixth International Conference on Trends in Welding Research*. 2002: Pine Mountain, Georgia.

57. Shi, L., Price, A.H., and Hung, W.N., *Use of Contour Method for Welding Residual Stress Assessment.* Procedia Manufacturing, 2018. **26**: pp. 276-285.

58. Ganguly, S., Fitzpatrick, M.E., and Edwards, L., *Use of neutron and synchrotron X-ray diffraction for evaluation of residual stresses in a 2024-T351 aluminum alloy variable-polarity plasma-arc weld.* Metallurgical and Materials Transactions A, 2006. **32**(2): pp. 411–420.

59. Zhang, Y., Ganguly, S., Edwards, L., and Fitzpatick, M.E., *Cross-sectional mapping of residual stresses in a VPPA weld using the contour method.* Acta Materialia, 2004. **52**(17): pp. 5225-5232.

60. Prime, M.B., Gnaupel-Herold, T., Baumann, J.A., Lederich, R.J., Bowden, D.M., and Sebring, R.J., *Residual stress measurements in a thick, dissimilar aluminum alloy friction stir weld.* Acta Materialia, 2006. **54**(15): pp. 4013-4021.

61. Sonne, M.R., Carlone, P., and Hattel, J.H., *Assessment of the Contour Method for 2-D Cross Sectional Residual Stress Measurements of Friction Stir Welded Parts of AA2024-T3—Numerical and Experimental Comparison*. Vol. 7. 2017. 508.

62. Zhang, C. and Shirzadi, A.A., *Measurement of residual stresses in dissimilar friction stir-welded aluminium and copper plates using the contour method.* Science and Technology of Welding and Joining, 2018. **23**(5): pp. 394-399.

63. Smith, M., Lévesque, J.B., Bichler, L., Sediako, D., Gholipour, J., and Wanjara, P., *Residual Stress Analysis in Linear Friction Welded In-Service Inconel 718 Superalloy via Neutron Diffraction and Contour Method Approaches.* Materials Science and Engineering: A, 2017. **691**: pp. 168-179.

64. Hosseinzadeh, F., Ledgard, P., and Bouchard, P.J., *Controlling the Cut in Contour Residual Stress Measurements of Electron Beam Welded Ti-6Al-4V Alloy Plates.* Experimental Mechanics, 2013. **53**: pp. 829-839.

65. Kapadia, P., Davies, C., Pirling, T., Hofmann, M., Wimpory, R., Hosseinzadeh, F., Dean, D., and Nikbin, K., *Quantification of residual stresses in electron beam welded fracture mechanics specimens.* International Journal of Solids and Structures, 2017. **106–107**: pp. 106-118.

66. Javadi, Y., Smith, M.C., Abburi Venkata, K., Naveed, N., Forsey, A.N., Francis, J.A., Ainsworth, R.A., Truman, C.E., Smith, D.J., Hosseinzadeh, F., Gungor, S., Bouchard, P.J., Dey, H.C., Bhaduri, A.K., and Mahadevan, S., *Residual stress measurement round robin on an electron beam welded joint between austenitic stainless steel 316L(N) and ferritic steel P91.* International Journal of Pressure Vessels and Piping, 2017. **154**: pp. 41-57.

67. Xie, P., Zhao, H., Wu, B., and Gong, S., *Using Finite Element and Contour Method to Evaluate Residual Stress in Thick Ti-6Al-4V Alloy Welded by Electron Beam Welding.* Acta Metallurgica Sinica (English Letters), 2015. **28**(7): pp. 922-930.

68. Smith, M.C. and Smith, A.C., *NeT bead-on-plate round robin: Comparison of residual stress predictions and measurements.* International Journal of Pressure Vessels and Piping, 2009. **86**(1): pp. 79-95.

69. Prime, M.B., Rangaswamy, P., Daymond, M.R., and Abeln, T.G., *Several Methods Applied to Measuring Residual Stress in a Known Specimen*, in *Proceedings of the SEM Spring COnference on Experimental and Applied Mechanics*. 1998, Society for Experimental Mechanics, Inc.: Houston, Texas USA. pp. 497-499.

70. Smith, M.C., Smith, A.C., Ohms, C., and Wimpory, R.C., *The NeT Task Group 4 residual stress measurement and analysis round robin on a three-pass slot-welded plate specimen.* International Journal of Pressure Vessels and Piping, 2018. **164**: pp. 3-21.

71. Muránsky, O., Hamelin, C.J., Hosseinzadeh, F., and Prime, M.B., *Mitigating cutting-induced plasticity in the contour method. Part 2: Numerical analysis.* International Journal of Solids and Structures, 2016. **94-95**: pp. 254-262.

72. Kaiser, R., Stefenelli, M., Hatzenbichler, T., Antretter, T., Hofmann, M., Keckes, J., and Buchmayr, B., *Experimental characterization and modelling of triaxial residual stresses in straightened railway rails.* The Journal of Strain Analysis for Engineering Design, 2014. **50**(3): pp. 190-198.

73. Moat, R.J., Pinketon, A., Li, L., Withers, P.J., and Preuss, M., *Residual stresses in laser direct metal deposited Waspaloy.* Materials Science and Engineering A, 2011. **528**(6): pp. 2288-2298.

74. Evans, A., Johnson, G., King, A., and Withers, P.J., *Characterization of Laser Peening Residual Stresses in Al 7075 by Synchrotron Diffraction and the Contour Method.* Journal of neutron research, 2007. **15**(2): pp. 147-154.

75. Frankel, P., Preuss, M., Steuwer, A., Withers, P.J., and Bray, S., *Comparison of residual stresses in Ti–6Al–4V and Ti–6Al–2Sn–4Zr–2Mo linear friction welds.* Materials Science and Technology, 2009. **25**(5): pp. 640-650.

76. Woo, W., An, G.B., Kingston, E., Dewald, A.T., Smith, D.J., and Hill, M.R., *Through-thickness distributions of residual stresses in two extreme heat-input thick welds: A neutron diffraction, contour method and deep hole drilling study.* Acta Materialia, 2013. **61**(10): pp. 3564-3574.

77. Thibault, D., Bocher, P., Thomas, M., Gharghouri, M., and Côté, M., *Residual stress characterization in low transformation temperature 13%Cr–4%Ni stainless steel weld by neutron diffraction and the contour method.* Materials Science and Engineering A, 2010. **527**(23): pp. 6205-6210.

78. Kundu, A., Bouchard, P.J., Kumar, S., Venkata, K.A., Francis, J.A., Paradowska, A., Dey, G.K., and Truman, C.E., *Residual stresses in P91 steel electron beam welds.* Science and Technology of Welding & Joining, 2013. **18**(3): pp. 271-271.

79. Frankel, P.G., Withers, P.J., Preuss, M., Wang, H.T., Tong, J., and Rugg, D., *Residual Stress Fields After FOD Impact on Flat and Aerofoil-shaped Leading Edges.* Mechanics of Materials, 2012. **55**: pp. 130–145.

80. Liu, C. and Dong, C., *Internal residual stress measurement on linear friction welding of titanium alloy plates with contour method.* Transactions of Nonferrous Metals Society of China, 2014. **24**(5): pp. 1387–1392.

81. Bouchard, P.J., *Code characterisation of weld residual stress levels and the problem of innate scatter.* International Journal of Pressure Vessels and Piping, 2008. **85**(3): pp. 152-165.

82. Kartal, M.E., Liljedahl, C.D.M., Gungor, S., Edwards, L., and Fitzpatrick, M.E., *Determination of the profile of the complete residual stress tensor in a VPPA weld using the multi-axial contour method.* Acta Materialia, 2008. **56**(16): pp. 4417-4428.

83. Hosseinzadeh, F. and Bouchard, P.J., *Residual Stress Measurement of a Hipped Bonded Valve Seat Using the Contour Method*, in *Proceedings of the ASME 2013 Pressure Vessels and Piping Division Conference*. 2013: Paris, France.

84. Zabeen, S., Preuss, M., and Withers, P.J., *Residual stresses caused by head-on and 45° foreign object damage for a laser shock peened Ti–6Al–4V alloy aerofoil.* Materials Science and Engineering: A, 2013. **560**: pp. 518-527.

85. DeWald, A.T., Hill, M.R., Benson, M.L., and Rudland, D.L. *Measurement of Residual Stress in Reactor Nozzle Mock-Ups Containing Dissimilar Metal Welds*. in *ASME Pressure Vessels and Piping Conference*. 2014. California, USA.

86. Isaac, D.D., Prime, M.B., and Arakere, N., *Residual Stress Measurement of Full-Scale Jet-Engine Bearing Elements Using the Contour Method*, in *Residual Stress, Thermomechanics & Infrared Imaging, Hybrid Techniques and Inverse Problems*. 2017.

87. Jacob, A., Oliveira, J., Mehmanparast, A., Hosseinzadeh, F., Kelleher, J., and Berto, F., *Residual stress measurements in offshore wind monopile weldments using neutron diffraction technique and contour method.* Theoretical and Applied Fracture Mechanics, 2018. **96**: pp. 418-427.

88. Kelleher, J., Prime, M.B., Buttle, D., Mummery, P.M., Webster, P.J., Shackleton, J., and Withers, P.J., *The Measurement of Residual Stress in Railway Rails by Diffraction and Other Methods.* Journal of neutron research, 2003. **11**(4): pp. 187-193.

89. Toparli, M.B., Fitzpatrick, M.E., and Gungor, S., *Improvement of the Contour Method for Measurement of Near-Surface Residual Stresses from Laser Peening.* Experimental Mechanics, 2013. **53**(9): pp. 1705-1718.

90. Elmesalamy, A., Francis, J., and Li, L., *A comparison of residual stresses in multi pass narrow gap laser welds and gas-tungsten arc welds in AISI 316L stainless steel.* International Journal of Pressure Vessels and Piping, 2015. **113**: pp. 49-59.

91. Xie, P., Zhao, H., Wu, B., and Gong, S., *Evaluation of Residual Stresses Relaxation by Post Weld Heat Treatment Using Contour Method and X-ray Diffraction Method.* Experimental Mechanics, 2015. **55**(7): pp. 1329–1337.

92. Zhang, Y., Pratihar, S., Fitzpatrick, M.E., and Edwards, L., *Residual Stress Mapping in Welds using the Contour Method.* Materials Science Forum, 2005. **490-491**: pp. 294-299.

93. Savaria, V., Hoseini, M., Bridier, F., Bocher, P., and Arkinson, P., *On the Measurement of Residual Stress in Induction Hardened Parts.* Materials Science Forum, 2011. **681**: pp. 431-436.

94. Levieil, B., Bridier, F., Doudard, C., Thevenet, D., and Calloch, S., *User Influence on Two Complementary Residual Stress Determination Methods: Contour Method and Incremental X-Ray Diffraction.* Experimental Mechanics, 2016. **56**(9).

95. Kartal, M.E., Turski, M., Johnson, G., Fitzpatrick, M.E., Gungor, S., Withers, P.J., and Edwards, L., *Residual Stress Measurements in Single and Multi-Pass Groove Weld Specimens Using Neutron Diffraction and the Contour Method.* Materials Science Forum, 2006. **524-525**.

96. Zhang, Y., Ganguly, S., Stelmukh, V., Fitzpatrick, M.E., and Edwards, L., *Validation of the Contour Method of Residual Stress Measurement in a MIG 2024 Weld by Neutron and Synchrotron X-ray Diffraction.* Journal of neutron research, 2003. **11**(4).

97. Dennis, R.J., Bray, D.P., Leggatt, N.A., and Turski, M., *Assessment of the Influence of Plasticity and Constraint on Measured Residual Stresses Using the Contour Method*, in *Proceedings of the ASME 2008 Pressure Vessels and Piping Division Conference*. 2008: Chicago, Illinois USA.

98. Nasri, H., Lanteigne, J., and Champliaud, H., *Usage of the contour method in measuring residual stress in welding and peen-welding applications*, in *IASTED Asian Conference on Modelling and Simulation*. 2007: Beijing, China.

99. Kerr, M., Prime, M.B., Swenson, H., Buechler, M.A., Steinzig, M., Clausen, B., and Sisneros, T., *Residual Stress Characterization in a Dissimilar Metal Weld Nuclear Reactor Piping System Mock Up.* Journal of Pressure Vessel Technology, 2013. **135**(4): pp. 041205-041205.

100. Hosseinzadeh, F., Toparli, M.B., and Bouchard, P.J., *Slitting and Contour Method Residual Stress Measurements in an Edge Welded Beam.* Journal of Pressure Vessel Technology, 2011. **134**(1).

101. Traore, Y., Bouchard, P.J., Francis, J., and Hosseinzadeh, F., *A Novel Cutting Stratergy for Reducing Plasticity Induced Errors in Residual Stress Measurement Made with the Contour Method*, in *Proceedings of the ASME 2011 Pressure Vessels and Piping Division Conference*. 2011: Baltimore, Maryland USA.

102. Hosseinzadeh, F., Traore, Y., Bouchard, P.J., and Muránsky, O., *Mitigating cutting-induced plasticity in the contour method, part 1: Experimental.* International Journal of Solids and Structures, 2016. **94-95**: pp. 247-253.

103. Hosseinzadeh, F. and Bouchard, P.J., *Residual Stress Measurement of a Ferritic Bead on Plate Benchmark Test Specimen Using the Contour Method*, in *Proceedings of the ASME 2012 Pressure Vessels and Piping Division Conference*. 2012: Toronto, Canada.

104. Traore, Y., Hosseinzadeh, F., and Bouchard, P.J., *Plasticity in the Contour Method of Residual Stress Measurement.* Advanced Materials Research, 2014. **996**: pp. 337-342.

105. Hill, M.R. and Olson, M.D., *Repeatability of the Contour Method for Residual Stress Measurement.* Experimental Mechanics, 2014. **54**(7): pp. 1269-1277.

106. Ismonov, S., Daniewicz, S.R., Newman, J.J.C., Hill, M.R., and Urban, M.R., *Three Dimensional Finite Element Analysis of a Split-Sleeve Cold Expansion Process.* Journal of Engineering Materials and Technology, 2009. **131**(3): pp. 031007-031007-031008.

107. Olson, M., DeWald, A.T., and Hill, M.R., *Repeatability of Contour Method Residual Stress Measurements for a Range of Material, Process, and Geometry*, in *Residual Stress, Thermomechanics & Infrared Imaging, Hybrid Techniques and Inverse Problems*. 2018. pp. 101-113.

108. Olson, M.D., Hill, M.R., Willis, E., Peterson, A.G., Patel, V.I., and Muránsky, O., *Assessment of Weld Residual Stress Measurement Precision: Mock-Up Design and Results for the Contour Method.* Journal of Nuclear Engineering and Radiation Science. 2015; 1(3): pp. 031008-031008-10.

109. Olson, M.D., DeWald, A.T., Prime, M.B., and Hill, M.R., *Estimation of Uncertainty for Contour Method Residual Stress Measurement.* Experimental Mechanics, 2014. **55**(3): pp. 577-585.

110. Bouchard, P.J., Ledgard, P., Hiller, S., and Hosseinzadeh, F. *Making the Cut for the Contour Method*. in *15th International Conference on Experimental Mechanics*. 2012. Portugal.

111. Shin, S.H., *FEM Analysis of Plasticity-Induced Error on Measurement of Welding Residual Stress by the Contour Method.* Journal of Mechanical Science and Technology, 2005. **19**(10): pp. 1885-1890.

112. Kim, H.K., Pavier, M.J., and Shterenlikht, A., *Plasticity and Stress Heterogeneity Influence on Mechanical Stress Relaxation Residual Stress Measurements.* Advanced Materials Research, 2014. **996**: pp. 249-255.

113. Bueckner, H.F., *Field Singularities and Related Integral Representations*, in *Mechanics of Fracture*, G.C. Sih, Editor. 1973. pp. 239-314.

114. Bouchard, P., Mark, T., and Mike, S., *Residual Stress Concentrations in a Stainless Steel Slot-Weld Measured by the Contour Method and Neutron Diffraction*, in *ASME 2009 Pressure Vessels and Piping Conference*. 2009: Prague, Czech Republic.

115. Sun, Y., Roy, M.J., Vasileiou, A.N., Smith, M.C., Francis, J.A., and Hosseinzadeh, F., *Evaluation of Errors Associated with Cutting-Induced Plasticity in Residual Stress Measurements Using the Contour Method.* Experimental Mechanics, 2017. **57**: pp. 719-734.

116. Kim, H.K., Coules, H.E., Pavier, M.J., and Shterenlikht, A., *Measurement of Highly Non-Uniform Residual Stress Fields with Reduced Plastic Error.* Experimental Mechanics, 2015. **55**(7): pp. 1211-1224.

117. Muránsky, O., Hamelin, C.J., Hosseinzadeh, F., and Prime, M.B., *Evaluation of a self-equilibrium cutting strategy for the contour method of residual stress measurement.* International Journal of Pressure Vessels and Piping, 2018. **164**: pp. 22-31.

118. Prime, M.B., *Private communication on bulge error correction procedure with Mike Prime*. 2015.

119. Dassault Systemes, ABAQUS, *Version 6.13*, 2013.

120. Paris, P.C., Tada, H., and Irwin, G.R., *The Stress Analysis of Cracks Handbook*. 2000.

121. Pook, L.P., *The linear elastic analysis of cracked bodies and crack paths.* Theoretical and Applied Fracture Mechanics, 2015.

122. Irwin, G.R., *Analysis of Stresses and Strains Near the End of a Crack Traversing a Plate.* Journal of Applied Mechanics., 1957. **24**: pp. 361-364.

123. Westergaard, H.M., *Bearing Pressures and Cracks.* Journal of Applied Mechanics, 1939. **6**: pp. A49-A53.

124. Anderson, T.L., *Fracture Mechanics: Fundamentals and Applications, 3rd Edition*. 2004, USA: CRC Press.

125. Williams, M.L., *On the Stress Distribution at the Base of a Stationary Crack*. Vol. 24. 1957. 109-114.

126. Irwin, G.R., *Analysis of Stresses and Strains Near the End of a Crack Traversing a Plate.* J. Appl. Mech., 1957.

127. Paris, P.C. and Sih, G.C., *Stress Analysis of Cracks. Fracture Testing and Its Applications*. Vol. ASTM STP 381. April 1965: American Society for Testing and Materials.

128. Sun, C.T. and Jin, Z.H., *Chapter 3 - The Elastic Stress Field around a Crack Tip*, in *Fracture Mechanics*, C.T. Sun and Z.H. Jin, Editors. 2012, Academic Press: Boston. pp. 25-75.

129. Pook, L.P., *Crack paths and the linear elastic analysis of cracked bodies*. Vol. 9. 2015.

130. Janssen, M., Zuidema, J., and Wanhill, R.J.H., *Fracture Mechanics*. 2nd edition ed. 2002, Netherlands: VSSD.

131. Creager, M. and Paris, P.C., *Elastic Field Equations for Blunt Cracks With Reference to Stress Corrosion Cracking.* International Journal of Fracture, 1967. **3**: pp. 247-252.

132. Rice, J.R., *Mechanics of Crack Tip Deformation and Extension by Fatigue*, J. Grosskreutz, Editor. 1967, ASTM International: West Conshohocken, PA. pp. 247-311.

133. Sih, G.C., *Handbook of stress-intensity factors : stress-intensity factor solutions and formulas for reference.* 1973.

134. Rooke, D.P. and Cartwright, D.J., *Compendium of stress intensity factors*. 1976, London: H.M.S.O.

135. Fett, T. and Munz, D., *Stress intensity factors and weight functions*. 1997, Southampton, UK; Boston, Mass. USA: Computational Mechanics Publications.

136. Wu, X.R. and Carlsson, A.J., *Weight functions and stress intensity factor solutions*. 1991, Oxford: Pergamon Press.

137. Gross, B., Srawley, J.E., and Brown, W.F., *Stress-intensity factors for a single-edge-notch tension specimen by boundary collocation of a stress function*. 1964, National Aeronautics and Space Administration: Washington, D.C.

138. Gross, B. and Srawley, J.E., *Stress-intensity factors for single-edge-notch specimens in bending or combined bending and tension by boundary collocation of a stress function*. 1965, National Aeronautics and Space Administration: Washington, D.C.

139. EDF Energy Nuclear Generation Ltd, R-Code Software: Implementing the R5 and R6 structural integrity assessment procedures, 5.0, 2015.

140. TWI Software, CrackWISE, *Version 5.0*, 2014.

141. Post, D. and Han, B., *Moiré Interferometry*, in *Springer Handbook of Experimental Solid Mechanics*. 2008. pp. 627-654.

142. Fett, *Stress intensity factors for edge-cracked plates under arbitrary loading.* Fatigue & Fracture of Engineering Materials & Structures, 1999. **22**(4): pp. 301-305.

143. Mahmoudi, A.H. and Saei, A., *Influence of Asymmetrical Cuts in Measuring Residual Stresses using Contour Method.* International Journal of Pressure Vessels and Piping, 2015. **134**: pp. 1-10.

144. Achouri, A., Advances in the contour method for residual stress measurement, a thesis in the School of Engineering and Innovation, 2018, The Open University.

145. Bouchard, P.J., Budden, P.J., and Withers, P.J., *Fourier basis for the engineering assessment of cracks in residual stress fields.* Engineering Fracture Mechanics, 2012. **91**: pp. 37-50.

146. EDF Energy Nuclear Generation Ltd, AGR Materials Data Handbook, R66 Rev. 008, 2010.

147. Vieira, M., Kenji, S., and Tomotake, F., *Smoothing of Noisy Laser Scanner Generated Meshes Using Polynomial Fitting and Neighborhood Erosion.* Journal of Mechanical Design, 2004. **126**.

148. Prime, M.B., *Plasticity effects in incremental slitting measurement of residual stresses.* Engineering Fracture Mechanics, 2010. **77**(10): pp. 1552-1566.

149. Press, W.H., Teukolsky, S.A., Vetterling, W.T., and Flannery, B.P., *Numerical Recipes in Fortran 77*. Second Edition ed. The Art of Scientific Computing. Vol. Vol. 1 of Fortran Numerical Recipes. 1997, Cambridge: Press Syndicate of the University of Cambridge.

150. The MathWorks, Inc., MATLAB, *R2014a*, 2014.

151. Chan, S.K., Tuba, I.S., and Wilson, W.K., *On the finite element in linear fracture mechanics*. Vol. 2. 1970. 1-17.

152. Paris, P.C. and Sih, G.C., *Stress Analysis of Cracks*, in *Fracture Testing and Its Applications*. April 1965, American Society for Testing and Materials. pp. 30-38.

153. Gross, B., Roberts, E., and Srawley, J.E., *Elastic displacements for various edge-cracked plate specimens*. 1967, National Aeronautics and Space Administration: Washington, D.C.

154. Cheng, W. and Finnie, I., *A Comparison of the Strains Due to Edge Cracks and Cuts of Finite Width With Applications to Residual Stress Measurement.* Journal of Engineering Materials and Technology, 1993. **115**(2): pp. 220-226.

155. Hossain, S., Truman, C.E., Smith, D.J., and Daymond, M.R., *Application of quenching to create highly triaxial residual stresses in type 316H stainless steels.* International Journal of Mechanical Sciences, 2006. **48**(3): pp. 235-243.

156. Aird, C., Smith, M., Kapadia, P., Venkata, K.A., and Ondrej, M. *Round Robin Prediction of Residual Stresses in the Edge-Welded Beam R6 Validation Benchmark Problem*. in *Pressure Vessels and Piping Conference*. 2013. Paris, France.

157. Nadri, B., Bouchard, P., Smith, M., Truman, C.E., and Smith, D.J., *Modelling and Statistical Treatment of Residual Stress Distributions in an Edge Welded Stainless Steel Beam.* Strain : an international journal for experimental mechanics, 2011. **47**: pp. 505-517.

158. Mayville, R.A. and Finnie, I., *Uniaxial stress-strain curves from a bending test.* Experimental Mechanics, 1982. **22**: pp. 197-201.

159. Prime, M., Newborn, M.A., and Balog, J.A., *Quenching and Cold-Work Residual Stresses in Aluminum Hand Forgings : Contour Method Measurement and FEM Prediction.* Materials Science Forum, 2003: pp. 435-440.

160. Smith, D.J., Bouchard, P.J., and George, D., *Measurement and prediction of residual stresses in thick-section steel welds.* The Journal of Strain Analysis for Engineering Design, 2000. **35**(4): pp. 287-305.

161. Dong, P., *On the Mechanics of Residual Stresses in Girth Welds.* Journal of Pressure Vessel Technology, 2006. **129**(3): pp. 345-354.

162. Naveed, N., Improving the spatial resolution of the contour method, a thesis in the School of Engineering and Innovation, 2015, The Open University.

163. Ganguly, S., Non-destructive measurement of residual stresses in welded aluminium 2024 airframe alloy, a thesis in the School of Engineering and Innovation, 2004, The Open University.

164. Wood, H.A. and Engle, R.M., *USAF Damage Tolerant Design Handbook: Guidelines for the analysis and Design of Damage Tolerant Aircraft Structures. Revision A*. 1979. 447.

165. Zhu, X.K. and Leis, B.N., *Effective Methods to Determine Stress Intensity Factors for 2D and 3D Cracks*, in *10th International Pipeline Conference*. September 29–October 3, 2014: Calgary, Alberta, Canada.

166. Vorel, M. and Leidich, E., *Accuracy of Determining Stress Intensity Factors in Some Numerical Programs.* Acta Polytechnica: Journal of Advanced Engineering, 2001. **41**(2): pp. 62-67.

167. British Standards Institution, Guide to methods for assessing the acceptability of flaws in metallic structures, BS 7910, 2013.

168. Kim, H.K., Stewart, B., Hosseinzadeh, F., Araujo de Oliveira, J., and Bouchard, P.J., *Slitting-Contour Measurements of Residual Stress for the NeT TG5 Edge-welded Ferritic Steel Beam Round Robin*. 2019, The Open University; Materials Engineering Report.